TRIBOEMISSION-LUBRICANT INTERACTIONS

Thesis submitted to Imperial College London
for the Degree of Doctor of Philosophy
and Diploma of Imperial College London (D.I.C.)

Submitted by

Debashis Puhan

Department of Mechanical Engineering

Imperial College London

October 2017

DECLARATION

I, Debashis Puhan, declare that this thesis titled, **' Triboemission-Lubricant Interactions**' and the work presented in it are entirely my own.

I confirm that:

- This dissertation is the result of my own work done during my PhD studentship at Imperial College London and includes nothing, which is the outcome of work done in collaboration except where specifically indicated in the text.
- It has not been previously submitted, in part or whole, to any university or institution for any degree, diploma, or other qualification.
- Where I have consulted the published work of others, this is always clearly attributed.
- Where I have quoted from the work of others, the source is always given.
- I have acknowledged all main sources of help.

Debashis Puhan,

Postgraduate Researcher

Imperial College London

Date: 20/02/18

ABSTRACT

There is need to increase the efficiency of machines in order to limit damage to the environment. The key to doing this is through the implementation of advanced materials, superior designs and better lubricants. For better formulation of lubricants, a complete knowledge of lubricant behaviour under full film and boundary lubrication conditions is a prerequisite. However, several aspects of the latter remain a mystery. For example, the pathways, by which certain anti-wear film form, are still not so clear. One possibly important factor, which limits understanding in this area, is a poor knowledge of the phenomena known as Triboemission. The aim of this PhD project is therefore to elucidate the tribological role of sub atomic particles and plasma emitted during the sliding process. To achieve this, two approaches are taken. Firstly, test equipment is developed to monitor the effects of emitted particles from a sliding contact under vacuum, ambient and submerged conditions. This staged approach is required due to the difficulty in detecting triboemission effects under submerged conditions. The second approach is to artificially introduce electrons into a sliding lubricated contact in order follow their effects. Particular focus is on non-conductive materials since these are known to produce intense emission behaviour when rubbed.

The study first presents spatially resolved measurements of electron emission from Polytetrafluoropolyethylene (PTFE) when scratch tests are carried out in a vacuum tribometer, in which microchannel plates coupled to a phosphor screen are used to image electron emission. The results show that electron emission occurs at specific locations on the worn surface and these sites remain active exhibiting after emission events which decay with a time constant of up to several seconds.

To study triboemission events under ambient and submerged conditions, a pin-on-disc tribometer is developed, whose transparent pin allows the contact to be viewed while sliding is occurring. This equipment is first used to detect the triboplasma caused by the discharge of air molecules on tribocharged surfaces under ambient conditions. Here, a range of polymer materials were tested (chosen due to their known ability to induce chemical reactions through rubbing) and maps showing plasma distributions were successfully obtained. Results show for the first time, the pronounced transient variations in plasma generation and have enabled a reasonably complete picture of polymer charging behaviour to be built up. Specifically, it is shown that the charge carrying ability of debris

plays an important role and that electrical resistivity and friction are not the primary factors controlling charge and triboplasma generation, as previously thought.

A fluorescence microscope coupled to this tribometer enabled viewing of the sliding contact submerged in a lubricant that contains a fluorescent dye and this was successfully used to detect in contact chemical changes due to the emission of charged particles. However, there is still some level of uncertainty regarding the detected chemical changes i.e. it is still a question whether the observed changes were a consequence of shear activated aggregation or electrons/radical initiated chemical reaction. This setup has potential for further improvement in order to detect and monitor chemical changes during rubbing.

Finally, various drivers for tribofilm formation are studied, such as the generation of fresh surface, shearing, mixing are studied on a mini traction machine using new and existing methods. It is concluded that fresh surface generation and mixing do not play a significant role in tribofilm growth whereas shearing does improve the mechanical properties and morphology of the tribofilm. Next, shear stimulated emission from oxide surfaces were induced in order to study links between tribo-film formation and electron emission, since emission has been correlated with oxide thickness. Results show that counter specimen oxide thickness, and therefore possibly electron emission, plays a role in the initial growth of ZDDP films. However, further work is needed in this area.

Another first of its kind test involved artificially stimulating electron emission from an additive/mineral oil covered steel surface with ultraviolet light to stimulate photoelectron emission. This was done in order to assess whether electron emission resulted in film growth. ToF SIMS analysis of steel surface following irradiation showed that electron emission resulted in very subtle changes to oil-steel interface. However, further high temperature UV tests confirmed that indeed electrons have the potential to cause tribofilm growth.

ACKNOWLEDGEMENTS

*First of all I would like to praise **The Almighty** for his benevolent shower of grace that led me throughout this arduous work, which would have been otherwise impossible.*

*I am struggling to find enough words to truly express my sincere gratitude to my supervisor **Dr. Tom Reddyhoff** because of whose impetus, sustained efforts, and peerless guidance, this research project could be undertaken. I have been extremely lucky to have a sensitive and approachable supervisor who promptly fostered the splendid vision of my thesis outline and bestowed me with freedom and the spirit to see to its culmination. I am thankful for his contribution towards my personal and professional capacity building by acting as my friend, philosopher and guide. I deeply appreciate his relentless resolve to facilitate my research endeavours and related travels by ensuring sufficient funding. This thesis has profited from his maddening attention to detail, which not only improved my scientific output from start to finish but also transferred valuable skills of designing oral presentation slides and posters. I owe my two best poster awards to his constructive criticism and generous appreciation. I dedicate this thesis to him.*

*My special thanks to **academic staff, seniors and colleagues in the Tribology Group**, for their all-time cooperation and help during the entire period. I express my indebtedness to **Dr Jason (Dr. Jie Zhang)** and **Dr. Janet Wong** for their esteemed support and knowledge transfer at various stages of my Ph.D.*

*I would like to thank all the officials and technical staff of **PCS Instruments**, UK and **KP Technology**, UK for their cordial association and services provided for this work especially **Prof Iain D Baikie**, **Miss. Susanna Challinger**, **Dr. Rich Baker** and **Dr. Matt Smeeth**. I am also thankful to **Dr. Patrick Mesquida (**Kings College London**), Sarah Fearn (**Imperial College London**),** and **Dr. Richard Thorogate (**University College London**)** for imparting knowledge and training on surface science techniques*

*My sincere thanks to all the faculty and staff of **Imperial College London** for the help and advice rendered during the tenure of this work especially **Mrs Chrissy Stevens, Mr. Tariq Rasheed, Miss Kate Lewis, Mr. Mark Holloway.** I also appreciate the suggestions by the **Staff in the Student Workshop** during manufacturing of my jobs and samples as well as cooperation of the **Security staff** for reminding me to go home and occasionally escort me out of college building when access ceases after midnight**.** I am extremely grateful to **Imperial College***

Graduate School *for enhancing my student experience by running various professional skills programme.*

I extend my gratitude to my ***Parents*** *and* ***Prof. Jayashree Bijwe*** *for their love and moral support which has ensured my wellbeing and kept me spirited throughout this work. A big shout out to Yuta, Antonio, Ale, Sorin, Oana, Aleks, Kostas, Ruby, Joanna, Francesco, Nico, Stefano, Carmine, Artemis, Jonathan, Jia, Peng, Xiang JiangMeihui, Mery Johanna, Diptargha, Alberto and Martina and all the friends I made in London, with whom I share wonderful memories of post conference travel, weekend outings, badminton and climbing sessions, Friday night beers, night outs, sumptuous dinner and barbeques.*

Table of Contents

List of Tables

List of Figures

List of Abbreviations

AFM	Atomic force microscopy
Al_2O_3	Aluminium oxide (Sapphire)
CF	Carboxyfluorescein
EDS	Energy dispersive spectroscopy
FITC	Fluorescein isothiocyanate
HDPE	High density polyethylene
KPFM	Kelvin probe force microscopy
KPT	Kelvin probe technology
MCP	Micro channel plates
MTM	Mini traction machine
NR	Neutral red
PC	Polycarbonate
PDMS	Polydimethylsiloxane
PEEK	Polyetheretherketone
PMMA	Polymethylmethacrylate
PP	Polypropylene
PS	Polystyrene
PTFE	Polytetrafluoroethylene
PVC	Polyvinylchloride
PVDF	Polyvinyldifluoride
SEM	Scanning electron microscopy
SLIM	Spacer layer imaging method
TE	Triboemission
ToF-SIMS	Time of flight secondary ion mass spectrometry
UHMWPE	Ultra high molecular weight polyethylene
WLI	White light interferometry
XPS	X-ray photoelectron spectroscopy
ZDDP	Zinc dialkyldithiophosphate

Chapter One

Introduction

Reducing the friction losses in tribological contacts of machine components is important so that, CO_2 emissions in the atmosphere can be reduced. This not only has great environmental impact but also has significant economic importance. Currently, this is being addressed by improving lubrication performance in all tribological contacts, particularly in the engines. Since a large percentage of today's machine components, such as the components in the valve train, are lubricated by an incomplete hydrodynamic film, it is of particular importance to reduce friction and wear under boundary lubrication (BL) conditions.

Typically boundary films are formed from additives (chemical compounds) incorporated in the lubricant to aid in reducing friction and wear. One of the most effective and most widely used of these additives is zinc dialkyldithiophosphate (ZDDP). Although researchers have attempted to explain the tribochemistry of ZDDPs, some unanswered questions remain such as what initiates a chemical reaction at the contacting asperities? It has so far, not been established conclusively whether it is the pressure at the asperities, the applied load, the local temperature rise, the shearing of molecules, triboemission, (or some combination of these) that initiates film formation. The focus of this study is understanding triboemission generation and interaction.

The emission of electrons, photons and other energetic particles that occur during the rubbing process at the contacting high spots between sliding components are collectively referred as "Triboemission" (TE) [1] (see Figure 1.1). This phenomenon has been suggested to be critically important, since charged particles may react to initiate boundary film formation. The electrons emitted from rubbing contacts are typically of low energy and may originate from the micro cracks initiated during sliding.

TE has also been a cause for concern. For instance it has been accused of causing lubricant degradation particularly of PFPE on hard disks [2]. If a gas rather than liquid is present, triboemission is accompanied by gas discharge and triboplasma is observed. The phenomena of discharge have been linked with simultaneous generation of intense UV radiation, shock waves and active radicals which make discharges particularly suitable for decontamination,

sterilization as well as polymerization purposes. However, the mechanisms and theories suggested in this regard either do not exist or are still not clear enough. Study and identification of similarities and dissimilarities in the generation mechanisms and the physical characteristics of such discharges and a triboelectric discharge (triboplasma) could identify the latter's use in a particular application.

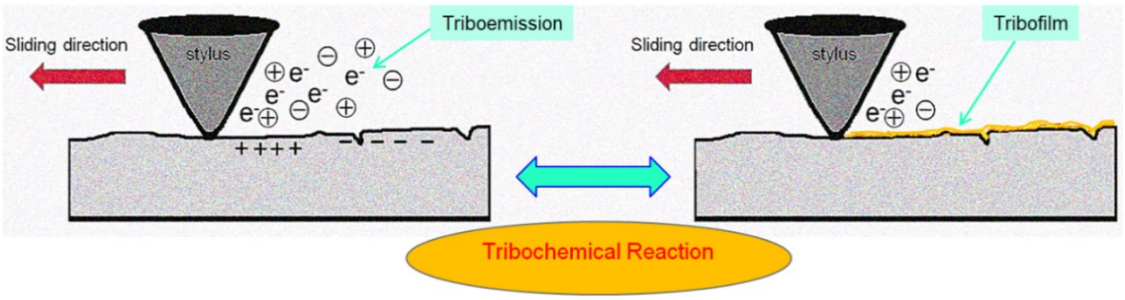

Figure 1.1: Schematic diagram showing the possible link between triboemission and boundary film formation.

From the literature review, it became apparent that triboemission is related to Mechanochemistry/Tribochemistry. Tribochemistry is essentially a branch of mechanochemistry that deals with all chemical reactions that occur as a response to mechanical stimulation at sliding contacts. Both tribochemistry as well as mechanochemistry play a role in transfer film formation involving polymer and its composites. Proteins have also been reported to form solid like films at the counter surface of artificial joint implants [3]–[5]. Therefore, it is not just the formation of additives film that might be driven by triboemission, but additionally the transfer film formation and protein interaction may be interconnected to triboemission and influence one another. When polymers are rubbed, contact charging occurs and this phenomenon is termed as Triboelectrification. Since triboemission and triboelectricity have common origins, *i.e.* mechanical sliding of surfaces, it is plausible that there exists a link between the two. Little has been reported about the relationship between triboemission, triboelectrification, and the resulting interactions at the surfaces such as additive film formation, transfer film generation and protein interaction.

The motivation behind this study is to prolong the useful life of a tribological components which range from hard interface between cylinder liner and a piston to soft interface between implants and biological tissues. The key to address this lies in further understanding the mechanism of the protective films formed at the sliding interface and its driving factors. This

could then provide answers to effective design of lubricant additives as well as high performance polymer composites.

1.1 Research Questions

- The central theme of this thesis lies in understanding of contributing factors of TE from a set of materials and appraising the interactions of TE in different environments and interfaces ranging from vacuum to air to liquid submerged condition. In particular, it is important to know how and why TE is generated from polymers under these varied conditions.

- An additional challenge is to determine possible links between triboemission (TE), triboplasma and triboelectrification and their roles in mechanochemistry. This is essential because all three phenomena have common origin, *i.e.* a shearing action at the contacting interface.

- The potency of TE, especially electron emissions' role in the formation of tribofilms is also not so clear. Therefore a part of the thesis will study growth of ZDDP tribofilms while isolating different factors, which have been suggested in driving film formation.

- This thesis will also explore aspects of lubricant degradation and the interaction of protein molecules with charged surfaces, using various techniques and determine the role of TE played.

1.2 Objectives and Plan of the Research

The overarching aim of this project is to explore the potential role of triboemission in influencing anti-wear film formation, transfer film formation, protein interaction and lubricant degradation. This has been achieved by following means:

- An extensive literature review is performed, focussing on published articles on topics including tribofilm formation and transfer film formation. Particular, emphasis is on: *i*) the additive ZDDP, its film formation mechanism and nature, *ii*) PTFE and its film forming mechanisms, *iii*) other related terms such as triboemission, triboelectrification and triboplasma, *iv*)factors affecting TE and its role in lubricant degradation and protein interaction.

- Another major objective of thesis is to develop new techniques and equipment for studying these sub-atomic to molecular level interactions that result in macroscopic changes under various surroundings.

- To answer the research questions outlined in section 1.2, a number of systematic studies are conducted. These include: *i*) examining the hypothesis that oxide layer thickness contributes to film formation, *ii*) testing whether TE can cause phosphate films without the action of shear using UV irradiation, *iii*) using dyes to study lubricant degradation and protein-surface interactions.

1.3 Presentation of the Research work in this dissertation

The structure of this thesis is outlined below:

Chapter 2 provides a literature review, which highlights the most important research work undertaken in the area of triboemission and related phenomena to date. This is a crucial step to ensure existing knowledge is built upon and the significant gaps in past research are adequately bridged. A number of studies on ZDDP tribofilm formation, PTFE transfer formation, lubricant degradation, protein-surface interactions where triboemission may play an important role, are reviewed.

Chapter 3- titled Materials and Methods - provides details of the experimental work done in this project. It introduces the various tribometers used in vacuum, air and liquid environments. A significant objective of this thesis was to develop a tribometer which would allow in-situ observation of the contact through a transparent sapphire (Al_2O_3) pin. This chapter presents a detailed account of key improvements made to an existing tribometer and explains the new components added to the system, alongside calibration procedures to achieve the stated goal. Information is also provided about test set-up, test procedures, environment and test materials.

Chapter 4 - titled Triboemission Interactions in Vacuum - is the first chapter of results section. It presents the experiments performed using the MCP tribometer under vacuum conditions, in which a diamond stylus scratches a PTFE disc material. Insights into what kind of material exhibit triboemission and the nature of such emissions is gained from this chapter.

Chapter 5 is titled Triboemission Interactions in Ambient air. The main aim of this chapter is to present experimental results from different materials (metals, inorganic oxides, polymers and polymer composites) in presence of air using the Air plasma Tribometer. The spatial distribution of air plasma in and around the contact as well as transient behaviour of plasma

observed through a pin specimen is shown for the very first time. A simple model based on Paschen's curve is developed to understand the spatial distribution of plasma. By interpreting the results of a series of tests, the factors which affect emission are identified and discussed. It also sheds light on the possible mechanisms responsible for the observed significant differences in emission among different type of materials.

Chapter 6 - titled Triboemission Interactions in Liquid Environment - is dedicated to exploring the emission activity in a fully submerged environment of water, salinized water, dye mixed water, and dye mixed oil. These tests are first of their kind which show the influence of liquid properties on triboemission as well as interaction with the dye molecules. In addition to this, it presents the results of protein interaction with polymer surface.

Chapter 7 - titled Investigation of Factors Effecting Film Formation - presents and interprets the results of studies that involved controlled tests for evaluating the effect of various drivers of film formation such as fresh surface, shearing, mixing and oxide thickness (linked with intensity of TE). It also demonstrates the growth of tribofilms without the action of shearing by using ultraviolet light to initiate artificial electron emission.

Chapter 8 summarises the conclusions and achievements of this research and evokes a range of thoughts to be investigated under future work.

Chapter Two

Literature Review

This project is aimed at understanding the interactions between charged particles emitted from rubbing surface and their environment. There are practically important situations where these interactions have been suggested to play a key role, namely the formation of protective boundary lubricating films, in the degradation of lubricants, the charging and reactive behaviour of polymer surfaces, and the interaction between proteins and biological rubbing interfaces. This literature review will therefore cover each of these four application areas and will also summarise the current state of understanding relating to the mechanisms of charging and emission behaviour.

The chapter will start by providing a review of main mechanism and various factors that influence the formation of protective boundary films on the surface of rubbing components, which help to reduce wear. First, it summarises the mechanisms of formation of such antiwear films, focussing especially on the most successful engine lubricant additive, zinc dialkyl dithio phosphates (ZDDP), the study of which has shaped the current understanding of antiwear films (section 2.1). Next, the mechanisms of polymer transfer film formation processes especially those of polytetrafluoroethylene (PTFE) are briefly summarised. In section 2.3, studies related to triboemission-initiated lubricant degradation are presented. Section 2.4 evaluates relevant literature on triboelectrification and triboplasma, exposing the gaps in the current understanding, thus highlighting the need and importance of the research undertaken in this thesis. A brief account of protein interaction is then presented in section 2.5. In section 2.6, the factors affecting triboemission from rubbing contacts is briefly discussed. Additionally, this section also reviews previous research on measurement techniques used for studying triboemission.

2.1 ZDDP film formation process

ZDDP forms a protective tribofilm of phosphate glass by mechanical activation at room temperature, which only occurs on the rubbing track as shown in Figure 2.1. The structure is similar to a thermal film (*i.e.* a film that forms at high temperature but without rubbing) but is stronger [6]. The layered structure of phosphates and metal oxides overlaid with layers of increasing hydrocarbon content has been confirmed by Bell *et al.* using ToF SIMS studies under cryogenic conditions [7]. They suggested that the resulting electrostatic attraction from sliding may contribute significantly to the adhesion. Several different mechanisms (*e.g.* [8]–[14]) and processes have been proposed that influence the formation of ZDDP tribofilms. However, four main mechanisms of ZDDP film formation on metal surfaces have been summarized by Spikes [6]. These are as follows:

- Ligand exchange mechanism which takes place between Zn and other labile metal cations or dithiophosphate ligands. This is based on hard and soft acid-base (HSAB) reactions [15], which require the exchange of Zn^{2+} and Fe^{3+} cations between the ZDDP and iron oxide wear particles which are subsequently digested within the tribofilm [16].
- Physical adsorption of ZDDP molecules on iron surfaces [14], [17] via the sulphur atom of the P=S bond that becomes irreversible when the temperature is above 60°C.
- Thermal degradation process [18]–[21], is activated at high temperature and leads to deposit of solid zinc phosphate, alkyl sulphides, mercaptans, hydrogen sulphide and olefins when lower levels of hydroperoxides or peroxy-radicals exist. The alkyl groups, which are initially bonded to oxygen atoms in ZDDP are transferred to the sulphur atoms.
- Decomposition of hydroperoxides [22] and peroxy-radicals [23]–[25] as an anti-oxidant, which leads to depletion of the quantity of ZDDP in oil so that less is available to form zinc phosphate antiwear film on the metal surfaces [26], [27].

Among other mechanisms are radical reaction [28], hydrolytic mechanism [29] as suggested by Spedding and Watkins, a chemical reaction of ZDDP with FeO and oxygen in the air [30], [31], or a combination of the above.

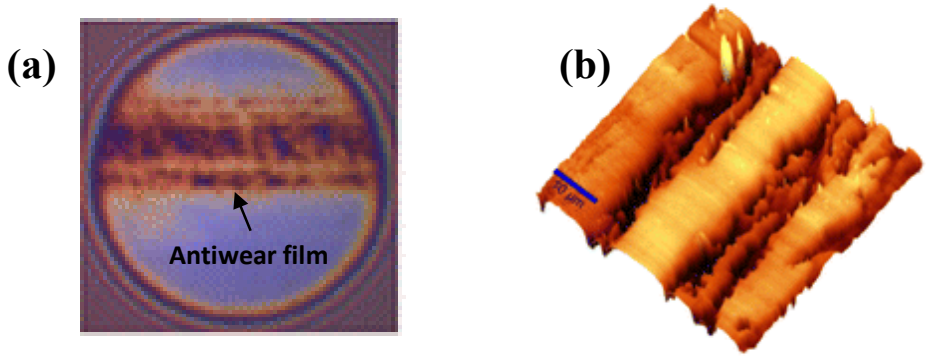

Figure 2.1: ZDDP films as imaged by (a) Spacer layer Interferometry (SLIM) method (b) Atomic force microscopy [32].

Numerous studies discussed above, strengthen the argument that these highly adherent load carrying tribofilms could never be formed by physisorption or chemisorption processes alone. From the review process five possible driving factors influencing the growth of such boundary films were identified and are discussed below. The drivers of tribofilm formation are as follows:

- Temperature
- Pressure
- Shearing
- Nascent surface/ Surface catalysis
- Triboemission

Temperature

Increased temperature at the contact can result from high operating temperature and pressure of the environment. It can also arise from frictional heating due to rubbing. It has been suggested that sliding could generate high flash temperatures at contacting asperities that can cause ZDDP tribofilm formation [8]. Questions that arise here are, what flash temperatures would be necessary and what is the driving mechanism?

Temperatures above 150 ºC can initiate a thermal degradation process of the ZDDP molecule involving exchange between oxygen and sulphur atoms leading to the formation of a ZDDP thermal film. Moreover, when ZDDP samples were heated to 200 °C, extensive thermal decomposition was observed which eventually lead to thinner films and inferior antiwear properties [14]. Furthermore, studies with ZDDPs at higher temperatures confirm that it forms thermal films which are similar to tribofilms but lack iron which is present in the tribofilm on

steel surfaces [33]. Studies have shown that mild sliding conditions at room temperatures (25 ^{o}C) are conducive for ZDDP tribofilms [34], [35].

In tribology literature, the flash temperature is the rapid temperature rise that takes place at the interface between two sliding surfaces [36]. Frictional heat is generated as result of asperity/asperity interlocking and welding which then act as miniature heat sources. Heat exchange from the sources (contacting asperities) occurs almost instantaneously due to the constriction of thermal flux at the contacting asperities which effectively provide the path of high conduction (least resistance). The thermal properties of the sliding pair and the contact dimensions play a major role in heat dissipation. The steady state heat generation per unit time of the source is equivalent to the work of the frictional force, which is given by

$$Q = \mu FV \qquad \text{Equation 2.1}$$

where μ is the coefficient of friction, F is the contacting force (external load), and V is the speed of sliding. From this equation, it can be concluded that flash temperatures rise can only reach high values at high sliding speeds. However, it has been confirmed that ZDDP films also forms at sliding speeds below 0.1 m/s [35] where flash temperature rise should be negligible. Hence, temperature alone does not seem to be a key driving factor for ZDDP film formation. These thermal spikes are too rapid to be measured by any measurement technique or equipment developed. However, flash temperature can be predicted based on mathematical calculations which assume a Boltzmann energy distribution and it has been suggested that a very intense energy dissipation at asperity conjunctions may lead to non-Boltzmann energy distributions. However, single-asperity sliding experiments by Gosvami *et al.* [37] have showed that growth rate of tribofilm increased exponentially with temperature whereas Martin *et al*. [16] refute the role of temperature as a driver.

Pressure

Contact pressure is a common terminology in tribology literature. It takes into account the normal load, the contact area and the contact geometry. It has been proposed that very high pressures present in rubbing contact may promote chemical reactions of ZDDP [38]. In addition to this, it has been observed that an applied tensile stress enhances the film forming effectiveness of certain antiwear additives [39]. Mosey *et al*. used first-principles molecular dynamics simulations [40] and worked out that very high pressures can lead to modification of the coordination number of zinc (Zn) atoms that induce cross-linking in a phosphate. Such

highly connected networks also improve mechanical properties. However, the pressures mentioned were far in excess of the yield strength of most materials and highly unlikely to occur in rubbing contacts. High-pressure infrared studies conducted by Tse *et al.* have shown no evidence of structural changes in ZDDP up to 21.2 GPa [38]. Their study confirms that at very high temperature and pressure (225 °C and 18.4 GPa), ZDDP undergoes substantial decomposition. The experimental results show that pressure cannot be the main driving factor as ZDDP films have been seen to form at milder contact pressures of 1 GPa.

Shearing

It has been suggested that the shear stress in sliding contacts may be sufficient to directly break the bonds between lubricant molecules and hence initiate chemical reactions that lead to film formation. This has been supported by recent studies by Gosvami *et al.* [37], who demonstrated the critical role of stress and thermal activation in tribofilm formation by conducting experiments in single-asperity sliding nano-contacts. The film growth rate increased exponentially with applied compressive stress. The films formed due to rubbing of a single asperity have the same nature (layered and patchy) as the films previously reported. Their study provides an explanation of the observed layered structure with variation in the mechanical property and thickness saturation property of tribofilms. At a constant load, the contact stress decreases as the tribofilm thickens because the tribofilm has a lower modulus than the substrate. As the contact stress decreases, stress-induced cross-linking and other reactions that produce the tribofilm also reduces, thus increasingly weaker and more compliant layers are formed on the top. This growth mechanism continues until the diminished contact pressure and weak layers on top are unable to sustain any further growth, which ultimately terminates any further growth thus making the tribofilm thickness self-saturating. Recently, tests conducted by Zhang and Spikes [32] also confirmed the hypothesis that ZDDP tribofilm formation in rubbing contact is driven by applied shear, thus validating a thermally activated, stress-assisted reaction rate model. However, the explanation provided in [32] for the pad-like rough structure of ZDDP film is not completely convincing. They suggested that these structures form on the tip of the asperities where the pressure is the highest. The reported dimension of a typical pad structure ranges from 1- 10 microns [6] while that of a single asperity is a few nanometers (similar to an AFM tip). It can be argued that the dimensions and distribution of the pads should then depend upon the surface roughness or statistical distribution of asperity heights, which is clearly not

the case as concluded by Goswami *et al.* [37]. Furthermore, no insights into whether short-chain or long-chain polyphosphate forms first were provided.

Although the layered structure could now be explained with the observed contact-pressure dependence of tribofilm formation the origin of patchy and pad like morphology is still not completely clear.

Nascent Surface & Surface catalysis

Plastic deformation and crack propagation lead to the creation of free surfaces which are reactive and may help in surface catalysis. From the experimental studies concerning sliding tests of tribo-pair containing iron in ZDDPs solution [15], it has been suggested that the sulphur in the ZDDPs reacts with freshly generated hard iron oxide wear particles to form iron sulphides. This is based on the hard and soft acids and bases (HSAB) principle. The hypothesis of surface catalysis causing a film growth cannot be accepted as both thermal films and tribofilms of ZDDPs have been reported to form on a wide range of materials other than iron, such as metals [41]–[43], ceramics [44]–[46], silicon [37] and DLC coatings [47].

Martin *et al.* who presented the model based on HSAB phenomena, later went on to investigate further into the origins of antiwear film formation using molecular dynamics and concluded that driving force is the entropy due to mechanical mixing at the atomic scale [16]. It can be commented that mechanical mixing comprises of plastic deformation, shearing action of top layers of the mating surfaces, wear debris formation which could result in triboemission as well.

Triboemission

Triboemission is a term used for the emission of electrons, ions, radical and photons as a response to friction and wear processes. It is speculated that triboemission can play a significant role in tribochemical reactions although little is known about the triboemission process itself [1], [48]–[50]. Furthermore, it has been suggested that triboemission may accelerate chemical reactions such as oxidation or polymerization of the lubricant under boundary lubrication conditions [51]. No direct evidence of triboemission contributing to tribofilm growth has been documented yet. However, researchers have proposed a few different mechanisms as described below.

Rubbing processes can bring mechanical transformation due to elastic or plastic strain energies worked into the material. The deformation and relaxation of materials could therefore activate exoelectron emission [52]–[55] or other particle emission through molecular strain release.

In certain materials such as dielectrics, plastic deformation and subsequent crack generation during sliding can cause charge separation along the opposite faces of the crack [51], [56], [57]. For example, when a crack develops in aluminium oxide, one side of the crack will contain oxide anions while the opposite side will contain aluminium cations. The narrow gap between the crack face causes a build-up of a large electric field gradient sufficient for electrons to escape from the anions. It is believed that not all the electrons which escape from the anions are collected by the cations on the opposite surface of the crack. This results in triboemission or the release of electrons into the wider environment under the action of sliding. Although triboemission has been extensively studied in vacuum conditions (*e.g.* [58]–[62]), it must also occur during sliding in air or under a lubricant but the electrons are not easily detected as their path length in air and liquid is much shorter than that in vacuum.

Gases, water vapour or liquids present in the environment may influence triboemission of electrons by chemisorption on the exposed surfaces of the crack about to release electrons [59, 66]. In gas environments and in air, emission of photons have also been reported and a new term triboplasma was coined. In this model the electrons, ions and photons are a product of gas discharge occurring due to high electric field generated on the crack surface or the differential tribocharging of the counter surfaces. The ionized gas molecules may then recombine generating molecules different from the original gas thereby contaminating the environment or possibly reacting with lubricant on the contact surfaces. Therefore, it is important to know whether the triboemission triggers the tribochemical reactions and whether these reaction products influence friction and wear characteristics.

A completely different mechanism of triboemission was also suggested by Dickinson *et al.* [50]. They attributed tribophotons from single crystal magnesium oxide (MgO) scratched by diamond to excited defects created by abrasion of ceramic-diamond contact. The emission of photons on mechanical or tribological stimulation is termed as Triboluminescence/Mechanoluminescence [64]–[66] and is too vast a topic on its own to be reviewed here in detail.

It should be noted that triboemission results from the shear stress in a sliding contact and can therefore be thought of as an intermediate step in the process by which shearing leads to film formation. In other words; shear stress applied to the surface may lead to triboemission which may in turn initiate film formation reactions. Triboemission may therefore be a part of the shearing activation process described above, rather than a separate process. This view is supported by research showing that shearing of molecules can give rise to triboelectric processes and volatile particles [67], [68].

No systematic studies have been carried out to confirm or refute the role of triboemission in tribochemical processes. If such process occurs at all, its mechanism is also not clear. To resolve this question, in-contact analysis needs to done, to observe the chemical intermediates present within the rubbing contact. This is very difficult due to technological limitations. However, it is possible to carry out near contact analysis. An unambiguous and conclusive proof would be provided by decoupling mechanical drivers such as shear stress and all other possible drivers such as temperature, pressure, shear force from triboemission and monitor ZDDP film formation process. Further studies can involve removing shear action at the contact and monitor the effect of emission only on film growth. The current PhD thesis, will conduct controlled tests to separate all other drivers from triboemission in an attempt to assess the capability of triboemission in promoting film growth.

2.2 Polymer Transfer Film Formation

Chemical reactions can also occur in sliding polymer contacts and this is therefore another area where triboemission may play a role. Solid lubricants are known to form transfer films which are able to reduce net wear and modify friction [69]. Solid lubricants such as PTFE, graphite, MoS_2 and other oxides when added as fillers in adequate quantity into polymer composites are able to detach from the base material and transfer a layer of low shear strength on the counterface [70]. The wear of polymer composites is reduced because of the reduced shear stress needed for sliding. Even when bulk polymers such PTFE, and UHMWPE are used in dry bearing applications, they form a preferential low wear transfer film. A review of transfer film formation was recently done by Ye *et al.* [71]. The process of transfer film formation has been categorized into three main categories as follows

- **Hypothesis of physical deposition**

Polymers simply deposit a bulk of their surface material by ploughing action of hard asperities [72]. The ploughing action by an asperity can lead to an extensive plastic deformation, followed by crack initiation, fracture and subsequent detachment from the surface. The detached lump of material sits between the asperities filling the troughs of the counter surfaces; as a consequence, counter face roughness is reduced leading to a low coefficient of friction and optimal wear due to lower asperity-asperity interlocking . The transfer films of this nature fail because they lack sufficient material to set up a new equilibrium and are easily removed [70].

- **Hypothesis of improved Adhesion/cohesion**

Makinson and Tabor [73] and Tanaka *et al.* [74] showed that transfer can occur not only in the form of lumps but also in the form of ribbons or sheets depending upon the sliding conditions. The thickness is generally a few tenths of a micrometre. Thin transfer films of PTFE of 300 Å thick [74] have been shown to originate from the destruction of its banded structure. It results from the slippages between crystalline slices and amorphous region and a relatively massive fragment is produced by the fracture at the boundaries between the bands. The transferred film adheres weakly and is continually removed and replenished as the wear proceeds discretely by the removal of a unit thickness of about 300 Å. Although this model appears acceptable, it fails to explain how fillers of the same size, same quantity but different chemical composition have different effects in reducing the wear of PTFE [18,19,20]. It is well known that bulk PTFE polymer is chemically inert, while fluorine is very reactive non-metal. The strength of adhesion is due to reactive fluorine which gives rise to bonding between the surface atoms of the PTFE polymer with surface atoms of the metal. It must be emphasized that any physical adhesion or mechanical bonding is primarily due to the Van der Waals forces of attraction. Studies by Gong *et al.*[75]–[77] showed that the transfer film of PTFE had a multilayer structure and the adhesion between the first layer of transfer film and its substrate (steel or aluminium) determined its stability.

In another study [78], it was shown that the fillers dispersed in PTFE matrix improved the cohesion between the layers of the transferred film. Few other studies [80, 81] have suggested that adhesion between the transfer film and its substrate is increased by inorganic compound fillers. Adhesion and cohesion depends upon the counterface roughness and texture which is altered by relative hardness [70] and shape [81] of the filler particles during sliding. However, physical Van der Waals forces of attraction alone cannot explain

the variation in wear behaviour and transfer films observed in different environments. Besides, it is known that when polymers are rubbed, they acquire net electrostatic charges which is known as tribocharging/triboelectrification/contact electrification. There is general consensus that resulting electrostatic attraction may contribute significantly to the adhesion [82]. However, very few of the studies with PTFE transfer films attributed any importance to this phenomenon.

- **The hypothesis of chemical reaction**

Chemical reaction at polymer/metal sliding contact can also lead to the formation of transfer film. This is another area where triboemission may play a role. The idea of chemical reactions occurring at sliding polymer contacts was presented in 1970s by Sviridyonok *et al.* [83]. It was hypothesised that in polar polymers such as polyamide and polymethylmethacrylate (PMMA), free radicals are generated as a result of sliding and their interaction controlled the transfer film formation process. These aspects have been previously studied under the branch of Mechanochemistry and is very relevant to the current study since free radicals which are produced during sliding and are also termed as triboemission.

Recently, the evidence of chemical reactions occurring in polymer contacts are being reported. For instance, studies using variable moisture environments have revealed that wear reduction mechanism in case of PTFE-Alumina nano-composites has of tribochemical origins [84]–[86]. The bonding between the transfer film and the counterface was attributed to chemical changes initiated due to sliding. Studies by Gong *et al.* [82, 83, 85, 94] also confirmed chemical bonding between the first layer and its substrate. Bahadur and Tabor [79] provided evidence of chemical reaction between the transfer film of CuS-HDPE composite and steel using. Bahadur and Gong [89, 90] found that reduction of copper filler in a sliding contact forms a transition layer which led to increased adhesion between the transfer film and its substrate. Buckley and Johnson [90], [91] concluded that high stress and high temperature sliding condition cause thermal degradation, formation of fluoride ions, and adhesion of filled PTFE to metal. Other studies indicate that sliding between metals or inorganic metallic compounds and polymers trigger tribochemical/mechanochemical reactions [87, 99]. Such induced reactions are beneficial if they produce an adherent transfer film but are a nuisance, if they cause degradation of the polymer or the counterface or the lubricant present in the system.

Evidence of tribochemical degradation of PTFE catalysed by rubbing against a metal surface has been shown by Onodera *et al.* [93]–[95]. Simulation results [93], [94] reveal a tribochemical reaction, which included de-fluorination of PTFE and the formation of aluminium fluoride. It was concluded that the aluminium surface acted as a catalytic Lewis acid in which the fluorine atom was removed from the PTFE polymer chain, thus the tribological performance of the system was reduced. Formation of aluminium fluoride inhibited the self-lubrication provided by PTFE because of an interfacial electrostatic repulsion. Most of these studies have been carried in dry conditions, however, it has been suggested that environment containing water vapour could improve the tribological performance [102, 103] of fluoride chains.

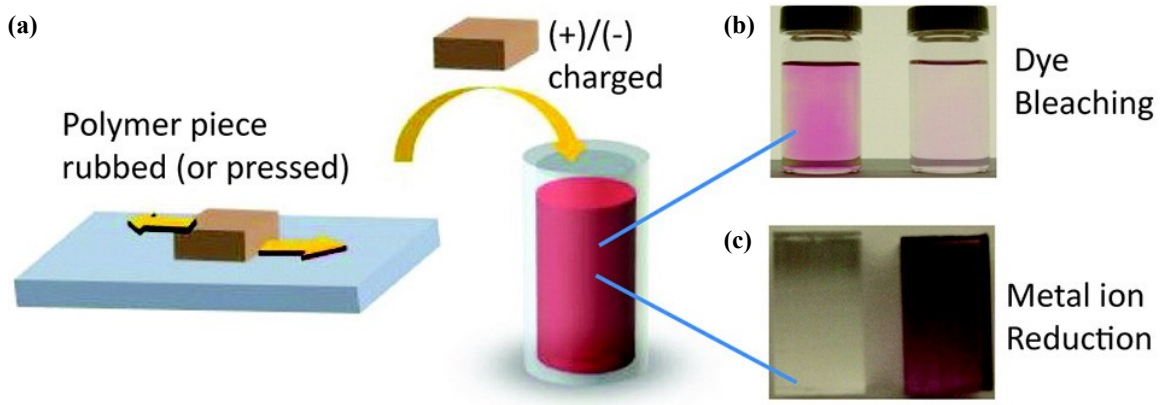

Figure 2.2: (a) Schematic of the experimental arrangement for charging of polymer pieces by rubbing or pressing and subsequently immersed into aqueous reagent solution. Both the negatively charged (−) and the positively charged (+) pieces can drive chemical reactions in solution. (b) Bleaching of Neutral Red dye (2.5 μM in water) by PVC pieces (four pieces, 16 cm^2 total surface area) positively charged by pressing against PTFE and placed into the solution.(c) How positively charged PDMS by rubbing against Teflon transforms $HAuCl_4$(aq) (1 mg/mL) into Au nanoparticles [97].

Recent research has shown that rubbing polymer specimens together can indeed cause certain chemical reactions to occur in liquids. This was first discovered by Liu and Bard [98], who showed that the submersion of freshly rubbed polymers into solutions caused metal salts to be reduced (*i.e.* gain electrons). This behaviour was first attributed to the production of "cryptoelectrons" which refers to the electrons that is transferred from the polymer to the species present in the liquid. However, Baytekin and co-workers later proved that mechano-radicals were responsible for the reduction of metal salts [97]. The question then arises, as to whether such radicals would be produced if rubbing took place under submerged conditions (*i.e.* could these chemical reactions occur in situ). If this were shown, this would provide the first evidence that triboemission can affect lubricant

behaviour. Figure 2.2 shows the schematic of rubbing process used by Baytekin *et al.* to show how charged surfaces transforms chemical solutions by bleaching of dye in one instance and reduction of metal in another.

In this section, various hypotheses related to transfer film formation are critically evaluated and the gaps in the research are identified. The current knowledge of the formation and evolution of transfer films is still clouded with mysteries and many conflicting views. Why some compounds decompose while others do not and what properties govern their decomposition are still not understood. For this purpose, a separate section of polymer tribocharging and triboelectrification (**Section 2.5**) is presented which will further highlight the gaps, provide more background information and help the reader map the research done in other overlapping research fields such as physics, electrostatics, and luminescence by providing links, and thus adding relevance to the research carried out in this thesis.

2.3 Lubricant degradation

The next area to be investigated where the emission of charged particles has been suggested as playing an important role is that of lubricant degradation. Various techniques have been used by researchers to explore the causes of degradation of PFPE type lubricants; these range from electron bonding apparatus [99] by Vurens to adapted tribometers by Nakayama [100]. Nakayama *et al.* have identified triboplasma (neutral gas discharge from rubbing contacts) as a direct cause of PFPE degradation [101]–[103]. Under the sliding condition used by Nakayama, the frictional temperature rise is negligibly small. The PFPE oil did not produce any decomposition products even under heating on a sapphire (single Al_2O_3 crystal) disc at 200 $^{\circ}$C thus proving that oils are decomposed by triboplasma in various real tribosystems where the sliding partners are insulators. Triboplasma generates mostly UV photons and these have high-energy. UV photons are known to cause photochemical reactions of oils and gas molecules leading to their degradation. In addition to this, Nevashupa *et al.* [104] showed that gas emissions occurred from sliding of various metals, elastomers and coatings due to structural deformation, and this may also lead to subsequent lubricant oxidation. Kajdas *et al.* [105] studied the process of tribopolymerization of perfluoropolyether (PFPE) lubricants under fretting conditions where triboelectrons were thought to play a role. Zhao *et al.* studied degradation of PFPE [2] in hard disk and explained the underlying mechanism. However no work has been carried out to study degradation of other lubricants such as engine oil due to triboemission.

Alternative ways to evaluate the effect of electrons on PFPE in the absence of frictional stimulation has also been attempted. Zhang *et al.* [106] investigated thin films of PFPE by measuring the surface energies and spreading characteristic of PFPE film and found that UV irradiation (184.9 nm and 253 nm) improved the bonding of lubricant end groups with the carbon surface and other lubricant molecule. Vurens [99], [107] examined the bonding of thin perfluoropolyether films using low-energy electrons and ultraviolet (UV) light in an electron bonding apparatus. It was found that photoelectrons can be generated from the substrate when irradiated with UV light. While D'Anna *et al.* [108] showed that low energy electrons below 15 eV did not cause decomposition of PFPE fluid (Fomblin Y-VAC 18/8) used in a vacuum pump fluid. In contrast to this, Pacansky demonstrated that an electron beam of 175 kV which is about 1.7-13 eV is able to decompose PFPE [109] and produces hydrogen fluoride which may cause severe surface damage.

An important possibility arises from this review is that UV photons can be used to stimulate electron emission, which may be employed as a tool to study boundary film formation.

2.4 Protein Interactions

Another area where triboemission may play an important role is the interaction of proteins and biological surfaces by virtue of the polarity of the protein molecules and the tissues. Tribological testing of artificial hip and knee joints have been ongoing for several decades in order to screen materials for biocompatibility and increase the longevity of the transplants. Various kinds of lubricants such as bovine serum and methyl cellulose which simulate human synovial fluid have been tested in vivo to study the friction and wear behaviour of implants [3]. Results show that lubricants have a significant effect on the friction developed between the mating surfaces. The mechanism proposed is as follows.

The proteins that are present within the bovine serum adsorb to the surfaces thus creating 'solid-like' films which rub together, protecting the joint surfaces from solid-solid contact [3]. This is undoubtedly beneficial for wear reduction but their influence of friction behaviour is not well understood. It has been observed that friction might increase or decrease between the contacting surfaces depending on the protein interaction. Further systematic studies need to be done to clarify what drives the protein adsorption on sliding surface. Other benefits might include new methods for development of protein initiated polymerization that are based on protein-reactive polymers conjugates [110], [111]. Much research work [112] in the biomedical field has

focussed on polymer surface modification for formation of biofunctionalized polymer surfaces, motivated to develop organ, joint, and soft tissue replacements. Since biological proteins are electrostatically charged molecules and are present in sliding contacts between nonconductive materials, it is likely that triboelectrification and particle emission plays a role in their film formation. In fact, triboemission is more likely to play a role in protein film formation than in that of anti-wear films, which were the primary focus of this thesis, since the latter involves conductive surfaces and less highly charged molecules.

Therefore, a part of this thesis will study the aspect of protein interaction with rubbing surfaces, and its possible link to triboemission and/or tribocharging.

2.5 Tribocharging & Triboplasma

Having introduced the areas where it has been suggested that triboemission may play a role, the following sections will review the details of related triboelectric phenomena.

Tribocharging, or triboelectrification, is defined as the electrical charging of contacting insulators that occurs when they are rubbed together or brought in contact and then separated. Many modern technologies exploit this phenomenon [113], including xerography [114], laser printing [115], electrostatic separations [116], and energy harvesting [117], [118]. On the other hand, uncontrolled triboelectrification can be problematic in damaging electronics [119], initiating explosions in grain and coal plants [120], [121], promoting dust storms by facilitating particle transport [122] and causing lightning [121].

The underlying physics of tribocharging is only now becoming understood fully, despite documents of its occurrence dating back thousands of years. Early research led to the development of a triboelectric series which ranks materials based on charge accumulation [123]–[125]. However, the exact order of this series is inconsistent [126], and even rubbing together identical materials can produce charge [127], [128]. Furthermore, whereas for metals electron transfer between valence levels is understood to be the dominant mechanism [129], there has been uncertainty regarding charge transfer for insulating materials such as polymers, which by definition have no free charge carriers. One of the most plausible tribocharging mechanisms in case of insulators is said to be driven by contact potential difference between the two contacting solid bodies [130]. Electrons are transferred from a surface with a low work function to the mating surface with a high work function, resulting in the former and the latter potential being positive and negative, respectively. Charge carriers in these contacts were

initially assumed to be electrons [98], [131] and then evidence suggested to be ions [127, 133, 134], with the latter now being the more accepted view. What has made this field challenging is that charging is not only an electrostatics problem but in reality involves tribological processes, which are system dependant.

During the last decade, the picture of how both micro- and nano-scale events are responsible for tribocharging and inconsistencies in triboelectric series has become clearer, thanks in part to the introduction of Kelvin Probe Force microscopy (KPFM) measurements [134]. Baytekin *et al.* showed that a mass transfer mechanism for tribocharging of polymers gives rise to nanoscale regions of positive and negative charge [135]. Following this, Burgo and co-workers showed that polyethylene (PE) and polytetrafluoroethylene (PTFE) were tribocharged due to the mechanochemical process of homolytic chain scission that follows an electron transfer process from hydrocarbon free radicals to the more electronegative fluorocarbon radicals [136]. However, further support of mass transfer as a mechanism came from Williams [137], Burgo and Erdemir [138].

An additional complication, which affects charging behaviour, is the role of ambient environment [138] and humidity [139]. Furthermore, as shown by Sow *et al.*, material strain can reverse the direction of charge transfer [140] and may play a key role in triboelectrification in general. Despite these system specific issues, several studies [138], [141], [142] suggest that tribocharging and friction force have a common origin and that measurements of the former provide fundamental information on the origins of the latter.

Although the details of charging mechanisms are becoming clear, discharging mechanisms, which clearly play a role in triboelectrification, have received considerably less attention and are not well understood [133]. Some evidence suggests that corona discharge does indeed limit the formation of charge during contact electrification [143], [144]. Moreover, when an electric field due to the accumulation of charge on components exceeds a threshold determined by the dielectric field strength [133] of the surrounding gas (30 kV/cm for air [145]), breakdown occurs by a Townsend discharge process that leads to the generation of plasma. During a discharge process, electrons undergo inelastic collisions with neutral species resulting in unstable species and ions, which then decay back to their ground state emitting photons [146]. Under ambient conditions, the surrounding gas is predominantly nitrogen, so these electron transitions produce photons with UV wavelengths (except in certain cases emission of photons

occurs at wavelengths around 695 nm, which has been attributed to secondary emission from defect centres in crystal surfaces which are excited by the friction induced plasma [147]).

The presence of plasma at sliding contact interface was first predicted in 1965 [148], [149], but it was not until 2002 that Nakayama and co-workers proved its existence by obtaining images of UV photon distributions in the vicinity of sliding contacts between a diamond tip and a soda-lime glass surface [149]. This led them to coin the term "triboplasma" [149]. Since then, the same group have shown that plasma is also generated when the sliding contact is submerged in oil, and, in this case plasma is generated within the gaseous cavitated region at the exit of the contact [101]. Figure 2.3 shows triboplasma generation from diamond/sapphire contact. It has been suggested that the generation of plasma is responsible for tribochemical behaviour that cannot be explained by classical means such as flash temperature rise [150]. For instance, plasma may induce reactions that alter contact conditions by forming breakdown products that deposit on component surfaces [151]. Plasma generated in this way can result in ion bombardment unto the lubricant molecules, and has been shown to cause the degradation, particularly in the case of computer hard drive applications [103]. At a larger scale, plasma generation at fault asperities, has been linked to seismo-electromagnetic radiation preceding earthquakes [152]. Plasma generation has also been linked to beneficial phenomena; for instance, when DLC surfaces are rubbed, plasma generation is thought to ionise hydrogen molecules in the surrounding gas which then passivates the dangling bonds of carbon atoms on the DLC surface to provide low friction [151]. Another application is in the generation of plasma for the deliberate modification of surfaces [153], [154] as an alternative to more costly methods such as microwave induction [146], [155].

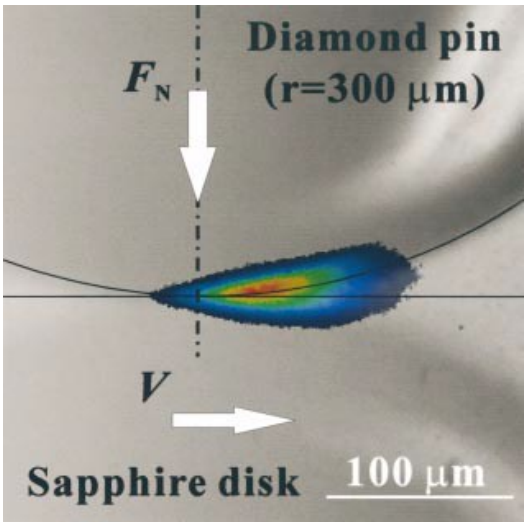

Figure 2.3: Triboplasma from diamond/sapphire contact captured as a two-dimensional photon image when observed from the side of the pin-on-disk sliding contact [63].

Despite the advances described above, there is still much uncertainty regarding triboplasma phenomena, its role in tribochemical process and its links with triboelectrification. Most critically, the vast majority of triboplasma measurements to date have been either time averaged [63, 102, 148, 150, 151, 153] or spatially averaged [133], and as a result, there is little understanding of the transient nature of this phenomenon. Furthermore, the focus of triboplasma studies has been on crystalline materials, with only a few studies ([133], [156]) addressing polymer materials, known to be important in tribocharging applications. Engineering polymers such polytetrafluorethylene (PTFE), ultrahigh molecular weight polyethylene (UHMWPE) because of their exceptional mechanical properties such as stiffness, toughness and low creep are used in the manufacture of structural products like gears, bearings, auto parts and electronic devices. The phenomena of triboelectrification and triboplasma occurring at the surface of the manufactured part may limit or enhance their performance, yet limited number of studies have been done to understand their effect [156], [157]. Selective attachment of proteins on artificial joint implants that employ polymeric materials may be influenced by triboelectrification and triboplasma.

2.6 Factors affecting Triboemission

This section reviews research on triboemission and various factors that affect it, such as intrinsic material properties, surface properties and environment. The triboemission behaviour of a large variety of materials such as metal oxides, inorganic materials, crystalline salts, polymers, adhesives and composites has been characterized by different researchers and most of these studies have correlated spatially averaged intensity measurements with specimen material properties.

2.6.1 Environmental conditions

Triboemission is known to occur under vacuum (*i.e.* its occurrence does not require a liquid or gaseous environment). However, the emitted particles are highly energetic and will immediately interact with their surroundings: (a) if a gas is present, electron emission causes discharge leading to plasma generation which is termed as ‘triboplasma’, (b) if a liquid is present, the emitted particles will react, though this process is poorly understood.

Triboplasma

Nakayama obtained two-dimensional side and plane images of emitted tribophotons originating mainly from the rear of a sliding contact and forming a circular (horseshoe shaped) area around the contact having one or two tails [149], [158]. However, under oil lubrication, plasma is generated along a frictional track only [101]. In addition to this Nakayama showed that triboplasma intensity increases with environmental gas pressure using various tribopairs including silicon nitride, aluminium oxide and a diamond stylus [51]. Under dry conditions, plasma consisted of UV (due to gas discharge), IR (due to blackbody radiation, thermoluminescence) and visible photons (due to surface defects and impurities). Nakayama also concluded that the maximum triboplasma intensity is independent of tribo-pair materials; however results in the current report contradict this. It was also shown that the spread of triboplasma increases with a decrease in air pressure.

2.6.2 Material Properties

In dry sliding tests under vacuum, ceramics have shown intense tribo-emission of electrons because of their ionic crystalline structure while metals reveal a lesser tendency, since the high electron mobility in a metal tends to equalize electron distribution on either side of the crack which are generated as a result of severe deformation of the surface.

Nakayama *et al.* conducted extensive studies on tribo-charge/emission from various materials including metals, semiconductors and insulators in scratch tests involving a hard stylus sliding on a substrate. It was found that the intensity of the tribocharge/emission increases with the resistivity of material in the order insulators>semiconductors>metals [159], and with the severity of surface damage in the sliding contacts (high load and sliding speed yielded higher tribo-charge/emissions) [51, 53, 161–163]. Triboemission and triboplasma have also been reported in various DLCs and correlated with differences in hydrogen content and electric resistivity [163]. Electric resistivity of DLC films in various environments including vacuum, ambient air, and oil lubrication have also been discussed by Nakayama [101, 164, 165].

Momose *et al.* investigated the tribo-electron emission intensity for 18 different metal surfaces when rubbed with PTFE [165]. They reported that for the following metal groups in the periodic table: group 4 (Ti, Zr), group 5 (V, Nb, Ta), group 10 (Ni, Pd, Pt) and group 11 (Cu, Ag, Au), the triboemission intensity increases with an increase of the periods of the metals. However, triboemission characterization based on periodicity does not aid in identifying the relevant

material property since many properties, such as size, valance electrons, electron affinity, and electronegativity also vary with periodicity.

2.6.3 Surface treatments

Momose and Kubo measured triboemission from copper, polytetrafluoroethylene and polyimide using a gas flow Geiger counter. Relative speed, pre-treatment (such as acetone cleaning, mechanical scratching, oxidizing) and tribo-pair material were all shown to influence triboelectron emission. A mechanism was proposed that comprised the formation of empty trapping sites on the polymer surface during the sliding process, which could accept the electrons transferred from the metal substrate for continued tribo electron emission [166]. This is followed by bond-forming process and subsequent breakdown of the sliding atmosphere on mechanical separation of the tribo contact with occupied trapping sites. The surface potential measurements were well correlated with tribo electron emission intensity which indicated that tribo-electron emission is promoted by the increase of the carbon content but suppressed by the increase of the surface oxide.

Oxide films play an important role in triboemission processes. Rosenblum *et al.* studied emissions from aluminium and nickel covered in their oxide layers [167]. They showed that the formation and propagation of cracks in the oxide film during the deformation process leads to triboemission. They also developed testing instruments to measure electronic emission from uniaxial deformation of oxide covered metals in ultra-high vacuum using single-particle counting techniques. The emission of positive ions, negative ions and photons during the propagation of fracture cracks in the different oxide thickness as low as 50 Å (≈5 nm) was measured. Thicker oxide films have peak emission at lower strains than thinner ones meaning that thicker oxides are prone to fracture. The total number of electrons and negative ions emitted is proportional to oxide thickness although electron count is one order higher than negative ion emission [56]. Electron emission and positive ion emission are dependent on the speed of crack propagation [168]–[170]. Tests performed on various inorganic glasses such as clear and cloudy (caused by voids or precipitates) forms of MgO, fused glass and sodium trisilicate glass showed that certain neutral masses were emitted instantaneously during fracture while others experienced a time lag before emission. Gieroszynski *et al.* studied electrons emitted from frictionally activated aluminium, copper, and iron surfaces under various partial pressures of oxygen [52]. It was concluded that exoelectron emission depends on the chemical nature and thickness of the oxide layer on the metal and appears only from irradiated, deformed surfaces.

It was estimated that a minimum oxide thickness of 500 Å (≈50 nm) is required for emission and there is practically no emission possible with pure metals. Larson *et al.* observed higher peaks of neutral emission with thicker oxide thickness about 2.8 times higher for an 8 times thicker film [171]. It was also observed that neutral emissions increases with oxide thickness and saturates at about 3000 Å (≈300 nm). Momose *et al.* showed that an increase of the work function of the oxide covered metal surface is not favourable for the electron emission from the metal surface [166]. Non mechanical excitation such as heat [172] or irradiation by high energy radiation such as gamma or UV rays can activate surfaces to significantly raise the level of triboemission.

It can be generalized that metal oxides and inorganic materials, which generally have higher resistivity values have a greater propensity for emission. This is possibly contrary to the hypothesis that electron emission causes boundary films to form, since many components metal and therefore conductive. However, some studies suggest that oxide film is essential for polyphosphate films formation [173]. In order to bring more clarity in this regard further studies need to be carried.

Loading conditions such strain rate and loading type also affect triboemission. Dickinson *et al.* [171, 175] measured acoustic emission along with positive ion emission and electron emission in titanium oxide and observed that the rate of each of these emissions exhibited a maximum intensity at a strain of 2.5- 3 %, (strain rate = 0.019 % s^{-1}) possibly due to oxide fracture. It has been shown that triboemission intensity decreases with increasing hardness [159], thereby linking triboemission to wear through the creation of fresh surfaces.

2.7 Summary of literature review

This chapter aimed at bringing together all aspects in the field of tribology where triboemission, tribocharging and triboplasma plays a role. The areas discussed are (a) formation of antiwear films in boundary lubricated conditions, (b) formation of transfer film in dry lubricated conditions (c) lubricant degradation (d) protein-surface interactions. Effects of emission of charged and neutral particles on these aspects were also reviewed briefly.

An overview of the current state of knowledge regarding mechanisms of ZDDP film formation and its drivers are presented. Although there is agreement concerning the overall process of the formation of ZDDP tribofilms, the conditions that lead to the initiation of such film is still not

completely clear. The widely accepted theory is that ZDDP adsorbs chemically or physically to the metal/oxide surface, as well as ZDDP decomposition products, followed by an oxidation and degradation of ZDDP. However, there is still debate and uncertainty as to the chemical reactions pathways that lead to the eventual formation of polyphosphate film under different conditions, *e.g.* whether the polyphosphate chains short or long form through same or different mechanism, whether through polymerisation or crosslinking or condensation, possible dependence on the number of cations in solution, or the significance of hydrolysis. The shear stress model does not explain the absence of thiophosphate chains and the presence of ZnS. The possible role of triboemission is also not clear since triboemission is known to result from plastic deformation of contacting asperities, and plastic deformation itself has been modelled using a stress-promoted thermal activation model. A conclusive proof that ZDDP film formation is promoted directly by triboemission requires this film formation to take place in the absence of all other possible drivers such as shear stress and plastic deformation. No studies have been done to assess contribution of one factor independent of the other driver at the contact. Moreover, the origins of the pad-like structure and patchy growth of ZDDP films is not clear.

The literature review also showed that triboemission is observed from a variety of materials and environment such as metals oxides, ceramics, DLC coatings, polymers. The mechanisms of emission range from excitation of impurities and defects to mechanical breaking of oxide layers to gas breakdown. The emission of charged particles and energetic photons during relative motion of contacting surfaces has been linked with tribochemical reactions such as polymerization, depolymerization as well as tribocatalytic processes. These processes have been shown to cause degradation of lubricant and could possibly drive transfer film formation in dry lubrication. These processes have been studied under the broader terms such mechanochemistry and tribochemistry which deal with the effect of mechanical action such shear force and plastic deformation on chemical phenomena on a molecular scale. Thus, triboemission and tribocharging can control friction and wear behaviour of the system by formation of transfer film or by selective attachment of polar molecules (additives/ protein molecules) to the tribocharged surfaces.

Although emission of electrons and ions have been studied for a plethora of materials including polymers, photon emission from sliding polymer surfaces has not been characterized. Since photons carry sufficient energy for polymerization or bond breaking (depolymerization), it is possible that triboplasma generated from rubbing contact might modify the surface of wear

track. Rubbing polymer contacts have been shown to initiate chemical reactions in liquids; however, this has been achieved ex situ and using only aqueous solutions rather than common lubricants. No conclusive studies have been done to observe the generation of plasma is liquid submerged conditions.

The uncertainty of role of triboemission process is a result of complex coupling of mechanical forces and chemical phenomena which is difficult to monitor at the microscale contact interface. A major technological limitation has been the lack of experimental techniques able to measure such phenomena. This explains why very few researchers who have attempted to study, have focussed on the effects of triboemission. New approaches are therefore required to tackle this problem and ascertain whether triboemission particles can to cause tribochemical reactions in real tribosystems.

The current research presented in this thesis addresses these shortcomings to a large extent, by designing and building test setups to capture, in situ changes using visual techniques in a spatial resolved fashion in various environment. The aim of the study is to understand the triboemission interaction in various environment such as vacuum, air and liquid submerged environment. The major focus of this research is to understand the interaction of various macromolecules such as polymer chains, proteins such Albumin and additives such as ZDDP to tribocharging and triboemission.

Other important aspects, requiring attention that were highlighted by this review, are (a) the characterization of the spatial and temporal distribution of triboplasma, (b) the elucidation its transient behaviour and (c) the study of the discharging phenomenon in relationship to charging. This is achieved by using high-speed camera measurements of plasma distributions around sliding polymer contacts and by comparing results with a simplified model. The investigation is conducted at three decreasing time scales; first steady state discharge is studied, then variations over a period of seconds, and finally emission events over the millisecond range.

A final important goal of this research, brought to the light by this review is to understand the role of triboemission in ZDDP tribofilm formation process by decoupling it from other drivers such as shear force and plastic deformation. In this thesis, various hypothesis concerning the formation of ZDDP tribofilm such as effect of fresh surface, shear stress and oxide film thickness are explored. This project employs polymers and metal oxides used in tribological applications as test specimens to maximise emission, since the review has shown that emission from conductive materials is limited.

Chapter Three

Material and Methods

This chapter describes the experimental techniques and setup used to test the hypotheses concerning triboemission described in Chapter 2. The main hypothesis is whether triboemission can initiate chemical reactions and more generally how it interacts with different environments, materials and contact conditions. The experimental methods, which primarily involve viewing of the contact under various environments, use a range of different tribometers and test setups. Therefore, in each section of this chapter, the ideology behind the choice of tribometer and measuring technique is presented. The methods section is arranged according to the sequence of chapters presenting the results. Firstly, for studying triboemission interactions in a vacuum environment, the components and functions of the vacuum tribometer used are presented. Next, for studying triboemission interactions in air, the improvements made to an existing tribometer are described, which enable viewing of a contact through a transparent sapphire pin specimen. The design and development of parts and components for complete transformation of an existing tribometer make up a significant part of this project. This tribometer is referred to as the Air plasma tribometer and is employed to study triboemission interactions in atmospheric conditions in conjunction with electrometer and spectrometer. Then, the development of a fluorescence microscopy tribometer to study triboemission interactions in a submerged environment is described. Other commercially used tribometers such as a UMT by CETR (USA) and Mini traction machine by PCS Instruments are also described. Finally, novel methods for investigation of factors effecting ZDDP tribofilm formation are discussed briefly followed by the relevant post-test surfaces analysis techniques. The test specimens and operating parameters used for each test conditions are also mentioned.

The tribometer and the measuring methods used to study TE interaction in various environment is summarized as follows:

a. **TE Interactions in Vacuum**

Tribometer: Modified PCS EHD rig → Vacuum tribometer

TE-stimulation: Stationary diamond stylus vs rotating disc sample.

Measurement method: Microchannel plates incorporating phosphor screen and camera.

b. **TE Interactions in Ambient air**

Tribometer: Modified PCS EHD rig → Air plasma tribometer

TE-stimulation: Sapphire hemisphere vs rotating disc sample

Measurement method: Camera and spectrometer

c. **TE Interactions under liquid submerged conditions**

- **Interaction of dyed solution with polymer surface**

  Tribometer: PCS EHD rig → Fluorescence tribometer

  TE-stimulation: Stationary ball vs a transparent rotating disc

  Measurement method: Fluorescence microscope and camera

- **Interaction of protein with polymer surface**

  Tribometer: Universal tribometer CETR

  TE-stimulation: Stationary sapphire hemisphere vs rotating polymer disc

  Measurement method: Fluorescence microscope and camera

d. **Investigation of Factors Effecting Film Formation**

- **Interaction of lubricant additive in sliding/rolling conditions**

  Tribometer: PCS Mini traction machine

  TE-stimulation: Stationary ball vs a transparent rotating disc

  Measurement method: SLIM and camera

- **Interaction of lubricant additive without sliding/rolling**

  Tribometer: Not applicable

  TE-stimulation: UV light

  Measurement method: ToF-SIMS

e. **Surface Analysis techniques**

- White light Interferometry (WLI)
- Atomic force microscopy (AFM)
- Kelvin Probe Technology (KPT)
- Scanning Electron microscopy (SEM)
- Time of Flight Secondary Ion Mass Spectrometry (ToF-SIMS)
- X-ray photoelectron spectroscopy (XPS)

3.1 Rationale for selection of test equipment and test methods

Measurements made under vacuum conditions

From the literature review, it was observed that the majority of tests were done under vacuum conditions involving channel electron multipliers (CEM). Measurements done using CEM, despite giving information regarding variation of emission with time and after-emission (a term used for emission even after sliding is stopped) are not designed to provide spatial information and are hence not able to help locate the sites of emission. To overcome this limitation, a newly developed vacuum tribometer that employs microchannel plates (MCP), (effectively an array of electron multipliers) coupled with phosphor screen is used. The MCP is located above the pin on disc contact and collects electrons, ions emitted from the entire surface of the disc placed inside the vacuum chamber. The phosphorescence of the phosphor screen captured by a camera, acts as a magnified image of triboemission from the contact as well as the entire surface. Thus, the positions where a triboemission event occurred can be located and the duration and lifetime of the emission can be calculated.

Measurements made under ambient conditions

Previous studies conducted in air environments involved viewing a pin-on-disc contact through a transparent disc. Consequently, the disc materials were limited to single crystal inorganic oxides. Any visual observation using a camera in conjunction with such a setup, only offers information from the surface of the disc around the contact and gives little information about what is occurring around the hemispherical pin surface which is in contact during the entire duration of the test. Viewing the disc material, can prevent the capturing of some photons and may also result in erroneous conclusions regarding shape and distribution of plasma around the contact as well as making the comparison of emission characteristics between different disc materials invalid. This is because of the fact that light travels in all directions and not all photons will travel towards the disc surface and through it. Therefore, the resulting image is only formed of all photons that reach the camera detector and not all photons that were produced in at the sliding contact. Factors such as low intensity of photons, its attenuation, the gap between the contours of pin and disc and optical properties of the material (such as refractive index and transmissivity) affect the number of photons reaching the camera through the transparent disc. Another consideration is that more action should be occurring at the pin surface, since the pin is the stationary component and is always in contact at the same position while the disc surface is continually passing into and out of contact. To address these shortcomings, it was necessary

to build a new tribometer that could enable the primary goal of viewing the contact through the pin specimen. Additionally, the diamond stylus used in vacuum condition was replaced by a large radius sapphire hemisphere. In section 3.2, the development of this tribometer is described, which shall be referred to as the Air plasma tribometer. In this rig, a high EM gain CCD camera acts as the detector of triboemission.

Measurements under liquid submerged conditions

There are many commercially available tribometers which house a lubricant bath that keeps the contact under fully submerged conditions, however, there are no methods available to study triboemission interaction in fully submerged conditions. The requirement of viewing the contact through a transparent specimen was met by PCS EHD tribometer. The use of this tribometer in conjunction with an upright fluorescence microscope, entitles this tribometer to be named Fluorescence Tribometer. The emitted light from a fluorescent dye mixed with a selected lubricant is captured using a monochrome camera. The test materials used here are same as those used in studies in air however the disc and pin materials are swapped.

Tests were also performed on contacts submerged in a fluorescent protein solutions. Understanding the protein interaction requires studying influence of protein on frictional properties of a chosen tribo-pair. Changes in friction values at low load are in micro quantities which need to be detected and measurement by a highly sensitive load cell with high precision and accuracy. All these conditions are fulfilled by 5g load cell of universal tribometer (UMT) from CETR, USA. Hence this tribometer is used to study protein interaction.

Measurements for investigation of factors effecting ZDDP tribofilm formation

From the review of literature, it was understood that oxide thickness is linked to electron emission such that thicker the oxide layer higher the emission intensity. If such is the relation between oxide thickness and electron emission, and the hypothesis of triboemission contributing to antiwear film growth is true, then oxide thickness could be linked to antiwear film growth. The antiwear film growth is best studied using a mini traction machine (MTM) coupled with spacer layer interferometry (SLIM) technique. Standard tests (rolling, sliding and combination of both) are performed to monitor ZDDP film formation on a steel ball when rubbed against aluminium discs with varying oxide layer thickness. Few other hypothesized drivers such as generation of fresh surface and effect of shearing and mixing are also put to test.

Another novel approach used to test the hypothesis of whether triboemission contributes to tribofilm growth, firstly involves decoupling the effect of rubbing, while artificially stimulating emission using UV light and consequently verifying antiwear film formation using a known surface analysis technique that can detect phosphate films. Since, there is no requirement of rubbing in this method, no tribometer is used.

Various kinds of surface analysis techniques are used to compliment the results obtained from tests using different tribometers in selected environment.

3.2 Rationale for selection of test samples

From the literature review it was clear that dielectric insulators such as aluminium oxide and polymers produce large amount of triboemission as compared to metals. Therefore, the materials selected in this study are materials which are known to produce triboemission as well as widely used in mechanical and tribological applications. The variety of test samples can be classified as metals, ceramics, polymers, and composites. They can also be categorized as conductors, semiconductors, and insulators. Generally, metals are conductors, polymers are insulators and oxides are semiconductors based on their band energy.

Measurements made under vacuum conditions

For the vacuum tests, the pin material is diamond while disc is material is polytetrafluoroethylene (PTFE). A vast majority of materials tested earlier have been oxides and ceramics hence for this study PTFE is chosen as representative material for all polymers.

Measurements made under ambient conditions

For the tests in air, the objective was to test a variety of materials for characterizing their triboemission and triboplasma behaviour. These materials are polymers, metals, alloys, ceramics and composites. They can be categorized based on their electrical properties as conductors, insulators, semiconductors. The aim is to identify if any material property influences triboemission.

The disc materials include 17 polymers such as PTFE, UHMWPE, Nylon, Oil-filled nylon, Polyvinylchloride, (PVC), Polypropylene (PP), High-density polyethylene (HDPE), Polyvinylidene fluoride (PVDF), Antistatic UHMWPE, PEEK (polyetheretherketone) which were supplied by Bayplastics, UK. Polydimethylsiloxane (PDMS) discs were synthesized in laboratory and the source of Polystyrene (PS) was a laboratory grade petridish. Two metallic conductors (AISI 52100 steel and Titanium alloy) were supplied by PCS instruments, UK, and

a semiconductor (Polycrystalline diamond) were kindly provided by visiting researcher Dr. Wen Yue from University of Geosciences (Beijing). Various composition of Titanium oxide (TiO_2) filled UHMWPE Composites were provided by Prof. J. Bijwe from Centre for Industrial Tribology, Indian Institute of Technology, Delhi. These discs were rubbed against a sapphire (single crystal Al_2O_3) hemisphere pin procured from Swiss Jewels, USA. Sapphire (Al_2O_3) is selected as pin material because it is transparent to a broad spectrum of light.

Measurements under liquid submerged conditions

For the submerged tests, a sapphire (single crystal Al_2O_3) disc is rubbed against a PTFE or UHMWPE ball. The submerged tests are carried out in various liquids such as deionized water, salt solution, dyed deionized water, and dyed oil. In the tests concerning interactions with bio-lubricants, polymers such as PTFE, UHMWPE, and Nylon were slid against sapphire in presence of protein-Albumin. Nylon is known to acquire net positive charges on its surface according to triboelectric series while PTFE and UHMWPE acquire net negative charges. Albumin carries negative charges. The net attraction or repulsion between dye tagged protein and polymer surface could influence the friction and wear behaviour. Fluorescein Isothiocyanate (FITC) dye tagged to Albumin obtained from bovine serum is supplied by Sigma Aldrich. The location of the protein-surface interaction is visualized using Fluorescence Tribometer.

Investigation of Factors Effecting Film Formation with Lubricant additive-ZDDP

When studying the interactions of an engine lubricant, discs with various thickness of aluminium oxide (5, 15, 25 μm) on aluminium disc were rubbed against a steel ball (AISI52100) under a combination of sliding and rolling conditions to understand the effect of oxide thickness on tribofilm formation. For understanding the effect of mixing and shearing, steel discs (AISI52100) were rubbed against a steel ball (AISI52100) using novel methods which will be discussed later. In order to completely remove the effect of shearing on tribofilm formation stationary tests involving artificial stimulation of emission, steel (AISI52100) discs were used. The lubricant was ZDDP (0.08%P) mixed with group II mineral oil. The samples are supplied by PCS Instruments, UK. The anodizing treatment to obtain various oxide thicknesses on polished aluminium discs was done at Metroplating, UK.

3.3 TE Interactions in Vacuum

3.3.1 MCP Tribometer

A schematic diagram of microchannel plate (MCP) tribometer is shown in Figure 3.1. The tribometer is of a pin on disc configuration where an external motor rotates the disc centrally inside a cylindrical vacuum chamber, via a dynamically sealed shaft. A 100 µm radius diamond tip mounted on a 1 mm diameter steel arm (obtained from Synton-MDP Ltd.), is loaded onto the disc sample at a set track radius using deadweight arrangement. A vacuum pressure of 10^{-5} Torr (10^{-8} Pa) is maintained using a turbomolecular pump and monitored using Pirani gauge (Edwards Vacuum).

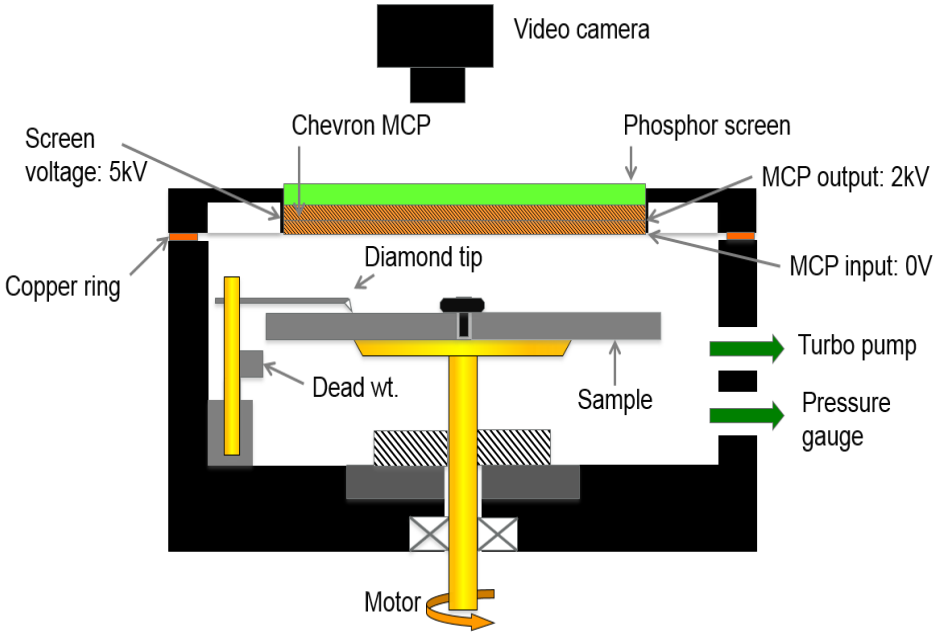

Figure 3.1: Schematic of vacuum MCP tribometer

A microchannel plate (MCP) is an array of electron multipliers used for detecting X-rays, ultraviolet radiation and charged particles. Each plate therefore consists of many tiny glass tubes fused together to form a thin disc. Both faces of the disc are metal-coated to provide parallel electrical connections to all channels. The Photonis MCP detectors (commercially available and used in this research) consists of two MCPs positioned together such that their detector channels are in a chevron arrangement. In vacuum condition, by applying a potential difference (usually 800 to 1400 V) across the plate, each channel acts as a continuous dynode electron multiplier that operates on the principle of electron avalanche. The output is a two-dimensional electron image which is used to excite a phosphor screen placed close to the output

thus providing an intensified high resolution visual representation which preserves the spatial resolution of the original input radiation pattern. Thus, it enables imaging of spatial distributions of triboemission generated from the rubbing contact.

This MCP detector with an effective diameter of 75 mm forms circular window on the top lid of the vacuum chamber and as such it is 10 mm above the sliding contact. The voltages applied to the upper and lower MCP and phosphor screen are 0, +1.5 and +5 kV, respectively. The lower MCP is set to 0 voltage so that the trajectory of charged particle emission remains unchanged. Important features of MCPs are high electronic gain, immunity from magnetic fields, fast response, low noise, low power consumption, high spatial resolution, small size, and ruggedness. The detection efficiencies [175] of the MCPs are as follows:

i) 0.01–50 keV electrons: 10–85%,
ii) 1–50 keV positive ions: 5–85%,
iii) UV radiation 300–1100 Å: 5–15%,
iv) UV radiation 1100–1500 Å: 1–5%,
v) Soft X-rays 2–5 Å: 5–15%,

The particles detected in the present setup of bias voltages are expected to be electrons. Positive ions which have energies above 1 keV can only be detected due to the bias applied to the plates. Photons of wavelength longer than 150 nm, on the other hand have zero detection efficiencies, while photons with wavelength between 30 and 150 nm, and have comparatively low detection efficiencies.

3.3.2 Camera

A Miro ex2 camera used for this set-up benefits from a CMOS sensor that can take 800 x 600 pixel images at up to 1200 frames-per-second (or 2252 frames/s at 512 x 512). At a reduced resolution of 32 x 16, frame rates greater than 111100 fps can be achieved. A 35mm f1.7 Fuji (focal length 35, max. aperture 1.7) lens was fitted to the camera and images were recorded at a capture rate of 170 frames/s. Phantom Camera Control software (PCC) was used for both data acquisition as well as camera control via ethernet cables.

3.4 TE Interactions in Air

3.4.1 Air plasma Tribometer

The test setup presented in Figure 3.2(a) shows the friction and load measurement apparatus (Figure 3.2(b)) mounted on the x-y-z control platform of the PCS high-speed EHD rig. The load is applied by rotating the z-direction screw on the platform such that the cantilever moves in negative z direction and the free end of the cantilever arm where the hemispherical pins are attached loads unto the rotating disc specimen. The x-direction screw was used to align the cantilever straight through the centre of the test specimen while the y-direction screw is used to select a wear track diameter. The cantilever is pivoted onto the frame (Figure 3.2a) in order to reduce friction between the mating parts. The rig uses two force sensors, for measuring load and frictional torque. The analogue voltage signals are amplified (see Figure 3.3) and sent to a self-developed LABVIEW program through multifunction DAQ USB Device NI USB-6008.

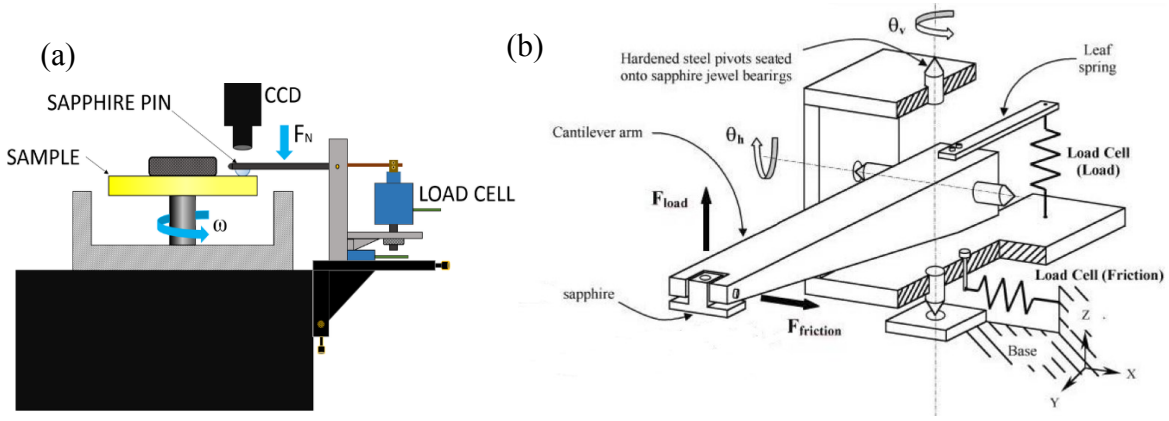

Figure 3.2: (a) Airplasma tribometer setup, (b) Principle on load and friction measurement adapted from [176].

3.4.2 Calibration of the rig

The calibration of the rig was carried out using a fine thread, a pulley, known weights (each 100 g) and an electronic scale. The resolution of the electronic scale was 0.01 g. The weights were attached to a fine thread on one end. The friction load sensor was calibrated for bidirectional measurements using a 100 g weight. To do this, a fine thread was hung through a pulley with one end attached to a 100 g (0.983 N) weight and the other end to the tip of the cantilever. Voltages readout for positive and negative loading direction were determined. A linear calibration function was fitted to the two points using a standard Labview virtual instrument (VI) that relates the digital readout voltage values to obtain friction readings in

newton (N). The voltage with slack thread was noted to confirm a co-linearity in both directions. The potentiostat present in the amplifying circuit (see Figure 3.3) can be turned to increase or decrease the sensitivity range.

For load cell calibration, the voltage readings without the cantilever was noted first. Then, the cantilever was loaded against an electronic scale up to up to a value of 400 g using the z-direction screw. The voltage at this point was noted. The no-load voltage and a voltage with known load of 400 g was noted. A linear calibration curve was fitted to relate the digital readout voltage values to obtain load sensor readings in newtons (N).

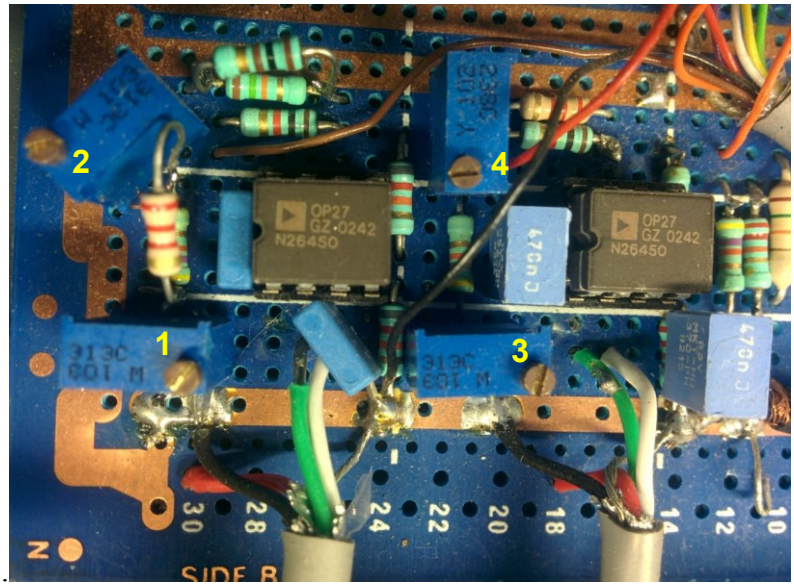

Figure 3.3: Amplifying circuit showing four potentiostats (numbered 1-4) which can be rotated to increase or decrease the sensitivity of the measurement.

3.4.3 The LabView Program

A Labview program was written to collect data in the form of spreadsheets and display variation in voltage, load, frictional torque and coefficient of friction in real time as shown in Figure 3.4.

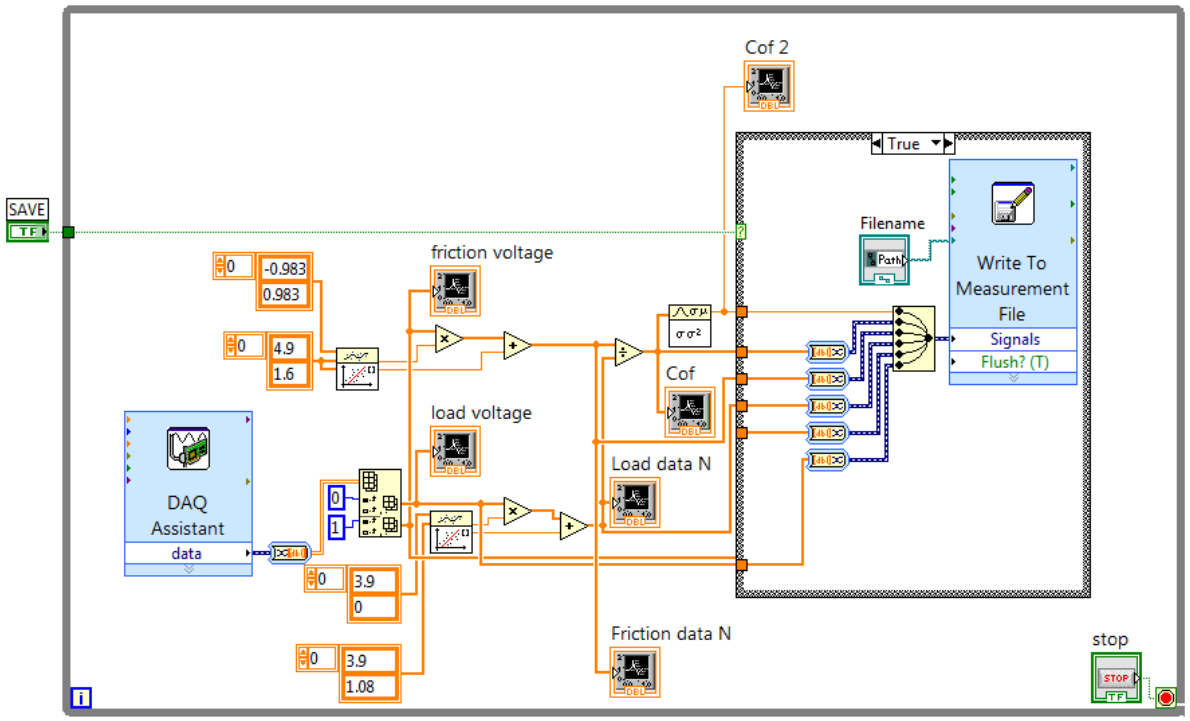

Figure 3.4: Labview program used for displaying, recording, and storing friction and load values into the computer.

3.4.4 Camera

Imaging of UV photons

Two cameras were used for the tests conducted in ambient atmosphere. A JAI CM-140GE-UV from Stemmer Imaging Ltd. and an ImagEM X2 from Hamamatsu Photonics UK Ltd. Review of literature, revealed that photon energies from triboplasma are in the ultraviolet (UV) range of the spectrum. These two cameras meet the requirement of high UV sensitivity of detecting units in the UV range of spectrum.

The CM-140GE-UV shown in Figure 3.5 is a monochrome camera with dimensions (H×W×L): 29×44×75mm that provides a resolution of 1.4 megapixel with an extended sensitivity to wavelength as low as 200 nm. It makes use of a Sony ICX407BLA CCD sensor which has been specially designed for UV sensitivity. The camera captures 16 frames/s in full frame in continuous (free-run) or trigger modes. Higher frame rates can be achieved by using the partial scan or vertical binning modes. A GigE Vision interface between the camera and the computer helps in fast transfer of high resolution captured images in realtime. JAI GigE Vision SDK and Control Tool software package along with programmable GPIO allows flexible configuration

of inputs/outputs functions and the timer/counter function. A sequencer function makes it possible to change exposure time, gain and region of interest (ROI).

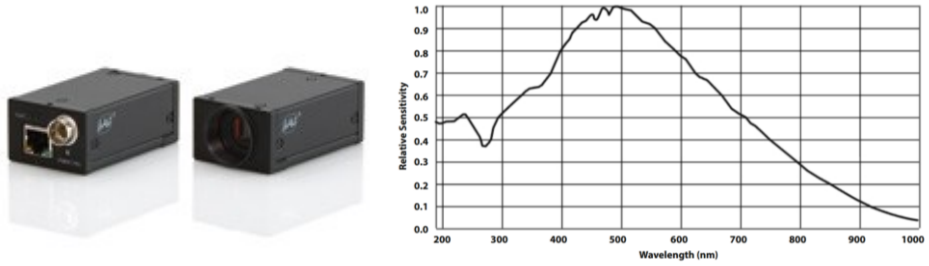

Figure 3.5: JAI CM-140GE-UV and its quantum efficiency.

The Jai camera has limitations such as low frame rate, small pixel size and hence struggles in ultra-low light conditions. At the highest frame rate of 17 fps, shorter exposure times permit only tens of photons per pixel in each shot which results in poor photon capturing resolution. Therefore, a frame rate 1.2 fps was chosen with this camera.

The ImagEM X2 camera with large pixels and advanced back thinned EM-CCD technology, has high QE, nearly zero readout noise, very high signal to noise in near dark conditions, extremely low dark current. It captures frames at 70 frames/s at full frame and can be increased up to 1076 frames/s with analog binning and regions of interest using a 512×512 EM-CCD sensor. This enables quantitative ultra-low light imaging both for long integration times and at high speed. With the use of IEEE1394b cables the images are sent at high speeds without dropping frames and stored in computer immediately. Additionally, it is an extremely versatile camera, with EM gain switched off, it can record low contrast bright images enabling it to be use in all the tests using fluorescence dyes. Figure 3.6 shows the ImagEX2 camera and its quantum efficiency for different wavelength of light while Table 3.1 shows a comparison between the two cameras.

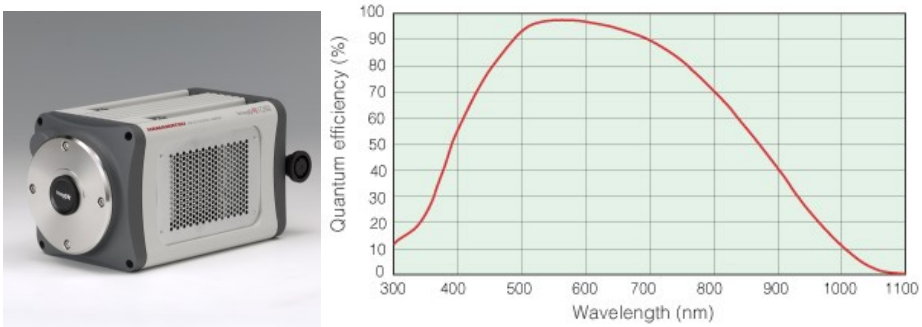

Figure 3.6: ImagEX2 camera and its quantum efficiency. Note that the QE below 200 has not been disclosed although it has been checked (with the supplier) to have one peak of 56% QE at 230 nm, another peak of about 35% at 260 nm, from 300 to 350 nm it slightly goes up from 27 to 30%, from 350-400 nm the QE rises from 30 - 65%.

Table 3.1: A comparison of the cameras

	JAI CM-140GE-UV	**ImagEM X2**
Effective number of pixels	1380 (h) × 1040 (v)	512 × 512
Cell size (square pixels)	4.65 µm	16 µm
Fast read out speed at full resolution	16 frames/second	70.4 frames/second

Imaging of IR photons

The imaging of thermal photons (IR photons) is carried out using an infrared (IR) camera that is positioned above the sapphire hemisphere and focuses through the sapphire into the contact in order to measure IR radiation from the contact region. A FLIR X6540 SC camera (Figure 3.7) that has a high resolution 640×512 detector, sensitive to IR wavelengths from 3 to 5 µm was used. In this study the contact surface is focused using a 5× objective lens and images are captured at 25 Hz for one minute of rotation.

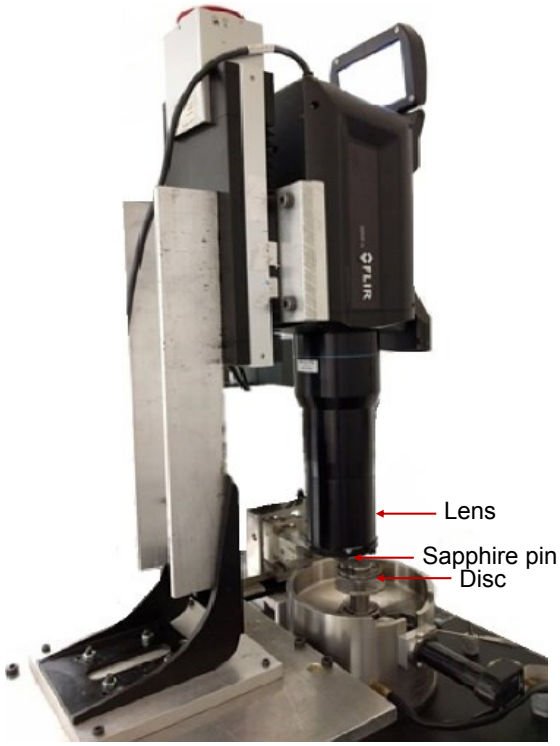

Figure 3.7: FLIR FLIR X6540 SC camera

3.5 TE Interactions in Liquid Environment

3.5.1 Fluorescence tribometer

The tribometer used for the liquid submerged studies is a high speed EHL tribometer by PCS Instruments. Figure 3.8 shows a generalized schematic of the fluorescence tribometer which can visualize the contact in two configuration (a) through a sapphire disc unto a ball made up of any material; (b) through a sapphire hemisphere unto a disc made up of any material as required.

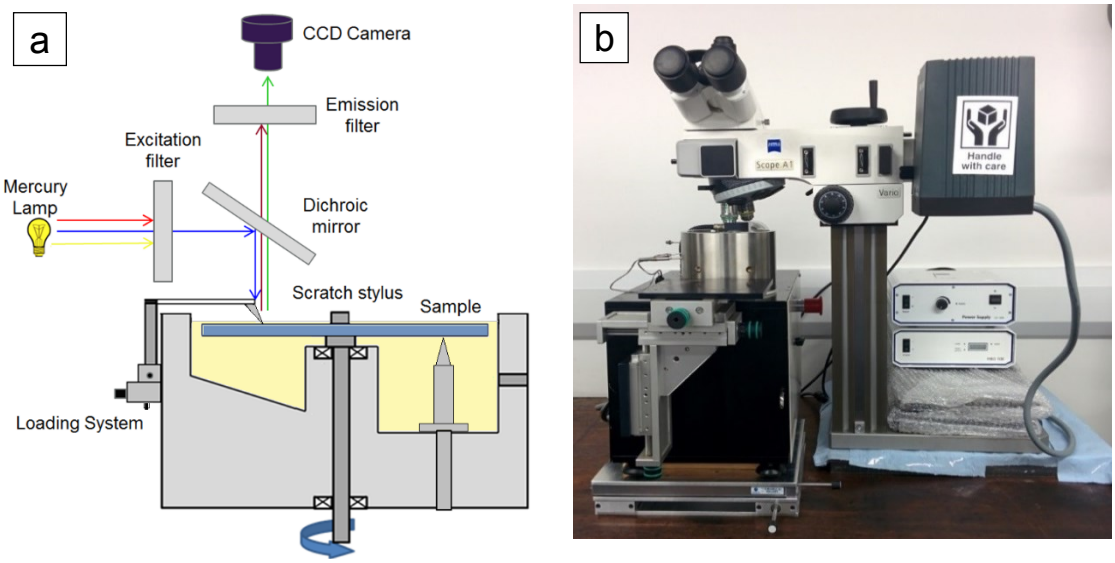

Figure 3.8: (a) Schematic of fluorescence rig (b) Image of the fluorescence tribometer.

For fully submerged tests, a transparent sapphire disc is securely tightened to a vertical shaft that is driven by a high-speed motor. The loading arrangement uses a hydraulic system that lifts the ball specimen and loads it onto the disc specimen from beneath. This enables the contact to be viewed from above using a Zeiss fluorescence microscope (Axiosope Vario) or a free standing camera. The disc sample is positioned centrally inside a chamber while the ball specimen holder stage is located off-center to the shaft and can be moved only in one direction about 10 mm which helps in selecting different wear track radii for each new test. The entire chamber can hold the lubricant and ensure fully submerged conditions at the contact. Completely submerged contact can also be achieved by a liquid column supported between a self-designed specimen holder and sapphire disc as shown in Figure 3.9. It can accommodate a 6 mm ball and ensure pure sliding conditions with the sapphire disc as well as hold a small quantity of liquid column around the contact. This overcomes the limitations of using large quantity of dye mixed liquid for submerging the whole contact. It also prevents any

contamination from known and unknown sources in the large pot which could result in change in concentration of the dye. The speed is kept low so as to ensure that the liquid film does not fly out of the contact by the action of centrifugal acceleration. The load and speed was kept at 20 N and 5.5 mm/s respectively.

Figure 3.9: Test set up for dye interaction tests showing a transparent sapphire disc loaded against a PTFE ball submerged in 1mM CF mixed deionized water.

At low sliding speed tests, a liquid film can also be sustained as a meniscus at the contact between sapphire pin and disc made up of any material which enables viewing the contact through a sapphire pin under submerged conditions. It is also possible to image any region on the disc always from the contact before rubbing, after rubbing as well as after adding a dye mixed lubricant.

Fluorescence images of the contact before and after the sliding test were viewed with the help of the fluorescence microscope (Axiosope Vario) and the images were captured using a high speed CCD camera ImagEX2. The base of the fluorescence microscope has been modified to accommodate the tribometer. The light source is a mercury bulb which emits light in a wide range of spectrum. From this any desired wavelength of excitation and emission can be selected by use of band pass filters. The choice of filters is guided by the excitation and emission spectra of the chosen dye.

Various candidate dyes were evaluated, and those which were selected for use in this study are shown in Table 3.2. 5(6)-carboxyfluorescein (CF) is a mixture of two isomers, 5-carboxyfluorescein and 6- carboxyfluorescein. Fluorescein isothiocyanate (FITC) is fluorescein functionalized with an isothiocyanate reactive group (-N=C=S) by replacing a hydrogen atom on the bottom ring of the structure while in CF a carboxyl group is added. Both dyes are fluorescein based and their chemical structure is shown in Figure 3.10. Their

absorption wavelength is 495 nm and emission wavelength 517-519 nm. They are commonly used as a tracer agents and used in the sequencing of nucleic acids and in the labelling nucleotides. Neutral red is a staining dye and has been used as a pH indicator. It has two forms: protonated (λ_{abs}=535 nm) neutral form (λ_{abs}= 452 nm). This is used for UV-VIS measurements. All three dyes were obtained from Sigma Aldrich.

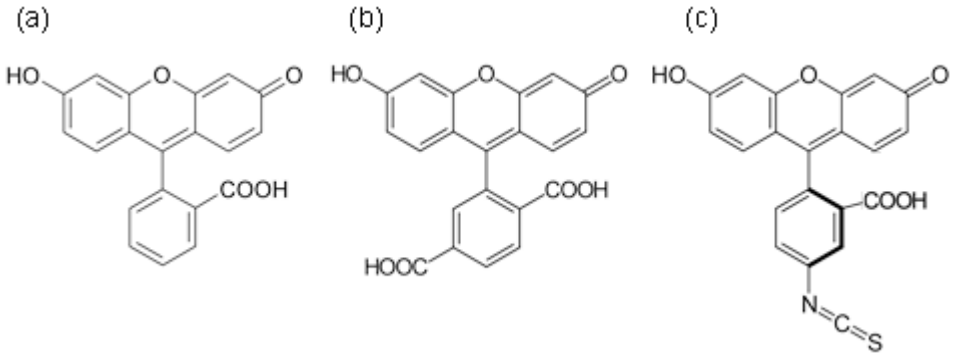

Figure 3.10: Chemical structure of dyes (a) Fluorescein (b) 6-carboxyfluorescein and (c) Fluorescein isothiocyanate. Commercially available carboxyfluorescein are a mixture of both these isomers.

Table 3.2: Candidate dyes and their excitation and emission wavelength

Dye	**Excitation wavelength nm**	**Emission Wavelength nm**
Carboxyfluorescein	504	525
FITC Fluorescein Isothiocyanate	495	525
Neutral Red	540	630

All tests were carried out at room temperature. The preparation technique of the liquids in which the samples were submerged is given below

(a) Deionized water and saline water

Deionized water was obtained from millipore installation in the laboratory and 10% (concentration by weight/volume) saline water was prepared using a measured quantity table salt and continuous mechanical stirring.

(b) CF mixed water

Measured grams of carboxyfluorescein (CF) were added to deionized water and mixed thoroughly using a vortex mixer to obtain a concentration of 1 mM.

(c) CF mixed Oil

In order to obtain a concentration of 1 mM CF in base II mineral oil, a magnetic stirring technique was used. A small magnet was put into the container and placed on a magnetic stirrer at 70 ^{o}C for 5 hours with additional shaking at regular intervals.

3.5.2 CETR UMT Tribometer

Figure 3.11 shows the CETR UMT Tribometer with a pin on disc configuration. Coefficient of friction (μ) is automatically recorded and displayed on the monitor of PC as a function of time. This is chosen for accurately measuring coefficient of friction at low load sliding while studying protein-polymer surface interaction.

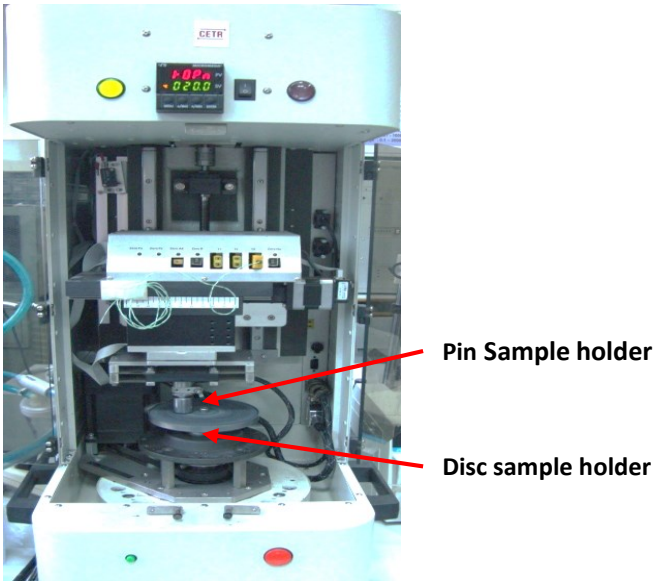

Figure 3.11: Universal Tribometer from CETR (now Bruker)

3.6 Investigation of Factors Effecting Film Formation

3.6.1 Mini Traction Machine

The mini-traction machine (MTM), developed by PCS Instruments involves a ball (or barrel) on disc configuration as shown in Figure 3.12. A wide range of entrainment speeds and slide roll ratios (SRRs) can be achieved with independently driven ball and disc. The lubricant reservoir is fitted with a heater to allow control of temperature. The MTM2 is widely used in measuring friction and boundary film thickness by incorporating 3D spacer layer imaging (3D-SLIM) option which uses optical interferometry to measure additive films on the specimens as they form during the test. A schematic of optical interferometry technique is shown in Figure 3.13.

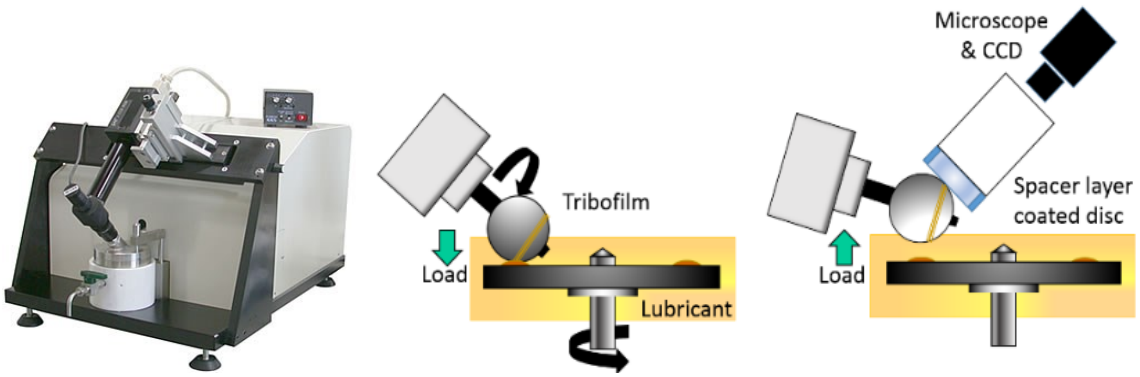

Figure 3.12: A Mini Traction Machine and its operating configuration.

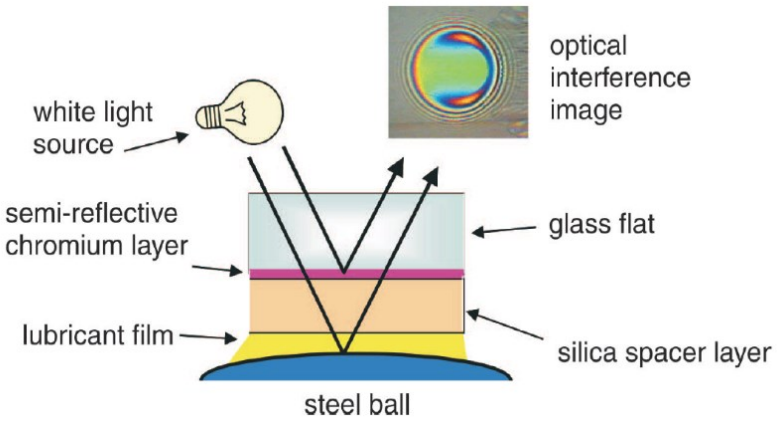

Figure 3.13: Optical interference technique used on the MTM [177].

While standard MTM tests under various SRRs were carried out to study effect of shearing and mixing on film formation and growth, another set of studies were conducted using the MTM rig to study effect of fresh nascent surface on film formation and growth on wear track of steel disc vs steel ball contact at 30 N load pure sliding as shown in Figure 3.14. In first case, rubbing was carried out for one rotation of the disc in presence of the heated 0.08% ZDDP containing oil while in second case hot oil kept at 100 ^{o}C was poured unto wear track immediately after one complete rotation of unlubricated sliding. The film growth is monitored using atomic force microscopy (AFM) and Time of flight Secondary ion mass spectroscopy (ToF SIMS).

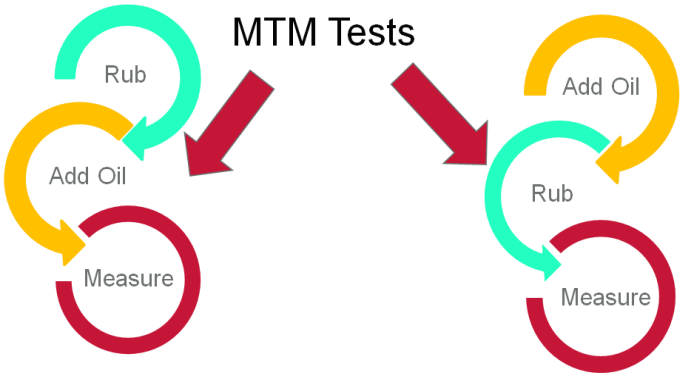

Figure 3.14: The test protocol for evaluating role of fresh surface/after emission/residual charges. Case I: Dry rub followed by pouring hot lubricant immediately on wear track; Case II: Rub in presence of hot lubricant.

3.6.2 Artificial stimulation of electron emission

This section describes the implementation of ultraviolet (UV) light to cause emission of electrons from a metal surface and monitor how these electrons affects the additive film formation. When the input of UV energy exceeds the work function of substances, electron emission is observed due to the photoelectron effect. The objective here is to check whether artificially stimulated electrons have the potential to form boundary films (see Figure 3.15) and can be achieved by the following procedure. First the sample was irradiated with UV light incident at about 60 degrees to the sample by means of a fibre optic cable. The energy was increased gradually from 4000 to 6000 meV (wavelength gradually decreased) to determine the work function of the sample which can be measured in electron volts or in terms of wavelength of the incident UV light. This point is determined by the current read by the detector due to electrons emitted from the surface. The point where a transition from no current horizontal line to a line with slope occurs is denoted as the work function of the material. This is done using the Air photoemission rig (APS02) shown in Figure 3.16 developed by KP technology, UK.

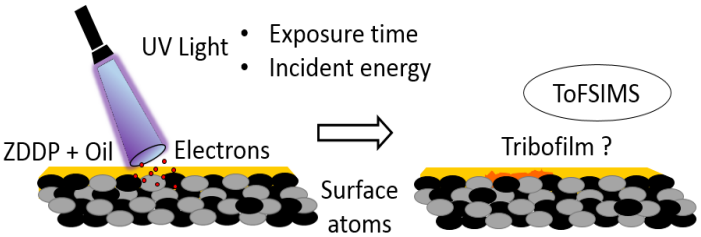

Figure 3.15: UV treatment of sample which might cause additive film to growth.

The procedure of this experiment are as follows:

- Metal sample is coated with a ~200 µm thick layer of oil containing ZDDP additive.
- UV light is then focussed upon a lubricant covered sample, using a Kelvin Probe Technology Air-Photoemission system as shown in Figure 3.16. Here, the test variables are the duration of UV stimulation, intensity, use of mask and the wavelength of UV light (different samples will be exposed to wavelengths above and below the work function of metal surface to elucidate the effect of electron emission due to UV irradiation on additive film formation.
- Atomic force microscopy (AFM) and Time of Flight Secondary Ion Mass Spectrometry (ToF SIMS) is then used to analyse the film thickness and reaction film compounds on the surface.

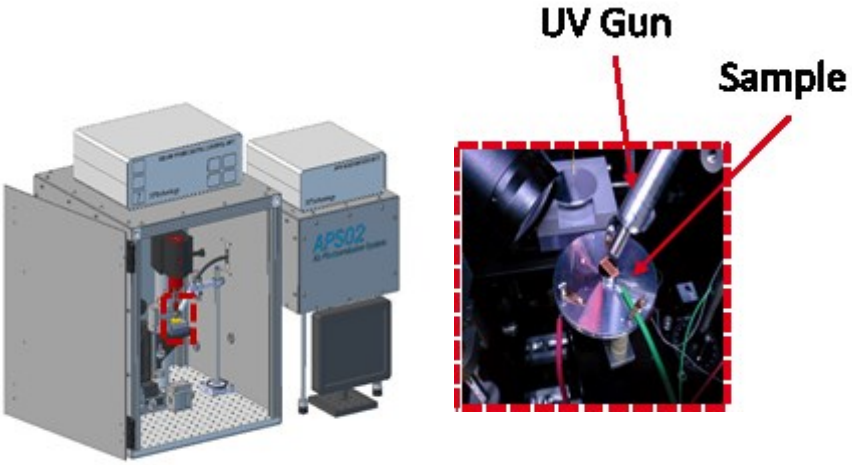

Figure 3.16: Air photoemission rig (KP Technology) and position of sample and UV light fibre optic.

3.7 Surface Analysis Techniques Used

3.7.1 Optical microscopy

Optical microscopy is a non-contact method widely employed to observe the appearance of samples before and after friction tests.

Principle of operation:

A digital camera allows images of specimen's surface observed by the microscope eyepiece and to be captured and saved onto a computer. The optical microscope can be calibrated using a graticule as a reference while modern state of the art digital microscopes such as HIROX RH 2000 comes with a set objectives that are pre-calibrated for each magnification. The dimensions

(along the x-y direction) of wear scars as well as material transfer on the surface can then be determined.

3.7.2 Mechanical profilometery

Mechanical profilometer or stylus profilometer is used to obtain information about the topography of a surface and various other surface parameters. A Taylor Hobson Talysurf is used for measuring dimensions of the width and depth of the wear track and determining surface roughness of the samples.

Principle of operation:

A diamond stylus is made to contact the surface at a set contacting force. The stylus is then traced across the surface where the changes in height of the asperities cause the stylus to be displaced. The height position of the diamond stylus generates an analogue signal which is converted into a digital signal, stored, analyzed, and displayed. The vertical displacement of the stylus can be thus used to generate a line profile. If desired, several line profiles can be stitched to generate a topographical map. The horizontal resolution is controlled by radius of diamond stylus (ranges from 20 nm to 50 μm), scan speed and data signal sampling rate. However, such a technique could damage surface adsorbed films and transfer films. Moreover its lateral and vertical resolution is lower than that which is achieved by atomic force microscopy.

In many ways, mechanical profilometry has been superseded by non-contact techniques such as optical profilometry (white light interferometry) where results can be obtained faster. However, mechanical profilometry continues to be employed for cases where optical profilometry is not suitable, for example transparent specimens, irregular shaped surfaces with large variations in height, extremely rough non reflective surfaces and large objects which would not fit into the optical profilometer.

3.7.3 White Light Interferometry

Optical profilometry is a non-contact technique widely used to determine the dimensions of wear scars and volume loss due to wear on the test surfaces. The topography of the surface can be mapped and a 3D representation can also be obtained. The optical profilometer used in this study is a Wyko model by Veeco (currently owned by Bruker). The Wyko can operate in two modes: Phase Shifting Interferometry (PSI) enables the measurement of smooth surfaces at

high, 0.1 nm, vertical resolution and Vertical Scanning Interferometry (VSI) enables the measurement of rougher surfaces at lower, 3 nm, and vertical resolution.

Principle of operation:

PSI mode employs a monochromatic light source to generate a series of interference fringes. The interference fringes are manually focused and the light intensity is adjusted so that a high contrast live image of the fringes is achieved. While, VSI mode uses a white light source to generate a series of interference fringes which need manual focussing similar to PSI. During this vertical scan by objective lens, snapshots of the fringes are continuously acquired. For each pixel in the image a snapshot is selected where the contrast of the interference fringe is greatest, *i.e.* where the fringes are most in focus. As the vertical position of the objective lens is recorded at each snapshot, a three dimensional topographical map is generated.

Although optical profilometry provides topographical information quickly without damaging the surface it is not an appropriate technique for studying transparent samples as no interference fringes will be generated. It is also not suitable for measuring thin monolayer films as such films interact with the light leading to anomalies including apparent augmentation of wear scar depth. Additionally, excess lubricant must be removed from specimens prior to optical profilometry as surface, which may cause optical aberration.

3.7.4 Atomic force microscopy

Atomic Force Microscopy (AFM) is form of scanning probe microscopy that can be used on any kind of surface not necessarily conductive. Even AFM measurements are possible on liquid immersed surfaces.

Principle of operation:

In AFM the tip is located at the end of a cantilever; in contact mode deflections of the cantilever are measured optically by monitoring the position of a reflected laser beam off the backside of the cantilever and in tapping mode the cantilever is made to resonate so that the tip intermittently contacts or ‘taps’ the surface. A tip is raster scanned across a surface and a topographical map is obtained at a very high resolution over a very small area (93×93 microns with the Bruker Dimension Icon shown in Figure 3.17). The information obtained by AFM is not limited to normal forces as it also enables the measurement of lateral friction forces. Imaging mode used in this thesis is ScanAsyst® which is a PeakForce Tapping® based image

optimization technique that enables creation of highest resolution AFM images using single-touch scanning where only the scan area and scan size is selected by the user.

Figure 3.17: Bruker's dimension icon AFM at London center for nanotechnology.

3.7.5 Kelvin probe force microscopy

Kelvin probe force microscopy (KPFM) is also called surface potential microscopy. The Peak Force KPFM™ accessory is mounted on the Bruker's Dimension Icon AFM provides high spatial resolution surface potential measurements on a wide range of samples. It can be operated in two powerful KPFM modes (amplitude modulated and frequency modulated) which are based on Bruker's patented PeakForce Tapping™ technology. A scanning kelvin probe apparatus at developed at KP Technology, Wick (UK) is also used for in this project.

Principle of operation:

The work function is the minimum energy (or work, usually measured in eV), needed to remove an electron from a solid, to a point immediately outside the solid surface (or energy needed to move an electron from the Fermi level into vacuum). When two different conductors are brought into electrical contact, for example via an external wire contact, electrons will flow from the one with lower work function to the one with higher work function, equalizing the Fermi energies.

If they are made into a parallel plate capacitor, equal and opposite charges will be induced on the surfaces. The potential established between these two surfaces is called the contact potential difference (CPD), contact potential, or surface potential, which equals the work function difference of the two materials. In order to measure the CPD an external potential (also called the backing potential) is applied to the capacitor until the surface charges disappear. At this point, the external potential equals the CPD. The various Kelvin probe techniques have been

recently developed which differ mainly only on how this charge free state is detected. The detection technique used by Bruker's KPFM accessory is shown in Figure 3.18.

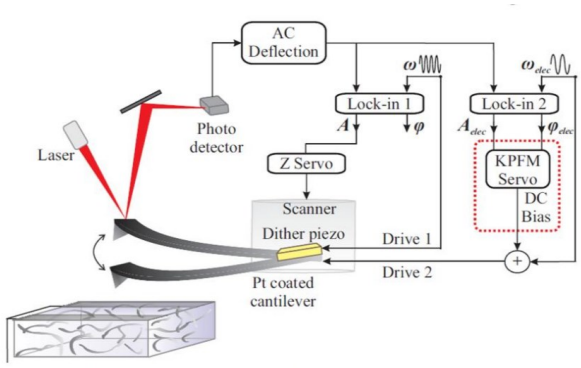

Figure 3.18: Schematic of KPFM [178].

A scanning Kelvin probe apparatus at developed at KP Technology, Wick (UK) is shown in Figure 3.19. It is used to measure the change in work function of a steel surface upon scratching (a form of plastic deformation) and ascertain the reactivity of fresh surfaces. This apparatus uses a scan stage to move sample with respect to the Kelvin probe and thus can produce maps showing variation of work function on a surface.

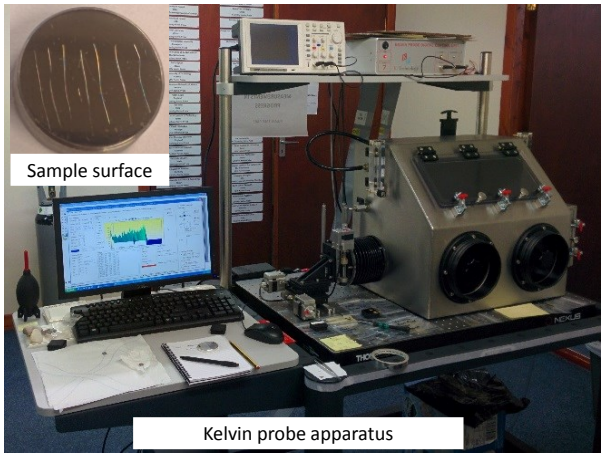

Figure 3.19: Image showing a 10 mm diameter scratched steel disc and scanning kelvin probe apparatus at KP Technology, Wick (UK).

3.7.6 Scanning electron microscope

Scanning electron microscope (SEM) is a mature technique of surface analysis and widely used in many scientific application. The interaction of bombarded electrons with the atoms in the sample surface, produce various signals that contain information about the sample's surface topography and composition. The high resolution SEM images have helped tribologists to observe and interpret the kind of wear (adhesive, abrasive) and failure (fracture, delamination, shear) occurring at the surface.

Principle of operation:

The basic principle is that a beam of electrons is generated by suitable source (tungsten filament or field emission gun). The electron beam is accelerated through a high voltage and passed through a system of apertures and electromagnetic lenses to produce thin beam of electrons. The beam scans the surface of the specimen by means of scan coils. Electrons are emitted from the surface of specimen by action of scanning beam and collected by suitable positioned detector. The scanning beam scans across from left to right, then drops a line and scans again to meet the required magnification set by a user.

All SEM images are black and white and can be seen on the screen. The beam scanning the specimen is synchronized with the screen in the sense that the brightness of a spot on the screen is proportional to the number of electrons sensed by the detector. The magnification of the image is the size of screen to size of area scanned. There are different types of electron image. The two most common are secondary electron image (ESED) or Backscattered electron image (BSE). SE is used to image fracture surface and has a higher resolution for observing topographical features while BSE is used to observe different composition or phases of the sample as it is sensitive to atomic number. The heavier atoms appear brighter than lighter atoms which results in the contrast of an image. BSE provides more information regarding distribution of polymer transfer films and debris around the wear scar.

Development of normal high vacuum scanning electron microscope has led to what is called an environmental SEM (ESEM) which can operate with air in the specimen chamber and the pressure is lower than atmospheric but higher than high vacuum of normal SEM. This has an advantage that wet specimens can be analyzed as well as not requiring a samples to be coated with gold.

Energy dispersive X-ray microanalysis (EDX) is complimentary to SEM. It enables the operator to analyses the composition of features in the SEM. The principle of EDX is that the electron beam generates X-ray within specimen. Many of these X-ray have energy characteristic of the elements that emitted them. Therefore not only the presence of a particular element but also its concentration can be determined.

The principle components are the X-ray detector (which intercepts the X-ray emitted), and pulse processor (the current generated by X-ray is converted to voltage pulse) that measures the size of voltage pulse corresponds to X-ray energy and a computer. The computer measures

voltage pulses over a time period and converts into histograms that shows the spectrum of X-ray energies, which can be examined to determine the elements present. The EDX may also be used to take control of the SEM system in order to collect elemental distribution maps (dot maps).

3.7.7 Time-of-Flight Secondary Ion Mass Spectroscopy

Time-of-Flight Secondary Ion Mass Spectroscopy (ToF-SIMS), sometimes referred to as static SIMS. In ToF-SIMS, the ejected ions give molecular information and the fragmentation pattern can be used to work out the structures of the species present; this makes ToF-SIMS suitable for studying thin tribofilms. ToF-SIMS have been used to identify products of tribochemical reactions post-friction tests. Figure 3.20 shows the particle-beam interaction that is utilized by ToF SIMS.

Principle of operation:

It uses low energy primary ion bombardment to eject secondary ions. The ejected secondary ions are then accelerated through a vacuum and the mean flight path of the ions is recorded and the corresponding mass is calculated. ToF-SIMS is static because, unlike standard SIMS techniques, the pulsed low energy primary ions only affect the uppermost surface of the material being analysed. Dynamic SIMS uses high energy ions that penetrate beneath the surface and this way a compositional depth profile can be obtained. However the high energy ion bombardment used in dynamic SIMS means that typically only atomic information can be obtained.

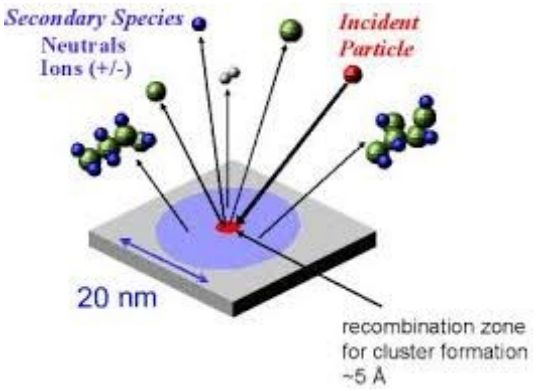

Figure 3.20: TOF-SIMS Particle-beam interaction [179].

The surfaces are analysed by using a TOF-SIMS IV instrument (ION-TOF GmbH, Münster, Germany). A 69Ga+ liquid metal ion source was used to produce a primary beam using an

acceleration voltage of 25 kV and an AC target current of 1.26 pA with a bunched pulse width of less than 0.7 ns. Both positive and negative secondary ion species were analysed. A raster of 256 × 256 pixels was used. The total primary ion beam dose for each analysed area was kept below 1012 ions cm^{-2} throughout, ensuring static conditions. ToF SIMS measurements performed on Combined IONTOF TOF.SIMS 5-Qtac100 LEIS instrument facility at Imperial College London uses Bismuth ions as primary beam. All data analysis was carried out using software supplied by the instrument manufacturer, IonSpec and IonImage (version 4.0).

3.7.8 X-ray photoelectron spectroscopy

X-ray photoelectron spectroscopy (XPS) is a surface-sensitive quantitative spectroscopic technique that measures more than just the elemental composition. It can provide information regarding empirical formula, chemical state and electronic state of the elements that exist within a material. K alpha XPS facility is used for XPS studies on the test samples.

Principle of operation:

XPS uses a beam of X-rays to irradiate a sample in high vacuum. During irradiation, electrons are ejected from the surface. It is possible to measure the kinetic energy and number of electrons leaving from from the top 0 to 10 nm of the material's surface. Each element gives rise to characteristic peaks depending on the kinetic energy. The intensity of the peaks can be used as a quantitative measure of the number of a particular atom in the sample.

3.7.9 Raman spectroscopy

Raman spectroscopy is a spectroscopic technique used to observe vibrational, rotational, and other low-frequency modes in a system. Raman spectroscopy is commonly used in chemistry to provide a fingerprint by which molecules can be identified. Alpha 300 Raman/AFM from WITec is used in this study.

Principle of operation:

In Raman spectroscopy, monochromatic light from the infrared, visible or ultraviolet part of the electromagnetic spectrum is shone onto a surface. Groups within molecules are energetically excited and promoted to a virtual high energy state. The energy is subsequently emitted and the majority of molecules fall back to their original ground state energy level, *i.e.* the light is elastically scattered. However, some of the molecules fall back to higher or lower energy states than their original ground level state, *i.e.* the light is inelastically scattered or

Raman scattered. If the incident light interacts with the electron clouds within molecules it can result in the molecule falling back to a different vibrational or rotational state. The scattered light therefore has a slightly different energy (frequency and wavelength) from the incident light.

3.8 Electrometer

A charge sensor (of the type developed in [153]) as positioned diametrically opposite the contact with its tip 2 mm above the disc surface and was connected to an electrometer (Keithley 6517B) to record the accumulated charge signal as shown in Figure 3.21 . Additionally the electrometer is used in conjunction with Model 8009 Resistivity Test Fixture [180] to measure the volume resistivity (up to 10^{18} ohm-cm) and surface resistivity (up to 10^{17} ohm) of polymers studied in this thesis.

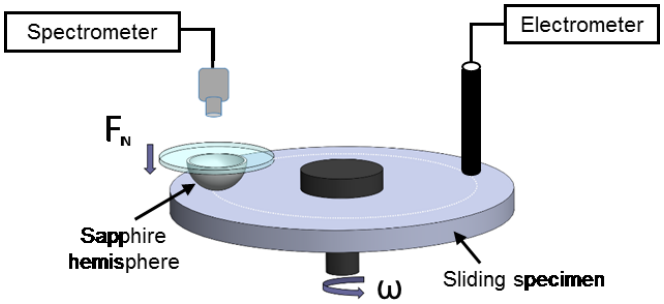

Figure 3.21: Schematic diagram of test set up showing the position of charge sensor and the sliding contact between Al_2O_3 hemisphere and disc.

3.9 Spectrometer

Spectrometers are instruments that are also used to measure a specific wavelength range. These use an optical grating or prism and multiple sensors to break down the incoming energy into different wavelengths or components. Spectrometers are not complete instruments and need to be paired with optics in order to work correctly. For certain tests, the camera was replaced by a spectrometer (Ocean Optics QE Pro) to measure the optical spectra of the plasma as shown in Figure 3.21. QE Pro uses the same back thinned CCD detector as the Hamamatsu camera ImagEX and therefore has high quantum efficiency, great signal to noise performance, stability and high-sensitivity spectrometer ideal for low light level applications such as fluorescence and Raman analysis. The grating number HC1 provides efficiency greater than 30% in wavelength range 200-950 nm.

3.10 Summary

This chapter provides a detailed description of the modification and transformation of existing test rigs to meet the requirements of the test conditions envisioned for this PhD. All the test rigs, test methods and procedures, test samples, test environment and test parameters used in the successive chapter have been described in details. Next chapter is the first results chapter that presents the studies done to understand triboemission interaction under vacuum conditions.

Chapter Four

Triboemission Interactions in Vacuum

The first step in this study was to determine which materials are prone to triboemission. From the literature survey, it was clear that the majority of insulating materials (ceramics, oxides, and polymers) have been reported to emit electrons upon fracture. However, the measurements were based on techniques that involved measuring a time varying signal for instance, channel electron multiplier. The limitation of these methods is that the sites of the triboemission could not be identified and as a result the lifetime of triboemission and after-emission events could not be obtained accurately. The measurements presented in this chapter benefit from the addition of a phosphor screen on top of multi-channel electron multiplier, which helps to visualize the sites where triboemission occurs, at the contact as well as over the entire wear track during the rubbing process. The pattern and triboemission sites are analysed and their sources are discussed. This data, obtained under vacuum conditions, provides a base line to which subsequent measurements under gaseous and liquid conditions can be compared. Important conclusions from this qualitative observation are also presented.

4.1 Triboemission from PTFE

This chapter presents the results of the tests performed in vacuum (2.7×10^{-5} Torr) using the MCP tribometer which incorporates a diamond tip stylus that scratches a disc made of the selected material, in this case polytetrafluroethylene (PTFE). The rationale behind material selection is presented in **Chapter 3**. The load and linear speed were kept at 0.5 N (mean contact pressure = 100 MPa) and 20 mm/s respectively. This load and speed was used to achieve a measurable emission intensity. The duration of sliding was two minutes. The triboemission from the sliding pair at a particular instant is considered equivalent to the intensity distribution of each individual 352×352 pixels phosphor screen image.

The results presented here show for the first time, the occurrence of triboemission from a PTFE surface. Figure 4.1(a) shows the location of the diamond tip and PTFE disc without the top

MCP and integrated phosphor screen. Figure 4.1 (b-i) shows eight individual frames captured through the MCP and phosphor screen during 0-30 seconds of the test in vacuum. In the absence of sliding there is no triboemission and all the observed phosphorescence on phosphor screen is termed as background emission as seen in image Figure 4.1(b). Images (c-i) show various triboemission events during the first 30 seconds of the test.

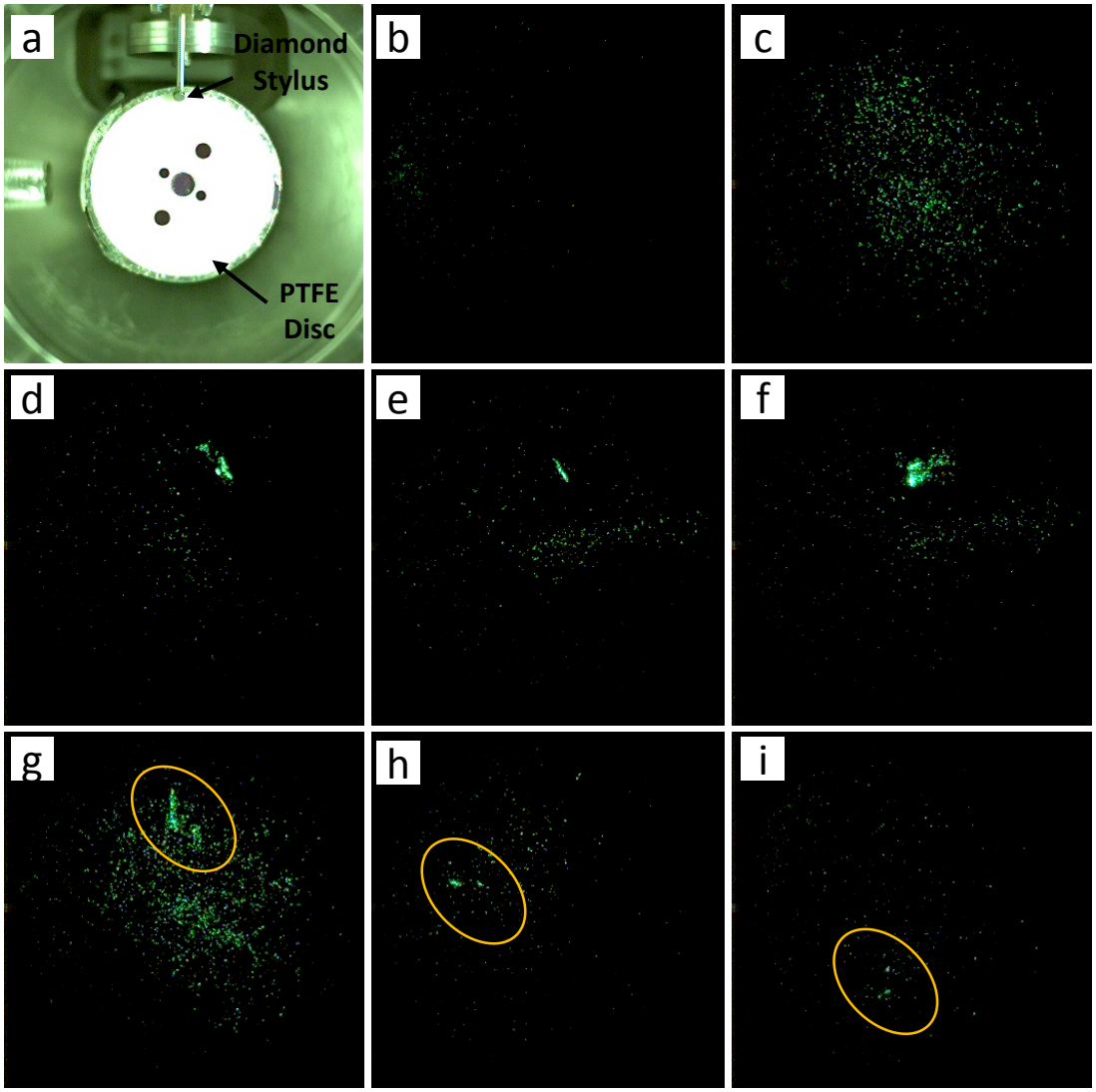

Figure 4.1: Selected individual frames during the first 30 seconds of the test showing various triboemission process.

When the disc is set in motion, the emission inside the chamber increases (c). This may be because of the release of gases trapped between components when the disc was stationary. Frames (d-f) show the triboemission at the contact. These may be a result of rupture of PTFE chains caused solely by the sliding of diamond tip on the PTFE disc. Frames (g-i) show a peculiar kind of emission which sustains for a longer period of time. The two pair points (encircled) generated on two opposite sides of the wear track continue emitting triboemission

until one complete revolution (Pair points have been discussed in [158]). This is likely to be from ion-electron recombination (electron bombardment) or strain relaxation. Such after-emission events were measured [181] but impossible to locate with previously used techniques. These after-emission phenomena will be discussed later in this chapter.

The variation of average triboemission with time in vacuum, presented in Figure 4.2, is variation of the average of all the pixel intensities obtained from a single phosphor screen image in grayscale. The RGB images captured by camera are first converted to grayscale using MATLAB script. Over a period of 150 seconds, 28530 frames were captured at rate of 171 frames per second and sliding starts just after 5 seconds. When the sliding commences, the triboemission from PTFE surfaces increases slowly during the next 30 seconds. The fluctuation in emission is periodic and the frequency of the emission corresponds to one rotation of the disc. It should be noted that the amount of TE and the kinetic energy of TE determines the brightness of the phosphor screen and hence the intensity counts of each pixel of a frame.

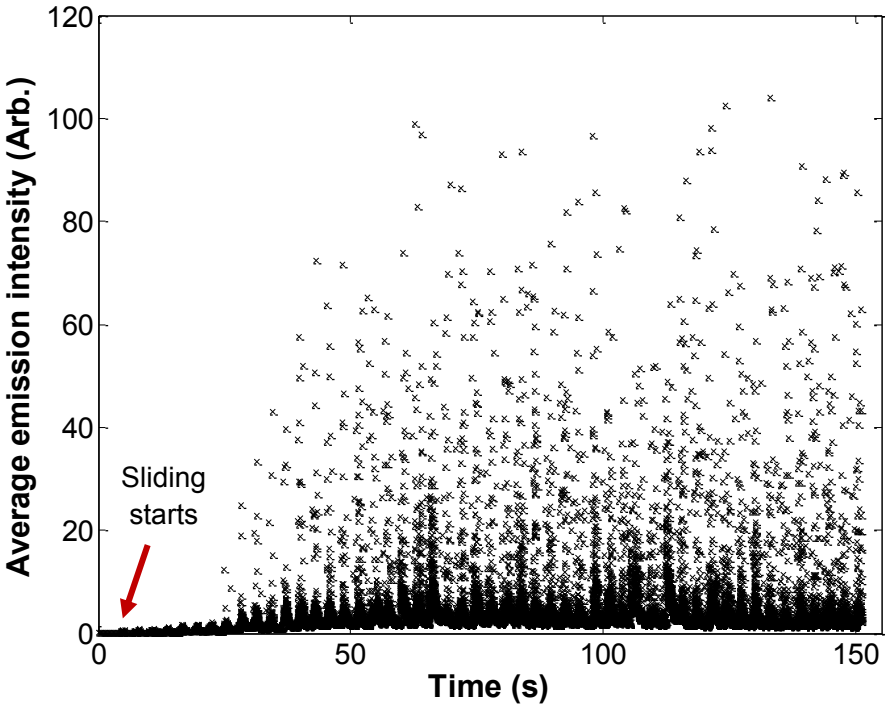

Figure 4.2: Variation of triboemission intensity with time showing intermittent triboemission.

It can also be observed in Figure 4.3(a) that peak emission intensity increases monotonically for the first 30 seconds after which the peak intensities do not follow any trend as seen in Figure 4.3 (b). The cyclic emission could be a result of several possibilities. Firstly, it could be either that the disc does not rotate in one flat plane, such that a particular section of disc is loaded more severely than other, or it may be that a particular section is more prone to emission

because of inhomogeneity. Alternatively, it could be because of a charging-discharging cycle. It was verified that there is no asymmetrical loading of disc as the wear depth remained similar at all sections along the wear track. Hence, this reason for the sporadic bursts of emission was discounted. Such rapid bursts of emission have been previously observed by Nakayama *et al.* [160] and Molina *et al.* [182] and more recently by Ciniero [183] *et al.* for ceramics (Al_2O_3) which are all electrical insulators. Molina concluded that frequency of occurrence of low-level electron-emission could be random, while large bursts of triboemission may arise from deterministic processes, pointing out that surface charge on insulators play an essential role in the large bursts of triboemission. Any comparison with previously reported trends of TE particularly, the observations regarding the duration between each burst as well as the rise and fall characteristics should take arrangement of the detector into consideration. Measurements by Molina *et al.* and Nakayama *et al.* were based on single point detectors located in close proximity to the stationary stylus specimen which enabled only measurement close to the contact to be obtained where as in this experiment, emission from the whole wear track is recorded. As discussed above, the current experimental set up is greatly sensitive to after-emissions away from the contact. The measurement of triboemission trends presented in this chapter is the first ever from PTFE surface, because previously reported measurement of emission from PTFE upon scratching did not concentrate on the variation of emission with time [159], [160]. Therefore, there is no data available to compare with this observation. A very high emission detected for this material, combined with the fact that many studies on triboelectrification have focussed on PTFE materials (including the study by Baytekin [184] showing rubbed PTFE could initiate chemical reactions), suggest that this material is an excellent candidate to be the focus of this study.

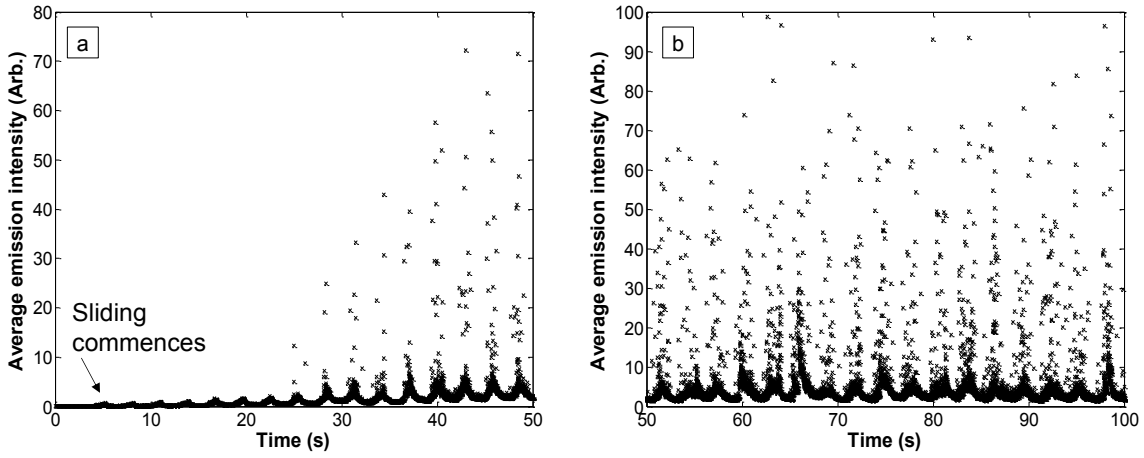

Figure 4.3: Cyclic nature of triboemission based on average phosphor-screen intensity data (a) 0-50 seconds (b) 50-100 seconds.

At this point, it is not possible to determine exactly the reasons for such characteristic large bursts. However, many factors such as resistivity of material, the surface hardness, surface charging, gas discharge, bond disintegration, stored strain energy, material inhomogeneity, decreased work function, defect excitation and material phase transformation have been suggested to affect triboemission, though several of these are unlikely to be applicable to PTFE (polymer and insulator).

Figure 4.4(a) shows the average emission during the entire duration of sliding. This is done by averaging 25820 frames. This figure shows that the maximum emission is at the position where tip contacts the disc. It also indicates that the emission occurs from the entire surface of the disc which is quite puzzling because the calculated effective Hertzian contact radius is only 50 microns which could increase to 200 microns as sliding progresses. Moreover, a magnification of ten times is observed for features at the disc level (Note that the bottom MCP is located 10 mm above the sliding surface). This is evidenced in Figure 4.4(b) which shows the shadow effect caused by the steel arm. The 1 mm diameter steel arm that holds the diamond tip showed up as 1 cm in dimension on the phosphor screen image. This magnification could be due to the arrangement of MCPs and phosphor screen or it could arise from the different collisional path lengths which could vary depending on the properties and energy of the emitted particles. Additionally, the steel could conduct some electrons thus preventing them to reach bottom plate of the MCP.

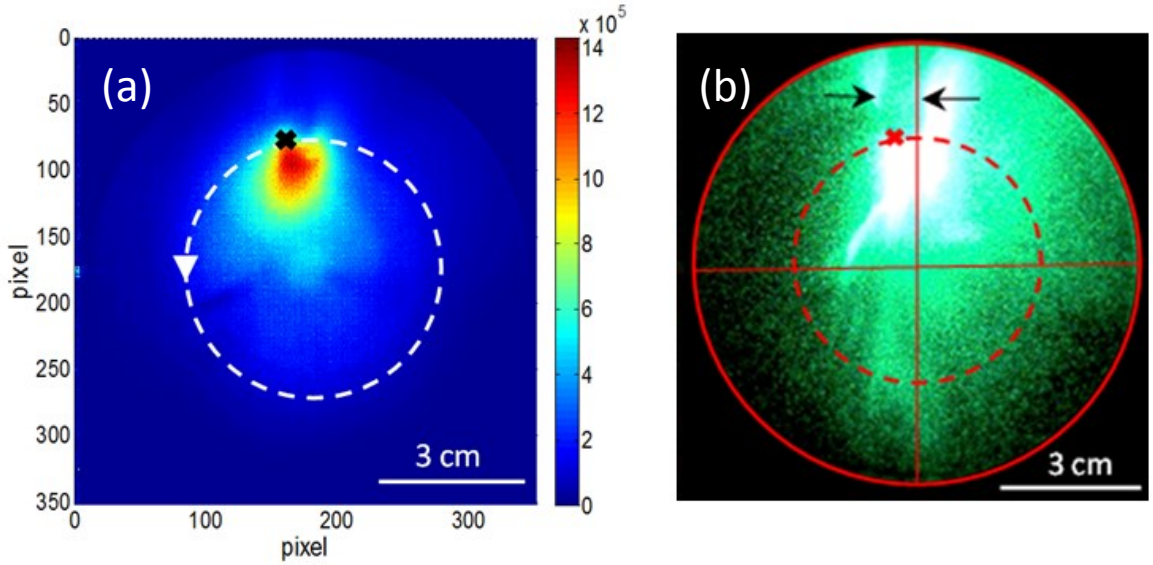

Figure 4.4: (a) Average triboemission during sliding for 150 seconds from sliding between diamond pin vs PTFE disc as observed from the phosphor screen. Dotted lines show the wear track and direction of rotation. (b) Single phosphor screen image showing wear track and position of the contacting tip. Black arrows show the dimension of the steel arm.

The average triboemission plot shown in Figure 4.4(a) does not account for rotation of the disc and therefore unable to provide information regarding the location of triboemission sites on the disc. Alternatively, if all the images are rotated back incrementally corresponding to the angle that the disc has rotated forward during the test, it would correspond to a condition where the disc is stationary while the contact moves in a circular path around the wear track. This is made possible by measuring the angular position of the disc and synchronising with the frame acquisition rate. Subsequent averaging of these rotated frames shows the variation in emission of the disc surface during the entire test and locates the site of intense triboemission on the disc surface as shown in Figure 4.5. From Figure 4.5 it is confirmed that maximum triboemission occurs from a certain location along the wear track. This constant source of emission gives rise to periodic fluctuation (corresponds to one rotation of disc) in emission intensity observed in Figure 4.3. The emission may be caused by damage of the specimen surface or inherent surface defect. This method of analysing thus provides a new technique of monitoring the location of defects as well as the evolution of wear in real time for various materials. The limitation of this technique is that it is a destructive technique that requires scratching the specimen and the location site of triboemission is still quite a large area and there are some out of track areas that seem to emit. To overcome this obscurity, individual frames should be studied.

However, triboemission, seemingly emitted from the entire disc surface could occur due to two possible reasons. Firstly, some triboemission events may occur away from the contact. Secondly, some emission events could release large quantities of energetic electrons, ions and photons which illuminate the entire phosphor screen. In this case, the emitted particles could undergo numerous collisions that alters their initial path of travel or triggers further emission and collisions. The former is referred as after-emission events while the latter is referred here as avalanche events. It should be noted that the asymmetric emission distribution shown in Figure 4.5 corresponds to the fluctuations in signal shown in Figure 4.3.

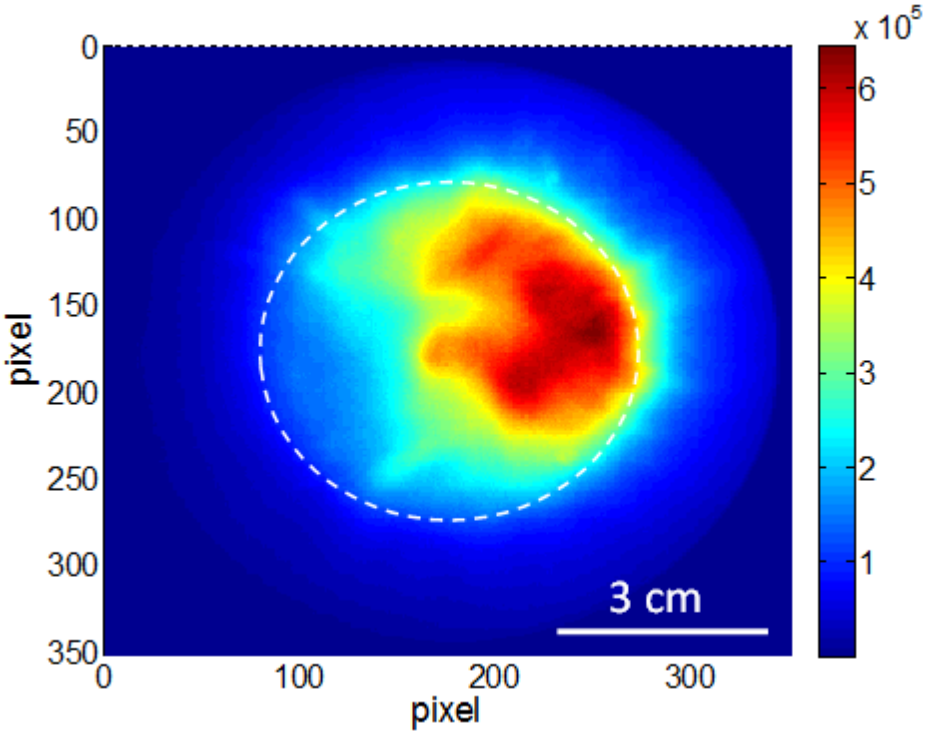

Figure 4.5: Rotated average for the entire test after each frame is rotated back to the angle it turned during the entire period of test. This provides the position of intense emission on the disc surface.

After-emission Events

Figure 4.6 demonstrates an after-emission event using selected frames between 92.8486 s and 95.8234 s which is the 31st rotation. The duration of such after-emission events is usually between 2.4-3 seconds which is one complete revolution of the disc. After completion of one revolution, the emitting site re-enters the contact. On re-entering, there is a possibility of two events occurring; either quenching of triboemission occurs or further boosting of emission occurs. However, there is little robust evidence to confirm whether there is any interaction between the spontaneous triboemission from the contact and after-emission from a damaged surface. Even though the cyclical trend of emission peaks is confirmed in Figure 4.2, the effects of the both emission events on each other *i.e.* whether such interactions lead to further intense emission or lowering of net emission could not be verified.

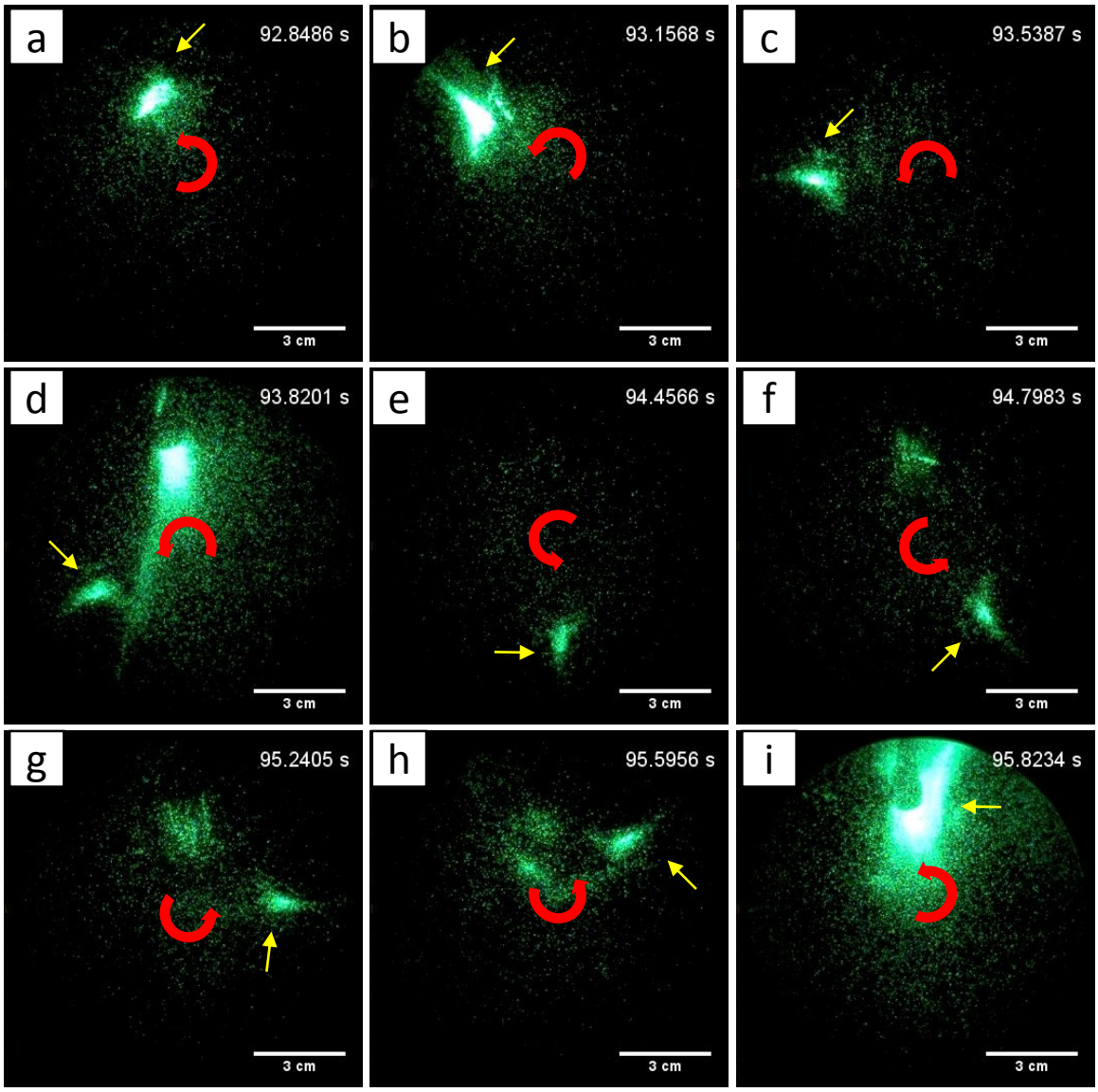

Figure 4.6 Selected frames between 92.8486 s and 95.8234 s (31st rotation) which illustrate after-emission from disc surface. The red arrow denotes the rotation of the disc.

Avalanche Events or High Intensity TE

Figure 4.7 presents selected frames which show high intensity triboemission events. These triboemission events are sporadic in nature, and of very short duration (less than 6 ms). Triboemission mostly emerge from the contact although powerful emissions away from the contact is common. Frames a-d, h and i show triboemission emitted from the contact while frames e-g show emission from disc surface, away from the contact. This spontaneous emission occurring outside the contact, has not been observed before, and is tentatively attributed to viscoelastic relaxation of the polymer material following deformation in the contact. As mentioned earlier, the periodic fluctuation in emission intensity also confirms that whenever a particular site on the wear track passes under the pin (corresponds to one rotation of disc), a

large amount of emission is observed. Various theories explain such avalanche events which range from gas discharge, debris detachment and fly-off, electron-recombination and subsequent collision based on their energy. Relevant mechanism and sources are discussed in detail in the next section.

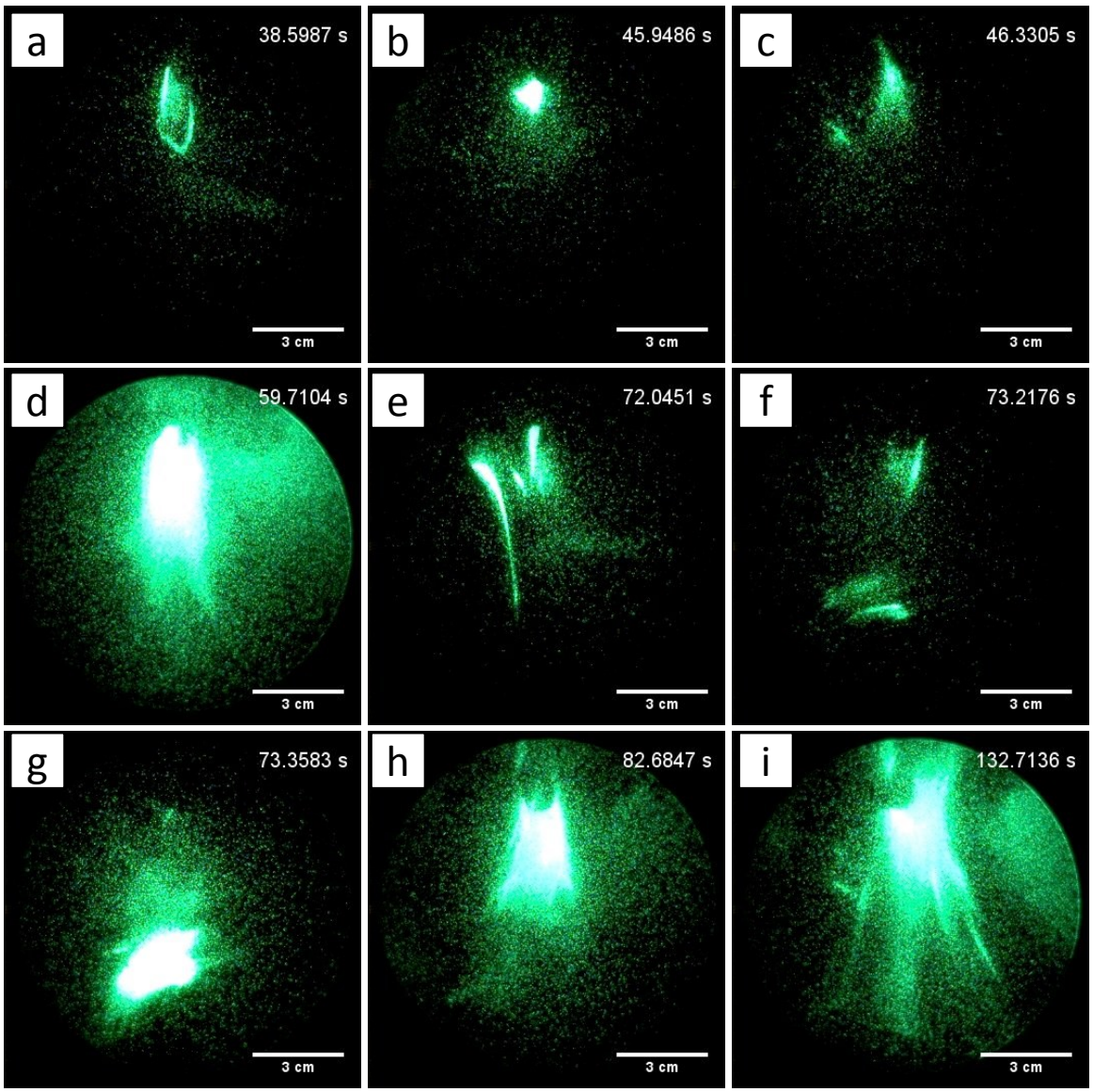

Figure 4.7: Selected high intensity triboemission events.

4.2 Mechanism and nature of the Triboemission in vacuum

Although no separate tests were done to confirm the proportion of electron, radicals, positive ions and negative ions comprising the emission, the manufacturers of the MCPs [175] claim that the detection efficiency for UV photons (30-150 nm) to be extremely low and nil for visible radiation. However, even if the detector cannot detect UV and visible light, it does not mean

that they are not emitted. In fact Nakayama *et al.* have observed tribo-photon emission upon scratching sapphire against a diamond pin under various dry air pressures ranging from atmospheric pressure to 10^{-1} Pa [130].

Triboemission (electrons or ions) from the surface act as seeding electrons and excite the molecules of the surrounding medium by colliding with them. If the energy is high enough, these collisions can also cause ionization. Another source of seeding electrons is tribocharging and subsequent charge separation between the surfaces that accelerates electrons e^- between the oppositely charged surfaces due to an intense electric field. These electrons then collide with air molecules, M, to cause electron avalanche producing additional electrons, e^-, and positive ions of the air molecules, M^+, ($e^- + M \rightarrow e + M^+ + e^-$). This is known as dielectric breakdown. Such a mechanism can sufficiently explain the high intensity avalanche events shown in Figure 4.7. Furthermore, UV photons are also likely to be emitted during this process when electrons in the excited state of a molecule fall down to the lower or ground level. The photons possess energies corresponding to the energy difference between the two energy levels.

However, the tests conducted here were done in high vacuum (10^{-2} Pa) hence gas breakdown is unlikely, due to low pressure test conditions. This conclusion comes from Paschen's law of gas discharge that states that the breakdown potential of a gas, *Vs*, depends on the product of the gas pressure p, and the electrode distance *d* [185]. The curve of *Vs* against *pd* gives a minimum at which breakdown of the gas occurs most easily. At the minimum, the value of *d* increases with a decrease in the value of *p*, since the *pd* value is constant for a given gas. Keeping *d* constant, as gas pressure *p*, is decreased the number of molecules per unit volume decreases, and the mean free path of the electrons becomes longer so that the probability of the collision of electrons becomes smaller. Moreover, Nakayama *et al*. reported that at pressures lower than 10 Pa, photon emission is due to frictional heating rather than plasma from gas discharge [130].

Nevertheless, a small number of residual gas molecules may remain in the system as well as a few trapped gas molecules could be desorbed from or through the polymer. The fracture products as well as remnant volatile gas may lead to a momentary increase in pressure within the crevices of the fresh surface and undergo breakdown because of the electric field gradient leading to emission of photons as well as products of gas discharge-electrons and ions. Additionally, some of the photons could be generated from the excitation of crystal defects.

Due to the detection efficiency of the MCPS, it can be assumed that much of the recorded emission consists of electrons and ions. Is it not necessary that all triboemission that are generated at the contact surface reach the detector as some particles could be conducted away by nearby metal surfaces such as the stainless steel stylus which holds the diamond tip. This raises two questions to be discussed. Firstly, how do these particles leave the surface of the PTFE and/or diamond and reach the detector? Secondly, where do they originate from in an organic polymer such as PTFE or an electrical insulator such as diamond? The emitted particles reach the detector according to their kinetic energy with respect to the bias voltage of the bottom MCP (grounded in this study). The second question regarding the source of TE is fundamental because the electronic configuration and chemical structure of both PTFE and diamond (*i.e*. the covalent bonding which makes them insulators) is very different to conductors (metals) and semiconductors (oxides) that have been widely used in triboemission studies, on which many accepted mechanisms are based. The mechanisms which are described in detail in **Chapter 2** are briefly summarized below.

Nakayama attributed TE to the creation of fresh surfaces and wear. He discussed that TE depends on the resistivity as well as surface hardness of the material. Subsequently, they proposed the mechanism of generation of triboplasma in a gaseous environment that occurs due to breakdown of gas molecules due to intense electric field generated between two contacting solid bodies because of tribocharging. It was proposed that tribocharging was driven by a contact potential difference between the tribopair. The electrons are transferred from a surface with a low work function to the mating surface with a high work function, resulting in the former having a positive potential and the latter a negative potential. According to this tribocharging mechanism, the diamond surface may transfer electrons to PTFE as it has a lower work function (5 eV, changes depending upon the crystal plane) compared to PTFE (5.75 eV [191]). The electric field generated by tribocharging could accelerate some electrons to be emitted from the contact surface as triboemission. Thus TE is related to the electron work function of a material which is defined as the energy required to extract an electron from its surface.

Another likely reason for electron emission is crack generation and subsequent dielectric breakdown of gas due to intense electric field owing to charge separation between the opposite faces of the cracks. Recently, Ciniero *et al.* reiterated this mechanism for TE observed in vacuum, where the fracture of the oxide layer causes crack faces with an uneven distribution

of charge leading to creation of high strength electric field, causing electron bombardment and subsequent gas discharge [183]. The uneven distribution of charges was attributed to piezoelectricity and crystal defects while the gas breakdown in their high vacuum setup was due to fracture products and desorbed volatiles which increased the pressure within the crack.

Dickinson *et al.* [186] and Molina *et al.* [187] suggested a mechanism entirely different to the field emission mechanism (dielectric gas breakdown caused by electron avalanche due to strong electric field) suggested by Nakayama *et al.* and Ciniero *et al.* They suggested that plastic deformation during sliding might locally reduce the work function of the surface because a strained surface leads to growth of surface defects, inhomogeneity and increased dislocation density. Meanwhile Abdel-Aal *et al*. [187, 188] linked TE to a semiconductor-to-metal phase transformation during sliding wear. However, Abdel's suggestion of semiconductor-to-metal phase transformation during sliding wear cannot be applied to polymers. From a polymer perspective, the mechanism of charge generation and TE can be quite different to that of oxides (semiconductor) mainly because polymers are insulators in which electrons in the valence band are separated from the conduction band by large band gap. Hence, the emission of electrons from covalently bonded materials such as PTFE and diamond is hard to conceive by many. Moreover, polymers are highly deformable and softer than any oxide which are typically very hard and brittle. PTFE is made of highly coiled $–(CH_2\text{-}CH_2)–$ chains having both crystalline and amorphous regions while oxides have a crystal lattice arrangement. Therefore, the representation of a well-defined micro-crack on PTFE surface setting up an electric field due to charge separation seems implausible.

It is understood that a polymer chain possesses dangling C bonds also known as immobilized radicals. However, scission of polymer chains generates free radicals are highly energetic, short-lived and possess kinetic stability. The free radicals immediately interact with an electron to acquire a net charge. This process is known as homolytic bond scission. Scratching a PTFE surface with diamond stylus can indeed cause homolytic bond disintegration [190] creating micro-sized fragments of cations or anions. For certain ionic molecules, electrons or ions could also be generated directly from the breaking of molecular bonds unevenly (heterolytic scission). However, this cannot happen for in PTFE because of the covalent bond strength and the hardness imparted by group electronegativity [191]. However, normal and shear forces at the contact can thermally stimulate electron emission.

Scratching a PTFE surface can also give rise to emission of low energy electrons (1-4 eV) termed as "exoelectrons". Exoelectrons are emitted from surface when it is excited by irradiation (photo-stimulated) or deformation (tribo-stimulated). The excitation results in a non-equilibrium state and exoelectron emission accompanies the relaxation process experienced by the surface to attain equilibrium.

Scratching of the PTFE surface can also release the trapped electrons present on a dielectric surface known as "cryptoelectrons". Cryptoelectrons [98] are defined as the electrons existing in a material, irrespective of their source (*e.g.* surface states, impurities, bulk defects), with energies significantly different from those expected from molecular states (or bands) in the material. The estimated electron density on PTFE is greater than 10^{13} electrons/cm^2.

Finally, tribocharging could also generate low-energy X-rays and Camara *et al.* reported the radiation of X-ray from peeling of 3-M scotch tape in vacuum for the first time in 2008 [192]. The tape did not emit X-rays continuously, but in short nanosecond bursts, accumulating enough energy to produce an X-ray image of a finger in a second. Of course, the X-ray produced is dependent on the electric field which will vary due to both the geometry of the system and the change in the charge density. Therefore, X-ray emission is also plausible and the detector efficiency is quite good for X-rays.

Based upon the discussion presented above, the following suggestion about the observed nature of emission can be made.

(i) High intensity or Avalanche TE whose duration is less than$1/10^{th}$ of a second and scintillates almost the entire phosphor screen (Figure 4.7) may be because of the trapped electrons (crypto electrons), energetic radicals that are liberated by scratching with the diamond tip and potentially X-rays.

(ii) After-emission phenomena (in Figure 4.6) could be due to exoelectron emission that accompanies the relaxation of strained polymer chain after contact with the tip.

(iii) The interaction of emitted electrons with charged ions and free radical may be accompanied by further emission of photons, electrons and ions due to gas discharge.

(iv) Some PTFE fragments (debris) after detaching from the surface can even reach the lower MCP, which is at 0 volts, and then lose their charge to the top plate at 1.5 kV and subsequently sucked out of the system by the turbo-pump maintaining the vacuum.

The triboemission, must also affect the charging of surface as these can also be considered as discharging events. Specifically, the emission of charged particles detected by the MCP suggests the PTFE surface will be left with regions of positive and negative charge. It is also possible that the emitted electrons (both exoelectrons and cryptoelectrons) may react with radicals on the surface to form charged electret (anionic or cationic) fragments. The distribution of cationic and anionic fragments and emission sites within the contact as well as on the wear track thus contributes to non-uniform contact electrification. This goes some way to explain the lack of consensus over the last two decades regarding the mechanisms of contact electrification in the case of polymers, *i.e.* whether it is due to electron transfer, ion transfer or mass transfer [193]. It is only very recently that concrete evidence supporting a mass transfer mechanism and an uneven distribution of charge upon rubbing surfaces has been provided [136, 139, 193, 194].

4.3 Conclusions

The current research presents the spatial distribution of triboemission from a PTFE surface for the first time when scratched with a diamond stylus in vacuum. The vacuum tribometer is integrated with a micro channel plate and phosphor screen to measure the distribution of emitted electrons, ions and photons. It also enabled the monitoring of 'after-emission' phenomena.

The majority of emission originates from the contact area of the tip while the after-emission is observed from a specific area of the wear track and occurs continuously over one cycle. The emission occurs in discrete bursts and varies cyclically with time between a minimum value and a maximum value. It is suggested this triboemission behaviour results from the breaking of certain polymer chains, relaxation of other chains and generation of micro sized debris. All these events influence the tribocharging that generates the electric field to be experienced by the emitted electrons.

The maximum or peak emission has been attributed to combined emission of cryptoelectrons, X-rays, gaseous ions, and radicals as well as charged polymer fragments. The after emission has been attributed to exoelectrons emitted from the surface due to strain relaxation. Some weak photons emission may originate from remnant gas breakdown, or electron-ion recombination, or defect excitation but their detection efficiency is very low.

Now that the emission from PTFE has been characterised in a vacuum, the next step is to study its behaviour under ambient and liquid submerged conditions.

Chapter Five

Triboemission Interactions in Air

In the previous chapter it was shown that polytetrafluoroethylene, PTFE, generates triboemission in vacuum conditions. One of the objectives of this thesis is to develop methods to study triboemission generation and its interaction with various environments. To achieve this, the current chapter delves further into the understanding the origins of triboemission from rubbing contact when air is the surrounding medium. This is done by using the Airplasma tribometer developed for the purpose of viewing the contact through a transparent pin specimen. From the literature review, it was discovered that some materials exhibit triboluminescence phenomena (an excitation of the crystal structure) upon mechanical excitation while some others generated triboplasma (an electric breakdown of the surrounding air, similar to atmospheric lightning phenomena). To explore this further, various kinds of materials (metals, polymers, ceramics, and composites) are tested to understand the influence of material properties and operating conditions on the resulting phenomena (triboluminescence or triboplasma generation). Triboplasma refers to the gas breakdown and the resulting ionization and excitation of gas molecules while triboluminescence is the excitation of atoms and molecules of the contacting surface upon mechanical shearing.

This chapter is divided into two parts titled ‘Mechanisms’ and ‘Materials’ respectively. The former elucidates the processes related to triboemission in air while the later explores into possible role of various material properties. From the literature survey, it was evident that although triboplasma has been studied for a wide range of materials, its evolution with time has been completely ignored. Therefore, the overarching aim of this chapter is to study the variation of emission with time and elucidate the transient behaviour of triboplasma generation and its relationship to charging and other factors that affect it. These transients are observed for the very first time, by rubbing polymeric materials against a transparent sapphire hemisphere. This is achieved by using UV-sensitive, EMCCD camera capable of high frame rate measurements of plasma distributions around sliding polymer contact. A simplified model is developed based on previous knowledge of the phenomenon of gas discharge between two separating electrodes

and compared with the experimentally observed triboplasma produced in situ during continuous rubbing. The section titled 'Materials', reports the emission characteristics of a range materials (previously not reported) such as certain polymers (Nylon, PVDF, Polycarbonate, Polystyrene, PMMA), titanium alloy, polycrystalline diamond (PCD) and composites of UHMWPE.

5.1 Mechanism

As discussed in the literature review, the mechanism of triboplasma generation in air (electric breakdown of surrounding medium) has been known for some time. However, little is known about the influence of various material properties and environmental conditions on this behaviour. First, a simplified model is developed which predicts the distribution of plasma around the contact and aids comparison with the experimental measurements.

5.1.1 Model for prediction of plasma distribution

The breakdown voltage, $\boldsymbol{V_B}$, necessary to cause an electric arc between electrodes during a Townsend discharge process, can be predicted as a function of the product of the gas pressure, p, and the gap length, d [185];

$$V_{Bi,j} = \frac{Bpd}{ln(Ap\boldsymbol{d_{i,j}}) - ln\left[ln\left(1+\frac{1}{\gamma_{se}}\right)\right]} \qquad \text{Equation 5.1}$$

where γ_{se} is the secondary ionization coefficient and A and B are constants; the former is the saturation ionization in the gas and the latter is related to the excitation and ionization energies [185]. These constants have been determined experimentally to be 112.50 kPa cm^{-1} and 2737.5 V kPa cm^{-1} respectively, for ranges of E/p from 450 to 7500 V kPa^{-1} cm^{-1} [185]. The well-known Paschen curve, obtained by plotting *pd versus* $\boldsymbol{V_B}$ from Equation 5.1, has a minimum at a *pd* value of around 1 Torr cm (~1.333 Pa m), with $\boldsymbol{V_B}$ increasing above and below this value. As explained in **Chapter 4**, this is because, at low *pd* values, there are fewer molecules between the electrodes so that high voltages are required to produce electrons to initiate the avalanche process; while at high *pd* values the density of molecules between electrodes increases the propensity of collisions that reduce electron energy and therefore requires a higher voltage to cause the gas ionisation.

Equation 5.1 can be used to predict the approximate distribution of plasma generated around the contact for the experimental test conditions used in this project. This approach involves the following steps:

1. Discretisation of the vertical gap heights, $d_{i,j}$, in the region around the contact - *i.e.* a 2D array is created where each value is the gap height between the disc and the hemisphere specimen at location *i,j* (Figure 5.1).This distribution of gap heights is obtained by measuring the topography of both specimens post-test using an optical profilometer.
2. The mesh of gap heights from Step 1 is used in two ways: *i*) to calculate the breakdown voltage at every point, $\boldsymbol{V_{Bi,j}}$, according to equation 1, *ii*) to calculate the actual electric field, $\boldsymbol{E}$, at every point according $\boldsymbol{E}_{i,j}=V_{i,j}/d_{i,j}= (Q/C)/d_{i,j}$, where Q is the surface charge – estimated by assuming it is proportional to the Hertz contact pressure in the wear track. C is the capacitance between the pin and disc surfaces– assumed to be a constant and entirely dependent upon the geometry of pin and wear track groove, and the separation between them. Thus, $\boldsymbol{E}_{i,j} \approx Q/d_{i,j}$.
3. The breakdown voltage at every point, $\boldsymbol{V_{Bi,j}}$, (from 2*i*) is divided by the $\boldsymbol{E}_{i,j}$ (in 2*ii*) to give a 2D map showing the propensity for emission at every point (locations where the potential difference due to triboelectrication is high compared to breakdown voltage will have a higher propensity to produce plasma and vice versa).

This simplified approach involves a number of assumptions: *i*) the accumulated surface charge density in the wear track is proportional to the contact pressure distribution, *ii*) counter specimens charge uniformly, with opposite polarity, *iii*) the gas pressure is constant and equal to atmosphere, *iv*) there are no aerodynamic effects so motion of the disc relative to the contact does not distort the distribution of plasma, *v*) no material transfer occurs by adhesion due to presence of charges of opposite polarity hence the generated wear debris do not remain at the contact to interfere with the contact geometry or net charge estimation. Further inaccuracy in this approach is due to the fact that Equation 5.1 is strictly one dimensional. In addition to this, deviations from Paschens' law have been reported for micron sized gaps [196].Thus asperity height distribution and topography will affect both the breakdown voltage and the electric field strength at a point at or near the contact.

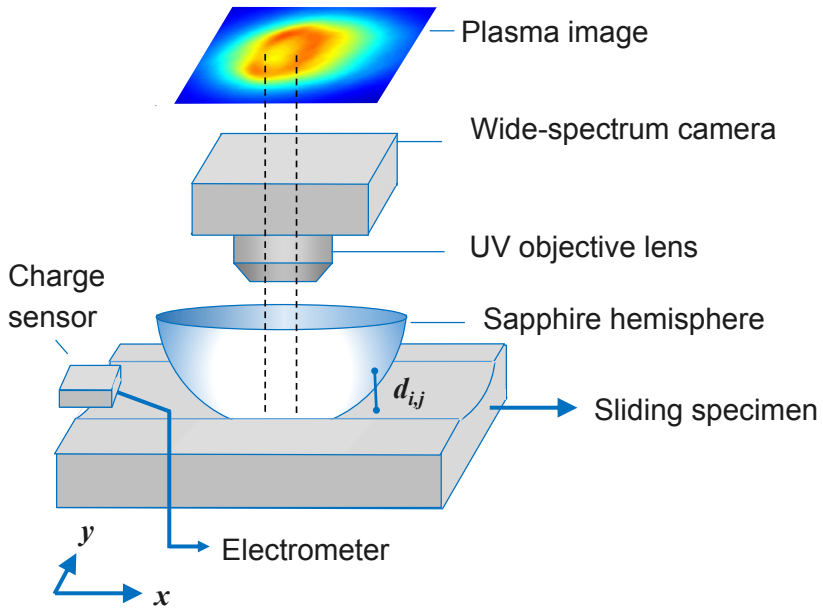

Figure 5.1: Schematic diagram of test set up showing the sliding contact between sapphire hemisphere and polymer disc wear track.

5.1.2 Experimental study of steady state and transient behaviour of plasma

To further understand the effect of material properties and charging on plasma characteristics, two widely used polymer material were chosen. In addition to PTFE (for which TE measurements in vacuum were presented in **Chapter 4**), Ultra-high molecular weight polythene (UHMWPE) is also tested in this chapter and the following chapter. The rationale behind choice of these two polymers is based on their low wear (UHMWPE) and low friction (PTFE) properties which facilitate its use as an ideal tribological material in engineering and biomedical applications. Furthermore, PTFE and PE have been studied extensively with respect to contact electrification behaviour [137, 197, 198]. It is understood that, when rubbed, their dominant charging mechanism is the homolytic scission of the C-C bond which produces free radicals with markedly different electronegativities followed by electron transfer to leave regions of cations and anions on surfaces [199]. The crystallinity of polymer samples was measured using X-ray diffraction and found to be 54% and 40% for UHMWPE and the PTFE respectively. As previously mentioned in **Chapter 3**, sapphire was used for the stationary specimen, since it is transparent and enables viewing of plasma discharge within the contact.

A sliding contact was produced by loading a single crystal Al_2O_3 hemisphere with diameter of 5 mm against a rotating polymer disc (Figure 5.1), while a UV sensitive camera (Hamamatsu ImagEM X2) with UV-13X lens (Newport) was focussed through the Al_2O_3 specimen (Swiss

jewel, USA) onto the contact to obtain images of the generated plasma. A charge sensor (of the type developed in [153]) as positioned diametrically opposite the contact with its tip 2 mm above the disc surface and was connected to an electrometer (Keithley 6517B) to record the accumulated charge signal. For certain tests, the camera was replaced by a spectrometer (Ocean Optics QE Pro) to measure the optical spectra of the plasma. All the tests were carried out at 2 N load (corresponding to initial average pressure of 40 MPa for PTFE and 16-52 MPa for UHMWPE) and 2.4 m/s sliding speed. After each test, scans of the specimen surfaces were performed using a variable pressure SEM (pressure of 60 Pa, 15 kV beam voltage and ×100 magnification) and a Veeco optical profilometer.

5.1.2.1. Steady State Plasma behaviour

Figure 5.2 (a) and (b) shows time-averaged plasma intensity images, recorded during rubbing tests on the PTFE and UHMWPE specimens using the high-speed camera with frame rate of 70 fps for 1 minute. Although the shape of the triboplasma region agrees with those obtained by Nakayama for single crystal oxides (*e.g.* [149][147]), there are two main differences. First, in this case the size of the plasma region is an order of magnitude larger (mm vs. 100s of μm), which can be attributed to more compliant specimens, which produce a smaller gap between specimens, and extends the region of the minimum breakdown voltage away from the contact. Second, as discussed below, the emitted plasma exhibits a protrusion at the front of the contact as well as the rear (note that PTFE image has been cropped to have the same scale).

Figure 5.2 c) shows the results from the plasma intensity model described in Section 5.1.1. The three images in this figure have certain features in common, namely *i*) an approximately elliptical distribution of plasma around the contact, *ii*) a minimum within the contact area, and *iii*) a tail stretching behind and in front of the contact This shows that the plasma distribution can largely be explained by Paschen's law in that: *i*) most intense plasma is generated at a distance where the breakdown voltage according to Equation 5.1 is lowest, *ii*) low levels of plasma are generated within the contact due to limiting values of *pd* that prevent discharge, *iii*) the tail is extended behind the contact due to the charged surface of the wear track as it leaves the contact, *iv*) the tail extending in front of the contact due to the re-entry of the charged wear track (*i.e.* the electric field on the wear track has insufficient time to be passivated between leaving and re-entering the contact on the subsequent disc rotations). This is supported by reports of the half-life of corona charged polyethylene being ca. 30 hours [136] and that of tribocharged PTFE being ca.60 hours [197], at 60% relative humidity.

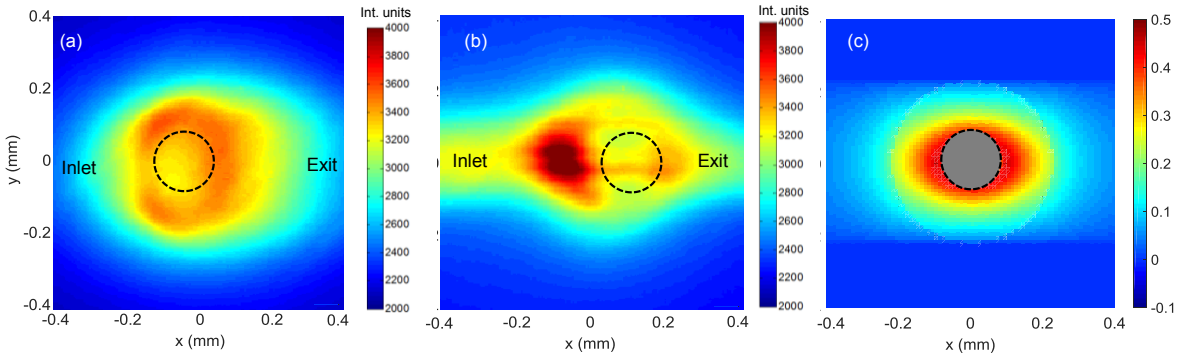

Figure 5.2: Plasma distributions; a) Measured from PTFE contact, b) Measured from UHMWPE contact, c) Predicted by simple air discharge model, based on contact conditions from PTFE test. The colour bar on (a) and (b) shows the intensity counts of the camera image while colour bar on (c) shows the propensity of discharge.

5.1.2.2. Spectra of Triboplasma

Further confirmation that the plasma generation results from air breakdown is given in Figure 5.3, which shows the emission spectra of the plasma, measured by the spectrometer during sliding tests on the two polymers. The excited atoms or ions emit characteristic photons which can be measured with optical emission spectrometry. Peaks are observed at 296, 314, 336, 355, 377, 386, 404 and 425 nm. The majority of peaks between 300 and 400 nm can be attributed to N_2 Second Positive System and N_2^+ First negative System (these band transitions are characteristic of lightning discharge [200]), and agree with those shown earlier by Nakayama for inorganic oxide materials (*e.g.* [148, 150]). The emissions recorded between 650 and 670 nm are attributed to the N_2 First Positive System (FPS). The emission peaks 404 and 425 nm is attributed to CH radicals.

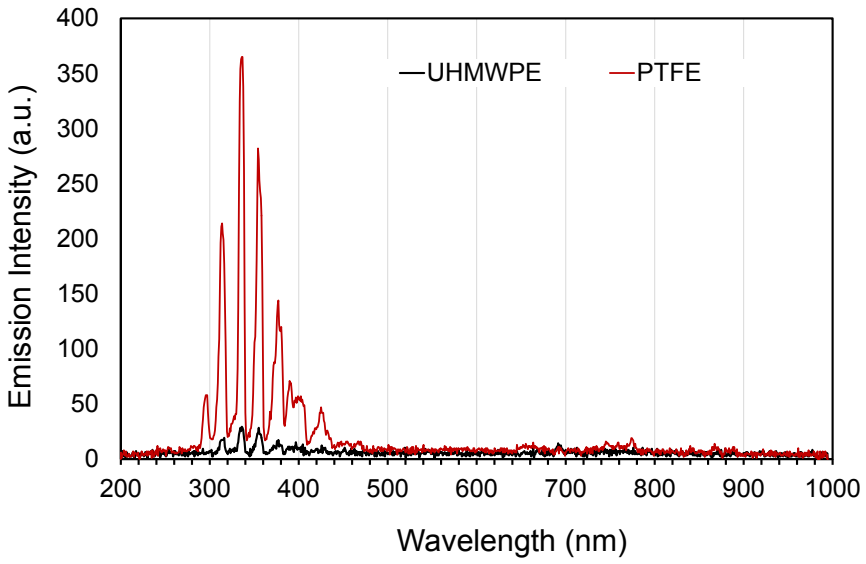

Figure 5.3: Plasma emission spectra for UHMWPE and PTFE sliding contacts.

Nitrogen FPS (first positive state), SPS (second positive state) as well as FNS (first negative state) are a result of direct electronic excitation and ionization which are likely to occur during the electronic avalanche propagation where bombarding electrons are highly energetic. Various kinds of reactions resulting in metastable molecules and molecular ions have been discussed in detail in [201]. A full kinetic study of the post-excitation phase requires analysis of the pressure dependence of temporal decays of the visible emissions and is beyond the scope of this research. It should be noted that the energies associated with the transitions states (2.9–4.18 eV) is comparable to the energies of many covalent bonds (discussed later), which highlights the possibility that the plasma generation may play a role in tribochemical reactions.

5.1.2.3. Transient plasma measurements – Seconds timescale

Figure 5.4 plots the maximum plasma intensity variation with time, at a frame rate of 2 Hz in order to monitor variations occurring over a period of seconds. In this figure, each data point represents the maximum intensity in a camera frame. It can be seen that there are marked differences between the materials tested; PTFE shows an initial sharp peak in plasma emission followed by a steady decline, while UHMWPE shows a fluctuating variation.

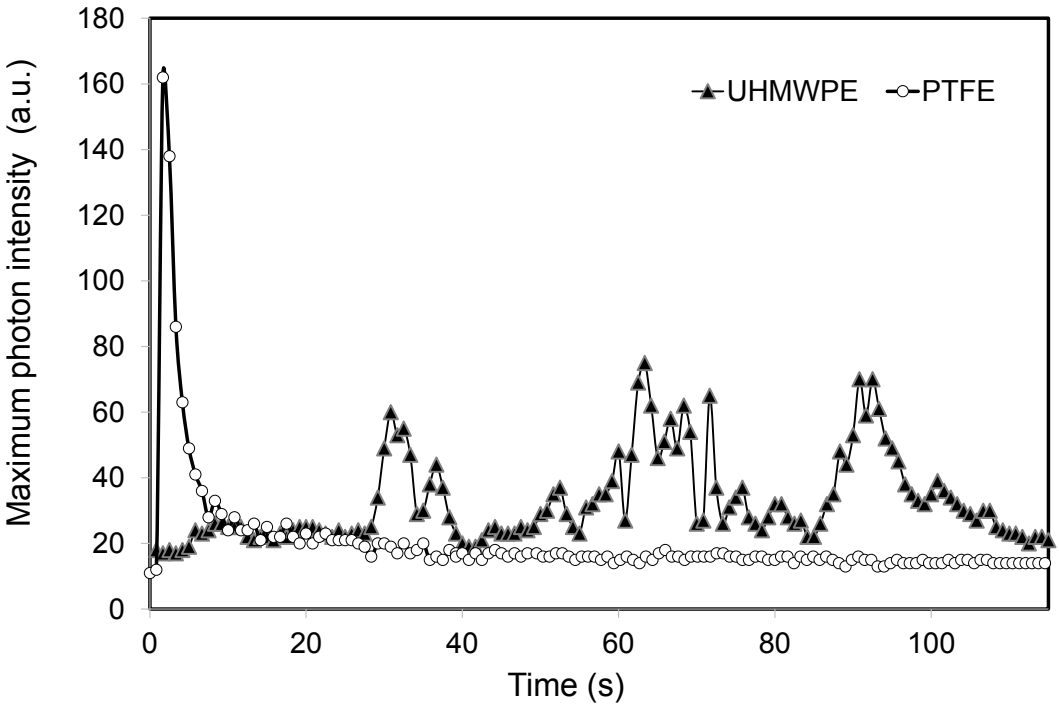

Figure 5.4: Variation in maximum emission intensity with time for PTFE/sapphire and UHMWPE/Al_2O_3 contacts, loaded with 1.4 N and sliding at a speed of 2.8 m/s obtained with frame rate of 2 Hz.

To investigate the cause of these transient variations, sliding tests were carried out on the PTFE specimen in which friction coefficient and wear depth were also monitored. From Figure 5.5,

it can be seen that friction remains approximately constant throughout the test, while photon emission intensity varied by a factor of seven. Although wear rate is highest during the first two seconds compared to the later stages (due to reduction in contact pressure), it is not proportional to the observed plasma intensity variations. This does not, however, preclude the indirect influence of wear, since a number of studies [136, 138, 139] have suggested that charging behaviour is governed by material transfer between specimens, which can be independent of wear rate.

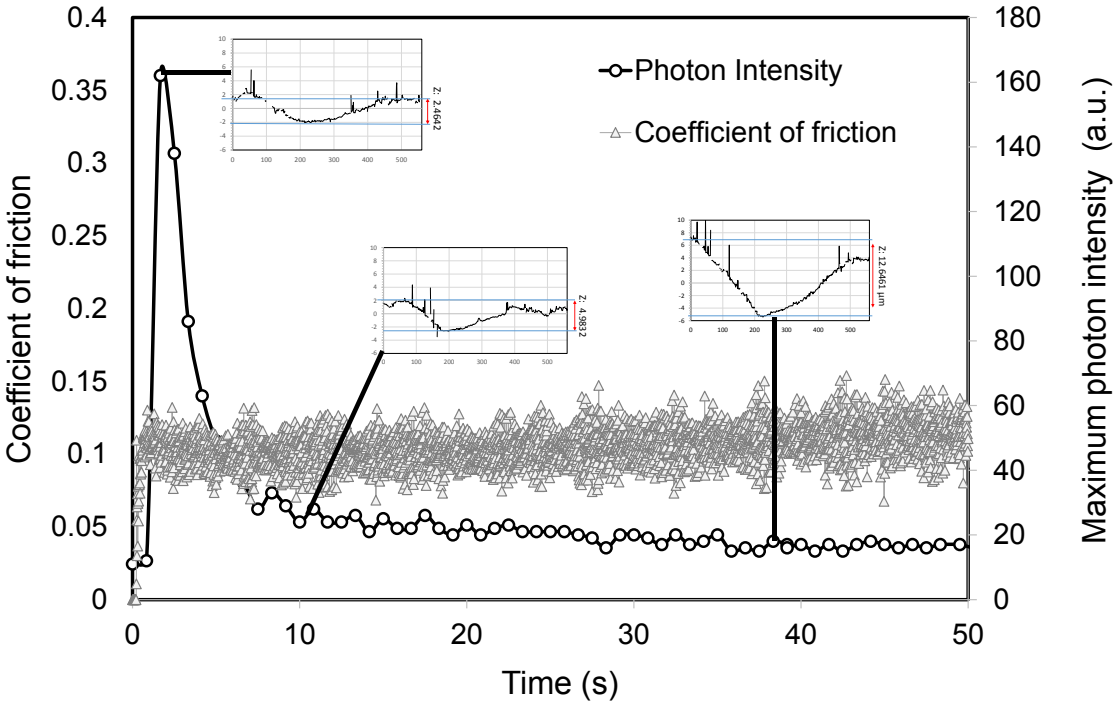

Figure 5.5: Variation in friction, wear depth and maximum emission intensity with time for PTFE/Al_2O_3 contact, loaded with 1.4 N and sliding at a speed of 2.8 m/s.

The next test involved recording the variation in plasma intensity as a function of time, alongside the accumulated surface charge measured using the electrometer, as shown in Figure 5.6. Also plotted in Figure 5.6, is the derivative of charge with respect to time. It is clear from this figure that plasma intensity is closely related to the rate of charging rather than the overall accumulated charge on the disc surface (after ~1.5 seconds of sliding, plasma intensity is reducing while charge is still accumulating). This is counterintuitive, since electrical breakdown and hence plasma intensity should increase with increasing field strength due to the accumulation of surface charge, however, the process may be explained as follows. Since, the charge is measured on the disc surface away from the contact; it gives no indication of the charge on the sapphire hemisphere specimen. Therefore, it is hypothesised that, over time, the hemisphere surface becomes less positively charge so that the difference in charge between the

two surfaces remains constant even when the discs becomes increasingly negative charged. Although this disagrees with the conventional behaviour of alumina, which should charge positively against PTFE according the triboelectric series, it can be explained by the transfer of material from the PTFE disc onto the alumina hemisphere, which is a known lubrication mechanism for this polymer [202, 203]. In other words, as sliding commences, PTFE molecules trapped in the contact are sheared leading to bond scission and the formation of ions [199] on the polymer surface. This results in tribocharging, as regions of negative fluorocarbon ions accumulate on the polymer surface. The shearing process also results in the transfer of PTFE from the disc to the alumina surface so the interface transitions from being PTFE/Al_2O_3 to PTFE/PTFE (as confirmed later by SEM). Therefore, although charge is continually accumulated on the disc with increased sliding, the charge differential between the two surfaces, and hence the plasma discharge intensity, reduces.

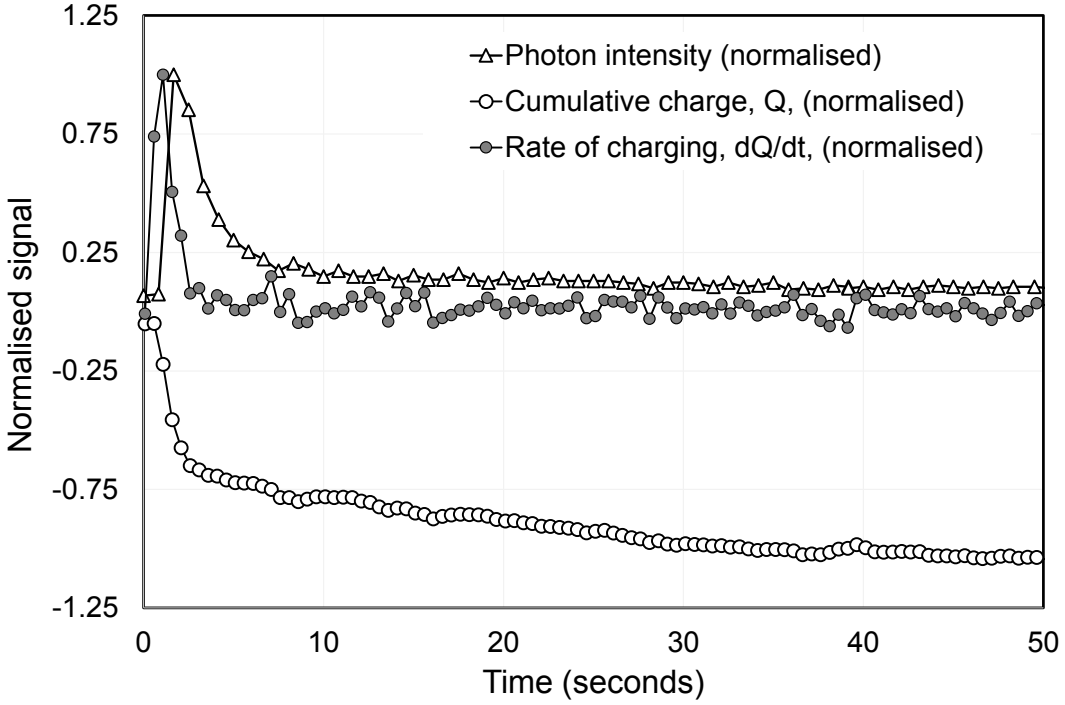

Figure 5.6: Variation in accumulated charge, derivative of charge with respect to time, and maximum emission intensity versus time for PTFE/Al_2O_3 sliding contact.

The rate of charge generation is thought to be linearly dependent on the rate at which asperity-asperity junction growth and detachment occurs in the contact area, which is proportional to sliding speed. The greater the number of contacts, the more microscopic material transfer occurs between the sliding specimens. This microgram material transfer was confirmed by EDX studies (Figure 5.7) is the leading cause of contact charging. Figure 5.7 also shows material transfer occurring from the harder (Al_2O_3) to softer (PTFE) surface and vice versa.

The mechanism by which aluminium oxide particles or aluminium ions transfer to PTFE surface could be mechanical in origin (such as abrasion and delamination). Alternatively, it may be driven by triboplasma. As mentioned earlier, triboplasma is an ionized gas consisting of electrons and ions which are accelerated by an electric field created due to charge build-up at the dielectric surfaces. When the ions and fast atoms from the plasma bombard the surface atoms or surrounding gas molecules, they not only release secondary electrons, but also depending upon their energy, release atoms of the cathodic surface (attracts positive charge: cations), which is called sputtering. The sputtered atoms are either ionized or excited. The excited atoms or molecules further emit photons when electron jump back to shells of lower energy level while the ionized metal could reach the anodic substrate (which attracts negative charge: electrons and anions) by diffusing through the plasma.

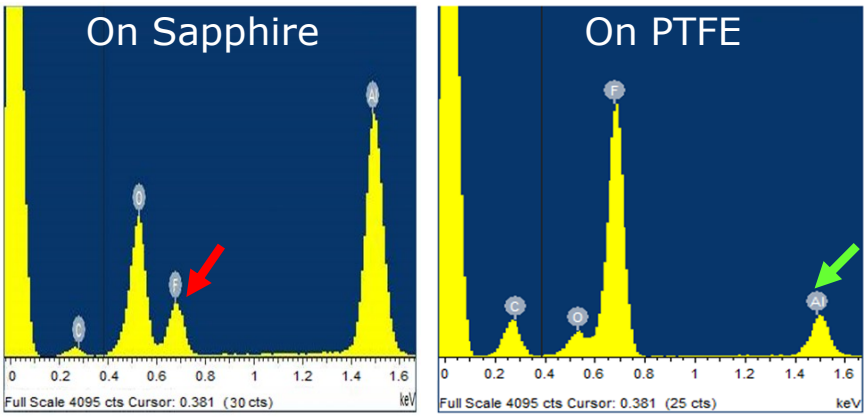

Figure 5.7: EDS results confirming material transfer from hard Al_2O_3 surface to softer polymer surface and vice versa. Red arrow shows fluorine on sapphire specimen while green arrow shows aluminium transferred unto PTFE surface.

The variation in maximum emission intensity with time for PTFE/Al_2O_3 at different sliding speeds is reflected in Figure 5.8. The higher the speed, the higher the charging and higher the peak intensity of emission (discharge). This figure further confirms the correlation between charging and discharging phenomena.

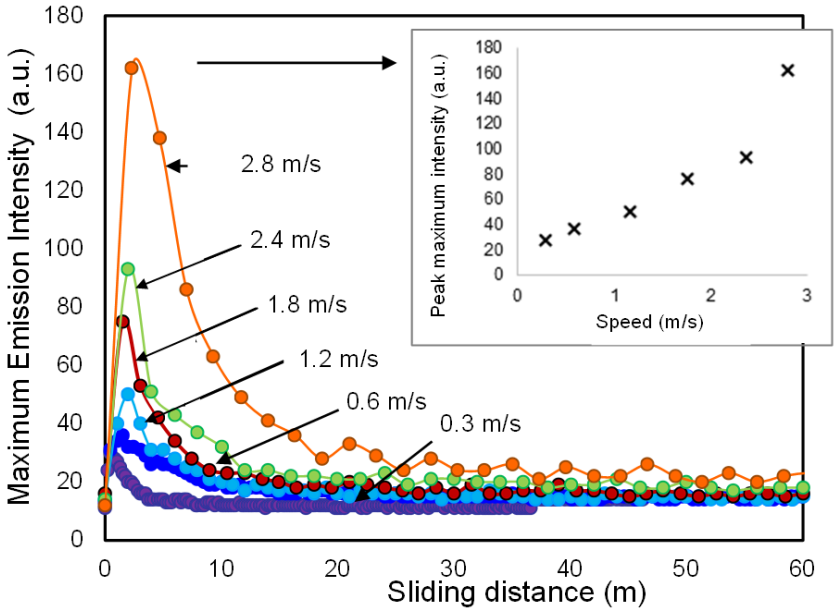

Figure 5.8: Variation in maximum emission intensity with sliding distance for PTFE/Al_2O_3. Inset: Graph showing correlation between peak intensity and sliding speed.

To test the hypothesis that material transfer is responsible for the variation in plasma and charging, repeat tests were performed on the same wear track (Figure 5.9), showing that emission resumes only after PTFE transfer has been removed from the alumina specimen. This strongly supports the idea that the reduction in plasma observed during the PTFE test is caused by charge equalisation due to predominantly negatively charged debris transferring to the positively charged hemisphere surface. The 65% reduction in emission between the test on the new and cleaned wear track can be attributed to the decrease in contact pressure due to wear, as the contact becomes conformal with larger contact area.

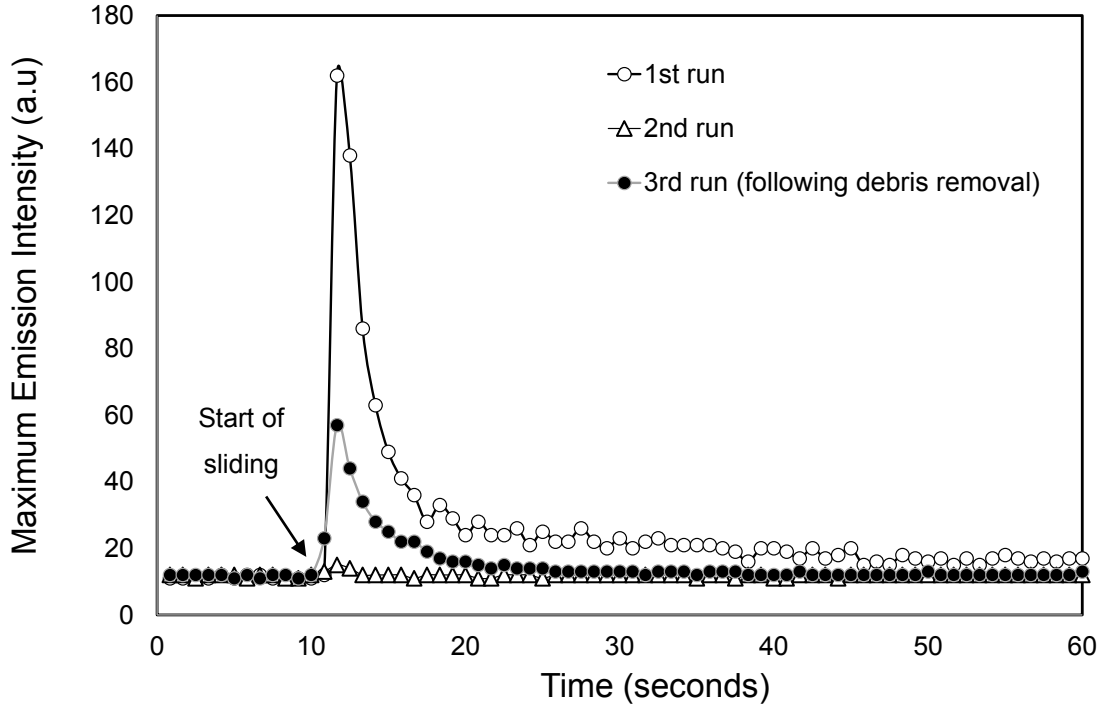

Figure 5.9: Variation in maximum emission intensity with time for PTFE/Al_2O_3, showing effect of repeated tests on same track and debris removal.

5.1.2.4. Transient plasma measurements - Milliseconds timescale

To investigate the transient nature of the plasma generation process at shorter timescales, photon emission images of the rubbing contact were recorded at a frame rate of 70 Hz (Figure 5.10). Here, the behaviour of the PTFE and the UHMWPE materials are highly contrasting, the former shows a continuous cloud of plasma, while the latter shows discrete breakdowns similar to atmospheric lightning. The differences between the two materials is also evident from the maximum plasma intensity as a function of time in Figure 5.11. Here, the same overall trends are observed as in Figure 5.4, with the PTFE showing an initial peak in emission intensity followed by a gradual decrease, while plasma generation from the UHMWPE undergoes a continual cyclic variation. However, high frequency fluctuations are superimposed onto the signals in Figure 5.11, due to the variations between plasma distributions observed in Figure 5.10

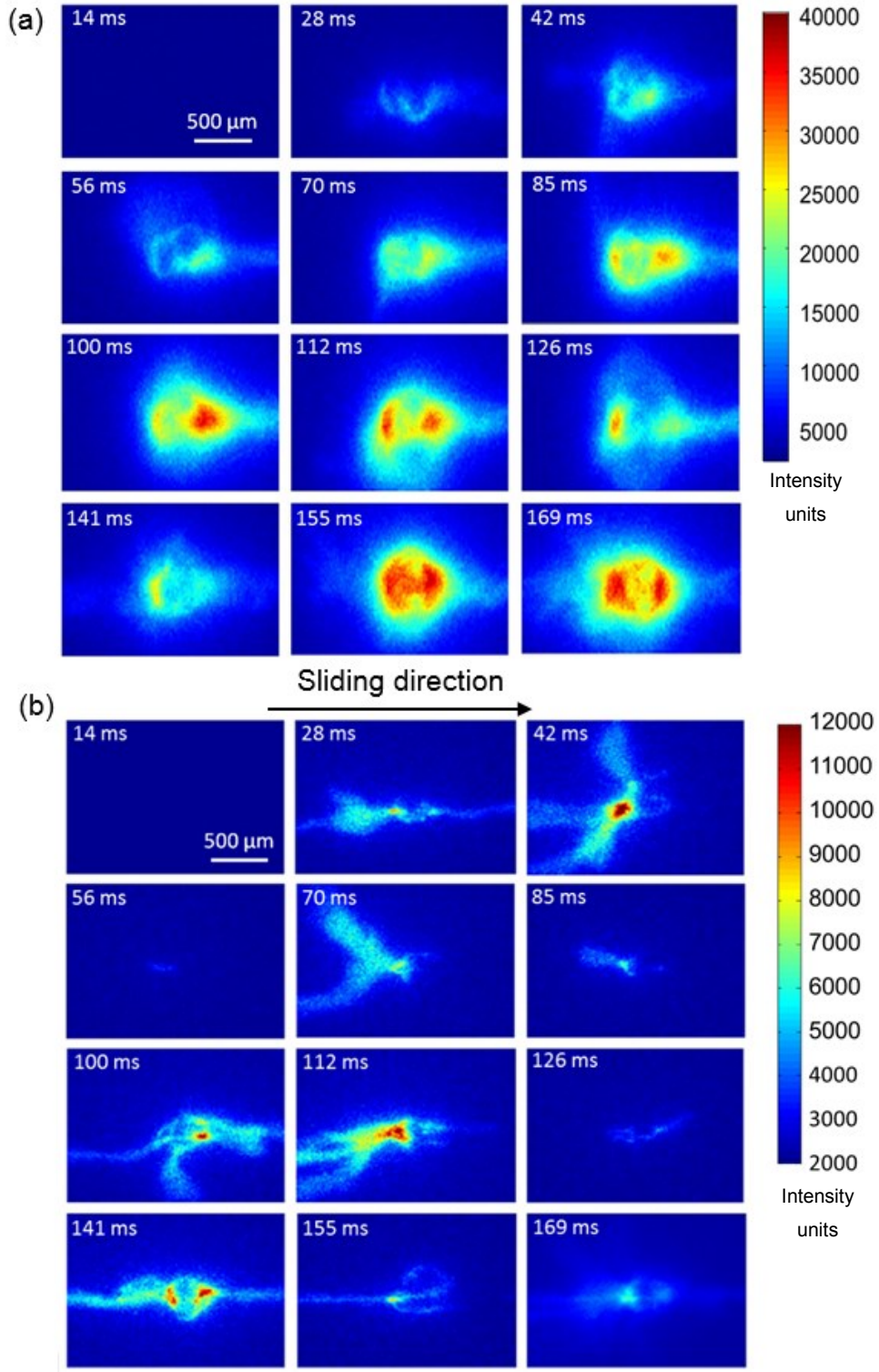

Figure 5.10: Images of transient plasma distributions, obtained with frame rate of 70 Hz for (a) PTFE and (b) UHMWPE. Sliding direction is from left to right.

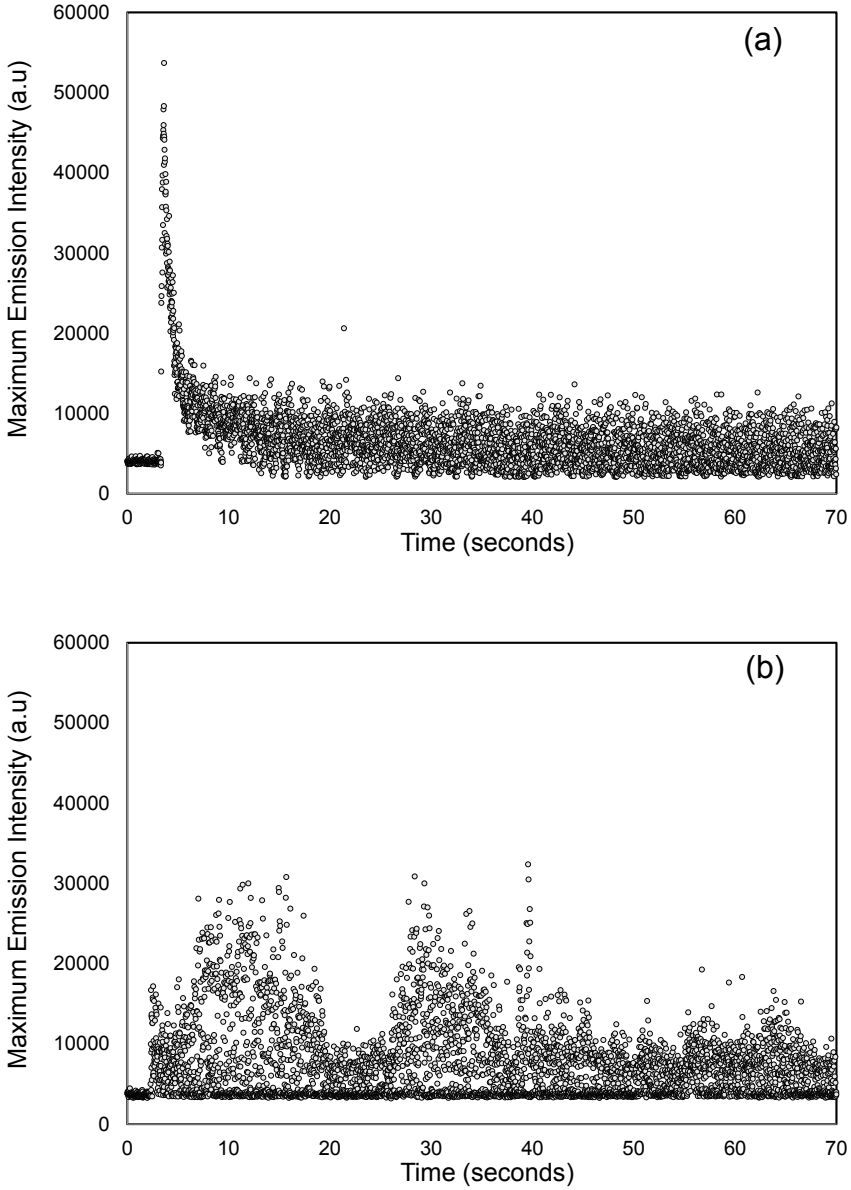

Figure 5.11: Maximum transient triboplasma intensity vs. time for a) PTFE/Al_2O_3 contact, b) UHMWPE/Al_2O_3 contact.

It should also be noted that the average plasma distribution around the contact, obtained by summing all the transient frames exampled in Figure 5.10 correspond closely to the images obtained at a longer exposure time in Figure 5.2. This is shown in Figure 5.12 and bears some similarity with steady maps obtained by Nakayama *et al.* particularly the tailing and the horse shoe shape. The colour bar shows the intensity counts of the camera.

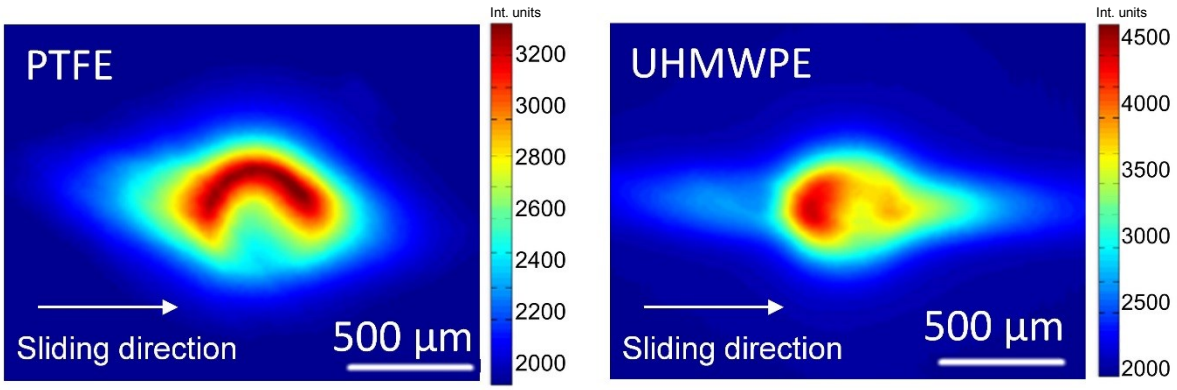

Figure 5.12: Average plasma distribution image for PTFE/Al_2O_3 and UHMWPE/Al_2O_3 contacts obtained by summing all the transient frames (6500 frames) during 60 seconds imaged at 70 frames/s. Sliding direction is left to right.

The millisecond timescale transient variation of plasma distribution suggests that the surface charge distribution is not uniform over the entire wear track. This results in different regions reaching the threshold electric potential required for breakdown of surrounding gas molecules at different time. There are several possible reasons for this fluctuation in emission, which range from *i*) triboemission, *ii*) variation in instantaneous gap heights, to *iii*) the distribution of charged sites.

The intermittent breakdown of gas molecules may also be initiated by triboemission, the emission of electrons and ions (observed in vacuum in **Chapter 4**) from the rubbed surfaces as suggested by Hiratsuka [156]. It was revealed in literature survey that numerous studies have reported emission of electrons from surfaces of rubbing insulators [161, 204] and have proposed various mechanism such as fracture [62], field emission [205], thermal emission [172] and strain relaxation [206]. It is a key new finding of this work that the emission of plasma under air conditions shows similar intermittent characteristics to the emission of electrons under vacuum conditions.

The trapped (immobilized) charges in the polymer surface also give rise to very high electrostatic potentials at the nanoscale. These charges can be measured using Kelvin probe force microscopy in high voltage (KPFM-HV) mode (discussed in **Chapter 3**) which has increased the measuring capability of electrostatic potential to up to 200 V with less than 15% relative error. The topography and surface potential of UHMWPE and PTFE surface before test is shown in Figure 5.13. Images (a) and (b) correspond to the UHMWPE surface while images (c) and (d) correspond to the PTFE surface. The potential is completely different from the topography measured on the selected area. It is evident that the location of the immobilized

charges on insulators are random. The distribution of these charges per unit area (charge density) gives rise to different values of potential (voltage) at different sites with specific polarities (positive or negative). The potential difference between these sites builds up the electric field required for triboplasma generation. Since these high potential sites do not have a constant voltage supply source, the plasma occurs as a spark that has a very short lifetime (ns to µs). Rubbing (contact electrification) further raises the electric potential (values greater than 200 V) and also leaves charged debris on the wear track which then interfere with the accurate measurement of surface potential after the test. The change in surface potential of polymer surface upon scratching with a SiO_2 AFM tip at 3 nN load is demonstrated in **Appendix A** . Three extremely smooth (R_a within few tens of nanometers) polymers such as PMMA, PS and PDMS were chosen for these measurements due to the high surface roughness (~600 nm) and presence of dangling polymer chains on PTFE and UHMWPE surface that interfere with surface potential measurements. Debris generation and removal also play an important role in charge generation and dissipation, and is discussed in the following section.

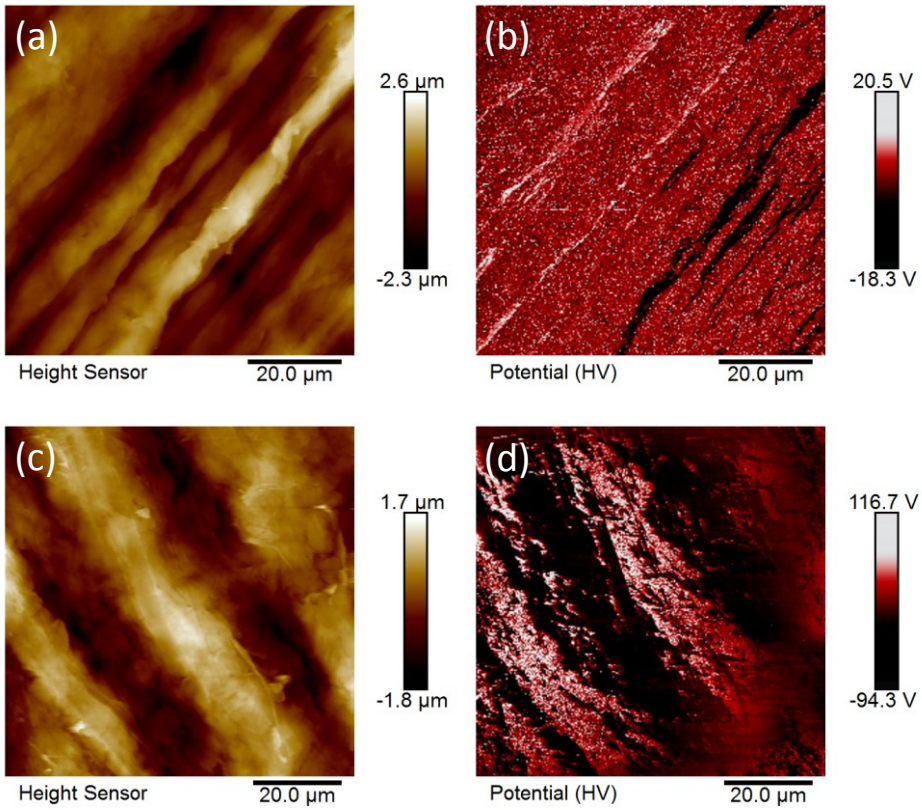

Figure 5.13: Topography and surface potential of UHMWPE and PTFE surface before test measured using peakforce Kelvin probe force microscopy. Images (a) and (b) shows UHMWPE surface while images (c) and (d) shows PTFE surface.

5.1.2.5. Correlation of breakdown with wear mechanisms

Figure 5.14 shows SEM images of the specimens obtained after each test, where clear differences can be observed between the two polymer materials. Figure 5.14 (a) shows charged PTFE debris transferred from the disc to the Al_2O_3 hemisphere, which are present inside the contact area. This supports the theory that both plasma discharge and charging rate decrease over time as the contact transitions from PTFE/Al_2O_3 to PTFE/PTFE. Figure 5.14 (b) on the other hand shows a UHMWPE transfer film on the sapphire hemisphere outside the contact area on the exit side. This explains the lower intensity of plasma observed at the contact exit for the UHMWPE presented in Figure 5.2 and Figure 5.12, since the transfer of polymer material to the hemisphere in this location will reduce the gap between the two surfaces so that the breakdown voltage according to Equation 5.1, increases. It is also important to note that the transfer of UHMWPE to the sapphire hemisphere must first occur in the contact area and then be transported to the exit due to the high shear stress within the contact. This building up and subsequent removal of material within the contact is likely to cause the fluctuations in plasma discharge observed in Figure 5.4.

The traditional theories postulate that charge transfer occurs through conduction (not applicable for polymers), induction during contact. Conduction requires electrons, whereas induction requires charge separation between two components that are separated by a dielectric medium. Only recently, it was proved that material transfer is the mode of charge transfer when contact between polymers is involved. The charged debris observed around the contact and its role as charge carrier is consistent with Baytekin's charge mosaic theory [135] in that, when components are rubbed together and become charged, their surfaces consist of microscopic regions of both positive and negative polarity. The observations of this study suggests that charge mosaics can be formed by charged debris, which are redistributed and mixed into the wear track.

Figure 5.14 (b) and (d) show SEM images of the wear track on the PTFE and UHMWPE discs. The contrasting wear behaviour of the two materials shown here sheds light on the differing plasma generation characteristics. In the case of PTFE, relative motion and adhesion to the sapphire hemisphere cause the polymer to shear and form lamellar flakes, which become flattened and embedded into the wear track (in agreement with [203]). During subsequent passes, these adhere to the hemisphere and are removed from the disc. In the case of UHMWPE, due to its higher yield stress (0.2 to 1.2 GPa vs 0.3-0.8 GPa for UHMWPE and PTFE

respectively [207]), shearing causes the material to form strands of fibrous debris, which do not readily adhere to the Al_2O_3 hemisphere.

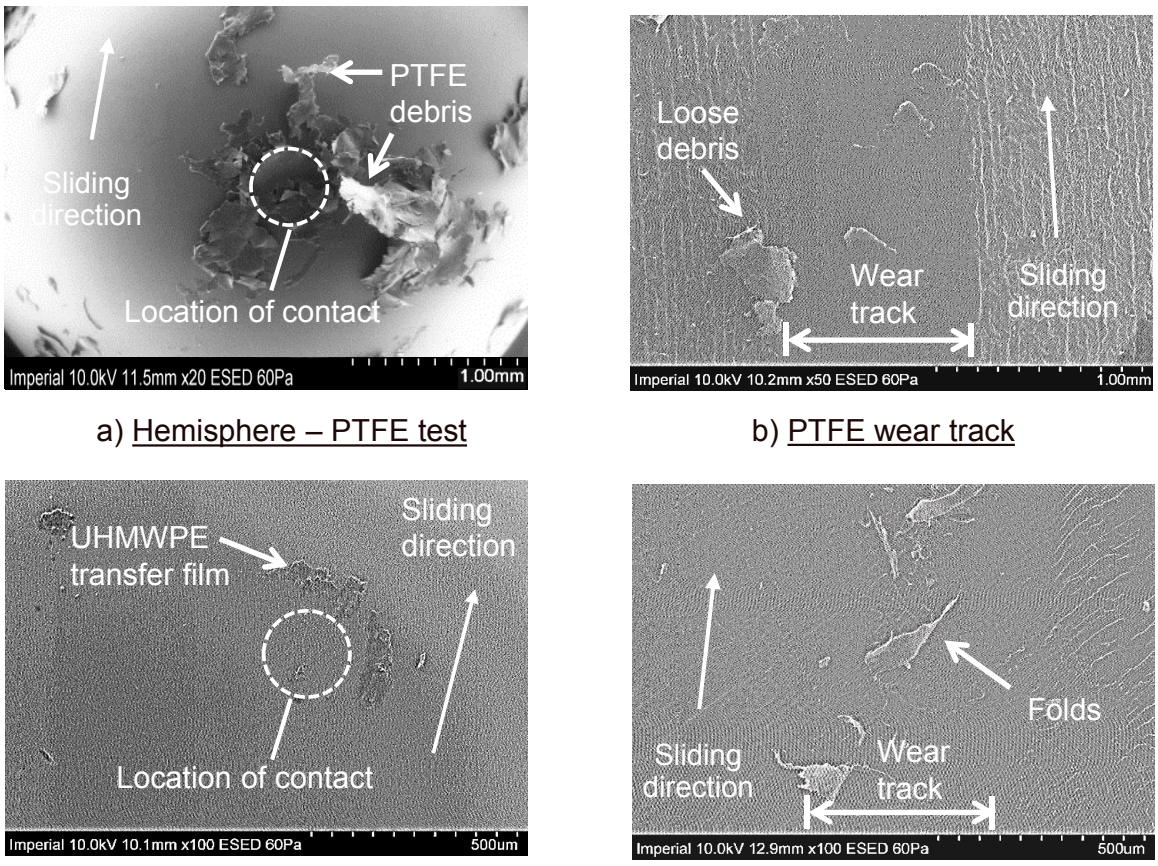

a) Hemisphere – PTFE test

b) PTFE wear track

c) Hemisphere – UHMWPE test

d) UHWPE wear track

Figure 5.14: SEM images of a) charged PTFE debris attached to Al_2O_3 hemisphere, b) wear track on PTFE disc, c) UHMWPE transfer film on Al_2O_3 hemisphere, d) wear track of UHMWPE.

The contrasting wear behaviours of the two polymers can be attributed to their molecular structures, morphology, and crystallite size and orientation. UHMWPE consists of very long, highly cross-linked molecular chains, which improve its wear resistance [208]. It also has a low glass transition temperature (around -150 °C) and a higher crystallinity (54%) compared to PTFE (40%). PTFE, on the other hand, has low wear resistance that is closely associated with the smooth profile of the rigid-rod-like PTFE molecule [203] and has a higher glass transition temperature around 115-130°C [209]. Due to the high shear rate sliding conditions used here, the frictional force will exceed the forces holding the PTFE crystallites together, and as a result, material in the form of thick laminar sheets is pulled out of the PTFE surface and is transferred to the counterface (Figure 5.14 a,b). In contrast, owing to the higher cohesive strength of UHMWPE, its low content of amorphous phase and very low glass transition temperature,

debris forms microfibrils or strands approximately half the size of debris from PTFE. It is proposed that the distribution of plasma in and around the contact is governed by the shape of the debris such as granules, splinters, fibrils, laminates or flakes. Since, charge distribution on any of the aforementioned shape gives rise to charge density owing to the debris surface area. The debris shape is influenced by material type, origin, size, shape. The transient bursts of plasma observed in Figure 5.10 and Figure 5.11 is suggested to occur from the combination of individual bond scission as well as creation of electric potential from charged debris. Multiple bond scission also generates burst of electrons (triboemission) as observed in **Chapter 4**. The triboemission events typically show short duration electron bursts with similar temporal characteristics to the plasma bursts in Figure 5.8 and Figure 5.9. It is therefore, speculated that intermittent electron emission from the worn surface (cryptoelectrons) is initiating the plasma. These electrons are then accelerated by the electric field potential (due to tribocharging) leading to ionisation of the gas medium by an electron avalanche process.

After having understood the core principles of gas discharge emanating from sliding polymer contacts, it is important to understand the effect of various kinds of materials on shape and distribution of plasma. The next section allows further understanding of plasma characteristics by expanding the test materials to include various polymers, Titanium alloys and Polycrystalline diamond.

5.1 Materials

As mentioned in **Section 3.2** of **Chapter 3**, discs made of various materials were tested to identify which material properties have greater influence on triboemission, triboluminescence and triboplasma behaviour. The materials used are summarized in Figure 5.15.

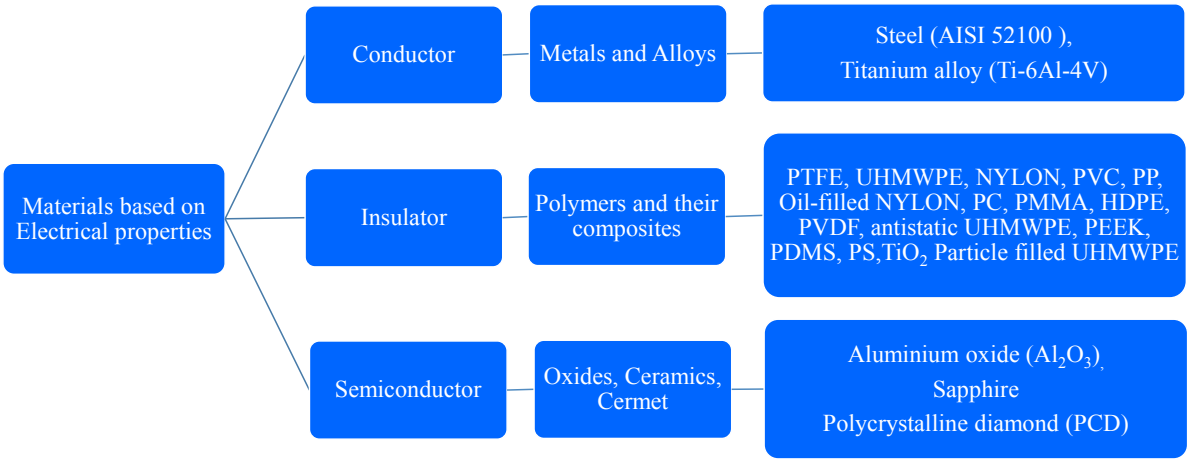

Figure 5.15: Materials characterized for triboemission studies in air.

The discs were rubbed against a sapphire (single crystal Al_2O_3) hemisphere pin and the differences in triboluminescence emission spectra and wear behaviour were examined. The load and speed was kept at 2 N and 2.4 m/s respectively. All tests were conducted in ambient atmosphere and room temperature and relative humidity varied between 20-50%.

5.1.1 Plasma from other polymers

Figure 5.16 shows averaged plasma distribution at the contact between various polymers and the sapphire pin during one minute of sliding. A variety of plasma distributions around the contact can be observed. Certain materials, e.g. Oil filled nylon and PVC, emit plasma with a horseshoe shape suggesting corona discharge, while some others have protruding tails along the wear track (in front as well as behind the contact) as observed with PTFE, UHMWPE. Only Nylon showed some spots of emission around the contact while polymers such PS, PMMA and Antistatic-UHMWPE (doped with carbon to increase conductivity) did not generate any triboplasma upon rubbing with Al_2O_3, therefore not shown in Figure 5.16.

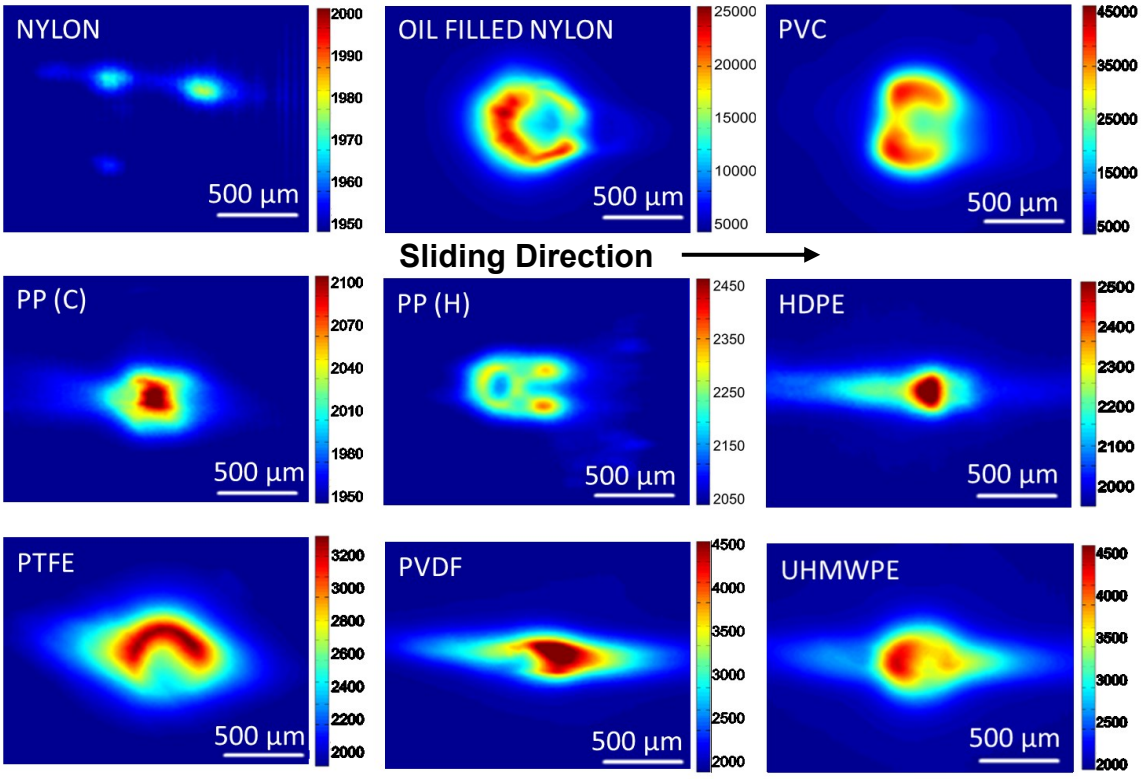

Figure 5.16: Plasma distributions measured from various polymer contact with Al_2O_3. The colour bar shows the average intensity counts of the camera image.

The addition of carbon black particle fillers in UHMWPE matrix made the surface conductive thus prevented any charge build-up and subsequent gas breakdown. Such particle filled

polymer composites have been used for manufacturing components operating at high line speeds and conveying rates because any charge build-up and subsequent gas discharge could potentially cause an explosion. To further understand the role of fillers on generation of triboplasma, a short study was conducted to discover the effect of amount of TiO_2 filler in UHMWPE matrix, on triboplasma generation and transfer film formation was conducted (See **Appendix B**). It is concluded that the addition of TiO_2 fillers leads to gradual reduction of photon emission and 10% (wt/wt) of fillers in UHMWPE matrix completely stops triboplasma generation.

It should be noted that the average plasma shape and size presented in this chapter show plasma generated during of 1 to 2 minutes of rubbing. Longer periods of rubbing can bring in further complexities that are known to affect plasma generation and its distribution. These factors are debris generation and accumulation, temperature rise, alignment of the polymer chains in the direction of sliding. The shape of the plasma distribution in and around the contact is reproducible but the intensity varies from test to test which can be attributed to the wear debris generation and removal which alters the charge distribution.

Figure 5.17 shows the general trend of photon emission for various polymer contact. A schematic is shown here for the purpose of brevity and measured variation of photon emission intensity with time can be found in **Appendix C** .

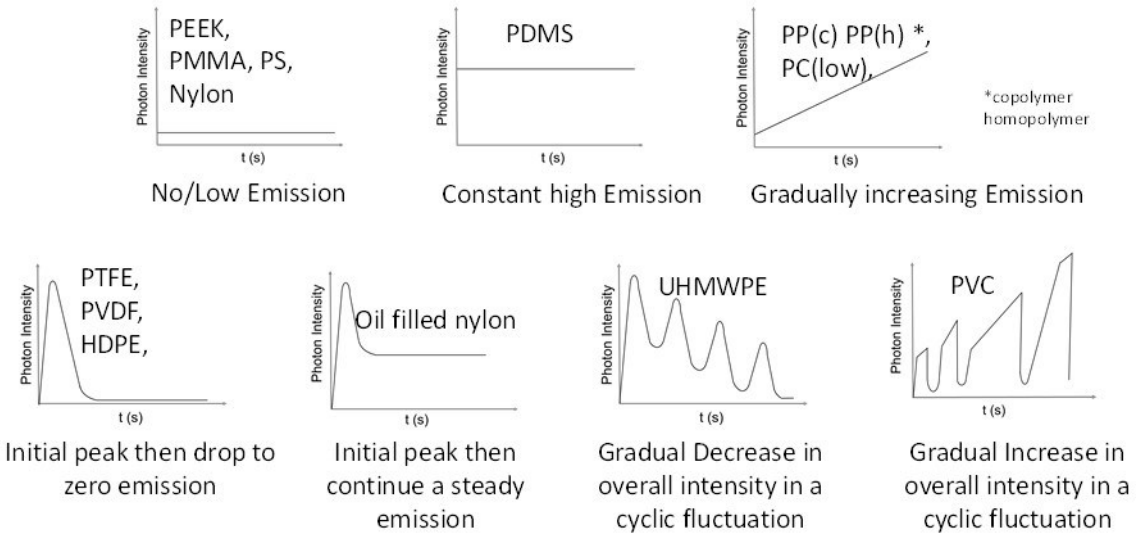

Figure 5.17: Trends of photon emission

The varying trends of averaged plasma with time and distribution around contact are dependent upon the material properties of the rubbed specimens. Of particular importance is the chemical

composition, chain structure *i.e.* straight, branched, and arrangement such as cross-linked or closed. These results contradict the conclusions of previous studies [159], which suggested surface resistivity is the primary factor in determining triboplasma generation. It is evident that, even if the resistivity of most polymers are comparable, the generation of triboplasma for different polymeric/Al_2O_3 contacts, its variation with time and its distribution around the contact is very diverse. The surface resistivity of these polymers, measured using Model 8009 Resistivity test fixture [180] along with their monomer weight, is shown in Table 5.1. It can also be concluded that monomer weight has no effect on the triboplasma behaviour. However, it is thought that the monomer 'group electronegativity' could play a vital role. "Group electronegativity is defined as the power of a group (G) to attract electrons to itself from another bonded atom or group". It is used to describe the bonding behaviours of group−atom or group−group bonds, which also determines the hardness of materials [191]. Group electronegativity of a monomer could be the main factor which influences the charge accumulation and charge transfer upon material transfer during sliding leading to tribocharging.

Table 5.1: Surface resistivity and monomer weight of some polymers

Polymer	**Surface resistivity Ohms**	**Monomer weight g/mol**
PEEK	1.8E+13	288.3
PP(H)	6.6E+13	42.1
Nylon (PA6)	1.22E+14	113.2
UHMWPE	9.89E+12	28.1
PP(C)	1.9E+13	42.1
PTFE	1.25E+13	100.0
PVC	1.96E+13	62.5
LDPE	2.66E+13	28.1
OIL FILLED NYLON	1.2E+13	113.157640<
ANTISTATIC UHMWPE	7.3+8	28.053160<

In relation to counter specimen material, it should be noted that plasma was also detected when a conductive steel hemisphere specimen was used in place of the sapphire. In this case, the contact was viewed from the side (Figure 5.18). This is important since steel-polymer material

are more prevalent than sapphire-polymer ones. Similar trend of maximum transient triboplasma intensity vs. time for PTFE/Steel contact further confirms that indeed shearing of polymers is plays an important role in triboplasma generation.

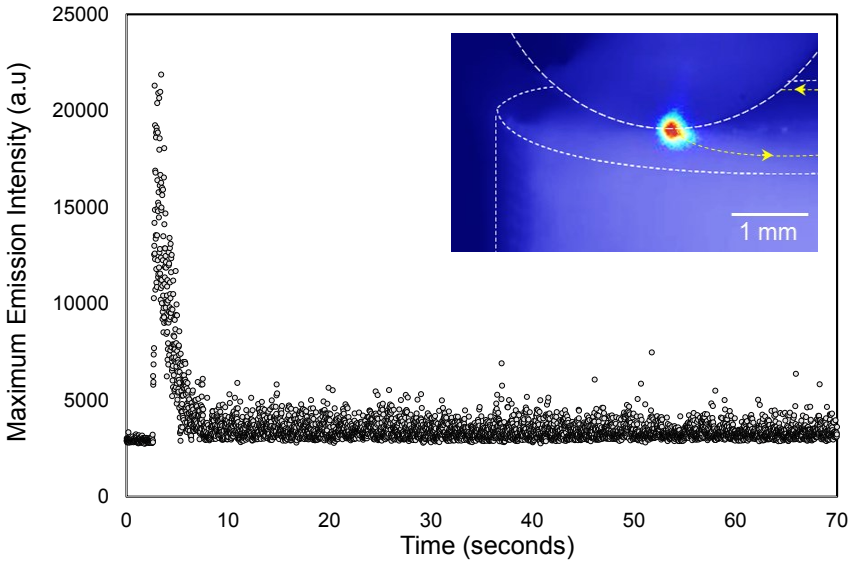

Figure 5.18: Maximum transient triboplasma intensity vs. time for PTFE/Steel contact. Inset: Recorded UV plasma intensity distribution, superimposed on a white light image of sliding PTFE/Steel contact.

The nature of emission was investigated for all polymer/Al_2O_3 contacts and was compared with available literature to understand the significance of each peak. It was found that apart from the nitrogen molecule dissociation and excitation, radicals such as OH, C, CH, CN are also emitted as shown in Figure 5.19 (a and b). Triboplasma from Nylon/Al_2O_3 contacts comprises of OH, CN and CH radicals while triboplasma from PVC/Al_2O_3 contacts includes additional chlorine radicals along with nitrogen discharge products. Thus, depending upon the composition of monomer unit, various radicals are produced *e.g.* in PVC, the monomer unit vinyl chloride contains chlorine while in Nylon, the OH radical, seen on the spectrum between 290-300 nm is from the hydrogen bonds formed by the carbonyl oxygens and amide hydrogens. The generation of visible light from PVC and Nylon by relative sliding (mechanical excitation) caused) is an example of Triboluminescence and different to Triboplasma which is essentially a nitrogen gas excitation and breakdown.

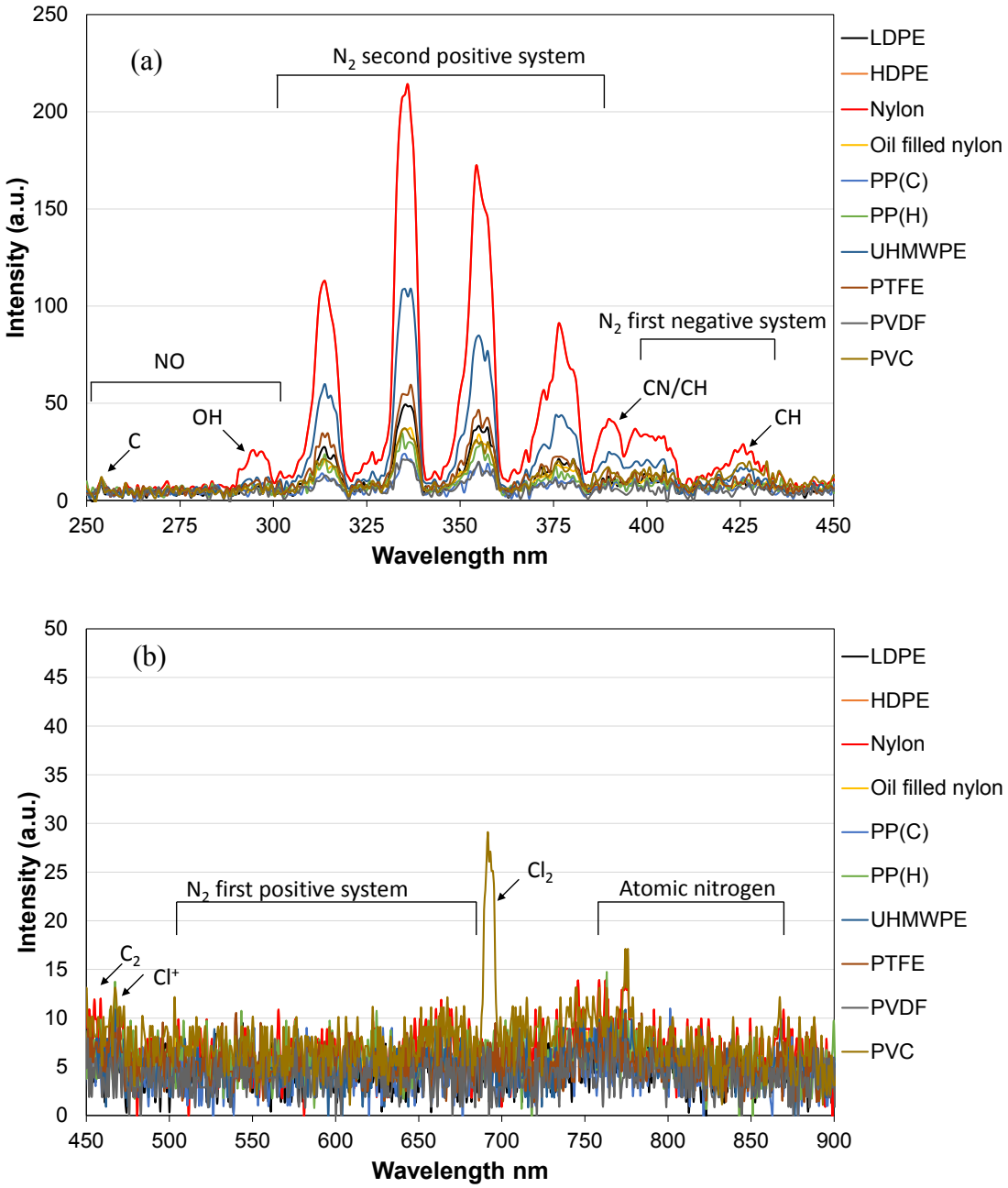

Figure 5.19: Optical emission spectra of triboplasma generated from various polymer/Al_2O_3 contacts. (a) 250-450 nm, (b) 450-900 nm.

There are two ways of excitation of the surface for light generation. First, as mentioned previously, when ions and fast electrons from the plasma impact the surface atoms, they not only release secondary electrons, but also atoms of the substrate material, which is called sputtering. These sputtered atoms/molecules are either ionized or excited in the plasma depending upon the energy transferred after collision. These molecules return to their stable form when electrons return to ground state emitting photons of characteristic wavelength. The second process is triboluminescence/ mechanoluminescence/ fractoluminescence which may

or may not involve the steps of the former process. The difference between the photons observed from triboplasma and photons from triboluminescence is the source of the photons. In triboplasma, the photons are emitted from gas molecules while in triboluminescence/ mechanoluminescence/ fractoluminescence the photons is emitted from the atoms constituting the crystal structure of the fractured material.

5.1.2 Plasma from metals and ceramics

This section presents triboplasma generation from polycrystalline diamond (PCD), titanium alloy, steel and copper discs sliding against a single-crystal sapphire (Al_2O_3) hemisphere of 5 mm in diameter under a load of 2 N and speed of 2 m/s in ambient air.

(a) PCD: Sapphire

Figure 5.20 (a) shows the spectrum of photons emitted while sliding a single-crystal sapphire (Al_2O_3) against PCD disc, while (b) shows the maximum two-dimensional image measured during sliding, obtained by the CCD camera in auto-contrast mode. The colour scale shows the photon intensity levels in and around the contact. Image (c) shows an electron microscope image of the contact area on the sapphire hemisphere after 60 seconds of rubbing.

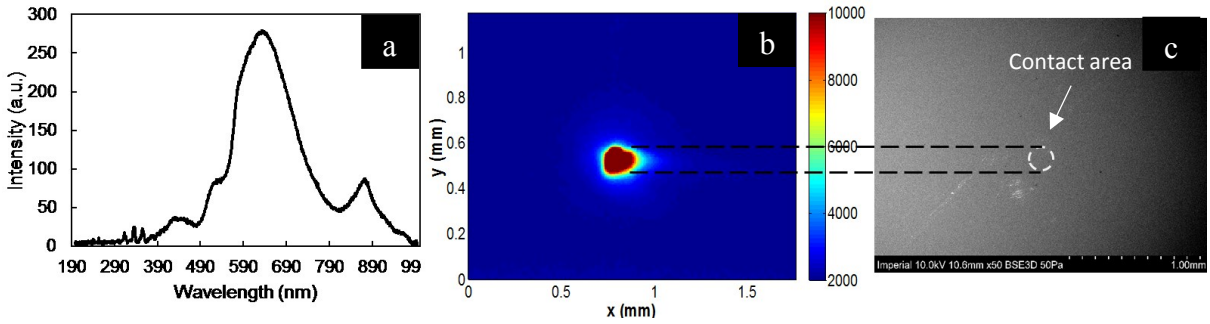

Figure 5.20: Photon emission spectra and its spatial distribution around the PCD-Sapphire contact.

The photon emission spectra of PCD/Sapphire shown in Figure 5.20 has 4 distinct peaks in the UV region: 313.806, 336.8, 355.02 and 377.55 nm which are from nitrogen second positive system; a broad band spectra in ranges 390-490, 500-800 and a IR peak at 871 nm. The broad spectra in the visible range is unlike any of the other materials tested and seem to resemble the fluorescence spectra of a diamond crystal with a nitrogen vacancy (NV) defect colour centre which also has a broad fluorescence spectra ranging from about 630 up to 750 nm along with a weak peak at 637 nm (zero phonon line) [21]. The broad peak could also arise from multiple excited states from same or different atomic species such as Cobalt (Co), Tungsten (W), Iron

(Fe), Copper (Cu), Bromine (Br) and Niobium (Nb). The presence of these atoms is typical of sintered polycrystalline diamond and EDX studies shown in Figure 5.21, confirms it. In the IR range, a peak at 871 nm is also observed. The near IR peaks from PCD could not be a result of thermal heating because the temperature rise as shown is not large enough to cause thermal photons. This peak is attributed to neutral atomic nitrogen excitation [30] in air. Thus, the photon emission in case of PCD/Sapphire system may originate from two sources. Firstly, UV photons from nitrogen gas discharge. Secondly, from the jumping of electrons from excited electronic states in surface atoms to lower energy shells. The surface atoms are ionized or excited by bombardment with the electrons /ionized gas molecules / fast atoms resulting from fracture and tribocharging.

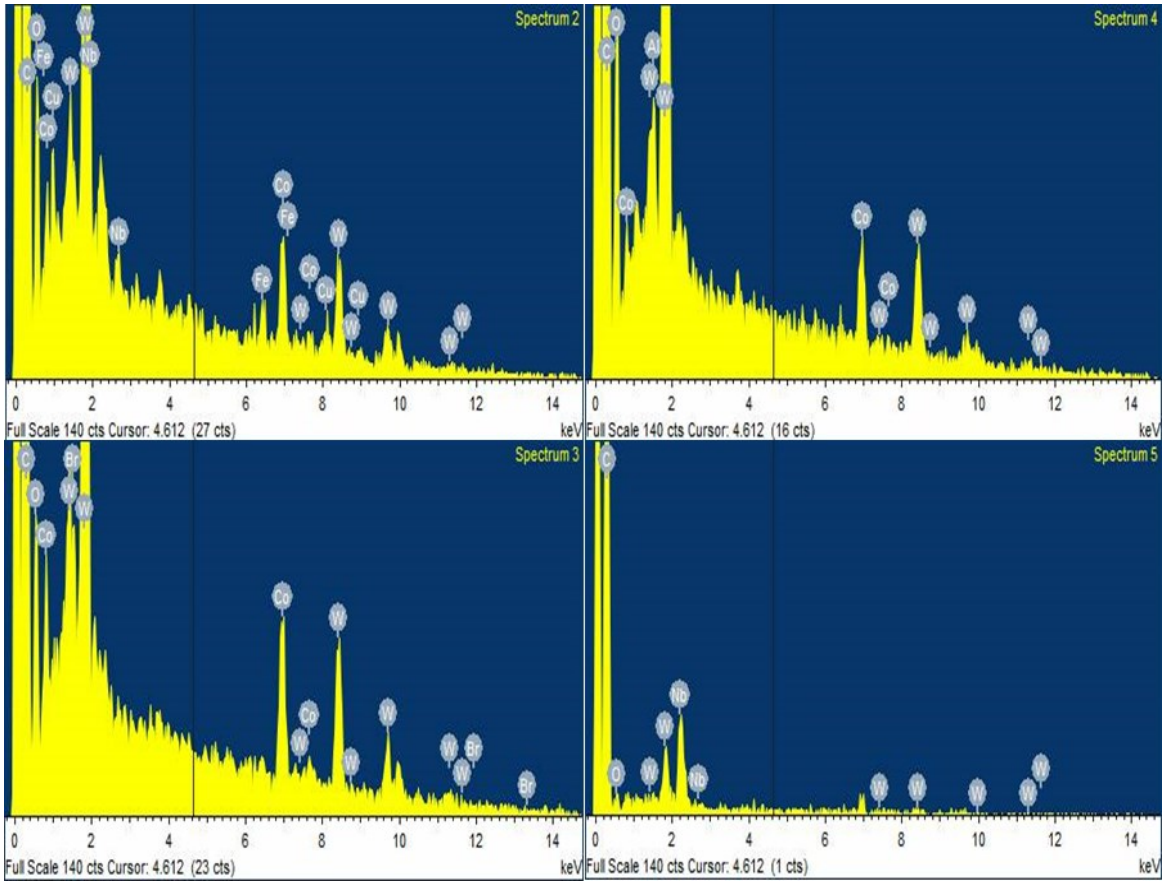

Figure 5.21: Detection of trace elements using EDS.

The photon emission intensity increases and then gradually decreases after 20 s to a low but steady value as shown in Figure 5.22. This may be due to severe abrasive wear of the Al_2O_3 surface during the running-in period of sliding after which the PCD surface only micro-polishes the Al_2O_3 surface. PCD is used as a cutting and grinding tool because of its hardness and high abrasion resistance, therefore shearing and fracture of smooth sapphire pin surface when rubbed against PCD cannot be avoided. A magnified SEM image of the fractured surface of sapphire

pin is shown in Figure 5.23. Image (a) shows PCD surface, while images (b) and (c) show Al_2O_3 surface after sliding. Image (b) confirms that PCD merely polishes the sapphire disc at most part of the contact while image (c) which shows the magnified region of Al_2O_3 contact surface, confirms fracture of Al_2O_3 crystal and hence provides evidence of abrasive wear.

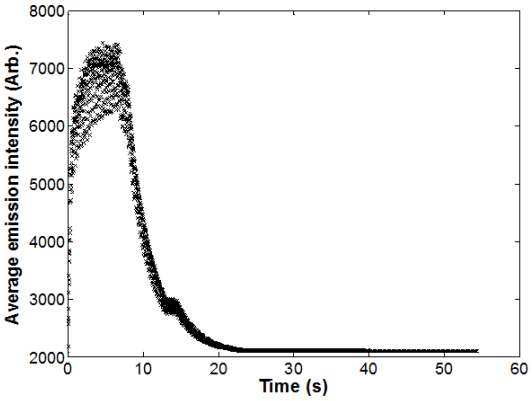

Figure 5.22: Emission of photons as a function of rubbing time from PCD/Al_2O_3 contact.

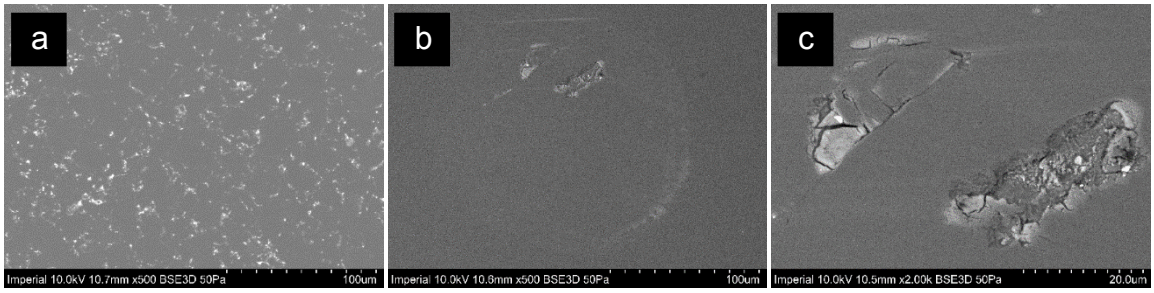

Figure 5.23: SEM micrographs of pin and disc surface after 60 seconds of dry sliding (a)PCD disc, (b) Al_2O_3 pin (c) magnified view of fractured Al_2O_3 pin.

(b) Ti: Sapphire

Figure 5.24 (a) shows the spectrum of photons emitted from Ti alloy/Al_2O_3 contact, while (b) shows the maximum two-dimensional image measured during sliding, which is displayed by the CCD camera in auto-contrast mode. The colour scale shows the photon intensity levels in and around the contact. The photon intensity from titanium-sapphire tribopair is at least 1000 times higher than PTFE/Al_2O_3 and PCD/Al_2O_3 sliding contact. Image (c) shows the two-dimensional electron microscope image of the contact area on the sapphire hemisphere after 60 seconds of rubbing.

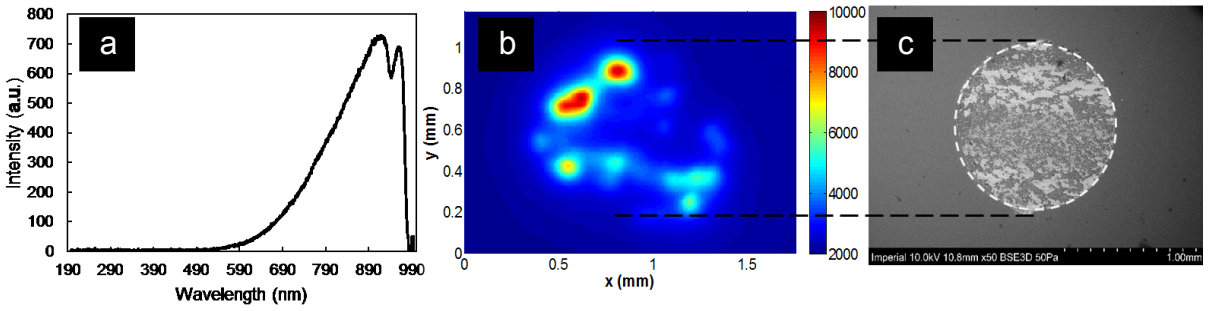

Figure 5.24: Photon emission spectra and its spatial distribution around the PCD-Sapphire contact.

The absence of narrow peaks in UV region in case of titanium alloy suggests a different mechanism other than nitrogen gas excitation and breakdown. In case of Ti/sapphire two distinct peaks in the IR range at 918.14 nm and 960.56 nm are observed (see Figure 5.24). Although there are no photons in the UV range, the visible photons are observable from 490 nm onwards to near IR range. This emission wavelength range is too low to be black body thermal radiation and theoretical calculations confirm this. The rapid drop in emission intensity above 960 nm could be due to the spectral response of the detector used in the spectrometer. These peaks may also result from excited to ground state transitions of rare-earth ions or transition metal ions. However, energy dispersive spectrum (EDS) studies, confirmed that no undesirable impurities were present. Therefore, it is conjectured that a tribocatalytic reaction might occur between the major constituents of the elements of the tribopair such as titanium, aluminium and oxygen resulting in luminescence.

The photon emission intensity gradually increases for Titanium/Al_2O_3 contact as shown in Figure 5.25. This may be due to severe wear of both the pin and the disc surface, in case of titanium/Al_2O_3 contact. Ti-6Al-4V alloy disc suffers from adhesive wear and Al_2O_3 hemisphere suffer from severe abrasive wear (Figure 5.26**)** under these sliding conditions. Poor wear resistance and severe adhesive wear of Ti-6Al-4V alloy is due to its low shear strength (550 MPa) [31]. Sapphire (Al_2O_3), on the other hand, is a scratch resistant ceramic material due to its high hardness and surface finish. The severe wear of sapphire hemisphere (Figure 5.26(b)) therefore comes as a surprise. The most probable cause of such damage could be a chemical recombination between the titanium and aluminium ions.

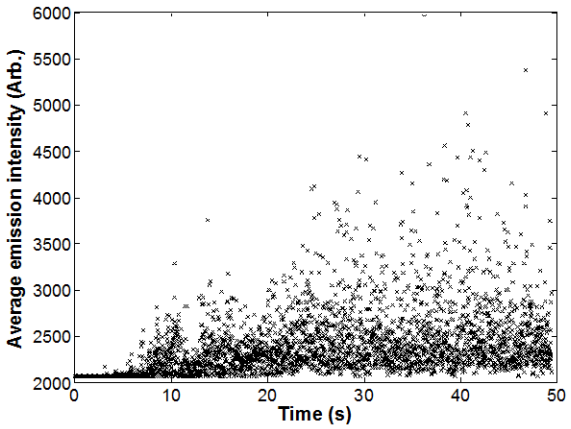

Figure 5.25: Emission of photons as a function of rubbing time from Titanium/Al_2O_3 contact.

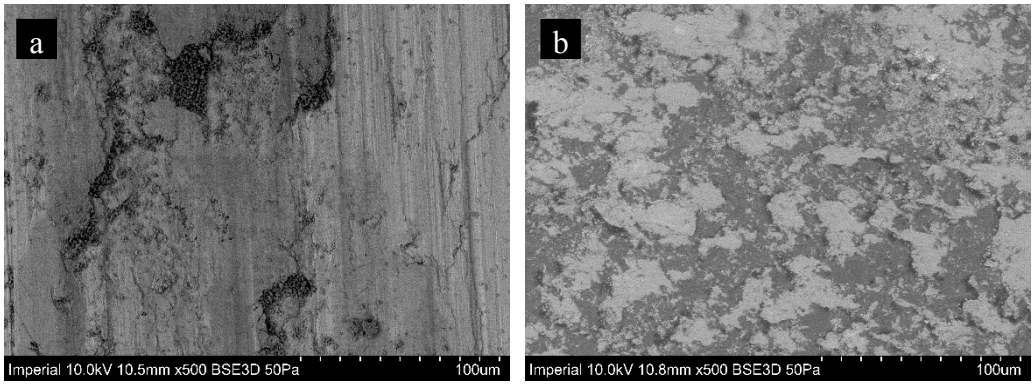

Figure 5.26: SEM micrographs of (a) Titanium alloy disc and (b) Al_2O_3 pin surface after 60 seconds of dry sliding.

The elemental composition of the sapphire hemisphere was analysed before and after the sliding experiment by its energy dispersive spectrum (EDS). The results show that the elemental composition of the sapphire surface changed drastically during the sliding experiment. The elemental composition of sapphire before the sliding experiment in terms of weight percentage is, Al = 48.83% and O = 51.17% while, the elemental composition of sapphire after the sliding experiment was found to be Al = 23.91%, O = 41.57%, Ti=25.4%, C= 7.84% and V= 1.29%. Thus, it is concluded that Ti ions substitute the Al in the crystal lattice of Al_2O_3 during relative sliding between the two materials. The first peak (at 918.14 nm) may be due to the excitation of Ti/sapphire microscopic crystals leading to stimulated emission of photons while second is an exothermic reaction of aluminium burning in air which would result in emission in the IR region. Although this is not detectable by the spectrometer, it can be visualized using thermal camera. Figure 5.27 presents a thermal image showing burning (oxidation) of aluminium ions from Titanium/Al_2O_3 sliding contact. Based on theoretical calculations, it is reiterated that there is no black body thermal radiation in far IR.

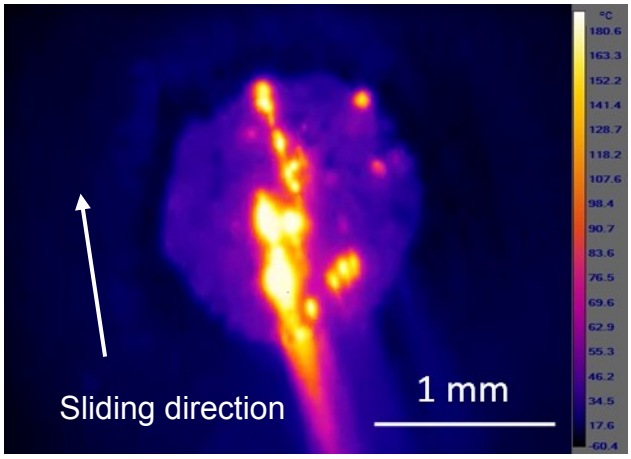

Figure 5.27: A thermal image obtained from Titanium/Al_2O_3 contact using FLIR IR camera.

From literature, it was found that emission in the range 680 to 1100 nm [32], peaking at around 800 nm is property of a Ti/sapphire crystal when excited by UV light. In a Ti/sapphire crystal, Ti^{3+} ion substitutes the Al^{3+} ion to be surrounded by six oxygen ions, resulting in octahedral ligand symmetry. Titanium exists in more than one charge state in sapphire as Ti^{3+} and Ti^{4+} [33] to form a Ti sapphire crystal which could be excited by emissions of lower wavelengths.

Additionally, Titanium oxide (TiO_2) is also known to transform into Magneli phases, Ti_nO_{2n-1} (n:3-10), at high temperatures and pressures [210]–[212]. During this formation process, electrons are formed in the vacancies. These electrons could initiate an excitation of the crystal. It is also known that oxygen deficient phases of TiO_2 are capable of storing charge [213]. The success of TiO_2 as solid lubricant in boundary lubrication [214]–[217] could be related to this transformation which provides additional electrons (triboemission) for reduction and decomposition of additives such as MoDTC and ZDDP. Further systematic studies need to be done to test this hypothesis of tribocatalysis and triboemission.

(c) Metal: Sapphire

Copper/Al_2O_3 (Freshly polished Copper surface) and steel/Al_2O_3 contacts did not produce any triboplasma or luminescence. However, on rare occasions, steel/Al_2O_3 emits some light which could be related to excitation of iron oxide formed on the steel surface. Since metals conduct the electrons, the high value of electric field necessary for breakdown of surrounding gas is never generated for metals. Therefore, the photons in case of metals may originate from defect centres such as presence of impurities or natural oxides that usually forms on metal surface, and not from dielectric breakdown of surrounding gas molecules.

5.2 Discussion

The results shown in this chapter confirm that triboemission occurs from non-conducting materials such as metal-oxides, ceramics, and polymers. A high-energy UV emission (triboplasma) is observed in cases of insulators (polymers) and semiconductors (PCD), as the propensity for contact electrification is higher in polymers and semiconductors compared to conductors (titanium alloy). Metals conduct away charge and share electrons, therefore triboemission and triboplasma is not observed. The intensity of photon emission is dependent upon speed (Figure 5.8) and the material in contact. The intensity of photons from Titanium/Al_2O_3 contact alloy is 1000 times greater than polymer/Al_2O_3 or PCD/Al_2O_3 contacts. Nevertheless, the different trend in emission with time suggests that the source and cause of such discharge is different and linked to respective wear behaviour. The wear behaviour controls the charging and discharging events in favourable materials.

Among polymers, it is proposed that the debris formation processes, which differ between polymers, are responsible for the transient bursts of plasma observed in Figure 5.10 and Figure 5.11. There are potentially two ways in which this may occur. Firstly, the gas breakdown could occur spontaneously between a newly formed, randomly oriented, charged debris and the stationary hemisphere. The gas breakdown is determined the by ratio of maximum electric field strength to the breakdown voltage (greater than or equal to 1 is favourable for breakdown). However, vacuum electron emission measurements typically show short duration electron bursts (Figure 4.2 and Figure 4.3) with similar temporal characteristics to the plasma bursts observed in Figure 5.4, Figure 5.8 and Figure 5.9. It is therefore, concluded that intermittent electron emission from the worn surface causes additional variation (transients in millisecond timescale) as compared to the plasma variation in second time scale. In other words, it is speculated that intermittent electron emission from the worn surface initiates the plasma by further collisions with surrounding gas molecules. Furthermore, Figure 5.19 also confirms the excitation and emission of moieties that form the molecular structure of the material surface such as C-H, O-H, C-C, and Cl radicals/ions. The same figure also confirms products of nitrogen gas discharge.

Inspecting Figure 5.2 and Figure 5.24, despite the similarities between the plasma images, there are a number of differences in shape between the plasma distributions from the various polymers, which deviate from the predicted elliptical shape. It is hypothesised that these are due to dynamics of the rubbing process, such as plastic flow and debris formation, and the

properties of material that govern the dynamics of the rubbing process such as group electronegativity, hardness and elastic modulus which are not taken into account in the simple model. Tribocharging and triboplasma is supressed by incorporation of conducting fillers such as carbon black or metal or metal oxide powders in polymer matrix by increasing the surface conductivity.

A shift from adhesive to abrasive wear modes of Al_2O_3 (based on post-test SEM images of Al_2O_3 hemisphere vs polymer, PCD and titanium alloy) seems to correlate with the shift from UV photons (high energy) to IR photons (low energy) summarized in Table 5.2. This means that, although the same amount of mechanical power was applied, the energy consumed for deforming and fracturing the surfaces is higher in the case of a tribopair where extensive material deformation and transfer occurs [34].

The spread of the plasma is larger for polymers owing to its large contact area and soft, easily sheared surface. Titanium emits IR photon from different spots at different times depending on the asperity-asperity interaction. These multiple intense excitation centres originate from defect centre cause by the migration of ions. This chemical recombination due to ion migration indicates occurrence of a tribocatalytic reaction, which lowers the energy for formation of Ti/sapphire crystals. The triboluminescence from Ti/Sapphire tribopair can be used as a cheaper source of an IR laser as it relies upon simple sliding and eliminates the use of expensive and inefficient pumped lasers traditionally used with IR lasers. Pump lasers diodes in the green spectrum range are not efficient and require considerable power while others might be expensive to operate or bulky.

Table 5.2: Summary of plasma emission characteristics from various materials

Sapphire against	Observation	Inference
Titanium (90%) Ti6Al4V	Plasma in IR, high wear	Ti-sapphire chemical recombination -LASER
Charge storing Polymer	Plasma in UV, medium wear	Gas discharge
Conducting Polymer or Metal	No plasma, medium wear	No gas discharge
Sapphire – PCD	Plasma in UV- VIS	Partly air discharge, partly defect excitation

In case of PCD, photoemission emission increases and then gradually decreases after 20 s to a low but steady value. This is attributed to severe abrasive wear of Al_2O_3 surface during first few rotations (the running in period) of sliding after which the PCD surface only micro-polishes the Al_2O_3 surface. UV emission from PCD suggests tribocharging and subsequent dielectric breakdown of surrounding nitrogen gas molecules in air. While in case of Titanium, UV emission is entirely absent due to its conductivity. The photon emission intensity trend keeps on increasing monotonically. The cause for such behaviour is the wear of both disc and sapphire surface leading to in an increased contact area between them. As sliding progress, more Ti^{+3} ions migrate to sapphire surface, and emit intense IR photons at these locations. The number of these localized micro asperity-asperity contact increase with sliding time due to widening of the wear track.

The variation in photon emission behaviour suggests that the triboemission from the tribological components may be caused by three mechanisms: *(i)* Electron and ionic (ionization) emission from material surfaces due to deformation and fracture *(ii)* electron and photon (ionization and excitation) emission from the gas discharge and *(iii)* fluorescence (excitation) due to excitation by the UV light from the gas discharge *(iv)* non-optically, by ion and electron recombination (relaxation/after emission).

It is suggested that triboemission and triboplasma strongly influence surface modification and new bond formation since it resembles low pressure atmospheric plasmas that have been used for surface cleaning, etching as well as polymerization. In practice, the different processes are often not separated, but occur simultaneously, *e.g.* cleaning may include sputtering or functionalization, or etching may occur along with deposition and/or sputtering. Therefore, the effect of triboemission and triboplasma may not be so evident.

5.3 Conclusion

Until now, very little has been known about how materials discharge following contact electrification and to address this the current study has developed a technique to image the distribution of plasma around a sliding contact. Different classes of materials classified electrically as conductors, semiconductors, and insulators; or on the basis of mechanical properties such as hardness were tested for triboemission events in air. The major findings are as follows

1. The time average of recorded transient plasma distributions can be predicted based on the accumulated surface charge and the geometry of the gap between components. However, the transient fluctuations in plasma distribution, which occur over two distinct time scales and vary between different polymers, are stochastic. Those that take place over a period of several seconds are shown to be caused by a combination of mechanical shearing, which increases charge due to molecular bond scission, and material transfer, which decreases charging. At shorter, millisecond, timescales, previously unseen rapid discharge events occur, is suggested to result from electron emission (trapped electrons) during debris formation processes.
2. Insights into the origins of the observed discharge behaviours are provided by SEM images of micro-scale wear features on the rubbed surfaces. Repeated tests on a single PTFE specimen reveal that the fluctuations in plasma that occur over a period of several seconds result from a competition between a) bond scission (due to the shear stress within the contact), which increase surface charge and hence the propensity for breakdown, and b) the transfer of material between the two specimens, which reduces charging.
3. Triboplasma generation among polymers is unaffected by their electrical resistivity but is greatly influenced by the shear strength of the surfaces, the bonds of the molecules and the electronic structure of the atoms of the molecules.
4. Spectrometric measurements show that the wavelengths of emitted photons correspond to band transition lines, characteristic of N_2 excitation and ionization along with radicals such as O-H, C-H, C-C and ionization and excitation of other moieties.
5. These studies observed a correlation between triboluminescence mechanisms and wear behaviour that influences the amount of photons and their energies. Metals did not emit while metal oxides and metal alloys (containing oxides) emitted intense light when fractured. For most polymers, the photon emission was in the UV range and mostly consisted of triboplasma due to nitrogen discharge while in the case of polycrystalline diamond the emitted photons were in the visible range. A remarkable observation with Ti:Sapphire emission spectra is that it does not include air discharge.
6. An important observation from testing different materials revealed that addition of conducting fillers at required amount completely stops generation of plasma.

Apart from shedding light on how charged surfaces dissipate charge, these findings also confirm that contact electrification is a tribological as well as an electrostatic process, and

suggest that contact electrification and breakdown can be controlled by selection of proper materials and lubricants. Furthermore, the interactions between contact electrification and wear particle formation have implications for biomedical implants contacts, where debris are known to interact with cells that are charge sensitive. Triboplasma resembles low pressure atmospheric plasma and therefore have the potential to facilitate chemical reaction because of the energy involved.

The next chapter studies the triboemission and triboplasma generation when the contact is submerged in liquid is present.

Chapter Six

Triboemission Interactions under Liquid Submerged Conditions

This chapter presents studies, focusing on triboemission behavior occurring when a sliding contact is submerged in a liquid environment. Since very few measurement techniques are in existence for this purpose, there has been the necessity to develop new ones. The development of three such techniques are described and the initial results they produced are discussed. The first is fully submerged in the presence of a liquid environment, the second is with fluorescent dye mixed with selected lubricant, and the third involves the interaction of a bio lubricant–protein with rubbed polymer discs. The first uses a newly developed fluorescence tribometer to visualize the effect of sliding in a liquid environment on triboemission generation. The liquids chosen here are deionized water, ionized water (10% NaCl solution) and a lubricating oil. The second technique uses a fluorescent dye mixed with chosen lubricants and observes the contact before and after sliding. This is to elucidate how the components of the lubricant interact with the worn surfaces and observe the sites from which triboemission was emitted. Finally, studies involving interactions of fluorescently tagged proteins with a freshly worn surfaces are presented. Proteins are used since 1) they are charged molecules and are therefore are affected by the formation of charged surfaces, and 2) they represent a practical application of these techniques, since the interaction of protein with charged surfaces is likely to be an important in the function of hip implants.

These new tests help to show how tribocharging plays an important role in determining how a lubricant will interact in a system. Finally, conclusions from the three aforementioned studies are presented.

6.1 Liquid submerged tests

The test setup adapted for the submerged liquid test is different to that presented in **Chapter 5** where a sapphire hemisphere and polymer disc is used to study triboplasma in air. Specifically, the configuration described here uses a sapphire disc and polymer ball as shown schematically in Figure 6.1. The tribometer used is a high speed EHL rig by PCS Instruments, UK. A PTFE ball (either 19.05 or 6 mm in diameter) is fixed onto a holder and a transparent disc sample is positioned centrally inside a pot. The ball was secured in a holder so that pure sliding conditions are ensured at the contact. The pot that can hold lubricant and ensure fully submerged conditions at the contact. The speed of rotation was such that the velocity at the contact was maintained at 1 m/s and the load between ball and disc was 20 N. The studies involved observing the contact with the high-speed CCD camera (ImagEX 2 from Hamamatsu photonics) to measure triboemission *i.e.* capturing photons during the sliding test with the liquid surrounding the contact. The tests presented in this section are sequenced as follows. Firstly, the generation of triboemission from this new configuration was determined by carrying out tests in dry conditions; next the environment was changed to deionized water, followed by 10% (wt/wt) NaCl solution. All tests were carried out at room temperature.

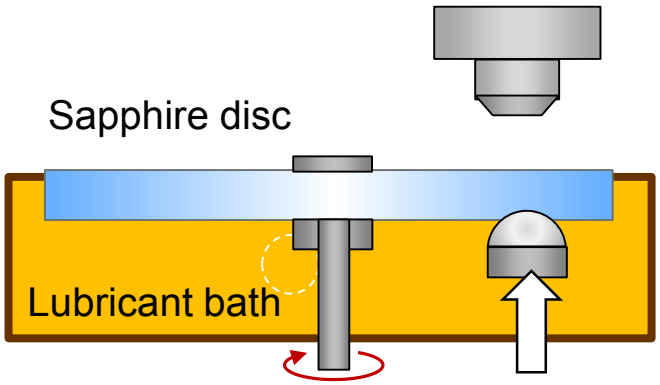

Figure 6.1: Schematic of the test set up.

In order to ascertain that plasma is produced even when the materials of the pin and disc configuration is interchanged (compared to the tests presented in **Chapter 5**) and provide a comparison with submerged triboplasma, dry sliding tests were first performed. A comparison of dry and fully submerged sliding of a PTFE ball against a sapphire disc at 20 N load and 1 m/s sliding velocity is shown in Figure 6.2 (a) and (b). The sliding direction is from right to left of the frame so the inlet is on the right and outlet is on the left of the dotted circle. In the case of dry sliding, the plasma is observed all around the contact. Although no tailing is

observed in this configuration, a higher intensity of photons is emitted from the outlet than the inlet. The absence of tail can be attributed to the lack of charge retention on the rotating sapphire disc. Low intensity of photon emission at the inlet is due to accumulation of charged debris at the inlet which results in lowering of electric field strength. This has been previously discussed in detail in **Chapter 5**. Figure 6.2 (b), shows miniature spots of photon emission in water submerged conditions. This is different to the streaks of emissions directed away from the contact as observed in Figure 6.2 (a). The triboplasma shape is reduced to a small sized spot at the outlet because of the electric field created between the sapphire disc and charged PTFE surface due to the liquid film separation at the contact outlet (also referred as starvation or cavitation). Sliding of a small contact area of the PTFE ball against sapphire disc at a high load of 20 N and high speed of 1 m/s sets up high shear stress which leads to large scale shearing, plastic deformation, and wear. The resulting PTFE debris generation is also charged. The charge generation on rubbing/scratching of polymers has been shown in **Chapter 5**.

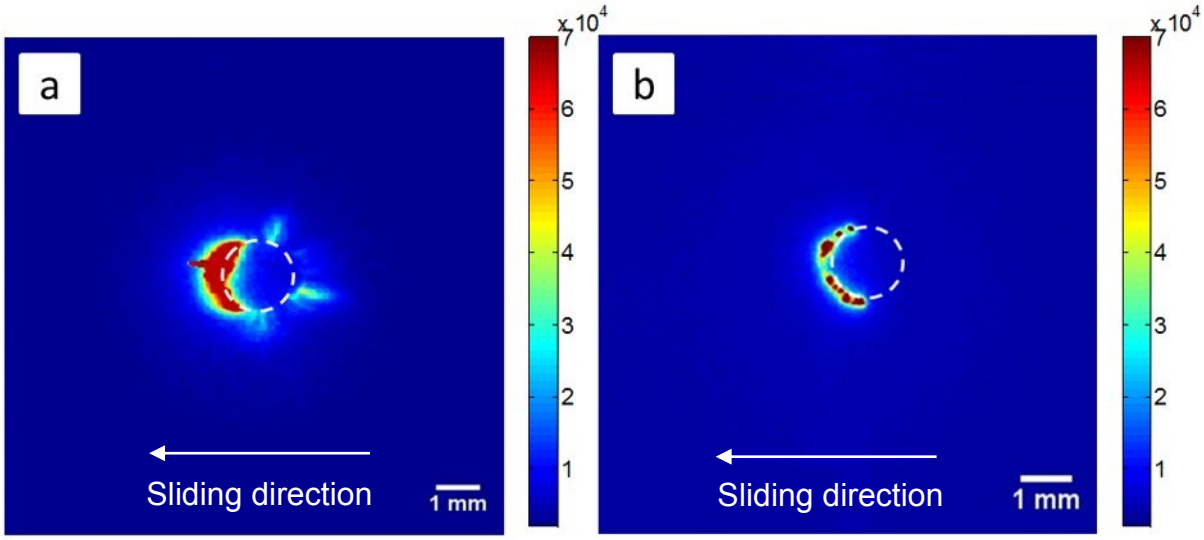

Figure 6.2: (a) Plasma from PTFE-sapphire interface in dry sliding. (b) Plasma under water submerged conditions. Sliding direction is from right to left of the frame so inlet is at right and outlet is on left.

Additionally, PTFE is hydrophobic in nature. This leads to an increased presence of trapped air in the vicinity of the irregular shaped debris and surrounding water by virtue of the meniscus formed by the liquid interface. Because of repeated high shear sliding, the detached PTFE debris accumulate around the contact due to electrostatic attraction. The net charge sets up an electric field which is sufficient to cause breakdown of the trapped air bubble. The debris that is smeared onto the sapphire disc collects at the front of the contact (inlet) as it is unable to enter the sliding contact and thus interferes with the electric field by decreasing gap height. This is why photon intensity is higher at the outlet and lower at the inlet. Figure 6.3 gives a

strong evidence as to why triboplasma is observed only from the exit of the contact in case of liquid submerged conditions. It shows an optical image taken (with ambient light) during sliding. Photon emission is observed from the cavitated region where liquid film separation occurs. Moreover, when the medium is changed to 10% NaCl solution in water the plasma is entirely absent as shown in Figure 6.4. This is due to the charge neutralization effect of the salt ions in the solution.

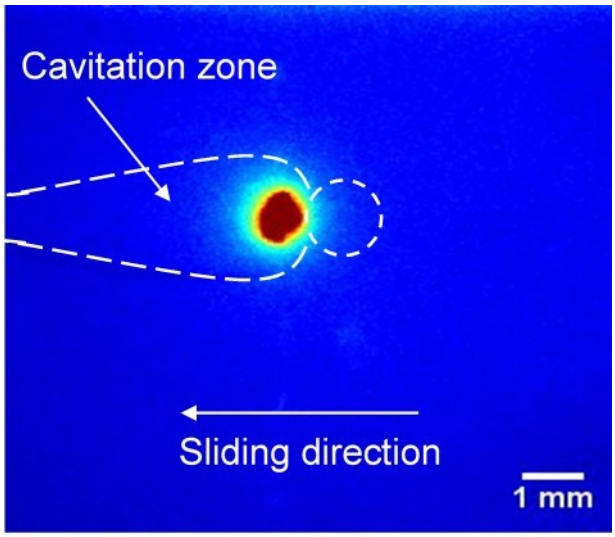

Figure 6.3: Optical image of the contact showing the cavitated zone. Note that the light is emitted from the contact outlet where the liquid film flow separation occurs.

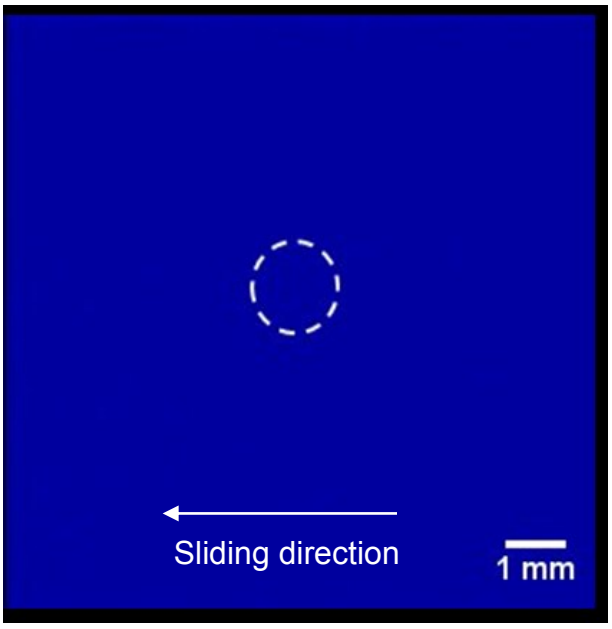

Figure 6.4: No plasma under ionized water (10% NaCl) submerged conditions. Sliding direction is from right to left of the frame so inlet is at right and outlet is on left.

The mechanism of discharge in this environment is the same as that described in the previous **Chapter 5**. The emission of photons is due to the dielectric breakdown of the air. Dielectric

breakdown occurs when the electric field due to charge build-up exceeds the electrical limit or dielectric strength of a material. Due to shearing of the polymer, charging and charge separation occurs, which sets up an electric field. Electrons from negative surface collide with molecules of the gas molecule and knock off electrons causing an avalanche of electrons. When electrons are removed from an outermost shell, the molecule becomes positively charged. The negatively charged electrons are pulled in the direction of the positively charged ions thus neutralizing charges of both polarities on opposing surfaces. Air is an insulator while ionized air is a good conductor and provides a path whereby charge flow and neutralization can occur. The surrounding air molecules which was ionized and excited by electron bombardment subsequently return to a stable state by emitting photons of equivalent energy. Thus, photon emission or sparks occur not only due to the recombination of the electrons and ions during the reformation process but also due to de-excitation of a gaseous atom or molecule where electrons from high energy shells return to their lower energy shells emitting the difference in energy as light. The combined term for ionized particles (electrons, ions) and photons is termed as triboplasma [218]. The dielectric strength of air is approximately 3 kV/mm (flat electrodes) [145]. Its exact value varies with the shape and size of the electrodes and increases with the pressure of the air. The dielectric strength (breakdown voltage) of deionized water is 65-70 kV/mm [145] which is 20 times higher than the dielectric strength of air. It is therefore likely that the electric field strength does not exceed the dielectric breakdown voltage of water. The absence of photon emission from liquid submerged contact could also be attributed to low number of photon generated owing to the pressure of the liquid and density which decreases the number of collisions. Moreover, these already low photon count will undergo optical diffraction due to the liquid medium and may become undetectable to the camera.

The transient variation of average triboplasma emission from PTFE-sapphire interface in dry sliding as well as under water submerged conditions is shown in Figure 6.5. Each point on the graph is a sum of the average of all the pixel intensities in an individual frame shown in Figure 6.2. There is initial peak observed during the first few seconds of sliding. This trend is similar to that observed in dry sliding of PTFE disc against sapphire hemisphere. This is because, the rate of the charge generation is high initially but then the accumulation of charged debris around the contact reduces the net electric field necessary to ionize the trapped air molecules.

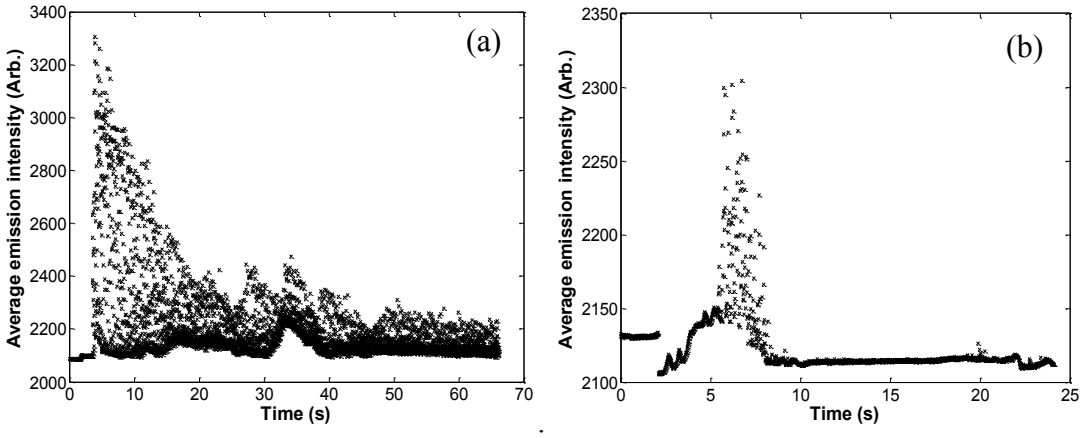

Figure 6.5: Variation of triboplasma with time from PTFE-sapphire interface (a) in dry sliding (b) under water submerged conditions.

6.2 Dye interaction tests

From the studies presented in **Chapter 5**, it was observed that the triboemission from the contacting materials varied at millisecond as well as second timescales. It was concluded that these variations were driven by presence of regions of charge of opposite polarity on the surface and charged debris. This section strives to build on the principles of interacting charges by using fluorescence to image these charged areas and their possible interaction with selected dyes. A fluorophore or a fluorescent dye molecule should interact with the tribocharged surface due to the presence of various functionalized or polar groups such as isothiocyanate group (-N=C=S) or carboxyl group. This interaction is achieved by either attraction to or repulsion from specifically charged sites and in doing so the dye could highlight areas of positive and negative charges. 5, 6 carboxyfluorescein (CF) was selected because of the presence of reactive functional group. CF is a fluorescein based dye (absorption wavelength is 495 nm and emission wavelength 517-519 nm) with an added carboxyl group, thus it is a highly charged derivative of fluorescein dye, and hence it will be attracted to oppositely charged surface. Furthermore, this interaction may be physical and chemical depending upon the dye-surface characteristics as well as mechanical and thermal conditions at the contact. It has been known that carboxyfluorescein which consists of a benzene moiety is highly fluorescent, while some of its derivatives containing an electron acceptor group such as NH_2 or an electron donor group such as NO_2, have almost no fluorescence due to photo induced electron transfer (PeT). This has been reviewed in [219] by Nagano. Figure 6.6 shows the mechanism of fluorescence quenching. Fluorescence of a derivative with an amino group on the benzene moiety (left column) is quenched by electron transfer from the benzene moiety to the excited fluorophore

(acceptor excited-PeT). For this to take place, the HOMO (highest occupied molecular orbital) energy level of the benzene moiety must be very high (in other words, the oxidation potential of the moiety is low). On the other hand, fluorescence of a derivative with a nitro group on the benzene moiety (right column) is quenched by electron transfer to the benzene moiety from the excited fluorophore (donor excited-PeT). For this to take place, the LUMO (lowest unoccupied molecular orbital) energy level of the benzene moiety must be very low.

Even if this phenomenon is known to occur, it is nearly impossible to determine if such derivatives were actually formed during sliding in water submerged contact. However, a transient quenching is plausible when excess of electrons are available to aid fluorescence quenching by electron transfer. Such a phenomenon was recorded and presented later in this chapter in Figure 6.10 and Figure 6.11.

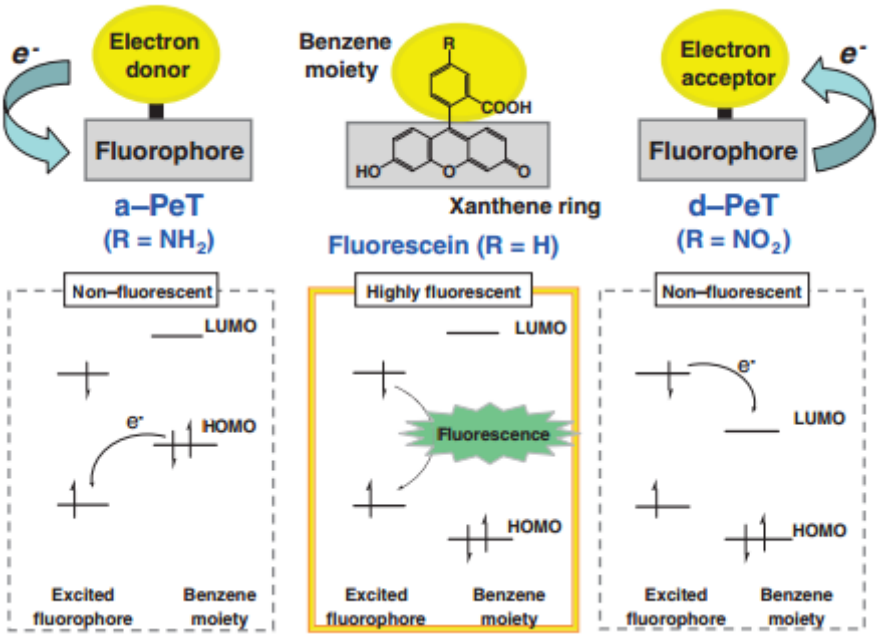

Figure 6.6: Schematic illustration of the change of fluorescence properties by the acceptor-excited PeT (a-PeT) mechanism (left column) and donor-excited PeT (d-PeT) mechanism (right column). Fluorescein derivatives can be regarded as conjugates of two independent moieties, the benzene moiety and the xanthene ring (fluorophore)of carboxyfluorescein (middle column) [219].

The interaction of carboxyfluorescein dye with triboemission at the rubbing contact was studied using PTFE and UHMWPE balls of 6 mm in diameter. CF was either mixed with deionized water or with group II mineral oil to obtain a 1 mM solution for two separate sets of experiments. Their preparation technique is given in the methods section. In this set of tests, the contact and the dye mixed liquid surrounding it, is viewed from top through the transparent

sapphire disc. Fluorescence images of the contact before and after the sliding test were viewed with the help of the fluorescence microscope and the images were captured using a high speed CCD camera. A mercury lamp in conjunction with Zeiss Filter Set 38 HE was used to excite the dye. The load used for this test was 20 N and motor speed and wear track diameter were set to ensure a low sliding speed of 5.5 mm/s. The ball was secured to the holder to ensure pure sliding conditions at the contact. All tests were carried at room temperature.

Figure 6.7 shows in-situ images of stationary sapphire versus 6 mm diameter PTFE ball contact Image (a) shows a white light image, (b) shows a fluorescence image before sliding and (c) shows a fluorescence image just after sliding in deionized water only while (d) shows white light image, (e) shows fluorescence image before sliding while (f) shows fluorescence image just after sliding in 1 mM CF mixed deionized water. The fluorescence image here refers to the wavelength of light emitted in the range of 500-550 nm. This is done by use of the filter set that allows wavelength of light only in range of 450-490 nm to be incident on the contact surface and filters out all wavelengths allowing only wavelength in range of 500-550 nm to reach the eye piece or camera. Since there is no dye present, there is no apparent difference between images (b) and image (c). The bright strands observed in both images are probably dangling PTFE fibers. The fluorescence image of the contact immersed in 1 mM CF mixed deionized water taken after sliding for one minute shows a marked change. The dye particles form non-fluorescent agglomerates which are seen as black patches in the contact. This kind of aggregations have been shown to arise from a competition between cohesive forces and flow rupture at the contact. Furthermore, the size of the aggregates have been correlated with the solution concentration and shear rates [220]. The black patches may also originate from a selective attachment of the dye molecule with the rubbed contact or with the debris. This is possible when fluorescence quenching of the dye occurs by interacting with charged debris. At the inlet of the contact (left side of image (f)), a crescent shaped region with different contrast to the background is observed. This is the polymer debris that is unable to enter into the contact, hence has accumulated there. The fibrous as well as lamellar shaped PTFE debris is seen at the exit of the contact is of different contrast as well compared. The black patches could be the dye fluorophores that were broken due to the high shear force at the contact which is a manifestation of mechanochemistry. Although this experiment provides some evidence of interaction of the fluorescent dye with freshly generated PTFE debris, it does not provide any information of the polarity of the charge present at these sites.

Figure 6.8 shows an ex-situ optical microscope image of the rubbed ball surface. The RGB color scheme has been adjusted to show the difference in dye stained PTFE debris seen as yellow patches and debris-dye agglomerates seen as red patches. This observed behavior is markedly different compared to the expected/desired outcome of these tests, which was that the fluorescent dye would be attracted to the rubbed surface and highlight areas of positive and negative charge. Although this has not be achieved, the results show that carboxyfluorescein dye is effective in interacting with charged sites and hence could potentially function as a charge detection probe. Additional tests confirming this interaction in case of PTFE-sapphire and UHMWPE-sapphire contact under liquid submerged conditions involving dye mixed water and dye mixed oil is presented in **Appendix D**

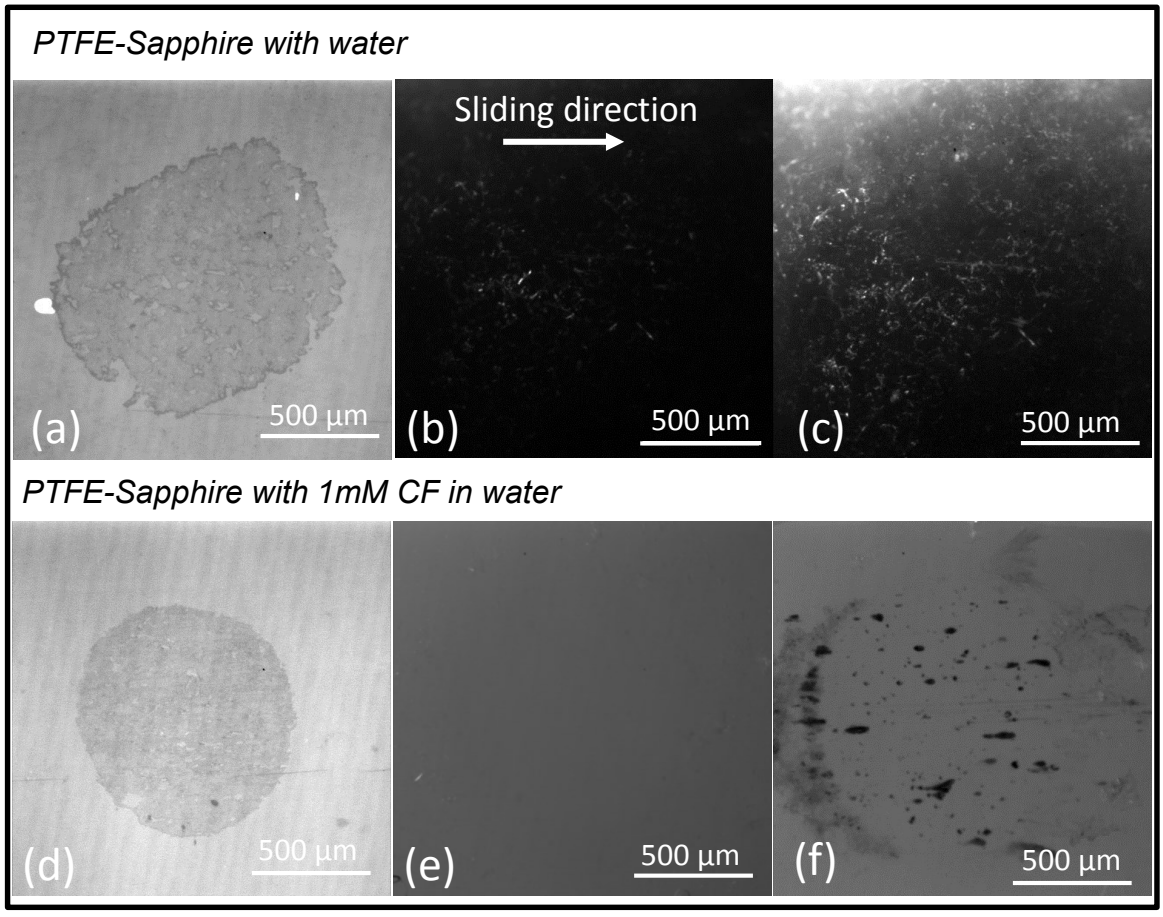

Figure 6.7:PTFE –Sapphire contact– submerged during sliding in water (no dye) – in situ fluorescence images (a) white light image (b) fluorescence microscope image before test (c) fluorescence microscope image after test [excited by 450-490 and observed in wavelength in range of 500-550 nm].PTFE –Sapphire contact– submerged during sliding in 1mM CF in water (a) white light image (b) in-situ fluorescence image before test (c) in-situ fluorescence image after test.

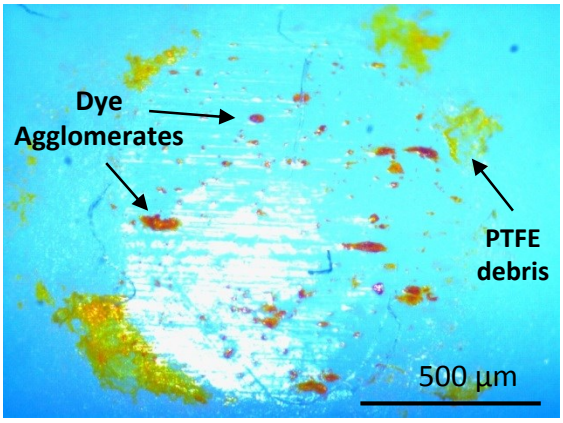

Figure 6.8: Contact area of the PTFE ball visualized under optical microscope after sliding test.

To overcome the effects of shear forces on the lubricant and to evaluate triboemission interaction on its own merits without issues such as dye agglomeration, another novel approach was employed. For this, dye interaction studies were performed away from the rubbing contact. After several seconds of dry sliding between a PTFE disc and sapphire hemisphere, a drop of 1mM CF dye solution was placed on the wear track and immediately covered with a cover slip. The fluorescence images were then recorded using the fluorescence microscope and camera. Figure 6.9 shows a white light image of the wear track after rubbing prior to dye drop placement. Figure 6.10 shows a sequence of fluorescent images captured immediately after adding a drop of dye, covering with coverslip and re-focusing.

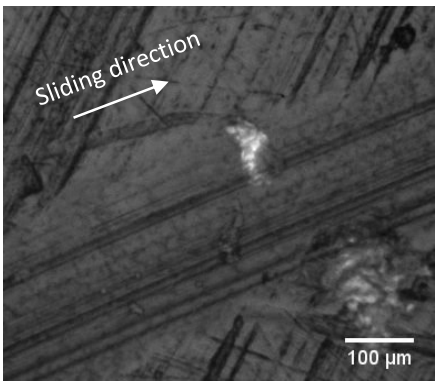

Figure 6.9: Optical white light image of the wear track on freshly rubbed PTFE disc against sapphire hemisphere

In the sequence of frames shown in Figure 6.10**,** an after-emission event is captured. More specifically, a site on the wear track highlighted in frame 4 undergoes a spontaneous fluorescence whose fluorescent intensity is plotted in Figure 6.11. The exposure time was 364.68 ms and frames were captured at a rate of 2.74 fps. Hence, the total time duration between the initiations to the attenuation of the fluorescence activity at the location is roughly

3 seconds. The time scale involved suggests that the observed phenomena is phosphorescence (delayed fluorescence) as fluorescence lifetimes are in general much shorter than phosphorescence lifetimes, *i.e.*, nanoseconds rather than milliseconds. In Figure 6.11, the minimum and average intensity remain unchanged while the maximum fluorescence intensity shows a peak value and gradually declines.

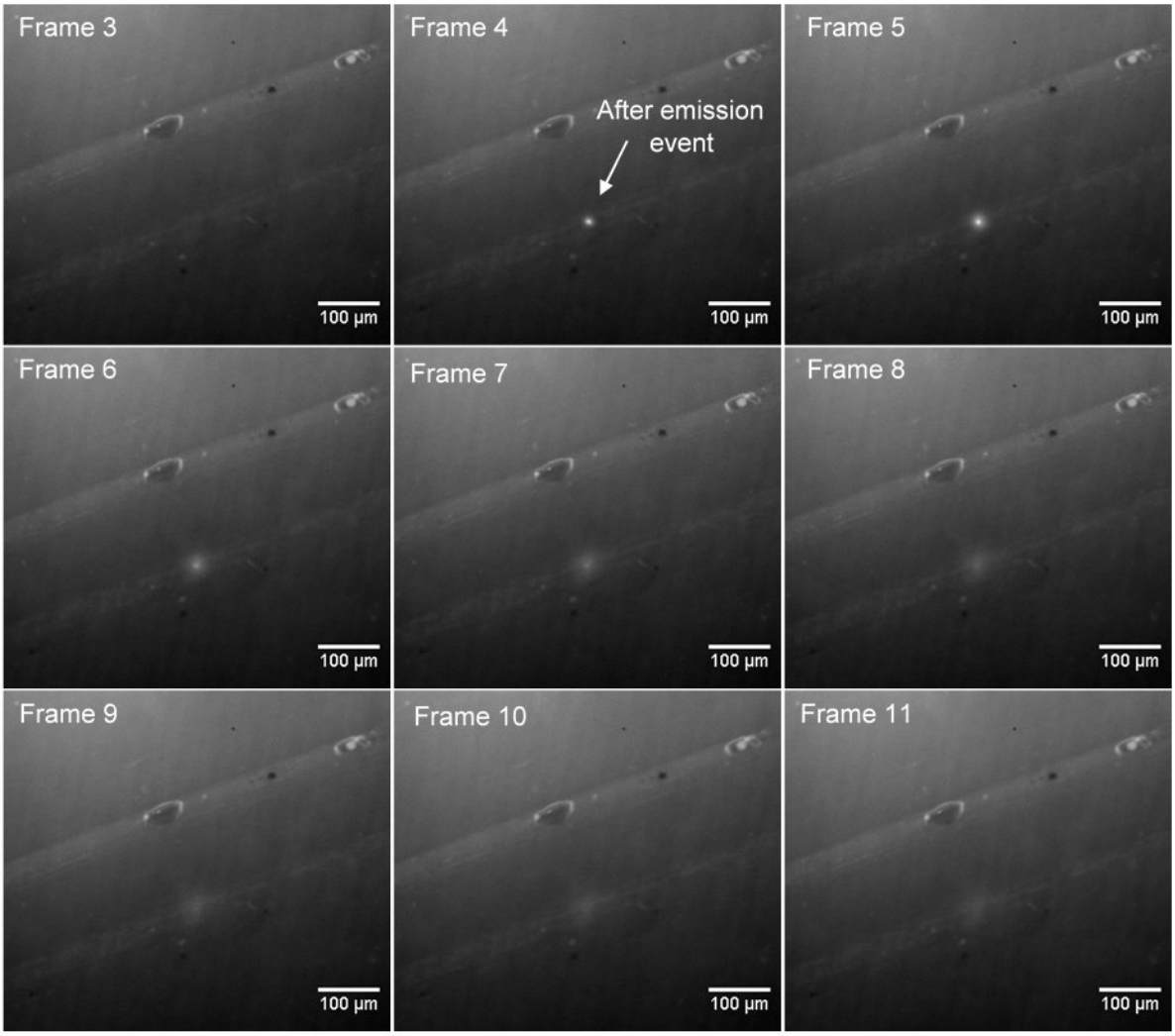

Figure 6.10: An after-emission event captured using CF dye in liquid submerged condition on PTFE wear track

This after emission event captured using the fluorescence of CF dye under liquid submerged conditions corroborates with the after-emission event observed on scratching PTFE disc with a diamond stylus discussed in **Chapter 4**. An after-emission event refers to emission of electrons or ions occurring after the sliding ceases. This provides direct evidence of how energy stored in the material due to work done in deforming it, generating cracks, and creating fresh surfaces could potentially affect the surrounding medium. Moreover, polymers undergo relaxation to relieve their state of stress (or strain), over a period of time and the amount of relaxation is a

function of time, temperature, stress level, and the degree of viscoelasticity. As discussed in **Chapter 4**, the strain relaxation is facilitated by rupturing of bonds and formation of microcracks. Only recently the effects of strain-relaxation on spatially-resolved photon emission from light emitting materials and substrates was reported [220]. It is believed that this stored energy is released to the surrounding medium as emission of the electrons and ions under conducive conditions. This available energy has the potential to either simply excite the molecules of the medium or disintegrate them to a favourable state that overcomes the activation energy for a chemical reaction.

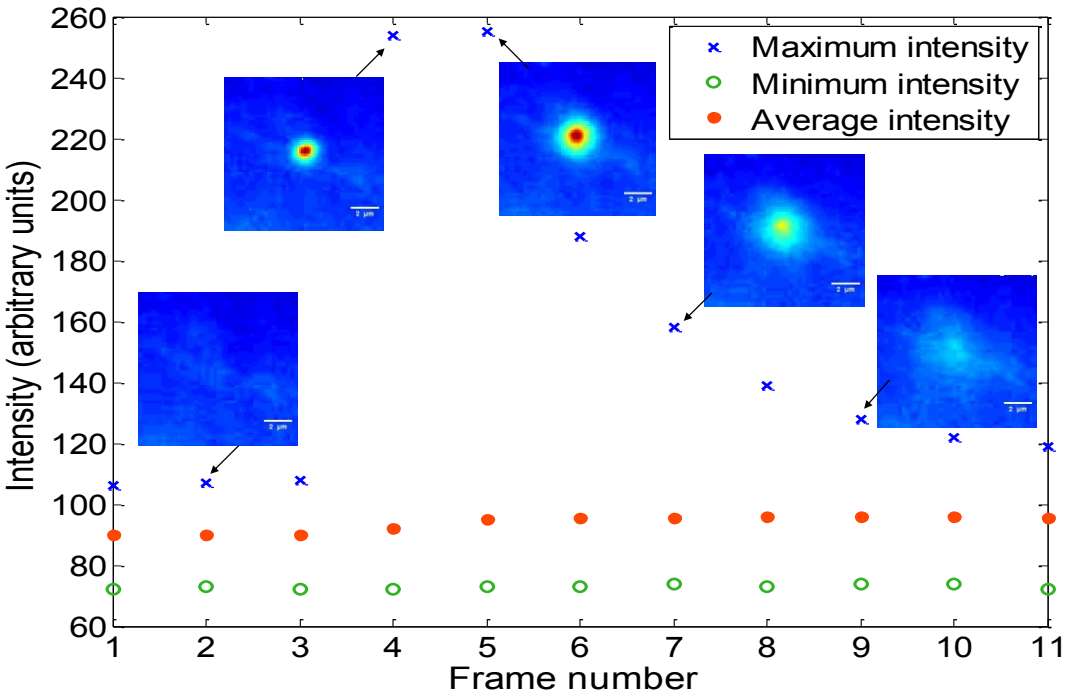

Figure 6.11: The rise and decline of maximum fluorescence intensity of an after emission event location obtained for a sequence of frames at 2.74 fps. The minimum and average intensity remain fairly unchanged.

In this case, the CF fluorophores may have undergone a phosphorescence process whereby a molecule relaxes from the triplet excited state to the singlet ground state [221]. The fluorophores could also be involved in a transient energy transfer process and interaction with the charged sites of the rubbed polymer surface leading to temporary deactivation of their excited electronic state following electron transfer as discussed earlier. These fluorophores could subsequently fluoresce and diffuse.

Although the exact mechanism needs to be explored, nevertheless it was evident that carboxyfluorescein fluorophore can respond to tribocharging and triboemission occurring from

rubbing contact. This technique could be improved to visualize triboemission under submerged conditions.

6.3 Protein interaction tests

Due to the complexities associated with conventional dyes (used in Section 6.2) to monitor charging behavior under submerged conditions, a series of tests were run using fluorescently tagged proteins as sensors. Fluorescein isothiocyanate (FITC) tagged Albumin was used to identify and visualize sites of protein interaction with the rubbed polymer by using the fluorescence microscope. Albumin is a protein extracted from bovine blood. FITC dye and FITC tagged Albumin were procured from Sigma Aldrich. These dyes were mixed with deionized water to obtain a concentration of 1 mM. FITC is a fluorescein based dye functionalized with an isothiocyanate reactive group (-N=C=S), replacing a hydrogen atom on the bottom ring of the structure. Its absorption wavelength is 495 nm and emission wavelength 517-519 nm. Pin on disc tests were performed using the CETR UMT Tribometer facility by loading a stationary hemispherical sapphire pin of 5 mm diameter unto a rotating polymer disc of diameter 50 mm and thickness 3-5 mm. The roughness (R_a) of discs were in the range of 0.5 to 1 μm. The sapphire pin was slid against three polymers namely, PTFE, UHMWPE and Nylon. Tests were performed at room temperature and the load was kept fixed at 2 N. The tests shown here were performed using the following test sequence. Two minutes of dry rubbing at 785 mm/s to produce a clear wear track for ease of visualization, followed by 2 minutes of rubbing at 785 mm/s with the test lubricant present at contact and on the wear track. The coefficient of friction (μ) was simultaneously recorded during sliding. The dye, and dye tagged Albumin solutions were dropped at the contact interface before the start of sliding such that the liquid is present at the contact. Tests with and without protein present at the interface were conducted to examine the extent of protein interaction with the rubbed surface and its effect on friction behavior. After completion of each experiment, the wear track on the disc samples were examined using the fluorescence microscope at 10× magnification.

Figure 6.12: shows optical and fluorescence images of the wear track on a UHMWPE disc rubbed against a sapphire hemisphere in presence of dye, mixed with deionized water (images a and b) and protein tagged with FITC dye, mixed with water (images c and d). It is evident that the dye attaches to the sheared surfaces of the UHMWPE disc (seen in (b)) where fluorescence is brighter on the ridges of the groove. When rubbing is carried out in the presence of FITC tagged protein, the rubbing interferes with the attachment of the dye tagged protein to the rubbed surface and consequently the wear track is less fluorescent (darker contrast in Figure

6.12b) as compared to the unrubbed surface. Albumin being negatively charged is repelled from negatively charged wear track. Figure 6.13 shows the variation of coefficient friction when UHMWPE is rubbed against the sapphire pin at 2 N and 785 mm/s under unlubricated, water lubricated and protein lubricated conditions. The scatter of the coefficient of friction is due to periodicity of the disc surface. A higher coefficient of friction is observed in dry sliding as compared to sliding in presence of water or protein which have nearly the same average friction coefficient. After 15 seconds of sliding, the water gets removed from the contact due to the centrifugal force acting due to the high speed rotation. This leads to increase in the coefficient of friction to the values observed in dry sliding. This phenomenon is not seen when protein is present, which suggests the retention of protein molecules at the contact. The evidence of protein repulsion from the negatively charged UHMWPE wear track is shown in Figure 6.12(d).

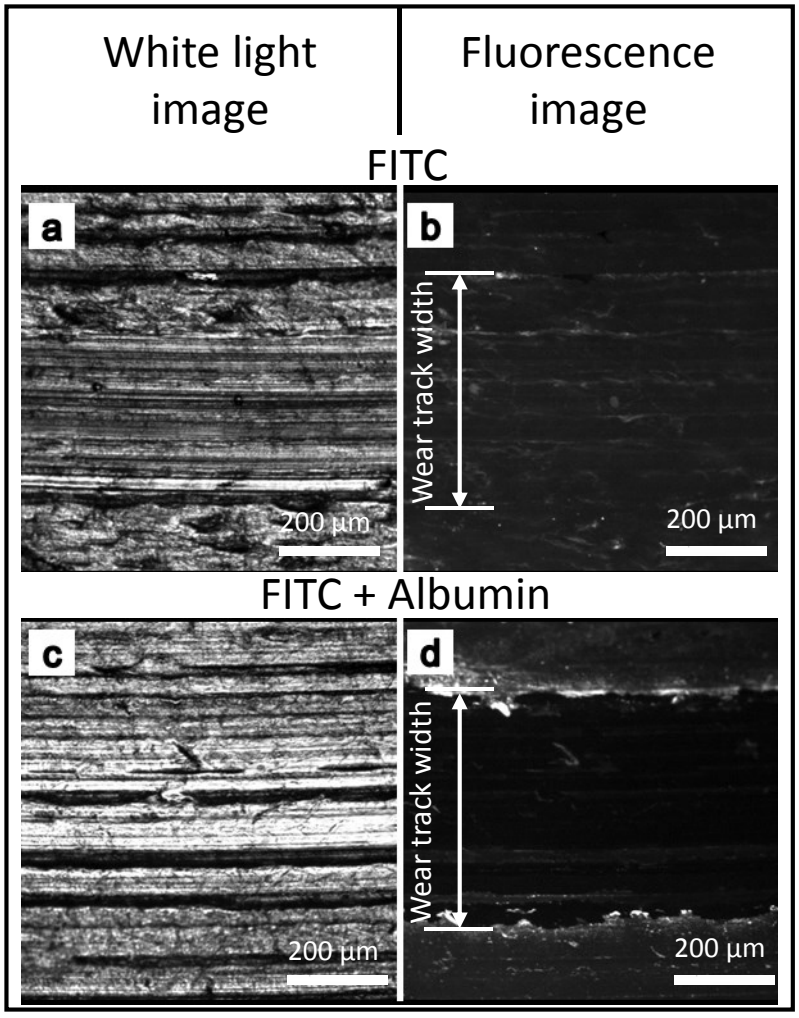

Figure 6.12: Optical (a and c) and fluorescence (b and d) images of wear track on a UHMWPE disc rubbed with sapphire hemisphere. Images (a) and (b) obtained after rubbing in presence of FITC dye mixed with deionized water. Images (c) and (d) are obtained after rubbing in presence of protein tagged with FITC dye mixed with water.

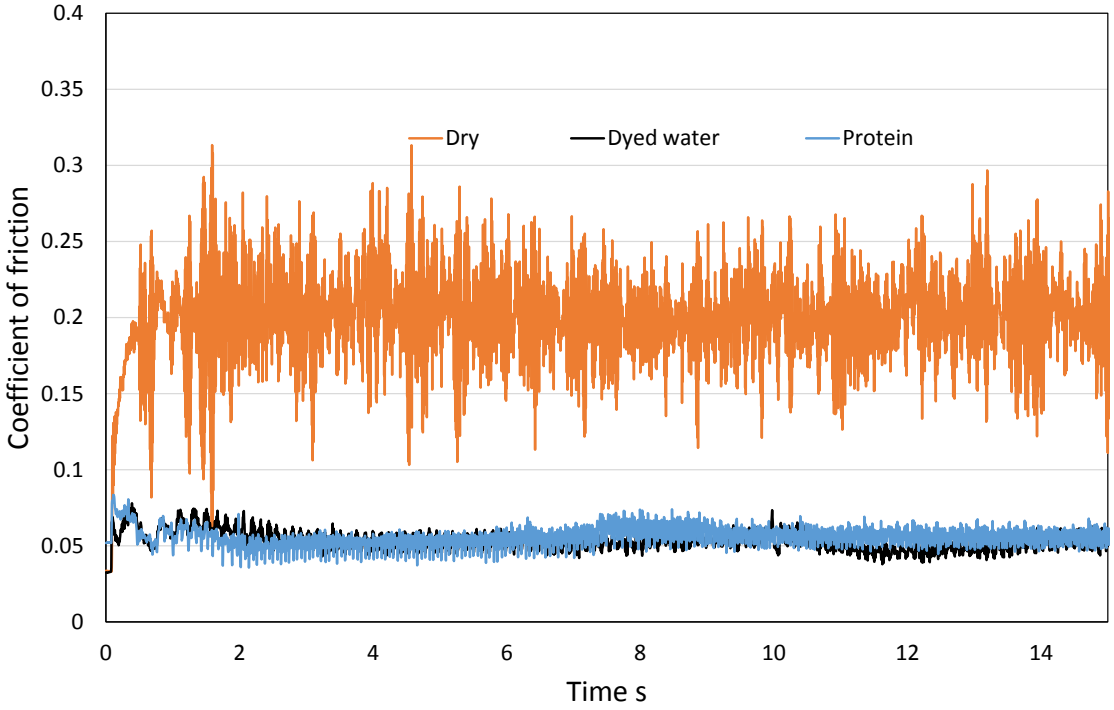

Figure 6.13: Variation of coefficient friction when UHMWPE is rubbed against sapphire pin at 2 N and 785 mm/s.

Similar observation is made with tests involving PTFE discs, where the coefficient of friction is highest under dry conditions followed by sliding in presence of water and protein (Figure 6.15). The dye attaching to the wear debris on the wear track is evident in Figure 6.14. The bright areas along the wear track are due to attachment of dye to charged sites of opposite polarity on the track and wear debris. There also appears to be some dyed debris on the protein-free sample as debris becomes fluorescent.

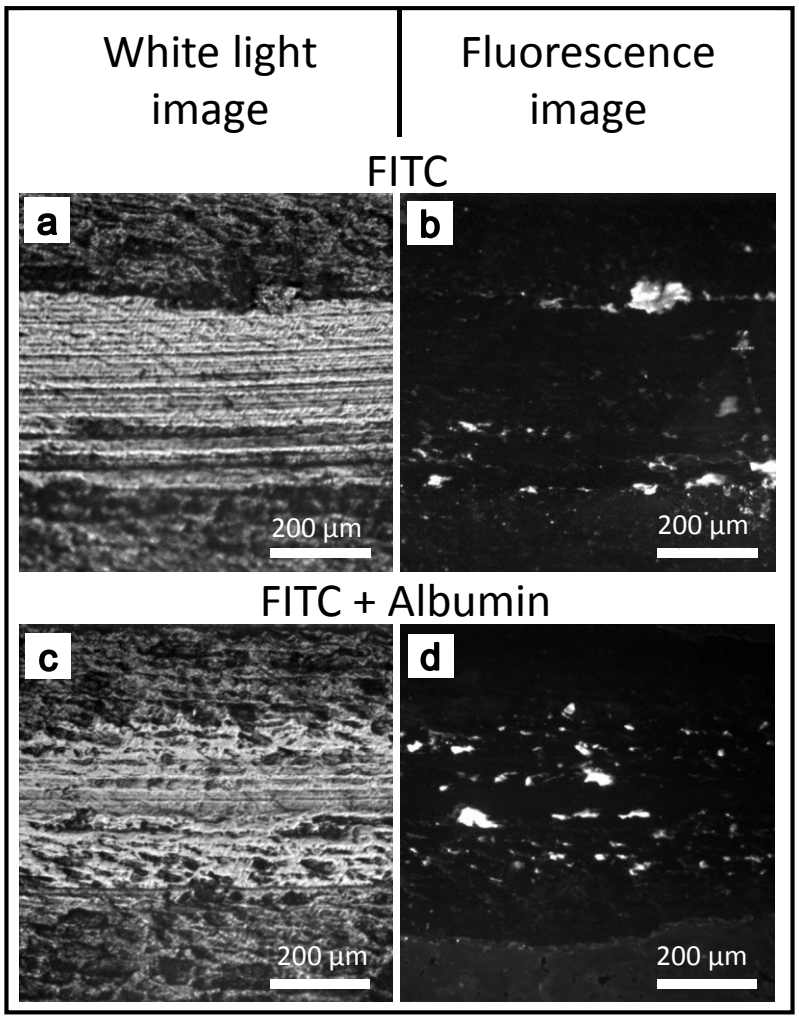

Figure 6.14: Optical (a and c) and fluorescence (b and d) images of wear track on a PTFE disc rubbed with sapphire hemisphere. Images (a) and (b) obtained after rubbing in presence of FITC dye mixed with deionized water. Images (c) and (d) are obtained after rubbing in presence of protein tagged with FITC dye mixed with water.

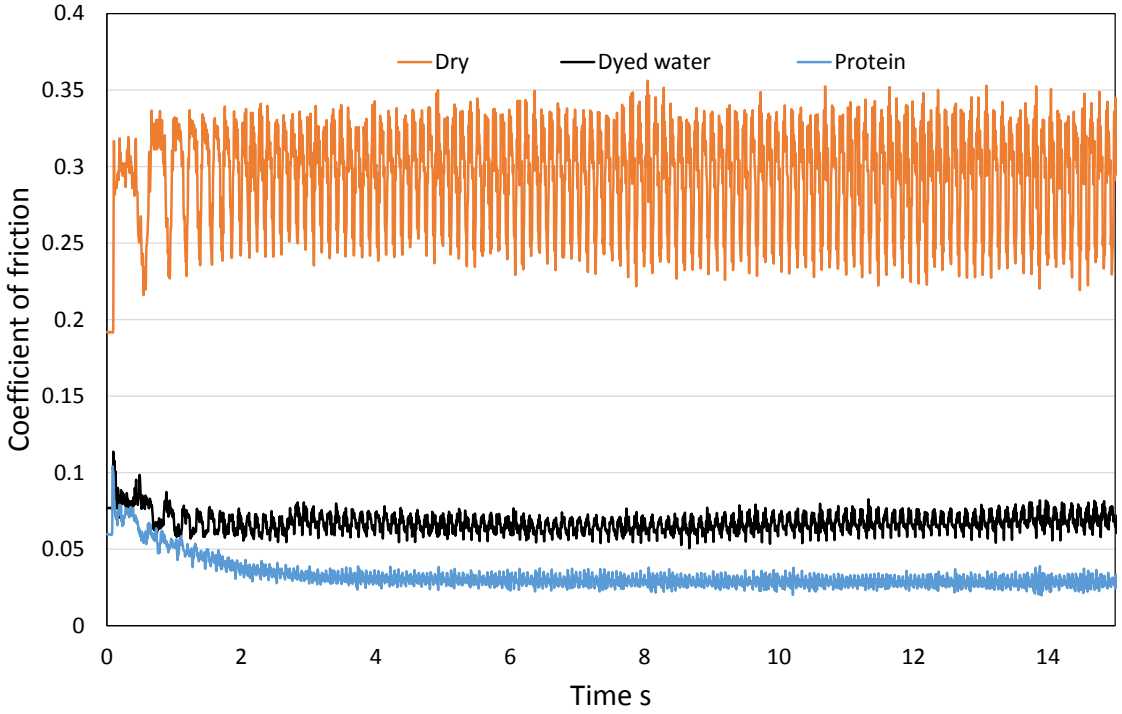

Figure 6.15: Variation of coefficient friction when PTFE is rubbed against sapphire pin at 2 N and 785 mm/s.

Different polymers become charged to different values and with different polarities during contact or rubbing through a process known as contact electrification/triboelectrification. The net polarity and the quantity of the charge acquired by a material generally follow the empirical triboelectric series. It was shown in **Chapter 5** that both PTFE and UHMWPE disc charge negatively while Nylon and PEEK charge positive on rubbing with sapphire. This would mean that the water and the negatively charged Albumin would attach readily to the rubbed Nylon surface which charges positive. This behaviour is confirmed from images c and d in Figure 6.16 which shows optical and fluorescence images of the wear track on a Nylon disc rubbed with sapphire hemisphere in presence of dye mixed with deionized water (images a and b) and protein tagged with FITC dye mixed with water (images c and d). In images c and d the dye attachment along the wear track is seen as bright areas which are mostly at the edges of the sheared polymer as well as debris.

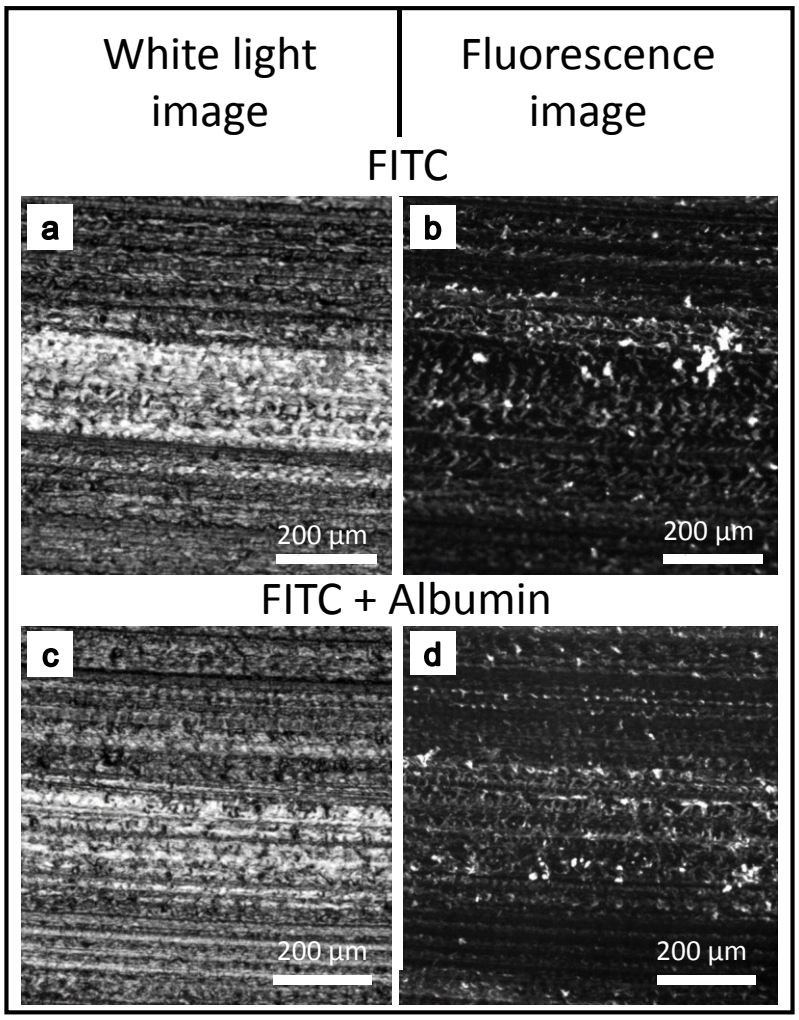

Figure 6.16: Optical (a and c) and fluorescence (b and d) images of wear track on a Nylon disc rubbed with sapphire hemisphere. Images (a) and (b) obtained after rubbing in presence of FITC dye mixed with deionized water. Images (c) and (d) are obtained after rubbing in presence of protein tagged with FITC dye mixed with water.

6.4 Conclusions

No techniques or methods were available to study the effect of triboemission and tribocharging in liquid submerged conditions. Therefore, new techniques to study triboemission and tribocharging when the contact is submerged in a confining liquid were developed. These techniques involved viewing the contact or the rubbed wear track using a fluorescence microscope by exploiting dye fluorescence and its charge sensitive attachment behaviour. To overcome the effects of shear forces on the lubricant, a novel approach was developed that uses a dye fluorophore as probe to monitor after-emission events on the wear track of polymer disc away from the rubbing contact. The new techniques developed here serve as tools to monitor triboemission/charging events under lubricated conditions and provide further understanding

about how tribocharging and triboemission interacts with a submerged environment. The major findings are as follows

1. The triboplasma which is observed in and around the contact in dry sliding conditions is only observed at the outlet of the contact which is a region of cavitation and flow separation under pure sliding conditions.
2. When an electrically conducting liquid is present the triboplasma is not generated even at the flow separation region because the charge generated by rubbing is neutralized by the ions of the solution.
3. Discharge also occurs inside air bubbles which have very short lifetime as they form and collapse during shearing of the liquid. Submersion in a liquid environment reduces plasma due to various reasons such as high breakdown voltage of the medium, low number of photons, or photon attenuation due to diffraction.
4. The after-emission phenomena for PTFE observed here in submerged conditions bears a close correspondence to that observed in vacuum conditions in **Chapter 4**.
5. From the in-situ fluorescence experiments, which showed reduced intensity regions due to rubbing, the interaction between dye and rubbed surface could be interpreted in three ways. Firstly, the non-fluorescent state can be attributed to the formation of a non-fluorescent dye derivative due to electron transfer from the rubbed surface. Secondly, the non-fluorescent state of dye may be due to agglomeration of the dye molecules resulting in precipitation out of the solution. The dye aggregates could also result from the adsorption of the dye molecules to the surface of the sheared polymer and generated debris following the sliding process. Meanwhile, the regions where the dye fluoresces more intensely may be due to increased concentration of dye molecules at these specific sites based on attraction to oppositely charged surface. It is not possible to determine the exact mechanism and whether agglomeration or formation of non-fluorescent state or both occur.
6. The preferential attachment of bio-lubricant-protein was explored. Albumin being negatively charged is repelled from the negatively charged wear track of UHMWPE. In the case of PTFE and Nylon, the protein is attached to the positively charged debris and positively charged regions on the wear track of Nylon. Dye tagged proteins thus can provide insight into charge distribution along wear track by locating charged areas with a different contrast in the fluorescent image. This in conjunction with friction data

provides further understanding whether the interaction is favourable or not from a friction and wear perspective.

Complex contributions from a large variety of energetic species as well as physical and thermodynamic forces make it impossible to provide definite answers with regards to the contribution of any force *i.e.* shear force, pressure, temperature or triboemission. The physico-chemical forces may break the physical and chemical bonds, yielding active nucleation sites, polar groups, and scission products onto the polymer surface. Overall, triboplasma like any other plasmas involved in atmospheric plasma treatment process may promote removal of molecules and fragments, and by limiting their interfacial diffusion and promoting specific interactions across the interface, cause the formation of new functionalised surface layer. This new surface would be favourable for dye and protein attachment which themselves possess functionalized moieties with some polarity.

This completes the triboemission studies in all three environments, vacuum, air, and liquid. The next chapter will present studies performed to elucidate the correlation between triboemission and tribochemistry by using a lubricant containing the anti-wear additive ZDDP and monitoring its formation and growth. Specifically, the final chapter shows for the first time, the formation of phosphate films on irradiation of additive containing surface with UV photons and hence, provides evidence for chemical reactions to be potentially triggered by electrons.

Chapter Seven

Investigation of Factors Effecting Film Formation

Triboemission generation in vacuum, air and liquid submerged conditions were investigated in the previous three chapters. This chapter explores deeper into the interactions between triboemission and a lubricant additive 'Zinc dialkyldithiophosphates' (ZDDPs) with the aim of establishing link between triboemission and tribochemistry.

There has been speculation about the role of triboemission, in particular, electrons in chemical reactions necessary for the antiwear tribofilm formation [1]. However, few systematic studies have been carried to test this hypothesis. It is therefore important that this chapter provides some evidence of chemical film formation on surface by a chemical reaction triggered by electrons produced in contact (in-situ) and electrons produced artificially (ex-situ).

This chapter is divided into three sections: 7.1 aims to understand the effectiveness of fresh surface formation on phosphate film growth by using a new approach. 7.2 shows the effect of shearing and mixing on ZDDP film thickness using two SRRs on the Mini traction Machine (MTM). 7.3 shows the effect of oxide thickness (hence electron emission) on ZDDP film growth in combined sliding and rolling condition; while 7.4; shows tests carried out using ultraviolet light to stimulate film growth, to evaluate the effect of electron emission. The rationale here is that electron emission has been shown to correlate with oxide thickness and therefore may be correlated with film growth. This method entirely removes the effect of shearing at the contact. Specifically, it uses a novel approach to produce electrons that does not need a vacuum environment or contact shearing. It uses ultraviolet light which produces photoelectrons from the irradiated surface via photoelectric effect. The resulting reaction films formed on the surface using both this technique and regular rubbing are analysed using ToFSIMS.

From the studies done in this chapter, it is concluded that fresh surface do not contribute ZDDP film formation while shearing has strong correlation with the kinetics as well as thickness of ZDDP film formation. The trends of film formation with varying thickness of oxide film shows a positive correlation between oxide thickness (previously correlated with quantity of emission [204]) and antiwear tribofilm thickness. ToFSIMS analysis of rubbed or irradiated surfaces also confirm formation of a zinc phosphate film. However, it should be noted that changing the oxide thickness changes the topography, pressure, subsurface stress distribution and debris formation which may also affect film growth.

7.1 Effect of fresh surface on antiwear film formation

To evaluate the role of fresh surface on film formation it is essential to evaluate difference between a fresh surface and surfaces that is usually covered with natural oxide layer. For this purpose, the surface of a steel sample was scratched with a diamond indenter and subsequently the variation in work function and gradient was measured using scanning kelvin probe (see Figure 7.1). Work function is defined as the minimum quantity of energy which is required to remove an electron from the surface of a given solid metal. From Figure 7.1, it is clear that work function is lowered due to scratching as it creates fresh surface that are free from oxide and therefore, very reactive. It was also observed that the work function changes back to usual value with time (see Figure 7.2) owing to the passivation by atmospheric oxygen. This is the first ever proof of concept study confirming the lowering of work function of freshly created surface.

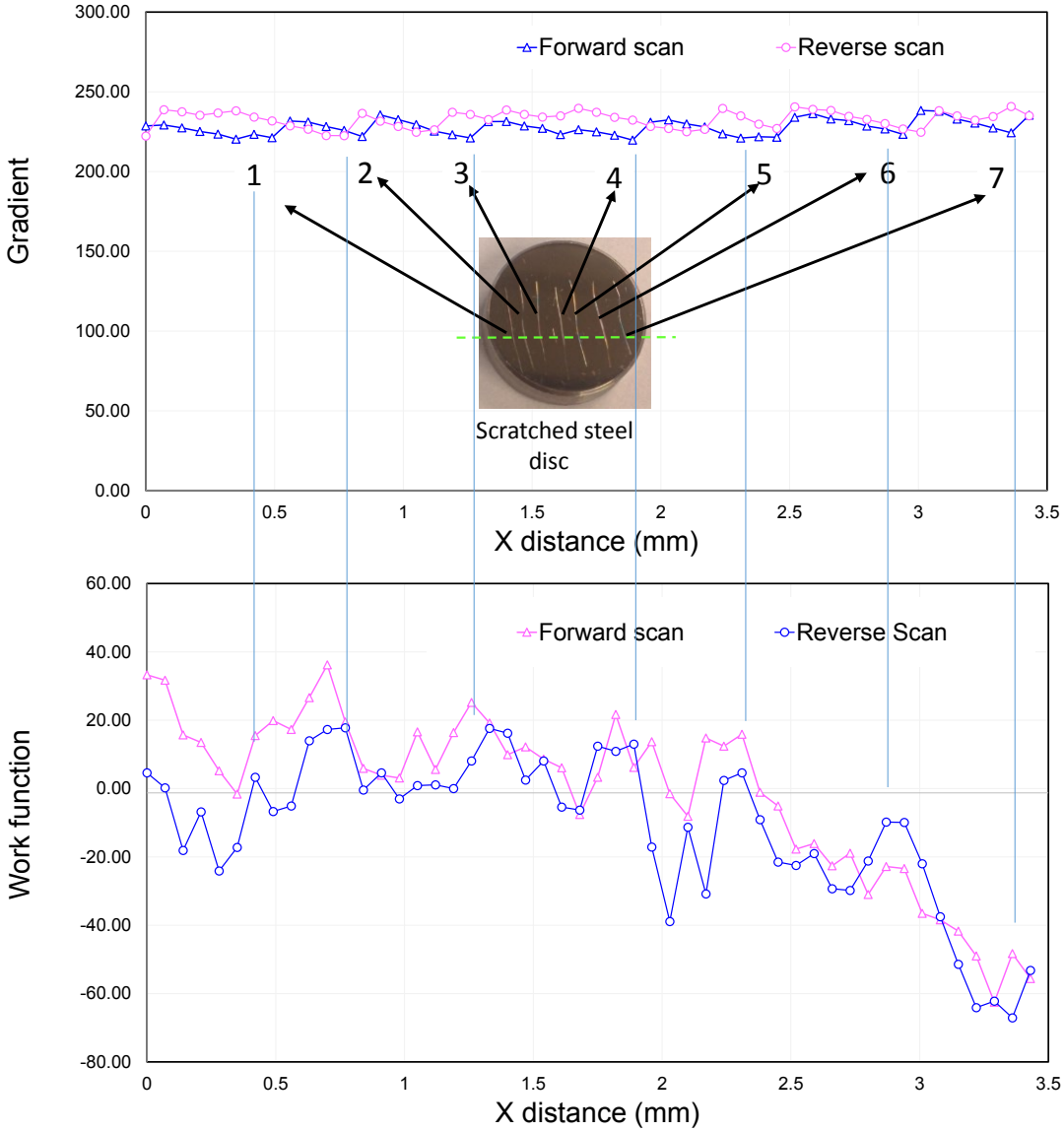

Figure 7.1: The line scans of gradient and work function variation of freshly scratched steel using line scan using Scanning Kelvin Probe.

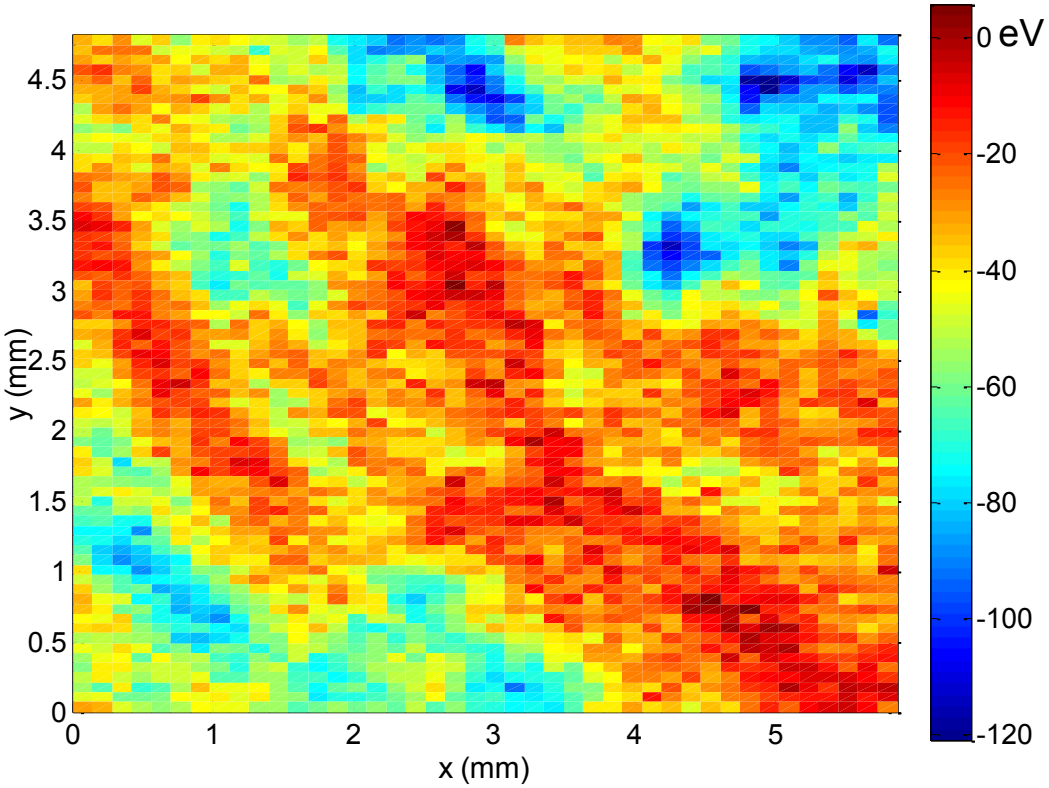

Figure 7.2: Mapping of variation of work function of the entire surface of freshly scratched steel using Scanning Kelvin Probe. The workfuction map doesnot show the 7 vertical scratches that were created on the steel surface.

A freshly generated surface may also retain some residual charge and/or exhibit after emission events. In order to evaluate the role of fresh surface formation, after emission or residual charges on tribofilm formation, a test protocol shown in Figure 3.14 was followed. **Case I**, involved dry sliding of a steel ball on a steel disc for one rotation of the disc at 100 ^{o}C, immediately followed by pouring lubricant maintained at 100 ^{o}C on the wear track; **Case II**: Involved rubbing in the presence of hot lubricant. Any resulting film formation was subsequently measured using AFM and ToF-SIMS after cleaning with cyclohexane to remove oil from the surface. The rationale here is that, if reactive nascent surfaces drive tribofilm formation, they will be formed during both sets of tests, (whereas if nascent surfaces are not the driver, films will only be formed for Case II tests). Combined sliding rolling (50% SRR) tests, one of short duration (10 seconds) and another of long duration (2 hours) were also carried out for comparison of morphology and film properties.

Figure 7.3 shows the comparison of average of normalized intensity counts of, PO_2^- and PO_3^- ions observed from the steel wear track surface shown in images (a) and (b) This semi quantitative analysis confirms the formation of phosphate films on the wear track of steel surface which was slid in presence of hot ZDDP lubricant. Any further comparison will lead to

erroneous conclusions, firstly because the ToF-SIMS technique is a surface sensitive technique and the film formed after single rotation is not uniform and very patchy. However, the AFM images clearly show that film are only formed during rubbing and the reactive surface alone is not sufficient to drive formation.

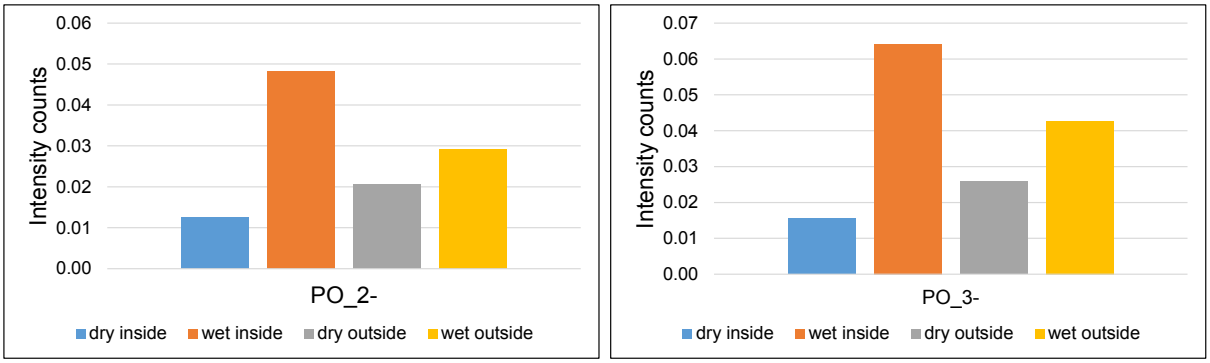

Figure 7.3: Comparison of averaged normalized intensity counts of PO_2^- and PO_3^- ions .Dry refers no oil while rubbing while wet means rubbed in presence of oil. Inside refers to the area inside the wear track while outside refers to area outside wear track.

Figure 7.4 shows AFM images of the wear track on a steel surface under various conditions. Image (a) shows that steel/steel sliding contact without any lubricant leads to high wear and no phosphate film formation is observed even after pouring hot lubricant on the wear track; (b) and (c) shows formation of distinct segregated pads which after a time transform into a more even and morphologically smoother coating over the steel substrate as shown in (d). The image (a) has a deep groove because of metal to metal contact. The wear track width, hence ZDDP film coverage increases with sliding distance/time. It reaches around 200 µm after 2 hour sliding test. All these observations corroborates the three stages growth mechanism proposed in [222]. It was suggested that the nucleation and growth of distinct segregated islands begin on active sites on the steel surface and on continuous rubbing, these islands coalesce causing the film to spread over a larger fraction of the surface and finally large islands fragment into smaller, densely packed structures.

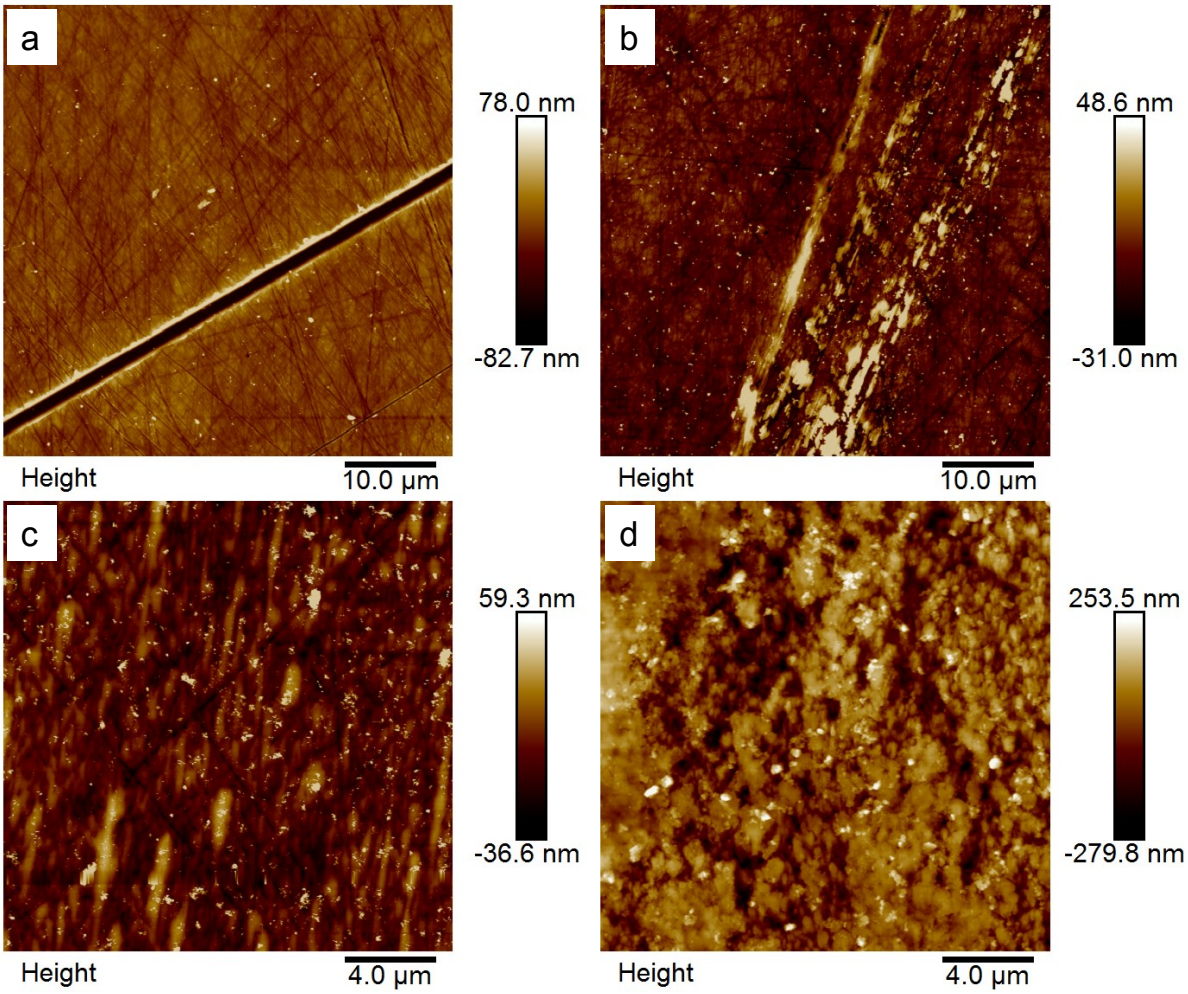

Figure 7.4: AFM images of the ZDDP tribofilm on steel/steel contact at 100 ºC illustrating the morphology difference on different sliding condition and rubbing time. (a) ZDDP oil added after dry sliding for 1 rotation. (b) Sliding for one rotation in presence of ZDDP oil (c) Combined rolling and sliding for 10 seconds (d) Combined rolling and sliding for 2 hours.

7.2 Effect of shearing and mixing on antiwear film formation

The film thickness growth for steel/steel contact under a load of 31 N and speed of 50 mm/s with two different slide to roll ratios (SRR) (0% and 50%) are shown in Figure 7.5. Here, the effect of shearing and mixing at the contact can be observed. For 0% SRR, the contact is entirely rolling while 50% SRR is a combination of sliding and rolling. It must be mentioned that 0 % SRR inevitably has a slight sliding motion. It is evident from Figure 7.5 that the film growth kinetics as well as final film thickness is lower in case of 0% SRR where the amount of shearing at the contacting interface is low.

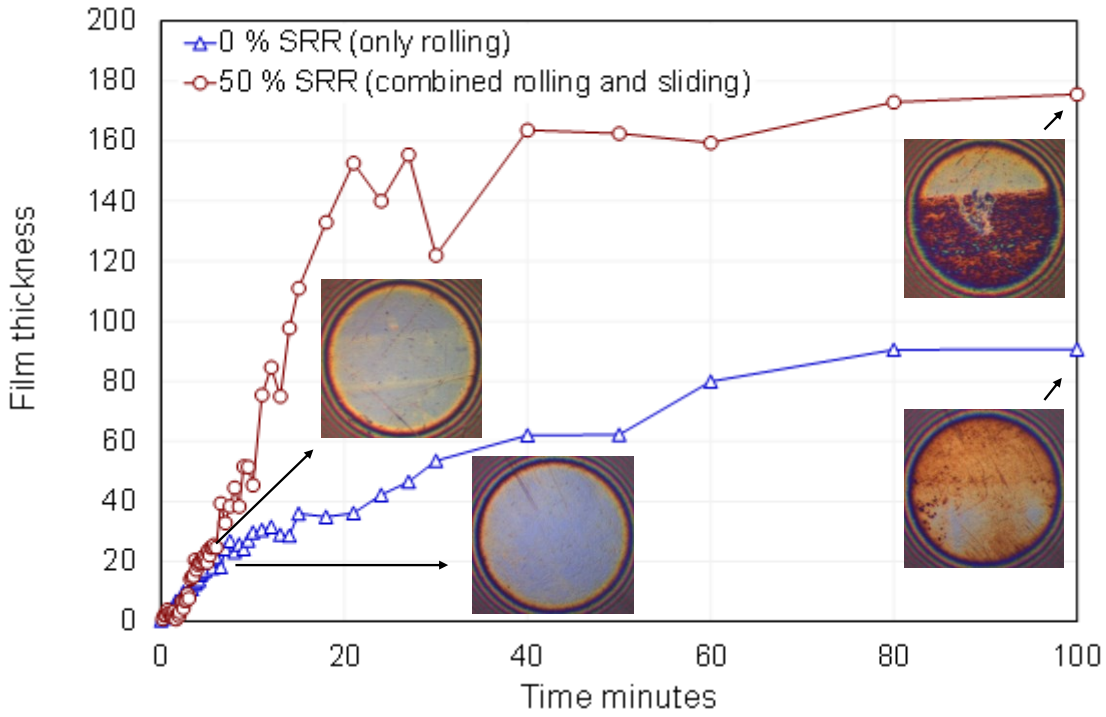

Figure 7.5: Growth of ZDDP film thickness on steel ball rubbed against steel at 0% SRR and 50% SRR

7.3 Effect of oxide thickness on antiwear film formation

This section presents the results of the tests carried out on a mini traction machine (MTM) where a steel ball is rubbed, under mixed sliding and rolling or pure rolling conditions, against aluminium discs which were covered in different oxide thicknesses. This was done in order to study links between ZDDP film formation and electron emission, since emission has been correlated with oxide thickness [56]. In each of these tests, steel (AISI 52100) MTM ball specimen were rubbed with either steel discs or aluminium discs. Aluminium discs with 5, 15, 25 µm of oxide thickness were used in this study. The disc specimens were rubbed against a steel ball of diameter 19.05 mm in the presence of a Group II mineral oil mixed with ZDDP (0.08% P) at 100 $^{\circ}$C under a constant load and speed of 30 N and 50 mm/s respectively. The slide to roll ratio (SRR) of 0.5 ensured equal sliding and rolling conditions at the contact.

Figure 7.6 and Figure 7.7 show the growth of a ZDDP film, measured on the surface of a steel ball using the an MTM SLIM. The graph displayed here is an average of three tests with their standard deviation shown as error bars. Each point on the graphs is obtained from SLIM images

using the SLIM offline analysis software that converts the RGB values of chosen area of the image into film thickness values by comparing with a pre-calibrated file.

The results show that counter specimen oxide thickness, and therefore possibly electron emission, plays a role in the initial growth of ZDDP films. The film thickness measurements show that thicker oxide surface layers result in higher tribofilm growth rates. In addition to this, it can be seen that the film forms more rapidly on the ball surface when it is rubbed against the oxide aluminum disc than when rubbed against the steel disc. It is known that oxide layers on aluminum emit significant quantities of electrons [204] when deformed and that emission intensity is linked to oxide thickness [56], [167]. It is also known that ZDDPs react more readily with oxides than with metallic iron [11], [223]. A natural oxide layer which is the present on polished aluminium disc was also tested (results not shown) but the growth could not be monitored because of high wear and it was concluded that tribofilms cannot form on this surface even though it has a naturally formed oxide layer. The naturally formed oxide layers are too thin (10 nm or less) and lack strong support from the relatively soft substrate, and therefore cannot survive the wear process at load and speed parameters used here.

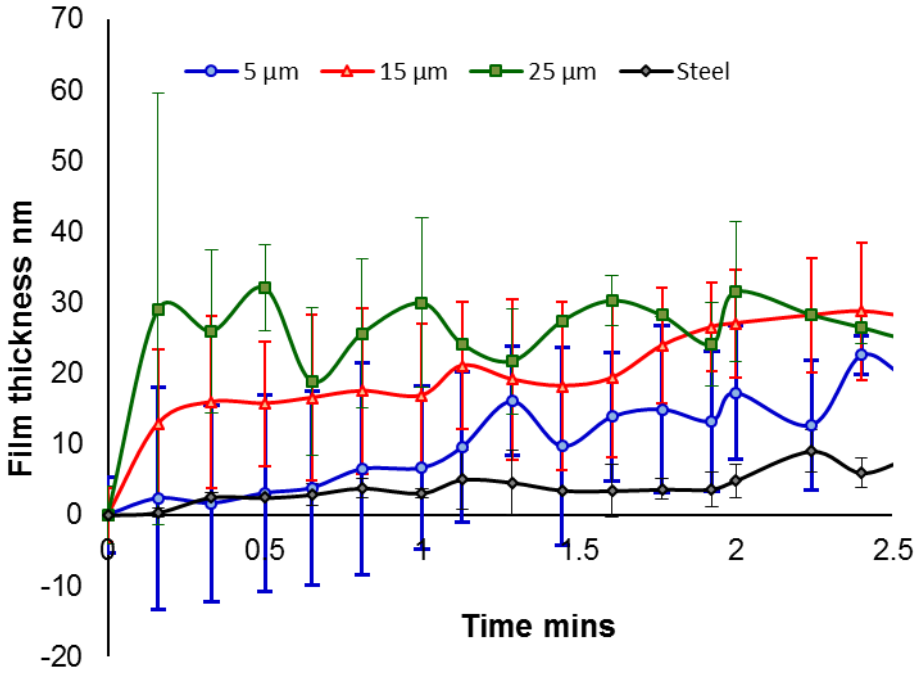

Figure 7.6: Growth of ZDDP film thickness on steel ball rubbed against different oxide thickness of Al_2O_3 in 50% SRR.

These results may suggest a link between triboemission and tribofilm formation. However, this effect is not distinct as it disappears over time *i.e.* these trends are only evident in the first

few minutes of film growth. The trend of growth of ZDDP film during the entire two hours is shown in Figure 7.7. After the first few minutes, the thickness of the film on the steel ball surface rubbed against steel counter surface overtakes those rubbed against the aluminium oxide surfaces which may suggest the electron emission is only a factor in the initial stages of film growth and after this shear stress take control of the growth of the antiwear tribofilm [32], [37]. Further support for this claim is presented later in the chapter.

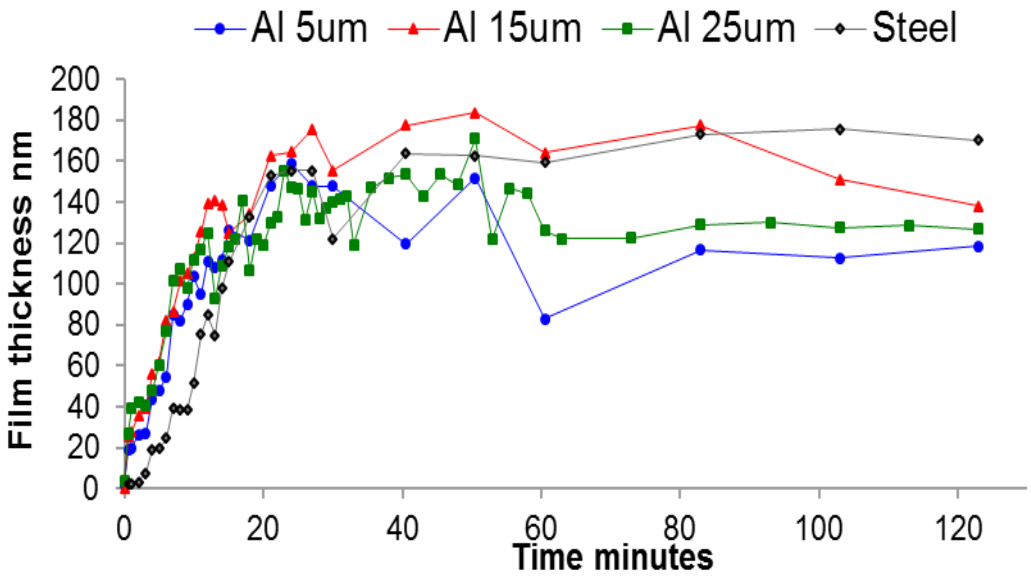

Figure 7.7: Growth of ZDDP film thickness on steel ball rubbed against different oxide thickness of Al_2O_3 during the entire 2 hours of test conditions in 50% SRR.

As mentioned earlier, each point on Figure 7.6 and Figure 7.7 and is obtained from SLIM images. Figure 7.8 and Figure 7.9 present the SLIM images captured at various intervals during the period of experiment. They show the growth of a ZDDP tribofilm on steel ball rubbed against a disc with a 15 µm thick Al_2O_3 layer at 100 °C in a mixed rolling and sliding (50% SRR) and pure rolling condition respectively. The antiwear tribofilm growth occurs on the wear track, and it is measured by loading the wear track on the ball surface against the mapper disc (see Figure 3.12 and Figure 3.13). Wear track refers to the region of the ball surface that is in contact with the disc surface and vice versa.

The similarity between these two figures is that the film formed on the contacting surface of the ball is patchy. The contrasting feature between the two figures is the directional orientation of the tribofilm. When sliding is involved the tribofilm is aligned along the sliding direction as evident in Figure 7.8. This is due the asperity ploughing through the top layers of newly formed tribofilm which are removed and formed again by shearing at the top of the asperities where film is thinnest during the initial stages of relative motion between the two

mating surfaces. This sacrificial nature of the ZDDP tribofilm is well documented [12], [224]. As sliding continues the thicker films with full coverage form on the wear track which are not removed easily [34]. In the case of pure rolling shown in Figure 7.9, due to the low shear forces at the contact, the antiwear tribofilms formed, are very poorly attached. Upon loading against the mapper disc (used for film thickness measurement) these loosely adhered tribofilms are transferred easily unto the mapper disc and continue to accumulate each time the ball is loaded against the mapper disc. As a result, a circular patch of accumulated tribofilm products grows at the centre of the contact. This circular patch at the centre is thicker the than around the edge of the contact and makes it difficult to identify the actual rubbed wear track. Film thickness data shown in Figure 7.9 shows the thickness measured from the edge of the central circular patch.

Figure 7.9 shows the growth of ZDDP film thickness on steel ball rubbed against different oxide thicknesses of Al_2O_3 in pure rolling (0% SRR) condition. Rolling against thicker oxide films have led to growth of thicker tribofilms. The formation of these films at 0% SRR suggests that even the slightest of metal to metal sliding and shearing can cause a tribofilm to form. The rate of formation of tribofilm under rolling condition is slower and the net thickness is lower than the tribofilm that forms at 50% SRR condition. Furthermore, this is line with the applied shear activation theory of tribofilm [32], [37] because pure rolling (0% SRR) will have lower values of mean shear stress generated at the contact than at 50% SRR. Practically, however, this low value of applied shear stress may be too low for any kind of shear induced thermal activation of tribofilm advocated in [32]. These observations also provides further evidence that although TE can aid formation of ZDDP films, the strength and toughness of the films is imparted by the action of normal and shear forces. The ZDDP tribofilms form very rapidly after initial two minutes of rubbing as seen in Figure 7.6 and Figure 7.10.

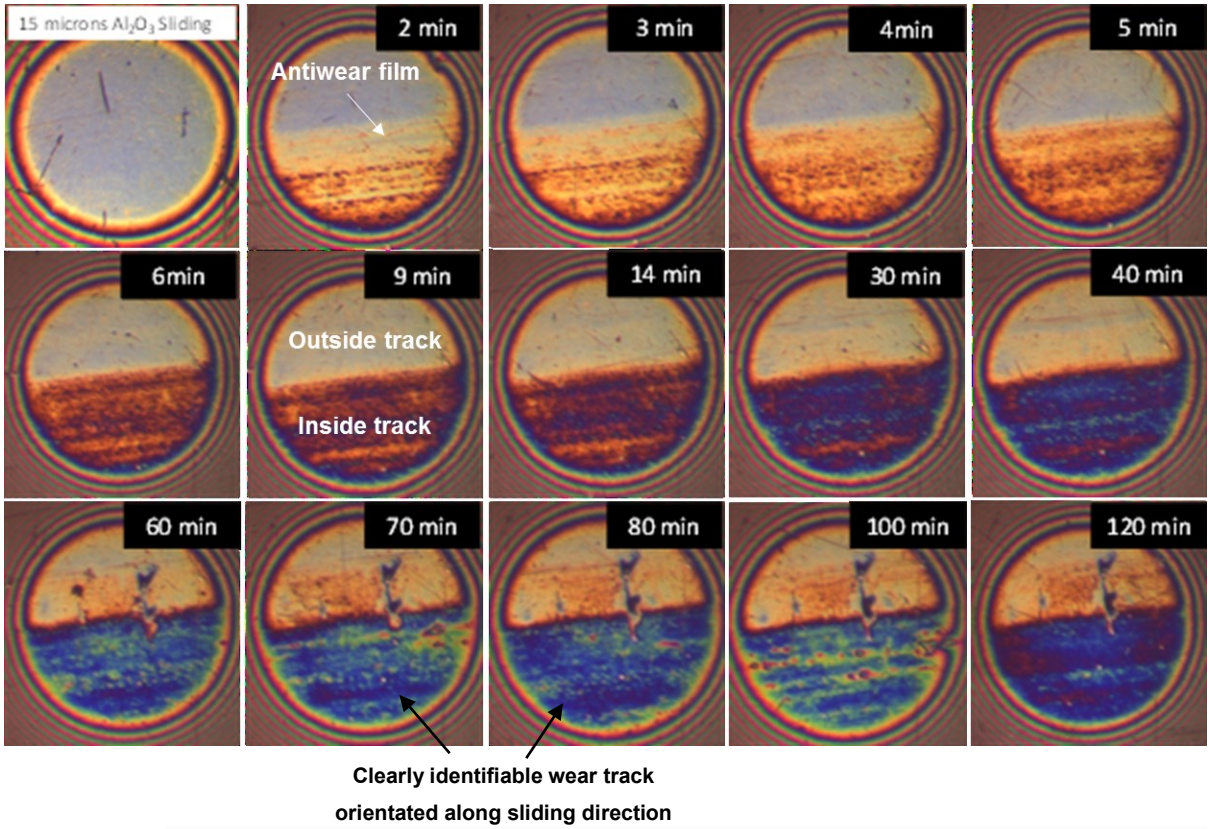

Figure 7.8: SLIM images showing ZDDP tribofilm formation in a rolling/sliding (50% SRR) condition on 15 microns thick Al_2O_3 /steel contact at 100 °C.

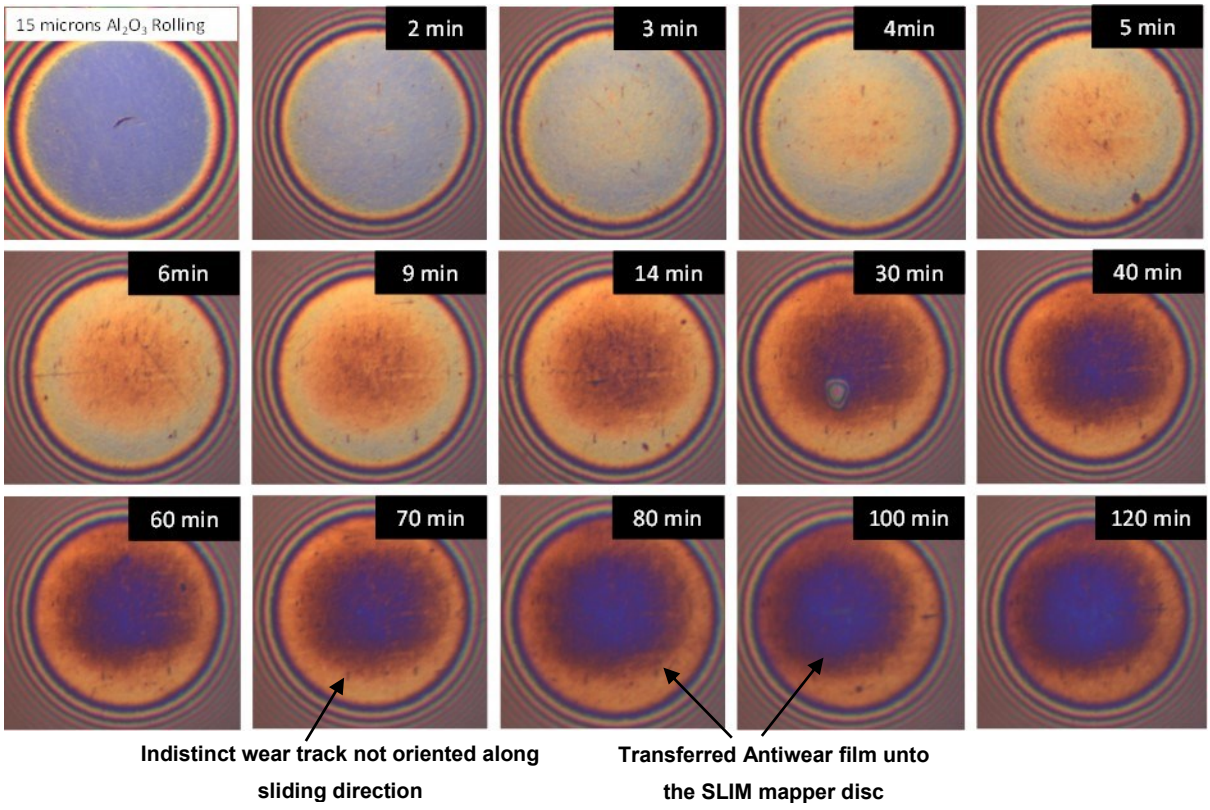

Figure 7.9: SLIM images showing ZDDP tribofilm formation in a rolling contact on 15 microns thick Al_2O_3 /steel contact at 100 °C.

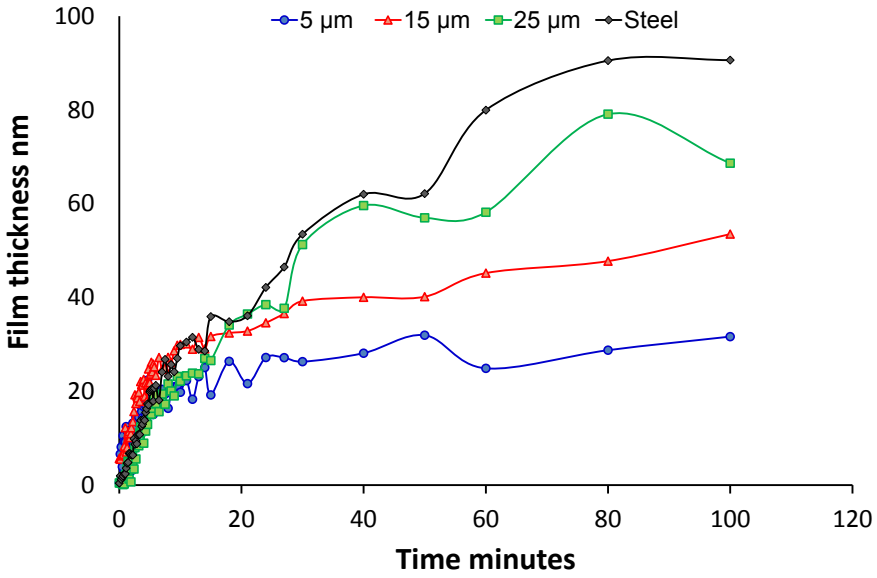

Figure 7.10: Growth of ZDDP film thickness on steel ball rubbed against different oxide thickness of Al_2O_3 in pure rolling (0% SRR) during the entire 2 hours of test conditions.

AFM images shown in Figure 7.11 confirm the patchy nature of the tribofilm formed on aluminium oxide films of different thickness. Images (a) and (b) show outside and inside the wear track on the 5 µm thick oxide covered aluminium disc taken after two hours of test under rolling/sliding (50% SRR) of Al_2O_3 /steel contact at 100 °C, while images (c) and (d) show outside and inside the wear track on 25 µm thick oxide covered aluminium disc. Here, it can be seen that the 5 µm thick oxide is rougher than 25 µm thick aluminium oxide and that some kind of flat oxide flakes along with ZDDP tribofilm are observed on 5 µm thick oxide. A marked increase in the roughness of the wear track because of the combined effect of wear and ZDDP film growth is observed in image (b) and (d). The surface of the 25 µm thick oxide was more uniformly covered by antiwear tribofilms of constant thickness. Thicker and less uniform antiwear tribofilms were present on the surface of the 5 µm thick oxide.

It was found that there is a difference in roughness and hardness values of different oxide thickness. Figure 7.12 shows the variation of (a) roughness (R_a), (b) hardness (HV_{10}) with oxide thickness. Thicker oxide is harder and smoother than thinner oxide films. This is in agreement with previous knowledge that the surface of the harder substrate (25 µm) was more uniformly covered by tribofilm while the soft substrates were covered with thicker and less uniform tribofilms [224]. Although the effects of oxide layer hardness and roughness on tribofilm formation have been reported earlier, the mechanism by which they bring the variation in tribofilm growth kinetics, the changes in morphology and nano-mechanical properties of

tribofilm is not so clear and needs to be investigated further. Variation in morphology and nano-mechanical properties from spot-to-spot and film-to-film have been linked to the heterogeneity in contact pressures owing to roughness of sliding surface [222]. Thus, while keeping in mind the above caveats, it is concluded that oxide thickness and hence electron emission from plastic deformation of oxide films are likely to affect the growth kinetics of ZDDP films during the initial phases of film formation, leading to increased thickness.

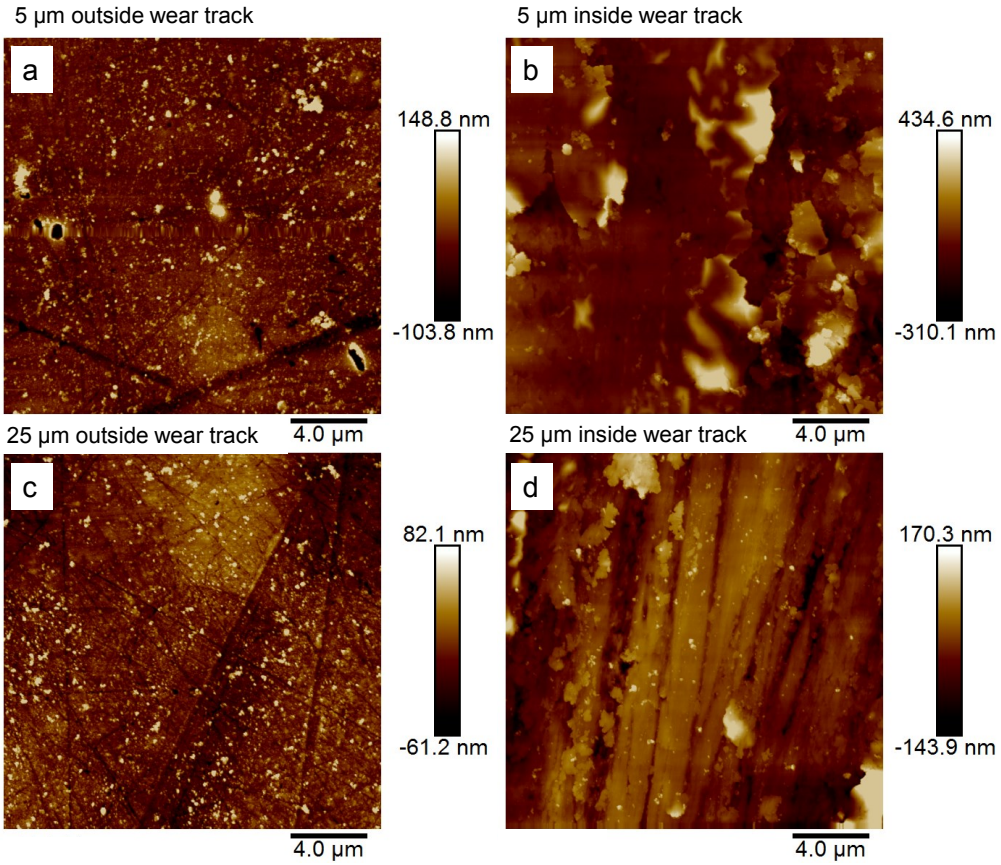

Figure 7.11: AFM images of outside and inside the wear track taken after two hours of test under rolling/sliding (50% SRR) of Al_2O_3 /steel contact at 100 °C. (a) and (b) 5 µm thick oxide covered aluminium disc; (c) and (d) 25 µm thick oxide covered aluminium disc

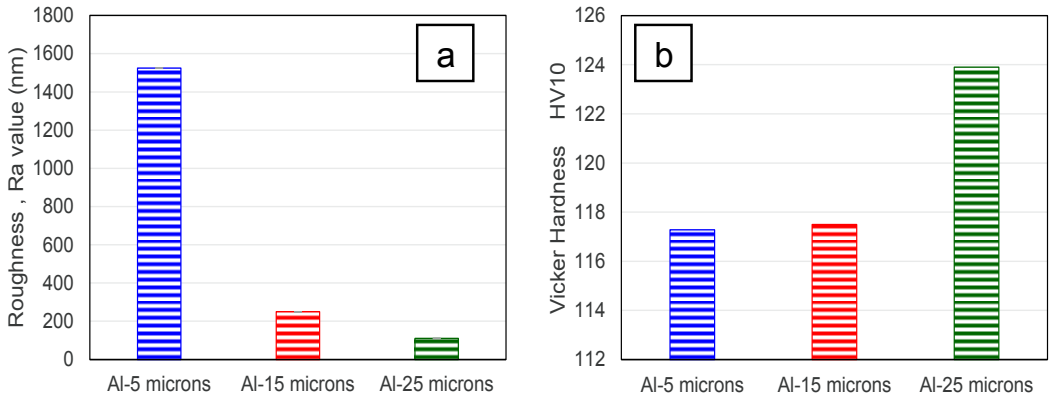

Figure 7.12: Variation of (a) roughness R_a (b) hardness (HV_{10}) with oxide thickness

In all the studies reported so far in this chapter, the action of shear forces upon sliding could not be eliminated and therefore a shear induced thermal activation model of ZDDP film formation still holds strong ground. In the next section, the influence of shear forces will be curtailed by eliminating relative sliding between the surfaces to avoid plastic deformation, triboemission as well as shearing of ZDDP molecules at the asperities. Instead, the electrons, which may be required for film formation reactions, are generated artificially using ultraviolet (UV) light.

7.4 Effect of electron emission on antiwear film formation

Artificial stimulation of electrons from a steel surface covered with a blend of ZDDP and mineral oil was achieved by irradiating with ultraviolet (UV) light. This was done to assess whether electron emission resulted in film growth. ToFSIMS analysis of the steel surface following irradiation showed that electron emission indeed result in changes to the oil-steel interface. This method exploits the Photoelectric Effect. The Photoelectric theory states that the kinetic energy of the ejected electron is equal to the energy of the incident photon minus the energy required to remove the electron from the material, which is called the work function. The energy of a photon (E) is given by

$$E = hf = hc/\lambda \qquad \text{Equation 7.1}$$

where, f is the frequency of the photon, λ is the wavelength, and c is the velocity of light. Thus, the shorter the wavelength the more energetic the photon.

This section is further divided into three subsection. The first subsection presents the proof of concept, the second subsection evaluates the role of energy semi quantitatively, and the final subsection uses a mask to make substantiate the argument qualitatively. The mask creates a pattern of incident radiation on the specimen to aid the identification of film growth.

7.4.1 Assessment of phosphate films using ToFSIMs

Figure 7.13 shows the resulting electron emission as a steel MTM disc is irradiated with UV light while slowly decreasing the wavelength of light. Here, it can be seen that electron emission occurs at energies above 4900 meV which is the work function of the steel. Once this value is known, the UV system is tuned to emit light at the wavelength required to produce photons at energies higher than the work function of steel. This ensures emission of electrons from steel surface during the test period. MTM samples were covered with a layer of ZDDP mixed with

mineral oil prior to irradiation. The irradiation was carried for 60 minutes. These irradiated surfaces were then analysed using ToF-SIMS to ascertain whether photoelectrons emitted from the surface had generated any antiwear film by reacting with the ZDDP molecules. The samples were rinsed with cyclohexane (to remove non-adhered ZDDP and oil) and dried prior to ToF-SIMS analysis.

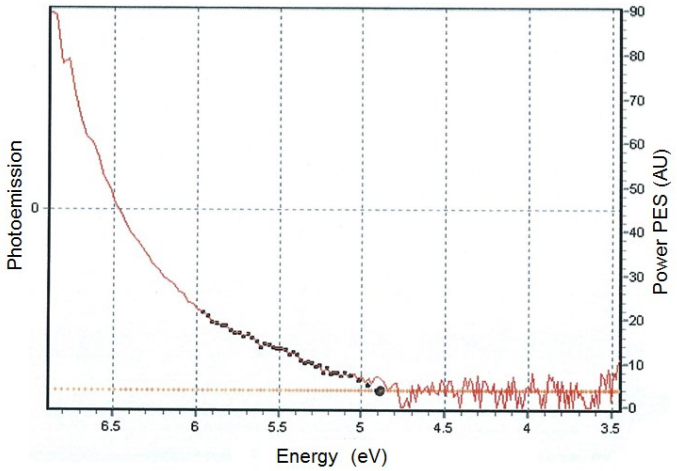

Figure 7.13: Photoemission from steel surface versus energy of incident UV light. Photoelectron emission is measured to start at 4.9 eV.

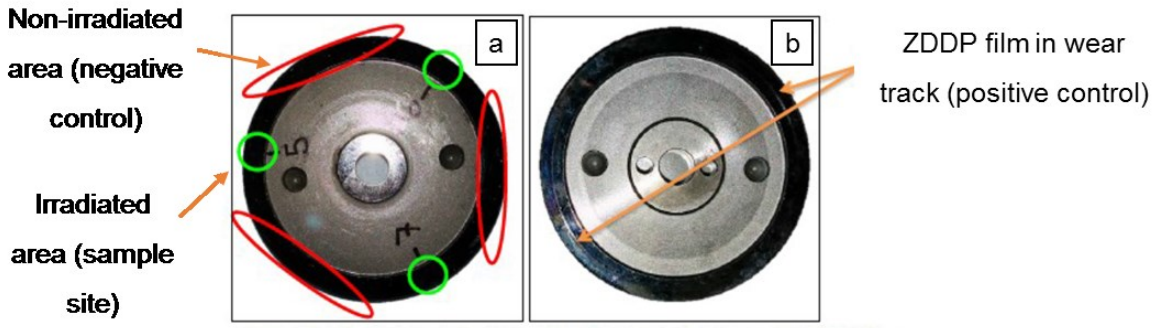

Figure 7.14: (a) UV treated specimen at position 5, 6 and 7. (b) ZDDP film formed on wear track while tribo testing.

Any reacted film formed on the surface after irradiation must essentially comprise predominantly of zinc and phosphates as has been pointed out in literature [6]. The site of the UV irradiation on the steel sample was compared with a positive control and a negative control (see Figure 7.14). The positive control is a section of wear track on a separate steel disc which had been rubbed against a steel ball at 30 N load, 50 mm/s speed at 50% SRR in the presence of lubricant kept at 100 ^{o}C, which was known to produce an antiwear tribofilm. The negative control is a non-UV treated area of the initial disc. The sample area and controls were imaged

via static SIMS and then also depth profiled using dynamic SIMS to assess whether the UV treatment had induced thin film formation.

There is only a very subtle difference between phosphate, iron and zinc between the UV treated and non-UV region as shown in Figure 7.15. Specifically, there are phosphate groups and zinc present at the surface of each sample with a significantly increased amount on the wear track region of the control sample which is a known fact. Importantly, it can be observed that there is a very slight increase in PO_2^+ peak in UV treated than in non-UV region as inferred from Figure 7.15(a) (see red horizontal lines)**.** Zinc and iron were also present at the surface of each sample. There is a significantly increased amount of zinc with a corresponding decrease in iron on the wear track region of the positive control sample. Cs^+ depth profiling demonstrated that the Zn is prominent at the surface of the wear track and not the underlying substrate. Zn signal drops gradually as profile progresses towards the substrate, Fe signals increase. Although not presented, depth profiling of both areas (irradiated and non-irradiated) of UV sample were comparable and indicated that the small Zn signal detected at the sample surface is not detected at any depth of the sample as substrate signals appear more rapidly.

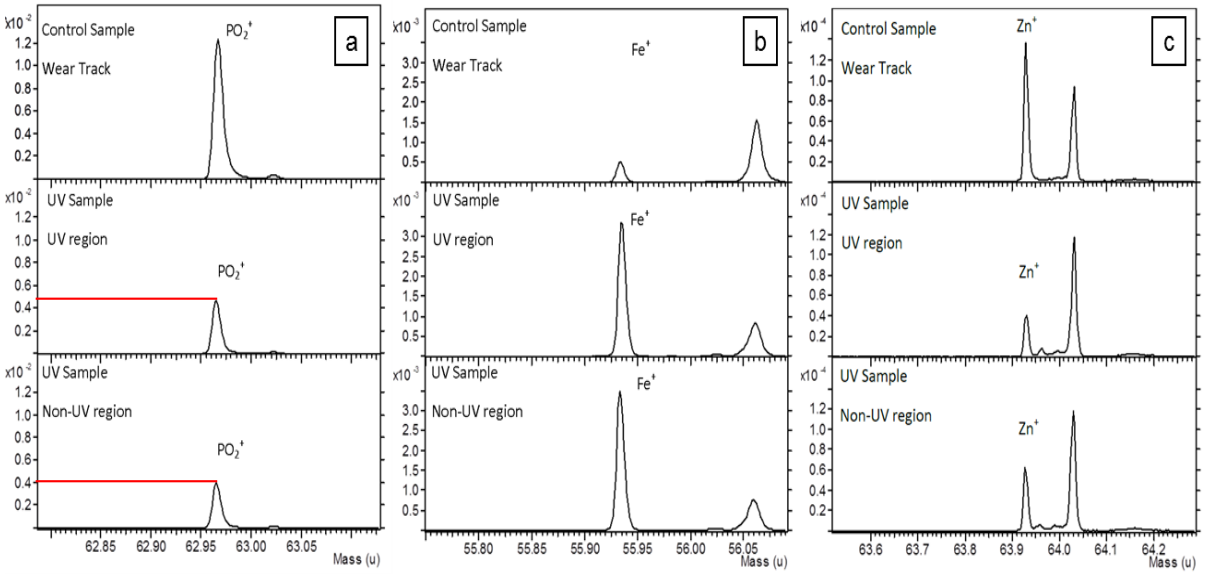

Figure 7.15: ToF-SIMS spectra comparison for PO^{2-}, Fe^+ and Zn^+. PO^{2+} ion is collected in negative polarity while Fe^+ and Zn^+ is collected in positive polarity.

A shortcoming of this experiment was that photoelectron emission took place at room temperature, whereas it is known that ZDDP molecules decompose and free zinc ions are generated above 60 ˚C [32], [223]. Therefore, further experiments were performed at 100 ˚C so that free Zn^+ ions would be available. The rationale for choosing this temperature is to

increase the rate of reaction only and prevent the ZDDP films from thermal decomposition which occurs at 150 ˚C.

7.4.2 Comparison with energy of irradiation

In this section the effect of energy of incident radiation is presented. A steel sample covered with ZDDP containing base oil was irradiated with photons at 4 eV and 5.63 eV. A comparison of phosphate groups (PO_2^- and PO_3^-) is presented in Figure 7.16. Both the phosphate groups are present in larger quantity when irradiated with photons at 5.63 eV than with 4 eV. Photons below 4.9 eV energy cannot produce photoelectrons and hence, this test is used as a control. The absence of phosphate film formation at the irradiated spot for the lower energy radiation shows that it is the increased electron emission which is responsible for the thicker films.

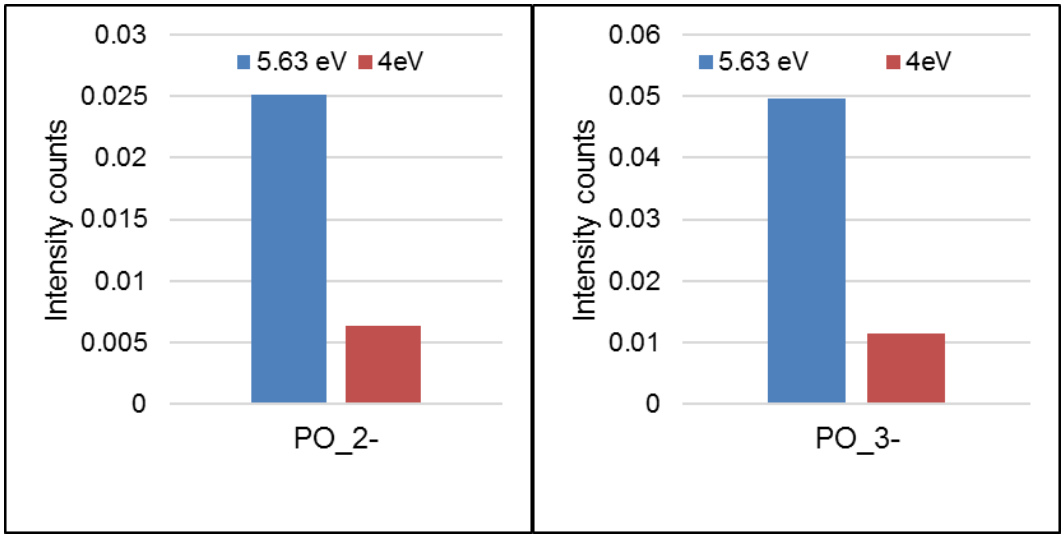

Figure 7.16: Comparison of average of normalized intensity counts of PO_2^- and PO_3^-

Although the graph shows a marked difference in the amounts of ions, the semi-quantitative significance may not be well appreciated. This is because of the fact that ZDDP films are patchy and their morphology and thickness are known to vary from spot to spot. However, the aim of this study is to demonstrate the potency of electrons to initiate a chemical reaction. Therefore, in the next subsection the formation of ZDDP antiwear film is shown qualitatively.

7.4.3 Use of mask and grid

To further understand the effect of photoelectrons on ZDDP molecules, a mask was used. This works under the assumption that, at places where the surface is masked from UV light, there are no incident photons to produce photoelectrons. In the absence of photoelectrons there

should be no chemical reaction. Thus, no film will be formed. A steel sample and silicon mask used for this study are shown in Figure 7.17. A drop of mineral oil containing ZDDP (0.8% P) was applied to the surface and irradiated with photons possessing energy of 6 eV for 1 hour. The spot size is 5 mm in diameter. The samples were maintained at 100 $^{\circ}$C to speed up the reaction. Another steel sample with silicon mask is also placed on the hot plate but is not irradiated with UV light. This acts as the control sample and helps separate the effect of temperature and effect UV irradiation.

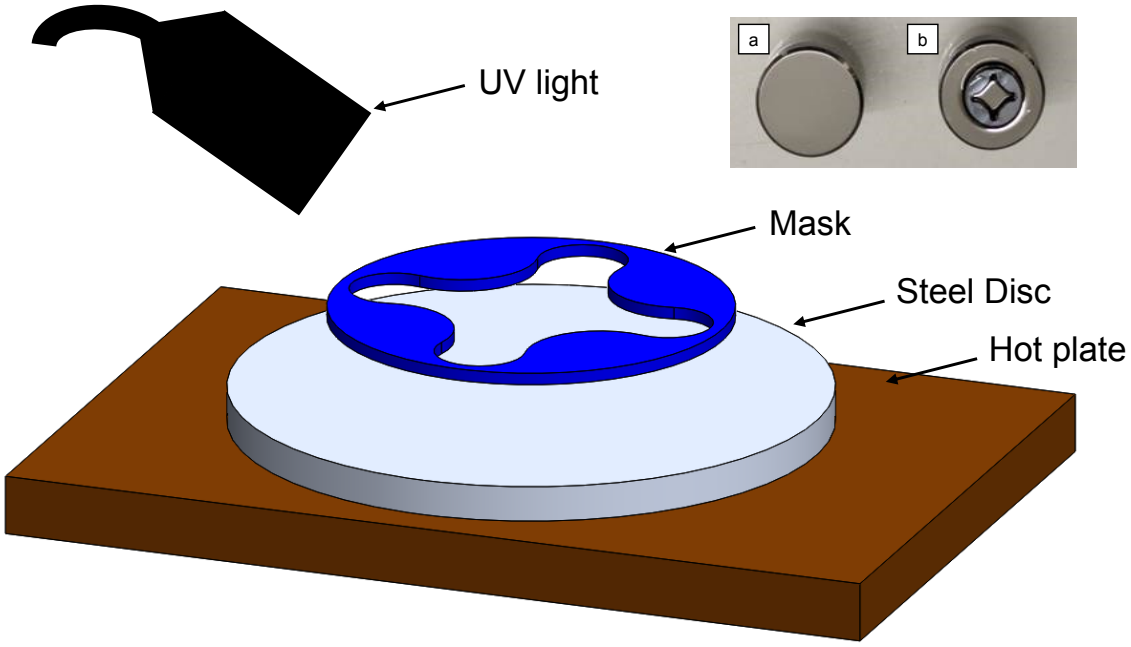

Figure 7.17: Schematic of irradiation method used. Inset (a) 10 mm diameter steel specimen (b) Steel specimen masked with silicon wafer mask

Prior to ToF-SIMS analysis, the samples were cleaned with cyclohexane to remove excess oil and then dried. All the ion distributions shown here are normalized to total intensity counts. Figure 7.18 shows ToF-SIMS negative polarity images. Images (a), (b), and (c) show the ion species distribution from the UV irradiated steel sample while images (d), (e), and (f) show the ion species distribution from the control sample that was not irradiated with UV. It is evident that phosphate ion groups are distributed on the unmasked areas of the UV irradiated steel sample. Figure 7.19 shows an overlay image of Fe^{+} ions and Zn^{+} ions obtained from positive polarity images for irradiated and un-irradiated steel surface. It shows that there are more Zn ions present on the unmasked region and more Fe^{+} ions on the masked region. The presence of zinc ions (distribution of green dots) on the unmasked region confirms that the difference is caused by UV irradiation.

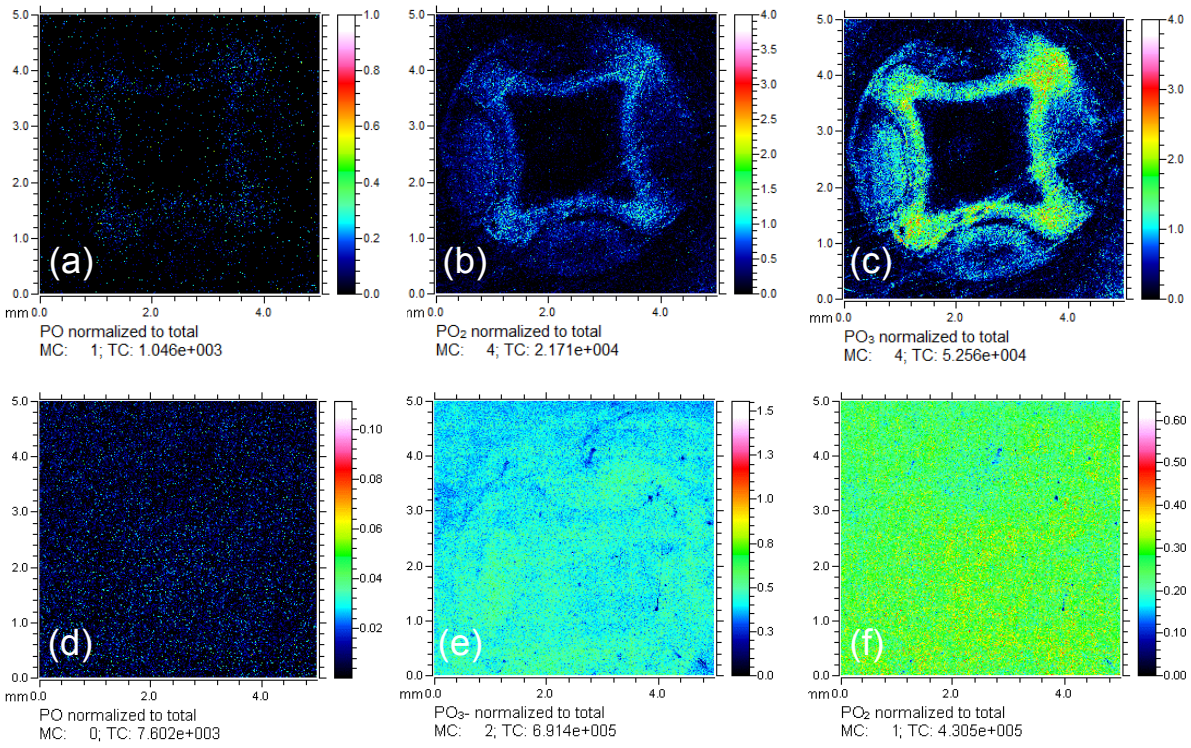

Figure 7.18: ToF-SIMS negative polarity images of the masked sample showing distribution of phosphate groups (a) PO^- (b) PO_2^- (c) PO_3^- ions on UV radiated surface while (d) PO^- (e) PO_2^- (f) PO_3^- on non-UV irradiated surface (control sample). Both samples were kept at 100 ^oC for 60 minutes.

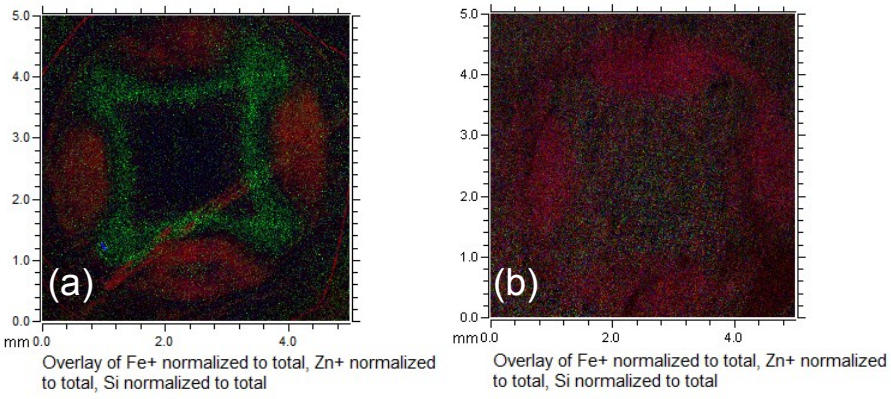

Figure 7.19: ToF-SIMS positive polarity images of the masked sample (a) UV irradiated (b) non-UV irradiated showing distribution of Fe^+ , Zn^+ and Si^+ ions using an overlay. Zn^+ ions are shown in green, Fe^+ ions in red and Si^+ ions in blue.

The Fe^+ ion concentration is low on the unmasked areas because the phosphate films are formed on the steel substrate. An intriguing feature of the ion distribution is that the central unmasked area has none of the ions that should be usually present on the surface. This is likely to be caused by formation of a convex meniscus by the oil drop on the steel surface, due to surface tension. This prevents the photons from reaching the steel surface as the incident photons would

undergo reflection, absorption, refraction, transmission, attenuation and eventual loss of energy. The probable cause of increased presence of phosphate groups along the edges of the mask could be due to increased supply of photoelectrons from the silicon mask itself. A comparison of average of normalized intensity counts of Zn^{+}, Fe^{+}, PO_2^{-} and PO_3^{-} ions are shown in Figure 7.20. This semi quantitative analysis confirms the formation of zinc phosphate films on the unmasked areas.

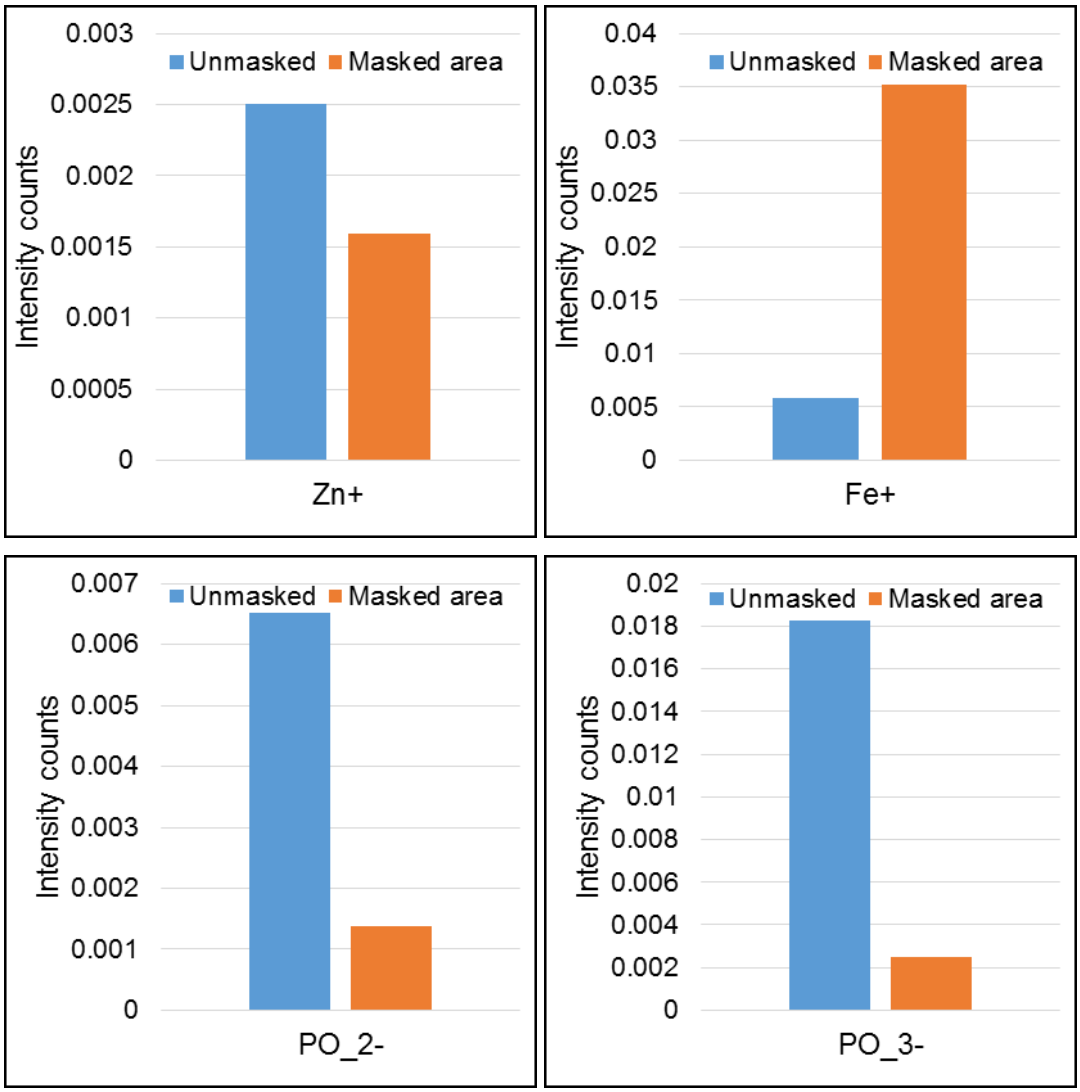

Figure 7.20: Comparison of averaged normalized intensity counts of Zn^{+}, Fe^{+}, PO_2^{-} and PO_3^{-} ions.

The formation of phosphate films at high energy (short wavelength) UV light and absence of phosphate films at low energy (longer wavelength) suggests that energy input into the system is a critical factor in film formation process. The formation of phosphate films upon irradiation with UV light with energy slightly above the work function of the material and its absence when the energy is below the work function suggests that emitted electrons play a major role

is phosphate film formation. The emitted electrons possess the energy to break ZDDP molecules and hence change the coordination between Zn^+, P^+, S^+, O^+ and Fe^+ ions, which then form new compounds by subsequent reaction. The correlations between UV photon irradiation, photoelectrons emission and phosphate film formation are shown for the first time. The exact pathway to film formation is still not clear, particularly regarding what starts the phosphate film formation, whether the UV energy is responsible for breaking of bonds and formation of new bonds or is it the bombardment of photoelectrons and production of secondary electrons or is it a photo-induced generation of ion-based reactive intermediates (radicals, acids, and bases) [225]. The growth of phosphate films on irradiated surfaces raises interesting questions such as whether ZDDP antiwear film formation is a photochemical process. If so, is this photochemical process a single photon-single reaction event or one that catalyses or induces a chain of reactions? If photons act as catalyst or initiate a chain reaction then the number of photons needed to trigger a chemical reaction is reduced significantly.

7.5 Discussions and Insights

The tests conducted in this study suggests that both shearing as well as triboemission have a positive influence on the formation of ZDDP tribofilm. Until now, the influence of triboemission on film formation have been hidden because triboemission is an intermediate step for formation of tribofilm that follows shearing at the contact as shearing can generate triboemission. However, the reason why the tribofilm is sulfur depleted and why ZnS precipitates are present, cannot be explained on basis of shear activated thermal model, and at the same time triboemission cannot explain the mechanical strength of the tribofilms. The fact that the film growth occurs at room temperature under mild sliding conditions confirms that the film is not product of thermal decomposition of the molecule on the substrate. However, both shearing and triboemission can increase the temperature at the contact and may even reach the thermal activation energy needed for a chemical reaction.

It is suggested that there may be more than one factor that affect the growth of tribofilm. Two processes *i.e*. shearing and triboemission must occur simultaneously for tribofilm formation and its growth. The formation and growth of tribofilm on a surface, depends on the properties of the substrate surface such its topography, hardness and presence of oxide as well as on the structure of ZDDP molecules. Therefore, the shearing of the ZDDP molecules and triboemission from the rubbing surface must act simultaneously to generate tribofilms. A variety of surfaces, such as steel, aluminium alloys, and DLC on which phosphate films are

formed are known to emit electrons and generate triboplasma in air upon sliding. The formation of a tribofilm is not continuous and occurs intermittently. The fluctuating nature of the film growth during the initial stages correlates subtly with the variation of triboemission intensity with time [183], [204]. The patchiness of tribofilm is either because shearing rate is higher at the thin gaps between contacting asperities, or it is because triboemission is localised at these points owing to the fracture of oxides present on the surface. The patchiness could also be due to decreased work function of freshly fractured surface. The reduction in work function of the freshly created surface could augment the thermal activation energy, E_a required for tribofilm formation. Freshly generated oxide surfaces also promote adsorption of molecules because of charge retention which is closely linked to triboemission. The phenomena of adsorption unto rubbed surface at specific sites was shown in **Chapter 6**, where the dye and protein molecules exhibited preferred attachment based on their polarity. The charge imbalance at the crack surface could lead to preferential chemisorption of zinc ions or there may be an initial ZDDP molecule–surface interaction that promotes adhesion due to attraction followed by cation and anion exchange reactions as discussed in [14, 225].

Furthermore, the difference in elasto-plastic properties of ZDDP tribofilms observed at different depths from the surface, *i.e.* the layer closest to the substrate has higher hardness and modulus as compared to top layers, can only be explained by considering both triboemission and shearing as drivers [226]. Since the hardness and modulus of tribofilm changes from base layer to surface layer, the mechanism of tribofilm formation at initial few minutes of rubbing must be different to that formed after 5 minutes of rubbing. Aktary *et al.* [222] showed that the indentation modulus and the hardness of a tribofilm formed after 5 minutes is similar to a tribofilm formed from 120 minutes of rubbing. This supports the suggestion that the action of triboemission (either by electron/ion flux or by aiding adsorption due to charging) initiates the first few monolayers of chemical reacted tribofilm after which shear induced thermal activation [32, 37] come into action and form the bulk of the film layer by layer. The mechanical strength to the tribofilm is provided by crosslinking induced by pressure [40, 230–232] or oligomerization process induced by shearing [230]. The plateauing of tribofilm, mostly observed around 140 nm is may be due to the formation of an adherent film on the surface that successfully prevents further oxide film fracture thereby stopping triboemission

No studies have been done regarding the measurement of localized charges that might accompany plastic deformation of polyphosphate films and in that case the electrical properties of phosphate glasses [6]. The fracture of phosphate films may generate triboemission too. It is

still not very conclusive whether these active sites where nucleation begins, are locations of high asperities, or sites of fresh surfaces, or sites of triboemission, or locally charged sites.

7.6 Conclusion

Studies were conducted to understand the impact of fresh surface, shearing, oxide film thickness, and triboemission on ZDDP tribofilm growth. This chapter also presents the first studies to elucidiate the role of electrons in ZDDP tribofilm formation on steel surface. This new approach involved artfitially stimulating emission from metal surface, and removed all the effects of normal load and relative sliding such as shear force, pressure, temperature hotspots, plastic deformation, crack propagation, charging, new surface creation and altering of work fuction that have been previously linked with tribofilm formation and growth. The major finds are as follows

1. Both shear force and triboemission have a positive effect on growth of ZDDP tribofilms.
2. Tests with various oxide thickness confirmed that higher the oxide thickness, higher is the tribofilm thickness. This is most likely because thicker oxide films produce higher number of electrons upon fracture.
3. From tests comparing the effect of rolling (0% SRR) and combined rolling and sliding (50% SRR), it was concluded that shear stress play an important role in modifying the mechanical properties of the tribofilm. The film formed with 0% SRR is poorly attached to the steel ball and is therefore easily removed and transferred to the other surface.
4. A link between triboemission and tribochemistry was shown using artificial stimulation of electron emission. UV irradiation onto ZDDP coated steel substrate resulted in phosphate film formation. The energy of the incident radiation is vital for releasing electrons from the top surface which subsequently cause growth of phosphate films.

Of course, the fact that electrons can initiate film growth does not prove that this is the only driving mechanism, however, it is nonetheless an important finding. Thus, tribofilm formation is result of a synergy between physical and chemical factors. The physical factors such as high pressure and shear stress can generate triboemission leading to chemical reaction. The patchiness of tribofilm is either because shearing rate is higher at the thin gaps between contacting asperities, or it is because triboemission is localised as these points.

There are still some questions that remain unanswered, such as the role of localized charges that result from fracture of oxide layer or the polyphosphate tribofilm itself. It is also not

definitive whether the active sites where nucleation begins are locations of high asperities, or sites of fresh surfaces, or sites of triboemission, or locally charged sites. Nevertheless, the consequence of any kind of surface interaction has been attributed to energy which transpires into various forms such as heat, pressure, shearing, charging and emissions. It appears that the weakest bond breaks, it does not matter whether energy input is thermal mechanical or triboelectric.

Chapter 8

Conclusions and Future work

For improved and advanced lubricants formulation, a complete knowledge and understanding of its components (*i.e*. lubricant additives) behaviour under full film and boundary lubrication conditions is essential. One possibly important factor, which limits understanding in this area, is a poor knowledge of the phenomena known as Triboemission. The subject of this thesis is to understand various triboemission phenomena and their interaction with the surrounding environment. To achieve this, two approaches are used. Firstly, test equipment and new methodologies were developed to monitor the effects of emitted particles from a sliding contact under vacuum, ambient and submerged conditions. This staged approach is required due to the difficulty in detecting triboemission effects under submerged conditions. This research extends the triboemission studies to liquid submerged conditions. The second approach is to study the expected precursors or drivers of ZDDP tribofilm formation such as fresh surface, mixing, shearing and electron emission in a sliding lubricated contact using various techniques that enable following their effects.

8.1 Development of New Methods and Main Achievements

In Chapter 2 a review of the relevant literature to identify issues in the current knowledge regarding ZDDP film formation, triboemission, triboplasma and tribocharging is presented. This covers areas such as drivers of ZDDP film formation and the related disparities, triboemission in vacuum, air as well as different gases, emission induced by fracture and the uncertainty concerning tribocharging particularly the charge carriers in case of insulators such as polymers.

In Chapter 3, various test equipment and methods (old and new) used for monitoring effects of emitted particles from a sliding from a sliding contact under vacuum, ambient and submerged conditions are laid out. New test equipment such as ‘Air plasma tribometer’ and 'Fluorescence tribometer’ are developed.

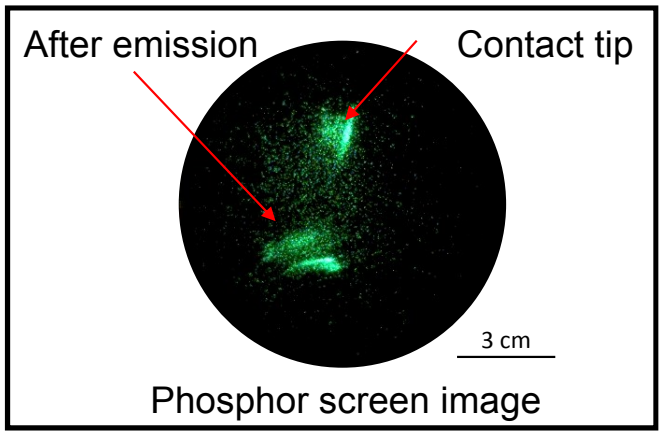

In Chapter 4, the spatial distribution of triboemission upon scratching of PTFE surface in vacuum were presented for the first time. The vacuum tribometer is integrated with a MCP and phosphor screen to measure the distribution of emitted electrons, ions or photons which enabled the monitoring of the 'after emission' phenomena. The emission occurs in discrete bursts and varies cyclically with time between a minimum value and a maximum value. It is suggested this triboemission behaviour results from the breaking of certain polymer chains, relaxation of other chains and generation of micro sized debris. The maximum emission has been attributed to combined emission of cryptoelectrons, gaseous ions, and radicals as well as charged polymer fragments while the after emission has been attributed to exoelectrons emitted from the surface during strain relaxation.

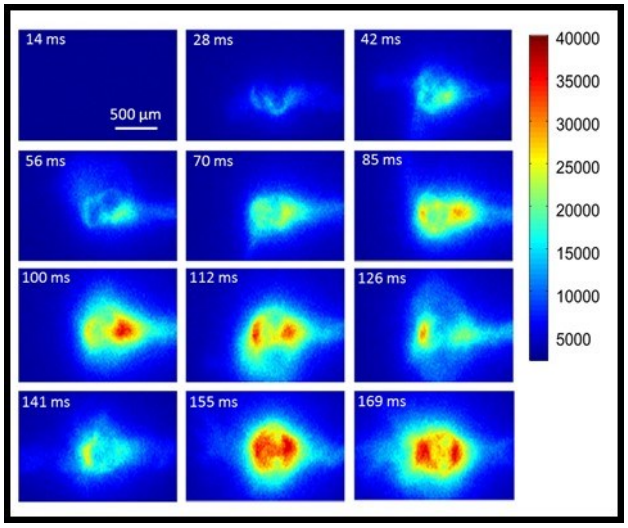

In Chapter 5, transient fluctuations in plasma for various polymers have been observed for the first time. The time average of recorded transient plasma distributions can be predicted based on the accumulated surface charge and the geometry of the gap between components. However, the transient fluctuations in plasma distribution, which occur over two distinct time scales and vary between different polymers, are stochastic. The characteristics of these unpredictable fluctuations are independent of the both the measured friction coefficient and wear volume but are strongly dependant on the polymer material being rubbed. These fluctuations result from a competition between a) bond scission (due to the shear stress within the contact), which increase surface charge and hence the propensity for breakdown, and b) the transfer of material from the polymer material between the two specimens, which reduces charging.

Spectrometric measurements show that the wavelengths of emitted photons correspond to N_2 discharge as well as radicals such as O-H, C-H, and C-C. Among different classes of materials

classified, metals did not emit while metal oxides and metal alloys (containing oxides) emitted intense light when fractured. For most polymers, the photon emission was in the UV range and mostly consisted of triboplasma while in case of polycrystalline diamond the emitted photons were in the visible range while UV emission is entirely absent from the emission spectra from Ti/Sapphire contact.

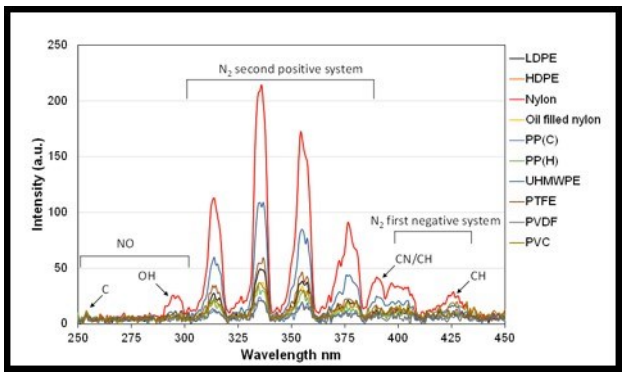

In Chapter 6, new techniques that involved viewing the contact or the rubbed wear track using a microscope by exploiting dye fluorescence and its charge sensitive attachment behaviour. The triboplasma which is observed in dry sliding conditions is only observed at the outlet of the contact which is a region of cavitation and flow separation under pure sliding conditions. Moreover, when an electrically conducting liquid is present the triboplasma is not even seen at the at the flow separation region due to charge neutralization.

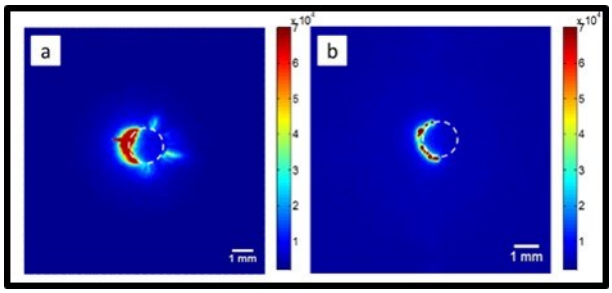

Another successful approach to monitor after-emission phenomena in submerged condition was developed which involved using dye fluorophore as probe and utilized. The observed after-emission event from PTFE wear track in submerged conditions bears a close correspondence to that observed in vacuum conditions. The interaction between dye and rubbed surface resulted in non-fluorescent state of the dye which can be attributed to the formation of some non-fluorescent derivative due to electron transfer from the rubbed surface or formation of aggregates because of preferential attachment to charged sites. The preferential attachment of proteins to charged sites was exploited using dye tagged proteins in order to obtain fluorescent images of the wear track based on the charge distribution. Albumin being negatively charged is repelled from negatively charged wear track

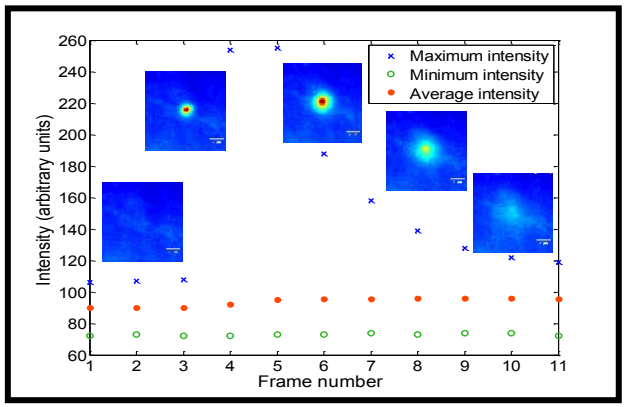

of UHMWPE. In case of PTFE and Nylon, the protein is attached to positively charged debris and positively charged wear track of Nylon respectively.

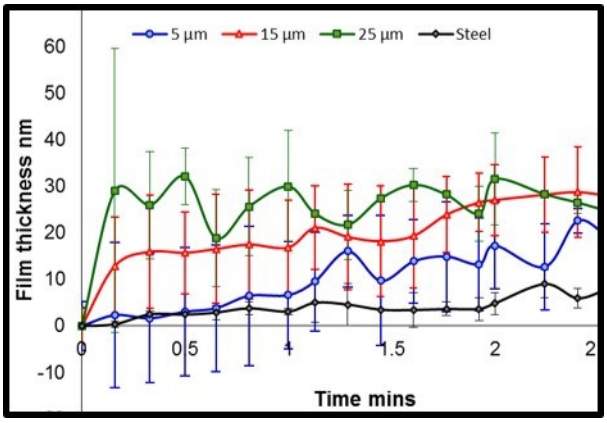

In Chapter 7, studies were conducted to understand the impact of fresh surface, shearing, oxide film thickness, and triboemission on ZDDP tribofilm growth. It was concluded that shear stress plays an important role in modifying the mechanical properties of the tribofilm while mixing and fresh surface do not affect ZDDP film formation. The film formed with 0% SRR is poorly attached to the steel ball and is therefore easily removed and transferred to other surface compared to film formed at 50% SRR. Tests with various oxide thickness confirmed that higher the oxide thickness, higher is the tribofilm thickness. This is because thicker oxide films produce higher number of electrons upon fracture.

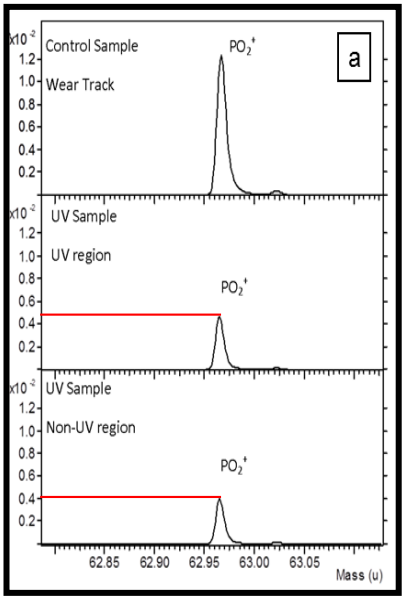

Chapter 7 also presented the first studies done to elucidiate the role of electrons in triggering a chemical reaction of ZDDP on steel surface that involved artfitially stimulating emission from the metal surface. This new method removed all the effects of normal load and sliding at the contact which introduces shear force, pressure and temperature hotspots at high asperities, plastic deformation, crack propagation, charging, new surface creation and altering of work fuction that have been previously linked with tribofilm formation and growth was developed. It was observed that the UV irradiation onto ZDDP coated substrate did indeed result in phosphate film formation. Thus, the energy of the incident radiation must have ejected electrons from the top surface which react subsequently to form ZDDP films.

8.2 Suggestions for Future Work

Time and resource constraints limited the testing of various materials in vacuum environment. As a future work it would be interesting to characterize spatially resolved triboemission from

various materials. Furthermore, it will be of great importance if the different particles leaving the surface could be characterized for their energy and mass by incorporating set ups similar to that used in mass spectrometers and Energy Dispersive Spectroscopy detectors. This would increase our understanding of the mechanisms behind triboemission phenomena.

A number of interesting additional questions arose over the course of this research, for example the experiments involving the interaction between dye and rubbed surface lead to the formation of non-fluorescent state and it was not possible to determine the exact mechanism *i.e.* whether the non-fluorescent state occurred due to electron transfer from the rubbed surface or it was due to the dye molecules forming aggregates. Additional surface analysis could improve our knowledge about the locations of fluorescent and non-fluorescent regions that occurred in dye mixed water as well as dye mixed oil environment.

There are still some questions that remain unanswered such as the role of localized charges upon fracture of oxide layer as well as polyphosphate glass. It is also not definitive whether the active sites where nucleation begins, are locations of high asperities, or sites of fresh surfaces, or sites of triboemission, or locally charged sites. Until this date, there has been an unresolved debate whether UV photons or radicals are responsible for polymerization process. With current techniques, it is very difficult to elucidate whether the final tribofilm molecule formed is electron initiated or radical initiated or photon initiated process.

Finally, since triboemission and triboplasma fall into the category of non-equilibrium molecular dynamics, non-equilibrium molecular dynamics (NEMD) simulations could be developed to examine the atomistic and molecular level collisions that occur due to contact electrification. The effect of localized charges, their effect on electric fields and hence interaction behaviour should be taken into account. Finally, what conditions of electronic configuration of additive molecules results in antiwear tribofilm generation could be investigated.

REFERENCES

[1] C. Kajdas, M. J. Furey, A. L. Ritter, and G. J. Molina, "Triboemission as a basic part of the boundary friction regime: A review," *Lubr. Sci.*, vol. 14, no. 2, pp. 223–254, 2002.

[2] X. Zhao, B. Bhushan, and C. Kajdas, "Lubrication studies of head-disk interfaces in a controlled environment Part 2: Degradation mechanisms of perfluoropolyether lubricants," *Proc. Inst. Mech. Eng. Part J J. Eng. Tribol.*, vol. 214, no. 6, pp. 547–559, 2000.

[3] S. C. Scholes and A. Unsworth, "The Effects of Proteins on the Friction and Lubrication of Artificial Joints," *Proc. Inst. Mech. Eng. Part H J. Eng. Med.*, vol. 220, no. 6, pp. 687–693, 2006.

[4] Y. S. Liao, P. D. Benya, and H. A. McKellop, "Effect of protein lubrication on the wear properties of materials for prosthetic joints," *J. Biomed. Mater. Res.*, vol. 48, no. 4, pp. 465–473, 1999.

[5] M. P. Heuberger, M. R. Widmer, E. Zobeley, R. Glockshuber, and N. D. Spencer, "Protein-mediated boundary lubrication in arthroplasty," *Biomaterials*, vol. 26, no. 10, pp. 1165–1173, 2005.

[6] H. Spikes, "The History and Mechanisms of ZDDP," *Tribol. Lett.*, vol. 17, no. 3, pp. 469–489, 2004.

[7] J. C. Bell and K. M. Delargy, "The composition and structure of model zinc dialkyldithiophosphate anti-wear films," in *Proc. 6th Int. Congress on Tribology*, 1993, pp. 328–332.

[8] Z. Yin, M. Kasrai, M. Fuller, G. M. Bancroft, K. Fyfe, and K. H. Tan, "Application of soft X-ray absorption spectroscopy in chemical characterization of antiwear films generated by ZDDP Part I: the effects of physical parameters," *Wear*, vol. 202, no. 2, pp. 172–191, 1997.

[9] Z. Zhang, E. S. Yamaguchi, M. Kasrai, and G. M. Bancroft, "Tribofilms generated from ZDDP and DDP on steel surfaces: Part 1, growth, wear and morphology," *Tribol. Lett.*, vol. 19, no. 3, pp. 211–220, 2005.

[10] J. Hershberger, O. O. Ajayi, and G. R. Fenske, "Zinc content of ZDDP films formed thermally and mechanically," *Tribol. Int.*, vol. 38, no. 3, pp. 299–303, 2005.

[11] K. Ito, J.-M. Martin, C. Minfray, and K. Kato, "Low-friction tribofilm formed by the reaction of ZDDP on iron oxide," *Tribol. Int.*, vol. 39, no. 12, pp. 1538–1544, Dec. 2006.

[12] H. So and Y. C. Lin, "The theory of antiwear for ZDDP at elevated temperature in boundary lubrication condition," *Wear*, vol. 177, no. 2, pp. 105–115, 1994.

[13] A. Morina and A. Neville, "Understanding the composition and low friction tribofilm formation/removal in boundary lubrication," *Tribol. Int.*, vol. 40, pp. 1696–1704, 2007.

[14] M. L. S. S. Fuller, M. Kasrai, G. M. M. Bancroft, K. Fyfe, and K. H. Tan, "Solution decomposition of zinc dialkyl dithiophosphate and its effect on antiwear and thermal film formation studied by X-ray absorption spectroscopy," *Tribol. Int.*, vol. 31, no. 10, pp. 627–644, 1998.

[15] J. M. Martin, "Antiwear mechanisms of zinc dithiophosphate: a chemical hardness approach," *Tribol. Lett.*, vol. 6, no. 1, pp. 1–8, 1999.

[16] J. M. Martin, T. Onodera, C. Minfray, F. Dassenoy, and A. Miyamoto, "The origin of anti-wear chemistry of ZDDP," *Faraday Discuss.*, vol. 156, p. 311, 2012.

[17] E. S. Yamaguchi and P. R. Ryason, "Inelastic Electron Tunneling Spectra of Lubricant Oil Additives on Native Aluminum Oxide Surfaces," *Tribol. Trans.*, vol. 36, no. 3, pp. 367–374, 1993.

[18] J. M. Martin, M. Belin, J. L. Mansot, H. Dexpert, and P. Lagarde, "Friction-Induced Amorphization with ZDDP—An EXAFS Study," *ASLE Trans.*, vol. 29, no. 4, pp. 523–531, 1986.

[19] M. Belin, J. M. Martin, and J. L. Mansot, "Role of Iron in the Amorphization Process in Friction-Induced Phosphate Glasses," *Tribol. Trans.*, vol. 32, no. 3, pp. 410–413, 1989.

[20] R. C. Coy and R. B. Jones, "The thermal degradation and EP performance of zinc dialkyldithiophosphate additives in white oil," *ASLE Trans.*, vol. 24, no. 1, pp. 77–90, 1981.

[21] M. A. Nicholls, T. Do, P. R. Norton, M. Kasrai, and G. M. M. Bancroft, "Review of the lubrication of metallic surfaces by zinc dialkyl-dithiophosphates," *Tribol. Int.*, vol. 38, no. 1, pp. 15–39, 2005.

[22] G. W. Kennerly and W. L. Patterson, "Kinetic Studies of Petroleum Antioxidants," *Ind. Eng. Chem.*, vol. 48, no. 10, pp. 1917–1924, 1956.

[23] T. Colclough and J. I. Cunneen, "Oxidation of organic sulphides. Part XV. The antioxidant action of phenothiazine, zinc isopropylxanthate, zinc di-isopropyldithiophosphate, and zinc dibutyldithiocarbamate, in squalene," *J. Chem. Soc.*, p. 4790, 1964.

[24] A. J. Burn, "The mechanism of the antioxidant action of zinc dialkyl dithiophosphates," *Tetrahedron*, vol. 22, no. 7, pp. 2153–2161, 1966.

[25] A. M. Barnes, K. D. Bartle, and V. R. A. A. Thibon, "A review of zinc dialkyldithiophosphates (ZDDPS): characterisation and role in the lubricating oil," *Tribol. Int.*, vol. 34, no. 6, pp. 389–395, 2001.

[26] P. A. Willermet, L. R. Mahoney, and C. M. Haas, "The Effects of Antioxidant Reactions on the Wear Behavior of a Zinc Dialkyldithiophosphate," *Tribol. Trans.*, vol. 22, no. 4, pp. 301–306, 1979.

[27] P. A. Willermet, L. R. Mahoney, and C. M. Bishop, "Lubricant Degradation and Wear III. Antioxidant Reactions and Wear Behavior of a Zinc Dialkyldithiophosphate in a Fully Formulated Lubricant," *ASLE Trans.*, vol. 23, no. 3, pp. 225–231, 1980.

[28] P. A. Willermet, S. K. Kandah, W. O. Siegl, and R. E. Chase, "The influence of molecular oxygen on wear protection by surface-active compounds," *ASLE Trans.*, vol. 26, no. 4, pp. 523–531, 1983.

[29] H. Spedding and R. C. Watkins, "The antiwear mechanism of zddp's. Part I," *Tribol. Int.*, vol. 15, no. 1, pp. 9–12, 1982.

[30] W. A. Glaeser, D. Baer, and M. Engelhardt, "In situ wear experiments in the scanning Auger spectrometer," *Wear*, vol. 162–164, no. PART A, pp. 132–138, 1993.

[31] J. C. Bell, K. M. Delargy, and A. M. Seeney, "The Removal of Substrate Material through Thick Zinc Dithiophosphate Anti-Wear Films," in *Tribology Series*, vol. 21, no. C, D. Dowson, M. Godet, C. M. Taylor, T. H. C. Childs, and G. Dalmaz, Eds.

Elsevier, 1992, pp. 387–396.

[32] J. Zhang and H. Spikes, "On the Mechanism of ZDDP Antiwear Film Formation," *Tribol. Lett.*, vol. 63, no. 2, p. 24, Aug. 2016.

[33] P. Njiwa, C. Minfray, M. Belin, E. Rigaud, and J.-M. Martin, "Friction response of ZDDP thermal film and tribofilm," *Tribol. - Mater. Surfaces Interfaces*, vol. 5, no. 4, pp. 129–132, 2011.

[34] H. Fujita, R. P. Glovnea, and H. A. Spikes, "Study of Zinc Dialkydithiophosphate Antiwear Film Formation and Removal Processes, Part I: Experimental," *Tribol. Trans.*, vol. 48, no. 4, pp. 558–566, 2005.

[35] H. Fujita and H. A. Spikes, "The formation of zinc dithiophosphate antiwear films," *Proc. Inst. Mech. Eng. Part J J. Eng. Tribol.*, vol. 218, no. 4, pp. 265–278, 2004.

[36] H. A. Abdel-Aal, "Flash Temperature Theory," in *Encyclopedia of Tribology*, Boston, MA: Springer US, 2013, pp. 1182–1194.

[37] N. N. Gosvami, J. A. Bares, F. Mangolini, A. R. Konicek, D. G. Yablon, and R. W. Carpick, "Mechanisms of antiwear tribofilm growth revealed in situ by single-asperity sliding contacts," *Science*, vol. 348, no. 6230, pp. 102–106, 2015.

[38] J. S. Tse, Y. Song, and Z. Liu, "Effects of temperature and pressure on ZDDP," *Tribol. Lett.*, vol. 28, no. 1, pp. 45–49, 2007.

[39] T. Sakurai, K. Sato, H. Hamaguchi, and K. Matsuo, "Effect of Internal Stress on the Wear Behavior of Steel during Boundary Lubrication," *ASLE Trans.*, vol. 17, no. 3, pp. 213–223, 1974.

[40] N. J. Mosey, M. H. Müser, and T. K. Woo, "Molecular Mechanisms for the Functionality of Lubricant Additives," *Science*, vol. 307, no. 5715, pp. 1612–1615, 2005.

[41] M. L. Suominen Fuller, K. L. De Jong, M. Kasrai, and G. M. Bancroft, "Electroless generation of phosphate films on metals from zinc dialkyldithiophosphates," *Chem. Mater.*, vol. 12, no. 5, pp. 1300–1304, 2000.

[42] M. Mee and A. A. Torrance, "A study of the lubricated wear of plain bearing materials in a ZDDP-containing lubricant," *Wear*, vol. 128, no. 2, pp. 201–217, Dec. 1988.

[43] D. Yang, J. Zhou, and Q. Xue, "Study of the tribochemical behavior of Al ion-implanted pure iron lubricated with ZDDP," *Surf. Coatings Technol.*, vol. 102, no. 3, pp. 223–232, Apr. 1998.

[44] J. S. Sheasby, T. A. Caughlin, and W. A. Mackwood, "A comparison of the boundary lubrication of 52100 steel, zirconia and silicon nitride by S, P, S/P and zinc dialkyl dithiophosphate additives," *Wear*, vol. 196, no. 1–2, pp. 100–109, Aug. 1996.

[45] B. Mingwu, Z. Xushou, and Q. Shangkui, "Tribological properties of silicon nitride ceramics coated with molybdenum films under boundary lubrication," *Wear*, vol. 169, no. 2, pp. 181–187, Oct. 1993.

[46] T. Haque, A. Morina, A. Neville, R. Kapadia, and S. Arrowsmith, "Non-ferrous coating/lubricant interactions in tribological contacts: Assessment of tribofilms," *Tribol. Int.*, vol. 40, no. 10–12, pp. 1603–1612, Oct. 2007.

[47] T. Haque, A. Morina, A. Neville, R. Kapadia, S. Arrowsmith, S. Tung, B. Kinker, M. Woydt, and S. W. Dean, "Study of the ZDDP Antiwear Tribofilm Formed on the DLC Coating Using AFM and XPS Techniques," *J. ASTM Int.*, vol. 4, no. 7, p. 100937, 2007.

[48] C. Kajdas, A. Kulczycki, and D. Ozimina, "A new concept of the mechanism of tribocatalytic reactions induced by mechanical forces," *Tribol. Int.*, vol. 107, no. August 2016, pp. 144–151, 2016.

[49] C. K. Kajdas, "Importance of the triboemission process for tribochemical reaction," *Tribol. Int.*, vol. 38, no. 3, 2005.

[50] J. T. Dickinson, L. Scudiero, K. Yasuda, M. W. Kim, and S. C. Langford, "Dynamic tribological probes: particle emission and transient electrical measurements," *Tribol. Lett.*, vol. 3, no. 1, pp. 53–67, 1997.

[51] K. Nakayama and H. Hashimoto, "Triboemission, tribochemical reaction, and friction and wear in ceramics under various n-butane gas pressures," *Tribol. Int.*, vol. 29, no. 5, pp. 385–393, 1996.

[52] A. Gieroszynski and B. Sujak, "Exoelectron emission in vacuum in the absence of light during plastic deformation of aluminum thickly coated with oxide," *Acta Phys. Pol.*, vol. 28, pp. 311–327, 1965.

[53] K. Nakayama, T. Fujiwara, and H. Hashimoto, "Exoelectron measurement apparatus incorporated in a scanning electron microscope," *J. Phys. E.*, vol. 17, no. 12, p. 1199, 1984.

[54] M. Tagawa, M. Mori, N. Ohmae, M. Umeno, and S. Takenobu, "Tribo and photo-stimulated exoelectron emission from graphite," *Tribol. Int.*, pp. 57–60, 1993.

[55] H. Ohuchi and Y. Enomoto, "Frictional heat- stimulated exo- electron emission from alumina sliding surfaces," *Appl. Phys. Lett.*, vol. 66, no. 10, pp. 1205–1207, Mar. 1995.

[56] B. Z Rosenblum, "Measurement of tribo-emission from oxide-covered metals," *J. physics. E, Sci. instruments*, vol. 10, no. 10, p. 1056, 1977.

[57] J. K. MUSUVA and J. C. RADON, "The effect of stress ratio and frequency on fatigue crack growth," *Fatigue Fract. Eng. Mater. Struct.*, vol. 1, no. 4, pp. 457–470, 1979.

[58] G. J. Molina, M. J. Furey, A. L. Ritter, and C. Kajdas, "Triboemission from alumina, single crystal sapphire, and aluminum," *Wear*, vol. 249, no. 3–4, pp. 214–219, 2001.

[59] K. A. Zimmerman, S. C. Langford, J. T. Dickinson, and R. P. Dion, "Electron and Photon-Emission Accompanying Deformation and Fracture of Polycarbonate," *J. Polym. Sci. Part B-Polymer Phys.*, vol. 31, no. 9, pp. 1229–1243, 1993.

[60] M. W. Kim, S. C. Langford, and J. T. Dickinson, "Electron and photon emission accompanying the abrasion of MgO with diamond," *Tribol. Lett.*, vol. 1, no. 2–3, pp. 147–157, 1995.

[61] D. L. Doering, J. T. Dickinson, S. C. Langford, and P. Xiong- Skiba, "Fracto-emission during the interfacial failure of a metal–oxide- semiconductor system: Au–SiO2–Si," *J. Vac. Sci. Technol. A Vacuum, Surfaces, Film.*, vol. 8, no. 3, pp. 2401–2406, 1990.

[62] J. T. Dickinson, L. Scudiero, K. Y. Ã, M. Kim, and S. C. Langford, "Dynamic tribological probes : particle emission and transient electrical measurements," *Tribol. Lett.*, vol. 3, pp. 53–67, 1997.

[63] K. Nakayama and R. a. Nevshupa, "Characteristics and Pattern of Plasma Generated at Sliding Contact," *J. Tribol.*, vol. 125, no. 4, 2003.

[64] A. J. Walton, "Triboluminescence," *Adv. Phys.*, vol. 26, no. 6, pp. 887–948, Nov.

1977.

[65] D. O. Olawale, O. O. I. Okoli, R. S. Fontenot, and W. A. Hollerman, *Triboluminescence : theory, synthesis, and application*. Springer, Cham, 2016.

[66] B. P. Chandra, "Mechanoluminescence," in *Luminescence of Solids*, Boston, MA: Springer US, 1998, pp. 361–389.

[67] A. R. R. Burns, R. W. W. Carpick, D. Y. Y. Sasaki, J. A. A. Shelnutt, and R. Haddad, "Shear-induced mechanochromism in polydiacetylene monolayers," *Tribol. Lett.*, vol. 10, pp. 89–96, 2001.

[68] T. E. Karis, V. J. Novotny, and R. D. Johnson, "Mechanical scission of perfluoropolyethers," *J. Appl. Polym. Sci.*, vol. 50, no. 8, pp. 1357–1368, 1993.

[69] J. K. Lancaster, "Polymer-based bearing materials," *Tribology*, vol. 5, no. 6, pp. 249–255, Dec. 1972.

[70] V. Tolieng, B. Prasirtsak, J. Sitdhipol, N. Thongchul, and S. Tanasupawat, "Identification and lactic acid production of bacteria isolated from soils and tree barks," *Malays. J. Microbiol.*, vol. 13, no. 2, pp. 100–108, 2017.

[71] J. Ye and D. L. Burris, "Characterizing PTFE transfer film properties to elucidate transfer film's role in ultra-low wear sliding of polymer nanocomposites," University of Delaware, Ann Arbor, 2014.

[72] B. Briscoe, "Wear of polymers: an essay on fundamental aspects," *Tribol. Int.*, vol. 14, no. 4, pp. 231–243, 1981.

[73] K. R. Makinson and D. Tabor, "The Friction and Transfer of Polytetrafluoroethylene," *Proc. R. Soc. A Math. Phys. Eng. Sci.*, vol. 281, no. 1384, pp. 49–61, 1964.

[74] K. Tanaka, Y. Uchiyama, and S. Toyooka, "The mechanism of wear of polytetrafluoroethylene," *Wear*, vol. 23, no. 2, pp. 153–172, Feb. 1973.

[75] D.-L. Gong, B. Zhang, Q.-J. Xue, and H.-L. Wang, "Study on tribochemical interaction of metals or metal oxides with polytetrafluoroethylene by X-ray photoelectron spectroscopy," *J. Appl. Polym. Sci.*, vol. 41, no. 1112, pp. 2587–2593, 1990.

[76] G. De-Li, Z. Bing, X. Qun-Ji, and W. Hong-Li, "Effect of tribochemical reaction of polytetrafluoroethylene transferred film with substrates on its wear behaviour," *Wear*,

vol. 137, no. 2, pp. 267–273, 1990.

[77] G. Deli, X. Qunji, and W. Hongli, "Physical models of adhesive wear of polytetrafluoroethylene and its composites," *Wear*, vol. 147, no. 1, pp. 9–24, Jul. 1991.

[78] G. Deli, X. Qunji, and W. Hongli, "ESCA study on tribochemical characteristics of filled PTFE," *Wear*, vol. 148, no. 1, pp. 161–169, 1991.

[79] S. Bahadur and D. Tabor, "The wear of filled polytetrafluoroethylene," *Wear*, vol. 98, no. C, pp. 1–13, Nov. 1984.

[80] S. Bahadur, "The development of transfer layers and their role in polymer tribology," *Wear*, vol. 245, pp. 92–99, Oct. 2000.

[81] C. J. Speerschneider and C. H. Li, "The role of filler geometrical shape in wear and friction of filled PTFE," *Wear*, vol. 5, no. 5, pp. 392–399, Sep. 1962.

[82] A. D. Roberts, "Surface charge contribution in rubber adhesion and friction," *J. Phys. D. Appl. Phys.*, vol. 10, no. 13, pp. 1801–1819, Sep. 1977.

[83] A. I. A. Sviridyonok, V. V. A. Bely, V. V. A. Smurugov, and V. G. V. Savkin, "A study of transfer in frictional interaction of polymers," *Wear*, vol. 25, no. 3, pp. 301–308, Sep. 1973.

[84] A. Pitenis, K. Harris, C. Junk, and G. Blackman, "Ultralow wear PTFE and alumina composites: it is all about tribochemistry," *Tribol. Lett.*, 2015.

[85] K. L. Harris, A. A. Pitenis, W. G. Sawyer, B. A. Krick, G. S. Blackman, D. J. Kasprzak, and C. P. Junk, "PTFE Tribology and the Role of Mechanochemistry in the Development of Protective Surface Films," *Macromolecules*, vol. 48, no. 11, pp. 3739–3745, 2015.

[86] A. Pitenis, J. Ewin, K. Harris, W. Sawyer, and B. Krick, "In vacuo tribological behavior of polytetrafluoroethylene (PTFE) and alumina nanocomposites: the importance of water for ultralow wear," *Tribol. Lett.*, 2014.

[87] D. Gong, Q. Xue, and H. Wang, "Effect of Tribochemical Reaction of PTFE Transferred Film with the Substrate on its Adhesion and Wear Behavior," in *Controlled Interphases in Composite Materials: Proceedings of the Third International Conference on Composite Interfaces (ICCI-III) held on May 21--24, 1990 in*

Cleveland, Ohio, USA, 1990, pp. 185–193.

[88] S. Bahadur and D. Gong, "The role of copper compounds as fillers in the transfer and wear behavior of polyetheretherketone," *Wear*, vol. 154, no. 1, pp. 151–165, Apr. 1992.

[89] S. Bahadur, D. Gong, and J. W. Anderegg, "The role of copper compounds as fillers in transfer film formation and wear of nylon," *Wear*, vol. 154, no. 2, pp. 207–223, 1992.

[90] D. H. Buckley and R. L. Johnson, "Friction, wear, and decomposition mechanisms for various polymer compositions in vacuum to 10-9 millimeter of mercury," NASA, Cleveland, Ohio, 1963.

[91] D. H. Buckley and R. L. Hohnson, "Degradation of polymeric compositions in vacuum to 10-9mm Hg in evaporation and sliding friction experiments," *Polym. Eng. Sci.*, vol. 4, no. 4, pp. 306–314, Oct. 1964.

[92] S. Bahadur and D. Gong, "The action of fillers in the modification of the tribological behavior of polymers," *Wear*, vol. 158, no. 1–2, pp. 41–59, Oct. 1992.

[93] T. Onodera, K. Kawasaki, T. Nakakawaji, Y. Higuchi, N. Ozawa, K. Kurihara, and M. Kubo, "Effect of Tribochemical Reaction on Transfer-Film Formation by Poly(tetrafluoroethylene)," *J. Phys. Chem. C*, vol. 118, no. 22, pp. 11820–11826, 2014.

[94] T. Onodera, M. Park, K. Souma, N. Ozawa, and M. Kubo, "Transfer-Film Formation Mechanism of Polytetrafluoroethylene: A Computational Chemistry Approach," *J. Phys. Chem. C*, vol. 117, no. 20, pp. 10464–10472, 2013.

[95] T. Onodera, K. Kawasaki, T. Nakakawaji, Y. Higuchi, N. Ozawa, K. Kurihara, and M. Kubo, "Chemical Reaction Mechanism of Polytetrafluoroethylene on Aluminum Surface under Friction Condition," *J. Phys. Chem. C*, vol. 118, no. 10, pp. 5390–5396, Mar. 2014.

[96] J. T. Shen, Y. T. Pei, and J. T. M. De Hosson, "Formation of metalF bonds during frictional sliding: Influence of water and applied load," *Appl. Surf. Sci.*, vol. 368, pp. 427–434, 2016.

[97] B. Baytekin, H. T. Baytekin, and B. a. Grzybowski, "What really drives chemical reactions on contact charged surfaces?," *J. Am. Chem. Soc.*, vol. 134, no. 17, pp. 7223–7226, 2012.

[98] C. Y. Liu and A. J. Bard, "Chemical redox reactions induced by cryptoelectrons on a PMMA surface," vol. 131, no. 18, pp. 6397–6401, 2009.

[99] G. H. Vurens, C. S. Gudeman, L. J. Lin, and J. S. Foster, "Mechanism of Ultraviolet and Electron Bonding of Perfluoroployethers," *Langmuir*, vol. 8, pp. 1165–1169, 1992.

[100] K. Nakayama, "Triboemission of electrons, ions, and photons from diamondlike carbon films and generation of tribomicroplasma," *Surf. Coatings Technol.*, vol. 188–189, no. 1–3, pp. 599–604, 2004.

[101] K. Nakayama, "The plasma generated and photons emitted in an oil-lubricated sliding contact," *J. Phys. D. Appl. Phys.*, vol. 40, no. 4, pp. 1103–1107, 2007.

[102] K. Nakayama, "Mechanism of triboplasma generation in oil," *Tribol. Lett.*, vol. 41, no. 2, pp. 345–351, 2011.

[103] K. Nakayama and S. M. Mirza, "Verification of the Decomposition of Perfluoropolyether Fluid Due to Tribomicroplasma," *Tribol. Trans.*, vol. 49, no. 1, pp. 17–25, 2006.

[104] R. A. Nevshupa, E. Roman, and J. L. de Segovia, "Contamination of vacuum environment due to gas emission stimulated by friction," *Tribol. Int.*, vol. 59, pp. 23–29, 2013.

[105] C. Kajdas, P. M. Lafleche, M. J. Furey, J. W. Hellgeth, and T. C. Ward, "A study of tribopolymerisation under fretting contact conditions," *Lubr. Sci.*, vol. 6, no. 1, pp. 51–89, 1993.

[106] H. Zhang, Y. Mitsuya, M. Imamura, N. Fukuoka, and K. Fukuzawa, "Effect of ultraviolet irradiation on the interactions between perfluoropolyether lubricant and magnetic disk surfaces," *Tribol. Lett.*, vol. 20, no. 3–4, pp. 191–199, 2005.

[107] G. Vurens, R. Zehringer, and D. Saperstein, "The Decomposition Mechanism of Perfluoropolyether Lubricants during Wear," in *Surface Science Investigations in Tribology*, vol. 485, no. 485, American Chemical Society, 1992, pp. 169–180.

[108] E. D'Anna, G. Leggieri, A. Luches, and A. Perrone, "Fragmentation spectra and appearance potentials of vacuum pump fluids determined by electron impact mass spectrometry," *J. Vac. Sci. Technol. A Vacuum, Surfaces, Film.*, vol. 5, no. 6, pp. 3436–3441, 1987.

[109] J. Pacansky and R. J. Waltman, "Decomposition of poly (perfluorinated ethers): Effect of end groups on main-chain degradation and product formation," *Chem. Mater.*, vol. 8, no. 12, pp. 2788–2791, 1996.

[110] K. L. Heredia and H. D. Maynard, "Synthesis of protein – polymer conjugates," *Org. Biomol. Chem.*, vol. 5, no. 5, pp. 45–53, 2007.

[111] B. S. Lele, H. Murata, K. Matyjaszewski, and A. J. Russell, "Synthesis of uniform protein-polymer conjugates," *Biomacromolecules*, vol. 6, no. 6, pp. 3380–3387, 2005.

[112] J. Goddard and J. Hotchkiss, "Polymer surface modification for the attachment of bioactive compounds," *Prog. Polym. Sci.*, 2007.

[113] D. J. Lacks and R. Mohan Sankaran, "Contact electrification of insulating materials," *J. Phys. D. Appl. Phys.*, vol. 44, no. 45, 2011.

[114] L. B. Schein, *Electrophotography and Development Physics*. Springer Science & Business Media, 2012.

[115] D. M. Pai and B. E. Springett, "Physics of electrophotography," *Rev. Mod. Phys.*, vol. 65, no. 1, pp. 163–211, 1993.

[116] D. K. Yanar and B. A. Kwetkus, "Electrostatic separation of polymer powders," *Electrostatics*, vol. 35, pp. 257–266, 1995.

[117] S. Wang, Y. Xie, S. Niu, L. Lin, and Z. L. Wang, "Freestanding triboelectric-layer-based nanogenerators for harvesting energy from a moving object or human motion in contact and non-contact modes," *Adv. Mater.*, vol. 26, no. 18, pp. 2818–2824, 2014.

[118] J. Yang, J. Chen, Y. Liu, W. Yang, Y. Su, and Z. L. Wang, "Triboelectrification-based organic film nanogenerator for acoustic energy harvesting and self-powered active acoustic sensing," *ACS Nano*, vol. 8, no. 3, pp. 2649–2657, 2014.

[119] William D. Greason, "Electrostatic damage in electronics: Devices and systems," *Letchworth*, vol. 8, 1987.

[120] N. Gibson, "Static electricity — an industrial hazard under control?," *J. Electrostat.*, vol. 40–41, pp. 21–30, 1997.

[121] L. Perrin, A. Laurent, V. Falk, O. Dufaud, and M. Traoré, "Dust and electrostatic hazards, could we improve the current standards?," *J. Loss Prev. Process Ind.*, vol. 20,

no. 3, pp. 207–217, 2007.

[122] J. F. Kok and N. O. Renno, "Electrostatics in wind-blown sand," *Phys. Rev. Lett.*, vol. 100, no. 1, p. 14501, Jan. 2008.

[123] A. Coehn, "Ueber ein Gesetz der Electricitätserregung," *Ann. Phys.*, vol. 64, p. 217, 1896.

[124] J. Henniker, "Triboelectricity in polymers," *Nature*, pp. 474–474, 1962.

[125] A. F. Diaz and R. M. Felix-Navarro, "A semi-quantitative tribo-electric series for polymeric materials: The influence of chemical structure and properties," *J. Electrostat.*, vol. 62, no. 4, pp. 277–290, 2004.

[126] L. S. McCarty and G. M. Whitesides, "Electrostatic charging due to separation of ions at interfaces: Contact electrification of ionic electrets," *Angew. Chemie - Int. Ed.*, vol. 47, no. 12, pp. 2188–2207, 2008.

[127] K. M. Forward, D. J. Lacks, and R. M. Sankaran, "Charge segregation depends on particle size in triboelectrically charged granular materials," *Phys. Rev. Lett.*, vol. 102, no. 2, pp. 1–4, 2009.

[128] J. Lowell and W. S. Truscott, "Triboelectrification of identical insulators : 11 . Theory and further experiments," vol. 19, pp. 1281–1298, 1986.

[129] W. R. Harper, *Contact and Frictional Electrification*. CA: Laplacian Press, Morgan Hill, 1998.

[130] K. Nakayama and R. A. Nevshupa, "Effect of dry air pressure on characteristics and patterns of tribomicroplasma," *Vacuum*, vol. 74, no. 1, pp. 11–17, May 2004.

[131] J. Lowell and A. C. Rose-Innes, "Contact electrification," *Adv. Phys.*, vol. 29, no. 6, pp. 947–1023, 1980.

[132] F. A. Diaz, "An ion transfer model for contact charging," *Langmuir*, vol. 9, no. 4, pp. 1009–1015, 1993.

[133] S. J. Vella, X. Chen, S. W. Thomas, X. Zhao, Z. Suo, and G. M. Whitesides, "The determination of the location of contact electrification-induced discharge events," *J. Phys. Chem. C*, vol. 114, no. 48, pp. 20885–20895, 2010.

[134] B. D. Terris, J. E. Stern, D. Rugar, and H. J. Mamin, "Contact electrification using force microscopy," *Phys. Rev. Lett.*, vol. 63, no. 24, pp. 2669–2672, 1989.

[135] H. T. Baytekin, A. Z. Patashinski, M. Branicki, B. Baytekin, S. Soh, and B. a Grzybowski, "The mosaic of surface charge in contact electrification," *Science (80-.).*, vol. 333, no. 6040, pp. 308–312, 2011.

[136] T. A. L. Burgo, T. R. D. Ducati, K. R. Francisco, K. J. Clinckspoor, F. Galembeck, and S. E. Galembeck, "Triboelectricity: Macroscopic charge patterns formed by self-arraying ions on polymer surfaces," *Langmuir*, vol. 28, no. 19, pp. 7407–7416, 2012.

[137] M. W. Williams, "Triboelectric charging of insulators - Mass transfer versus electrons/ions," *J. Electrostat.*, vol. 70, no. 2, pp. 233–234, 2012.

[138] T. A. L. Burgo and A. Erdemir, "Bipolar Tribocharging Signal During Friction Force Fluctuations at Metal-Insulator Interfaces," *Angew. Chemie*, vol. 126, no. 45, pp. 12297–12301, 2014.

[139] C. A. Rezende, R. F. Gouveia, M. A. da Silva, and F. Galembeck, "Detection of charge distributions in insulator surfaces.," *J. Phys. Condens. Matter*, vol. 21, no. 26, p. 263002, 2009.

[140] M. Sow, R. Widenor, A. Kumar, S. W. Lee, D. J. Lacks, and R. M. Sankaran, "Strain-induced reversal of charge transfer in contact electrification," *Angew. Chemie - Int. Ed.*, vol. 51, no. 11, pp. 2695–2697, 2012.

[141] R. Budakian and S. J. Putterman, "Correlation between charge transfer and stick-slip friction at a metal-insulator interface," *Phys. Rev. Lett.*, vol. 85, no. 5, pp. 1000–1003, 2000.

[142] J. Krim, "Friction at the Atomic Scale," *Sci. Am.*, vol. 275, no. 4, pp. 74–80, 1996.

[143] A. Fabian, C. Krauss, A. Sickafoose, M. Horányi, and S. Robertson, "Measurements of electrical discharges in Martian regolith simulant," *IEEE Trans. Plasma Sci.*, vol. 29, no. 2 I, pp. 288–291, 2001.

[144] S. W. Thomas, S. J. Vella, G. K. Kaufman, and G. M. Whitesides, "Patterns of electrostatic charge and discharge in contact electrification," *Angew. Chemie - Int. Ed.*, vol. 47, no. 35, pp. 6654–6656, 2008.

[145] W. M. Haynes, Ed., *CRC handbook of chemistry and physics*, 96th ed. CRC Press, 2015.

[146] C. Tendero, C. Tixier, P. Tristant, J. Desmaison, and P. Leprince, "Atmospheric pressure plasmas: A review," *Spectrochim. Acta - Part B At. Spectrosc.*, vol. 61, no. 1, pp. 2–30, 2006.

[147] K. Nakayama, "Triboplasma generation and triboluminescence: Influence of stationary sliding partner," *Tribol. Lett.*, vol. 37, no. 2, pp. 215–228, 2010.

[148] P. A. Thiessen, "Physical and chemical investigations in tribomechanical events," *Zeit Chemie*, vol. 5, pp. 162–171, 1965.

[149] K. Nakayama and R. A. Nevshupa, "Plasma generation in a gap around a sliding contact," *J. Phys. D. Appl. Phys.*, vol. 35, no. 12, pp. L53–L56, 2002.

[150] C. Matta, O. L. Eryilmaz, M. I. De Barros Bouchet, A. Erdemir, J. M. Martin, and K. Nakayama, "On the possible role of triboplasma in friction and wear of diamond-like carbon films in hydrogen-containing environments," *J. Phys. D. Appl. Phys.*, vol. 42, no. 7, p. 75307, 2009.

[151] K. Nakayama and J.-M. M. Martin, "Tribochemical reactions at and in the vicinity of a sliding contact," *Wear*, vol. 261, 2006.

[152] J. Muto, H. Nagahama, T. Miura, and I. Arakawa, "Frictional discharge at fault asperities: Origin of fractal seismo-electromagnetic radiation," *Tectonophysics*, vol. 431, no. 1–4, pp. 113–122, 2007.

[153] S. V. Singh, Y. Kusano, P. Morgen, and P. K. Michelsen, "Surface charging, discharging and chemical modification at a sliding contact," *J. Appl. Phys.*, vol. 111, no. 8, p. 83501, 2012.

[154] Y. Kusano, S. Taormina, P. K. Michelsen, and K. Nakayama, "Triboplasma – its generation and application for surface modification," in *4th Mikkeli international industrial coating seminar*, 2008.

[155] Y. Kabouzi, M. D. Calzada, M. Moisan, K. C. Tran, and C. Trassy, "Radial contraction of microwave-sustained plasma columns at atmospheric pressure," *J. Appl. Phys.*, vol. 91, no. 3, pp. 1008–1019, 2002.

[156] K. K. Hiratsuka and K. Hosotani, "Effects of friction type and humidity on triboelectrification and triboluminescence among eight kinds of polymers," *Tribol. Int.*, vol. 55, pp. 87–99, 2012.

[157] "Diamond Tool Wear when Cutting Amorphous Polymers," *CIRP Ann. - Manuf. Technol.*, vol. 53, no. 1, p. 447, 2004.

[158] K. Nakayama, "Triboplasma Generation and Triboluminescence: Influence of Stationary Sliding Partner," *Tribol. Lett.*, 2009.

[159] K. Nakayama, "Triboemission of charged particles and resistivity of solids," *Tribol. Lett.*, vol. 6, no. 1, pp. 37–40, 1999.

[160] K. Nakayama, N. Suzuki, and H. Hashimoto, "Triboemission of charged particles and photons from solid surfaces during frictional damage," *J. Phys. D. Appl. Phys.*, vol. 25, no. 2, 1992.

[161] K. Nakayama and H. Hashimoto, "Triboemission of Charged Particles and Photons from Wearing Ceramic Surfaces in Various Gases," *Tribol. Trans.*, vol. 35, no. 4, p. 643, 1992.

[162] K. Nakayama and H. Hashimoto, "Triboemission from various materials in atmosphere," *Wear*, vol. 147, no. 2, pp. 335–343, 1991.

[163] K. Nakayama, "Triboemission and Triboplasma Generation with DLC Films," in *Tribology of Diamond-Like Carbon Films*, C. Donnet and A. Erdemir, Eds. Springer US, 2008, pp. 291–310.

[164] C. Matta, O. L. Eryilmaz, M. I. D. B. Bouchet, A. Erdemir, J. M. Martin, and K. Nakayama, "On the possible role of triboplasma in friction and wear of diamond-like carbon films in hydrogen-containing environments," *J. Phys. D. Appl. Phys.*, vol. 42, no. 7, p. 75307, 2009.

[165] Y. Momose, Y. Yamashita, and M. Honma, "Observation of Real Metal Surfaces by Tribostimulated Electron Emission and Its Relationship to the Analyses by XPS and Photoemission," *Tribol. Lett.*, vol. 29, no. 1, pp. 75–84, 2007.

[166] Y. Momose and K. Kubo, "Observation of triboelectron emission from real copper surfaces in sliding contact with polytetrafluoroethylene and polyimide," *Tribol. Int.*, vol. 47, pp. 212–220.

[167] B. Rosenblum, P. Bräunlich, and L. Himmel, "Spontaneous emission of charged particles and photons during tensile deformation of oxide- covered metals under ultrahigh- vacuum conditions," *J. Appl. Phys.*, vol. 48, no. 12, pp. 5262–5273, Dec. 1977.

[168] J. T. Dickinson, D. B. Snyder, and E. E. Donaldson, "Electron and Acoustic-Emission Accompanying Oxide Coating Fracture," *Thin Solid Films*, vol. 72, no. 2, pp. 223–228, 1980.

[169] J. T. Dickinson, P. F. Braunlich, L. A. Larson, and A. Marceau, "Characteristic Emission of Negatively Charged-Particles during Tensile Deformation of Oxide-Covered Aluminum-Alloys," *Appl. Surf. Sci.*, vol. 1, no. 4, pp. 515–537, 1978.

[170] J. T. Dickinson, E. E. Donaldson, and M. K. Park, "The Emission of Electrons and Positive-Ions from Fracture of Materials," *J. Mater. Sci.*, vol. 16, no. 10, pp. 2897–2908, 1981.

[171] L. A. Larson, J. T. Dickinson, P. F. Braunlich, and D. B. Snyder, "Emission of Neutral Particles from Anodized Aluminum Surfaces during Tensile Deformation," *J. Vac. Sci. Technol.*, vol. 16, no. 2, pp. 590–593, 1979.

[172] H. Ohuchi and Y. Enomoto, "Frictional heat- stimulated exo- electron emission from alumina sliding surfaces," *Appl. Phys. Lett.*, vol. 66, no. 10, pp. 1205–1207, 1995.

[173] C. S. Saba and N. H. Forster, "Reactions of aromatic phosphate esters with metals and their oxides," *Tribol. Lett.*, vol. 12, no. 2, pp. 135–146, 2002.

[174] J. T. Dickinson, E. E. Donaldson, and D. B. Snyder, "Emission of Electrons and Positive-Ions Upon Fracture of Oxide-Films," *J. Vac. Sci. Technol.*, vol. 18, no. 2, pp. 238–242, 1981.

[175] J. L. Wiza, "Microchannel plate detectors," *Nucl. Instruments Methods*, vol. 162, no. 1–3, pp. 587–601, Jun. 1979.

[176] J. H. Choo, R. P. Glovnea, A. K. Forrest, and H. A. Spikes, "A Low Friction Bearing Based on Liquid Slip at the Wall," *J. Tribol.*, vol. 129, no. 3, p. 611, Jul. 2007.

[177] K. Topolovec-Miklozic, T. R. Forbus, and H. A. Spikes, "Film thickness and roughness of ZDDP antiwear films," 2007.

[178] A. Raman, "nanoHUB.org - Courses: nanoHUB-U: Fundamentals of Atomic Force Microscopy, Part 2: Dynamic AFM Methods: 01a." [Online]. Available: https://nanohub.org/courses/AFM2/01a/outline/week5dynamicafmforelectrostaticsmagneticbiology/l51dynamicafmforelectrostaticsmagneticbiology-measuringelectrostaticforcesi?time=00:24:36. [Accessed: 06-Sep-2017].

[179] "TOF-SIMS Particle-beam interaction." [Online]. Available: https://serc.carleton.edu/details/images/8382.html. [Accessed: 06-Sep-2017].

[180] "Model 8009 Resistivity Test Fixture Instruction Manual Rev. C | Tektronix." [Online]. Available: https://www.tek.com/keithley-accessories/test-fixtures-manual-4. [Accessed: 20-Feb-2018].

[181] J. T. Dickinson, L. C. Jensen, and W. D. Williams, "Fractoemission from Lead Zirconate-Titanate," *J. Am. Ceram. Soc.*, vol. 68, no. 5, pp. 235–240, 1985.

[182] G. J. Molina, M. J. Furey, and C. Kajdas, "A Deterministic-Chaos Study of Electron Triboemission Outputs," *J. Tribol.*, vol. 129, no. 3, p. 679, 2007.

[183] A. Ciniero, J. Le Rouzic, I. Baikie, and T. Reddyhoff, ""The origins of triboemission – Correlating wear damage with electron emission," *Wear*, vol. 374–375, pp. 113–119, 2017.

[184] B. Baytekin, H. T. Baytekin, and B. A. Grzybowski, "What Really Drives Chemical Reactions on Contact Charged Surfaces?," *J Am Chem Soc*, vol. 134, no. 17, pp. 7223–7226, 2012.

[185] E. Husain and R. S. Nema, "Analysis of Paschen Curves for air, N2 and SF6 Using the Townsend Breakdown Equation," *IEEE Trans. Electr. Insul.*, vol. EI-17, no. 4, pp. 350–353, 1982.

[186] J. T. Dickinson, L. C. Jensen, and A. Jahanlatibari, "Fracto-Emission - the Role of Charge Separation," *J. Vac. Sci. Technol. a-Vacuum Surfaces Film.*, vol. 2, no. 2, pp. 1112–1116, 1984.

[187] G. Molina, M. Furey, C. Kajdas, and N. Steika, "On the mechanism of electron triboemission from ceramics," *Ann. Univ. "Dunărea Jos " Galaţi Fascicle VIII*, pp. 17–23, 2005.

[188] H. A. Abdel-Aal and R. Ysai, "On the strength of tribo-induced emission of charged particles from mono-crystalline silicon surfaces scratched with diamond styli," *Ann. Univ. "Dunărea Jos " Galaţi Fascicle VIII,* pp. 119–124, 2005.

[189] H. A. Abdel-Aal, "Discussion: 'A Deterministic-Chaos Study of Electron Triboemission Outputs' (Molina, G. J., Furey, M. J., and Kajdas C., 2007, ASME J. Tribol., 129(3), pp. 679–683)," *J. Tribol.*, vol. 132, no. 1, p. 15501, 2010.

[190] L. Beraldo da Silveira Balestrin, D. Del Duque, D. Soares da Silva, and F. Galembeck, "Triboelectricity in insulating polymers: evidence for a mechanochemical mechanism," *Faraday Discuss*, vol. 170, pp. 369–383, 2014.

[191] K. Li, P. Yang, L. Niu, and D. Xue, "Group Electronegativity for Prediction of Materials Hardness."

[192] C. G. Camara, J. V Escobar, J. R. Hird, and S. J. Putterman, "Correlation between nanosecond X-ray flashes and stick–slip friction in peeling tape," *Nature*, vol. 455, no. 7216, pp. 1089–1092, 2008.

[193] L. S. McCarty and G. M. Whitesides, "Electrostatic Charging Due to Separation of Ions at Interfaces: Contact Electrification of Ionic Electrets," *Angew. Chemie Int. Ed.*, vol. 47, no. 12, pp. 2188–2207, Mar. 2008.

[194] T. A. L. Burgo, T. R. D. Ducati, K. R. Francisco, K. J. Clinckspoor, F. Galembeck, and S. E. Galembeck, "Triboelectricity: Macroscopic charge patterns formed by self-arraying ions on polymer surfaces," *Langmuir*, vol. 28, no. 19, pp. 7407–7416, 2012.

[195] M. W. Williams, "Triboelectric charging of insulators – Mass transfer versus electrons/ions," *J. Electrostat.*, vol. 70, no. 2, pp. 233–234, 2012.

[196] D. B. Go and A. Venkattraman, "Microscale gas breakdown: ion-enhanced field emission and the modified Paschen's curve," *J. Phys. D. Appl. Phys.*, vol. 47, no. 50, p. 503001, 2014.

[197] T. A. L. Burgo, C. A. Rezende, S. Bertazzo, A. Galembeck, and F. Galembeck, "Electric potential decay on polyethylene: Role of atmospheric water on electric charge build-up and dissipation," *J. Electrostat.*, vol. 69, no. 4, pp. 401–409, 2011.

[198] T. A. L. Burgo, C. A. Silva, L. B. S. Balestrin, and F. Galembeck, "Friction coefficient dependence on electrostatic tribocharging.," *Sci. Rep.*, vol. 3, p. 2384, 2013.

[199] L. B. S. Balestrin, D. D. Duque, D. S. Silva, and F. Galembeck, "Triboelectricity in insulating polymers: evidence for a mechanochemical mechanism," *Faraday Discuss.*, vol. 170, pp. 369–383, 2014.

[200] L. M. Sweeting, "Triboluminescence with and without air," *Chem. Mater.*, vol. 13, no. 3, pp. 854–870, 2001.

[201] N. Sewraj, N. Merbahi, J. P. Gardou, P. R. Akerreta, and F. Marchal, "Electric and spectroscopic analysis of a pure nitrogen mono-filamentary dielectric barrier discharge (MF-DBD) at 760 Torr," *J. Phys. D. Appl. Phys.*, vol. 44, no. 14, p. 145201, Apr. 2011.

[202] G. Jintang, "Tribochemical effects in formation of polymer transfer film," *Wear*, vol. 245, no. 1, pp. 100–106, 2000.

[203] S. K. Biswas and K. Vijayan, "Friction and wear of PTFE - a review," *Wear*, vol. 158, no. 1–2, pp. 193–211, 1992.

[204] J. Le Rouzic and T. Reddyhoff, "Spatially Resolved Triboemission Measurements," *Tribol. Lett.*, vol. 55, no. 2, pp. 245–252, 2014.

[205] R. A. Nevshupa and K. Hiratsuka, *Fundamentals of Friction and Wear*. Berlin, 2007.

[206] J. T. Dickinson and E. E. Donaldson, "Autographs from peeling pressure sensitive adhesives: Direct recording of fracture-induced photon emission," *J. Adhes.*, vol. 24, no. 2–4, pp. 199–220, 1987.

[207] "Polymer - Mechanical Properties." [Online]. Available: http://www.goodfellow.com/catalogue/GFCat2C.php?ewd_token=XpPnkdkV9gNjqr420971o4c3tlUoxx&n=mn7piwtGpI1iwrzRYjBQHy9hRUix9b&ewd_urlNo=GFCat26&type=30&prop=3. [Accessed: 09-Sep-2016].

[208] M. C. Sobieraj and C. M. Rimnac, "Ultra high molecular weight polyethylene: Mechanics, morphology, and clinical behavior," *Journal of the Mechanical Behavior of Biomedical Materials*, vol. 2, no. 5. pp. 433–443, 2009.

[209] P. J. Rae and D. M. Dattelbaum, "The properties of poly(tetrafluoroethylene) (PTFE) in compression," *Polymer (Guildf).*, vol. 45, no. 22, pp. 7615–7625, 2004.

[210] M. N. Gardos, “Magnéli phases of anion-deficient rutile as lubricious oxides. Part I. Tribological behavior of single-crystal and polycrystalline rutile (TinO2n−1),” *Tribol. Lett.*, vol. 8, no. 2/3, pp. 65–78, 2000.

[211] M. N. Gardos, H. S. Hong, and W. O. Winer, “The effect of anion vacancies on the tribological properties of rutile (Tio2-x), part ii: Experimental evidence,” *Tribol. Trans.*, vol. 33, no. 2, pp. 209–220, Jan. 1990.

[212] M. N. Gardos, “The effect of anion vacancies of the tribological properties of rutile (Tio2-x),” *Tribol. Trans.*, vol. 31, no. 4, pp. 427–436, 1988.

[213] A. C. M. Padilha, H. Raebiger, A. R. Rocha, and G. M. Dalpian, “Charge storage in oxygen deficient phases of TiO2: defect Physics without defects.,” *Sci. Rep.*, vol. 6, p. 28871, Jul. 2016.

[214] M. Laad, V. Kumar, and S. Jatti, “Titanium oxide nanoparticles as additives in engine oil,” *J. King Saud Univ. - Eng. Sci.*, no. February, pp. 6–11, Feb. 2016.

[215] K. G. Binu, B. S. Shenoy, D. S. Rao, and R. Pai, “A Variable Viscosity Approach for the Evaluation of Load Carrying Capacity of Oil Lubricated Journal Bearing with TiO2 Nanoparticles as Lubricant Additives,” *Procedia Mater. Sci.*, vol. 6, pp. 1051–1067, Jan. 2014.

[216] M. Roy and J. P. Davim, *Thermal Sprayed Coatings and their Tribological Performances*. IGI Global, 2015.

[217] A. Skopp, N. Kelling, M. Woydt, and L. M. Berger, “Thermally sprayed titanium suboxide coatings for piston ring/cylinder liners under mixed lubrication and dry-running conditions,” *Wear*, vol. 262, no. 9–10, pp. 1061–1070, Apr. 2007.

[218] K. Nakayama and R. A. Nevshupa, “Plasma generation in a gap around a sliding contact,” *J. Phys. D. Appl. Phys.*, vol. 35, no. 12, p. L53, 2002.

[219] T. Nagano, “Development of fluorescent probes for bioimaging applications.,” *Proc. Jpn. Acad. Ser. B. Phys. Biol. Sci.*, vol. 86, no. 8, pp. 837–47, 2010.

[220] Y. Zhang, J. A. Huang, K. H. Li, D. Bai, Y. Wang, T. Wang, and H. W. Choi, “Influence of strain on emission from GaN-on-Si microdisks,” *J. Phys. D. Appl. Phys.*, vol. 49, no. 37, p. 375103, Sep. 2016.

[221] M. P. Lettinga, H. Zuilhof, M. A. M. J. van Zandvoort, P. J. Quinn, G. van Ginkel, Y. K. Levine, J. Thomas-Oates, and H. Zuilhof, "Phosphorescence and fluorescence characterization of fluorescein derivatives immobilized in various polymer matrices," *Phys. Chem. Chem. Phys.*, vol. 2, no. 16, pp. 3697–3707, 2000.

[222] M. Aktary, M. T. McDermott, and G. A. McAlpine, "Morphology and Nanomechanical Properties of ZDDP Antiwear Films as a Function of Tribological Contact Time," *Tribol. Lett.*, vol. 12, no. 3, pp. 155–162, 2002.

[223] K. Ito, J. M. Martin, C. Minfray, and K. Kato, "Formation Mechanism of a Low Friction ZDDP Tribofilm on Iron Oxide," *Tribol. Trans.*, vol. 50, no. 2, pp. 211–216, Apr. 2007.

[224] Y. R. Li, G. Pereira, M. Kasrai, and P. R. Norton, "The effect of steel hardness on the performance of ZDDP antiwear films: A multi-technique approach," *Tribol. Lett.*, vol. 29, no. 3, pp. 201–211, Mar. 2008.

[225] S. Chatani, C. J. Kloxin, and C. N. Bowman, "The power of light in polymer science: photochemical processes to manipulate polymer formation, structure, and properties," *Polym. Chem.*, vol. 5, no. 7, pp. 2187–2201, 2014.

[226] J. Ye, M. Kano, and Y. Yasuda, "Evaluation of Local Mechanical Properties in Depth in MoDTC/ZDDP and ZDDP Tribochemical Reacted Films Using Nanoindentation," *Tribol. Lett.*, vol. 13, no. 1, pp. 41–47, 2002.

[227] M. A. Nicholls, P. R. Norton, G. M. Bancroft, M. Kasrai, T. Do, B. H. Frazer, and G. De Stasio, "Nanometer Scale Chemomechanical Characterization of Antiwear Films," *Tribol. Lett.*, vol. 17, no. 2, pp. 205–216, Aug. 2004.

[228] N. J. Mosey and T. K. Woo, "Insights into the chemical behavior of zinc dialkyldithiophosphate anti-wear additives in their isomeric and decomposed forms through molecular simulation," *Tribol. Int.*, vol. 39, no. 9, pp. 979–993, 2006.

[229] N. J. Mosey, T. K. Woo, M. Kasrai, P. R. Norton, G. M. Bancroft, and M. H. Müser, "Interpretation of experiments on ZDDP anti-wear films through pressure-induced cross-linking," *Tribol. Lett.*, vol. 24, no. 2, pp. 105–114, Nov. 2006.

[230] R. B. Jones and R. C. Coy, "The chemistry of the thermal degradation of zinc dialkyldithiophosphate additives," *ASLE Trans.*, vol. 24, no. 1, pp. 91–97, Jan. 1981.

Appendix A AFM and Potential Scan of selected polymers

Appendix A presents AFM and potential scans on surface of three polymers namely Poly(methyl methacrylate (PMMA), Polystyrene (PS) and Polydimethylsiloxane (PDMS). A silicon oxide (SiO_2) AFM tip was used to scratch the sample in contact mode to create a pattern of 3 lines 15 micron apart. AFM and potential scan of the same area were obtained using same tip in tapping mode. Only these materials could be used for this study, because of two essential requirement of the technique. Firstly, surface to be measured needs to have surface roughness in nano-scale range for AFM measurement. Secondly, the potential measurements requires an electrical circuit between the sample and tip. If the sample is thick, the potential measurements does not give accurate values. Therefore, the polymer materials need to be made into thin films by spin coating or molded into thin sheets.

The PMMA surface charges positive upon scratching and attains a potential of +170±60 mV as shown in Figure A1 while Polystyrene surface charges negative and attains a very high negative potential of -3800±500 mV as shown in Figure A2. Spin coated PDMS after scratching with SiO_2 tip attains a positive potential of +252±200 mV. For PS and PDMS, the absence of sharp drop in potential between scratched and unscratched areas suggest that some charge leaks into to neighbouring unscratched areas.

Despite the fact that PS and PMMA attain opposite potential upon scratching, both do not give generate plasma within 1 minute of high speed sliding. This further reinforces the hypothesis that a positive/negative or a high/low values of surface potential of the individual samples are not as much a crucial factor for triboplasma generation as the net potential difference between pin and disc sample.

Table A.1: Surface potential of polymers measured after scratching with SiO_2 tip

Polymer against SiO_2 tip	**Potential**
PMMA	+170mV ± 60mV
PS	-3800mV ± 500mV
PDMS	+252mV ± 200mV

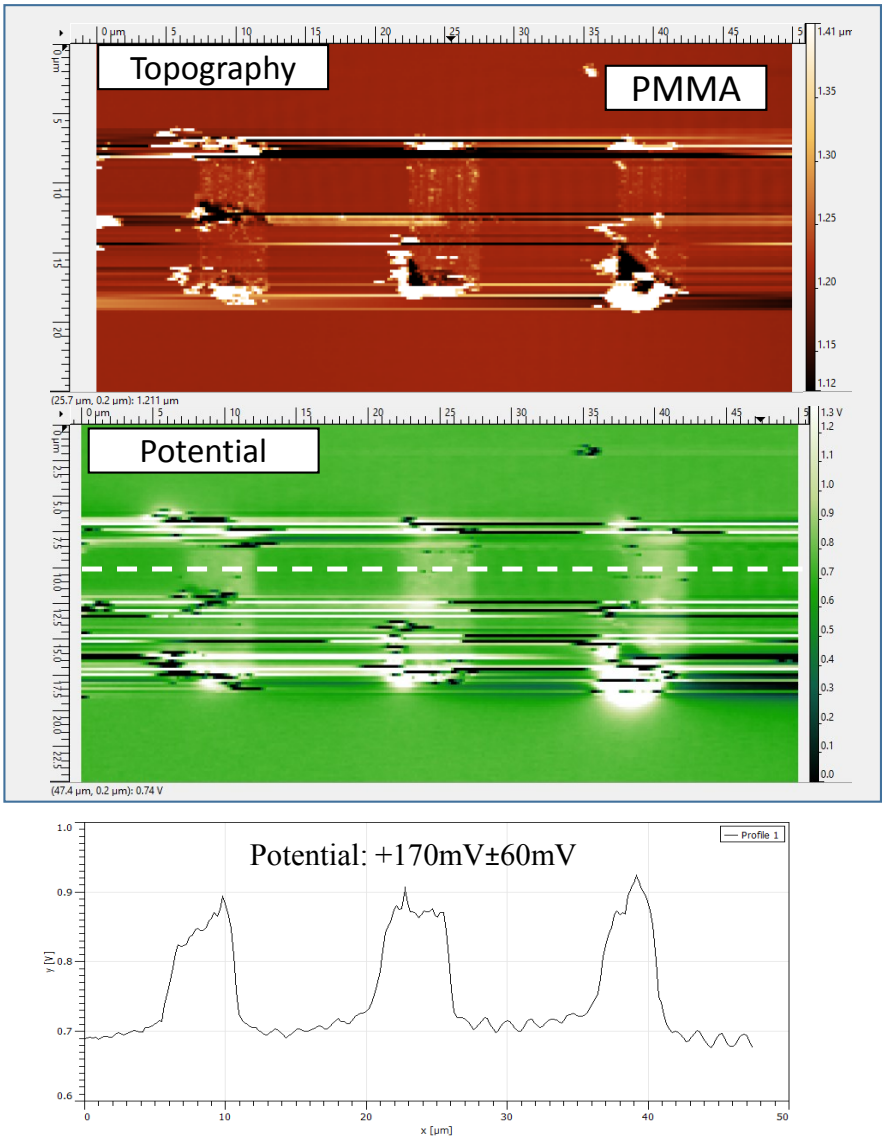

Figure A2.1

Figure A.1: Topography and potential distribution on spin coated PMMA after scratching with SiO_2 tip.

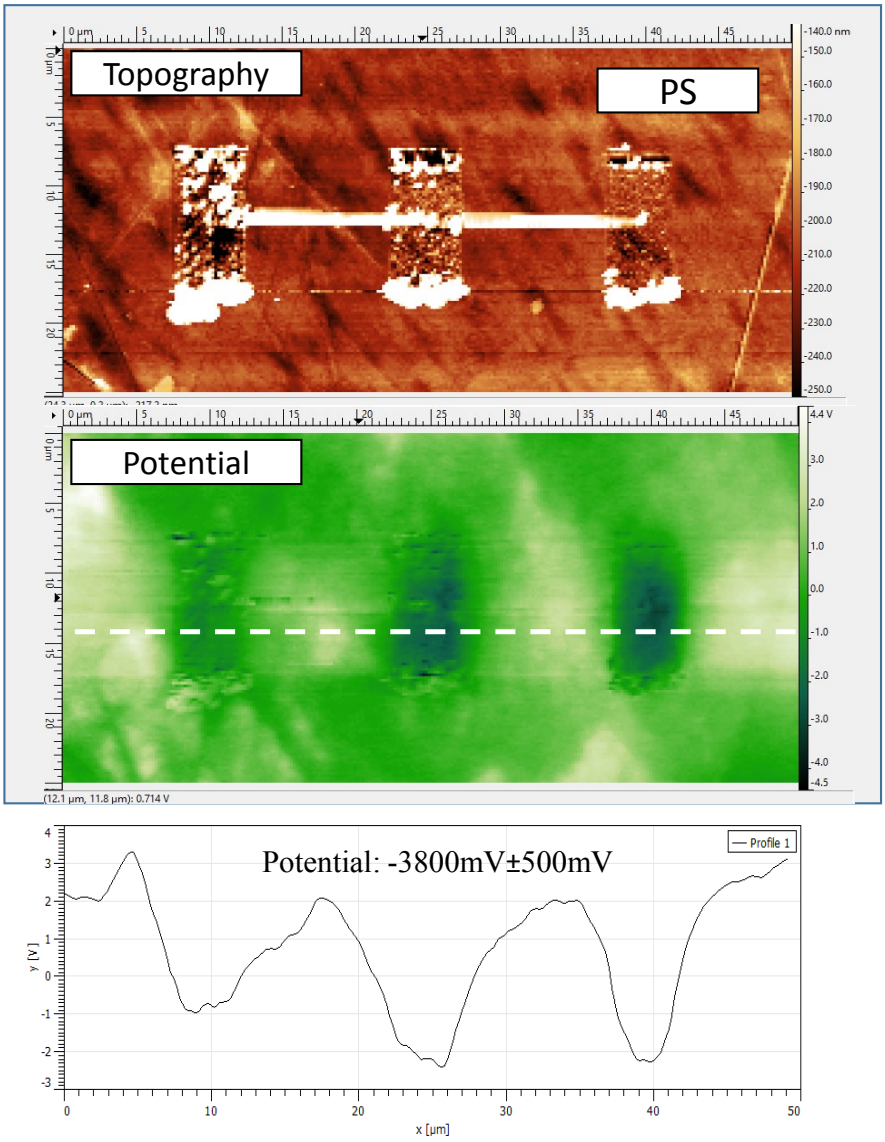

Figure A2.2

Figure A.2: Topography and potential distribution on Polystyrene petridish after scratching with SiO_2 tip.

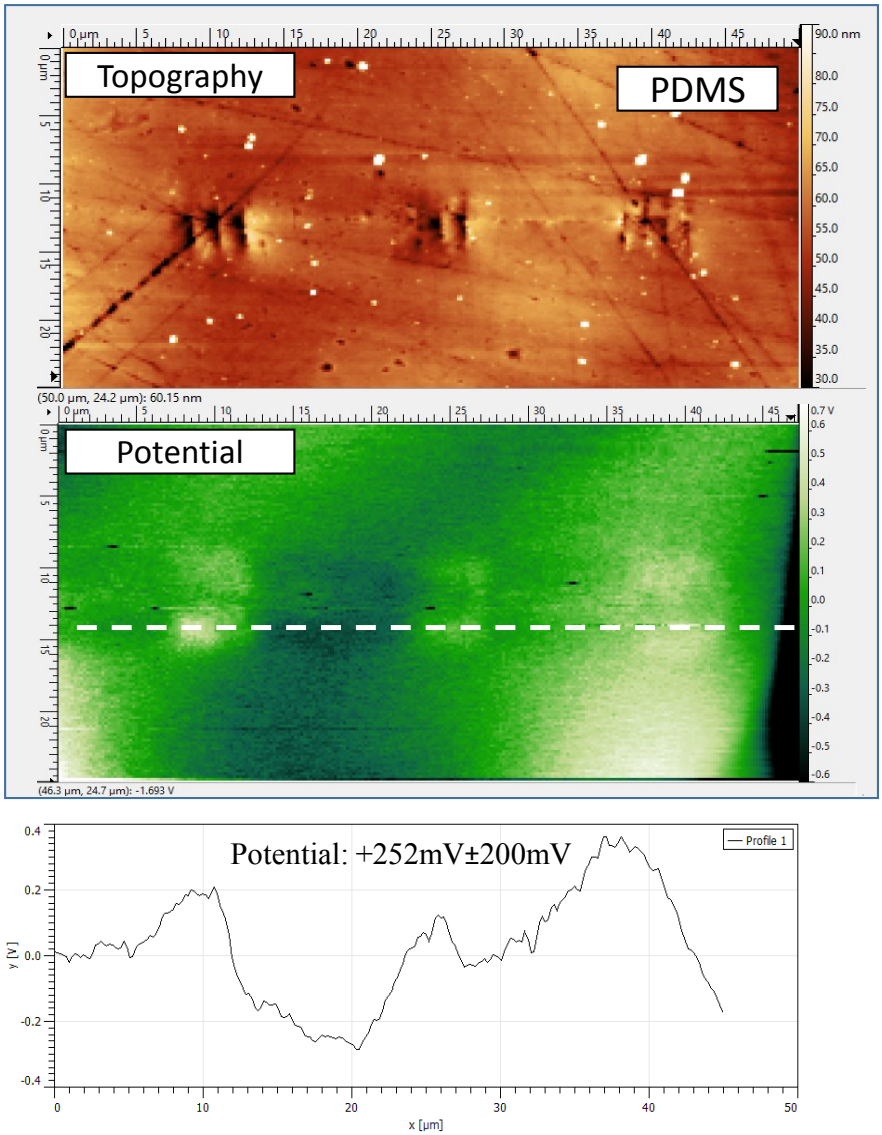

Figure A.3: Topography and potential distribution on spin coated PDMS after scratching with SiO_2 tip

Appendix B Plasma from TiO_2 filled UHMWPE composites

TiO_2 filled UHMWPE composites of various compositions (see Table B.1) were rubbed against Al_2O_3 hemisphere at a load of 40 N and speed of 2.4 m/s. The choice of TiO_2 particles result from the discussion above *i.e.* TiO_2 crystals have the potential to generate triboemission. The temperature and relative humidity was kept at 20 °C and 47% respectively. Triboplasma generation from the composites is shown in Figure B.1. The spread as well as intensity of emission reduces as the amount of TiO_2 increases.

Table B.1: Nomenclature and composition of UHMWPE composites

Nomenclature	Amount of TiO_2
T_0	0%
T_2	2%
T_4	4%
T_6	6%
T_8	8%
T_{10}	10%

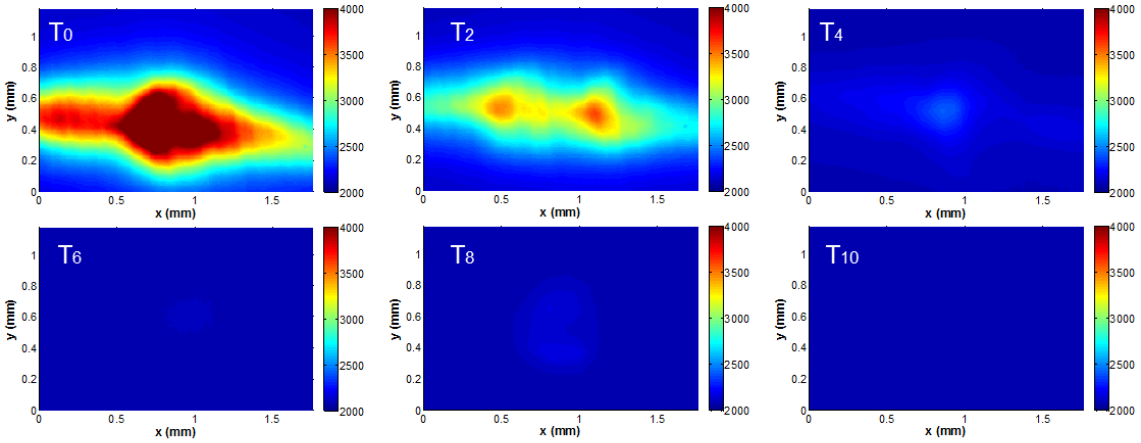

Figure B.1: Plasma distributions measured from various TiO_2 filled UHMWPE/Al_2O_3 contact

The maximum emission intensity also falls as the amount of TiO_2 filled in the UHMWPE matrix increases (Figure B.2). Furthermore, the addition of TiO_2 also leads to a change of variation of photon emission with time (Figure B.3). The cyclically fluctuating trend of UHMWPE changes to the trend characteristic for PTFE/Al_2O_3 contact (Section 5.1.2.3) upon addition of fillers.

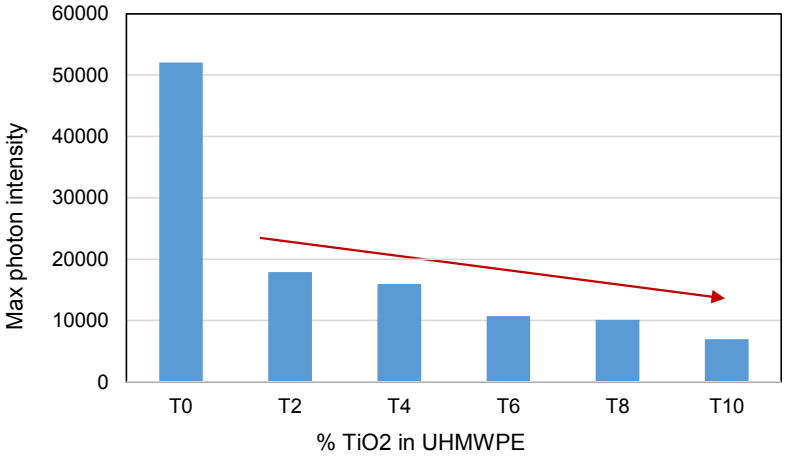

Figure B.2: Effect of TiO_2 loading on maximum photon emission

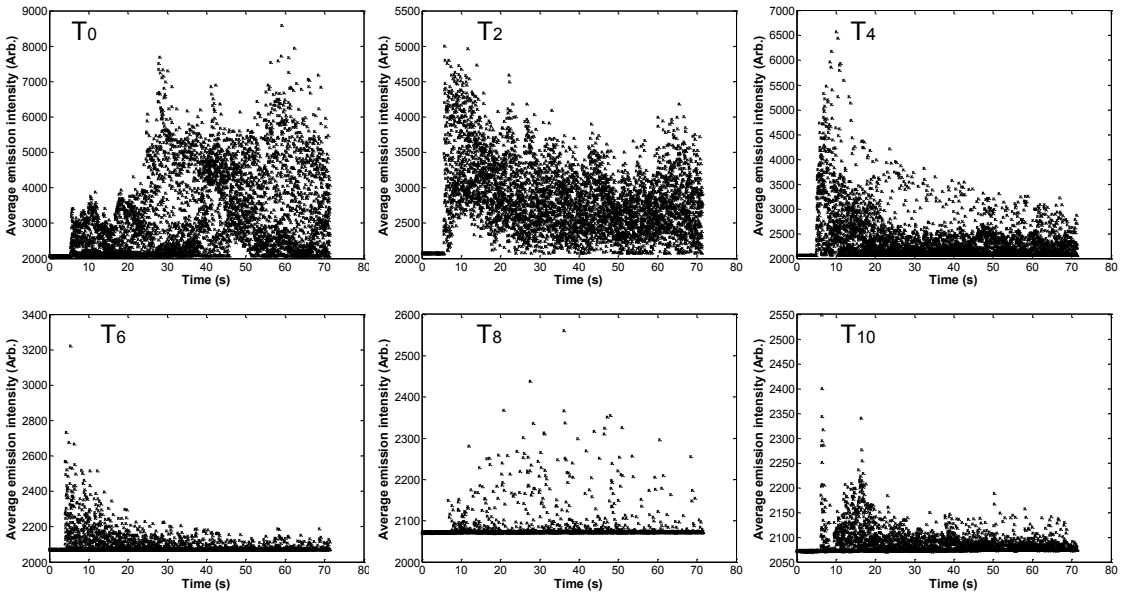

Figure B.3: Variation in average emission intensity with time for various TiO_2 filled UHMWPE/Al_2O_3 contact, loaded with 1 N and sliding at a speed of 2.4 m/s.

SEM images of transfer film and debris deposit on Al_2O_3 hemisphere after a sliding test at load of 40 N and speed of 1 m/s are presented in Figure B.4. The transfer film is observed adhering to both inlet as well as outlet of the contact along with debris of all sizes. Unfilled UHMWPE composite has highest plasma but no film compared to filled UHMWPE. All other composites form similar shaped transfer film on the Al_2O_3 surface.

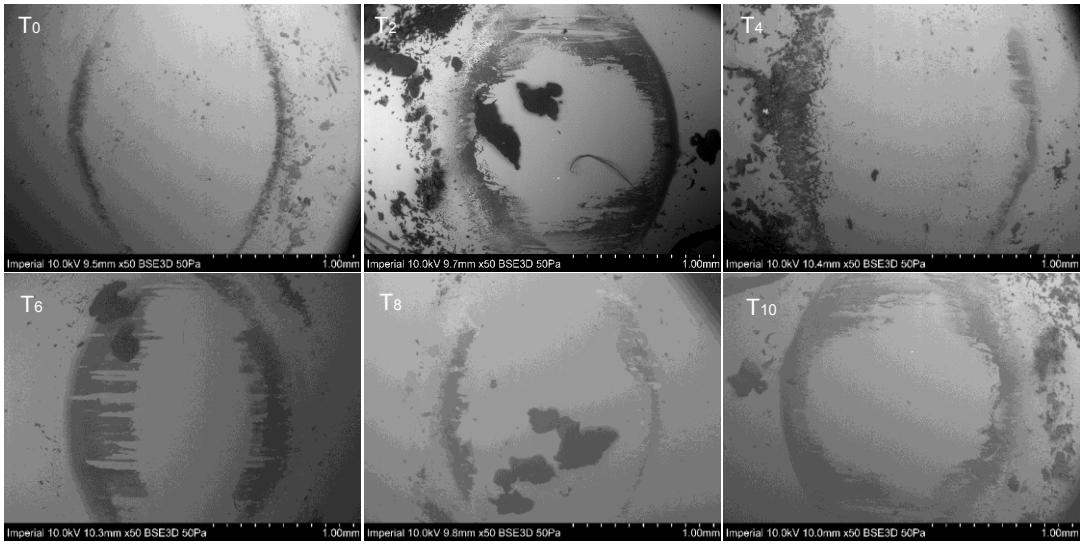

Figure B.4: SEM images of transfer film and debris deposit on Al_2O_3 hemisphere.

It is concluded that triboplasma is not a major contributor for transfer film formation. It the shearing and temperature that causes film formation. Metallic titanium (50%) filled UHMWPE composites/Al_2O_3 contacts produced no plasma as well because of the conducting metal dispersed in the UHMWPE matrix. This is similar to the behaviour of antistatic UHMWPE in which conducting carbon is dispersed in UHMWPE matrix arrests the charging and subsequent discharging.

Appendix C Variation in photon emission intensity with time for selected polymer/sapphire contacts

Appendix C shows the raw data for variation of average photon emission with time for various polymers tested and summarized in **Section 5.1** of **Chapter 5**. Figure C.1 shows the transient variation in average photon emission intensity with time for PMMA/ Al_2O_3, PS/Al_2O_3, PEEK/Al_2O_3 and NYLON/Al_2O_3 contacts, loaded to 1 N and sliding at a speed of 2.8 m/s. These kinds of photon emission intensity have been categorized as No/Low emission. In Figure C.2, an example of constant high emission type variation in average photon emission intensity with time as observed for PDMS/Al_2O_3 contact loaded to 1 N and sliding at a speed of 2.8 m/s is shown.

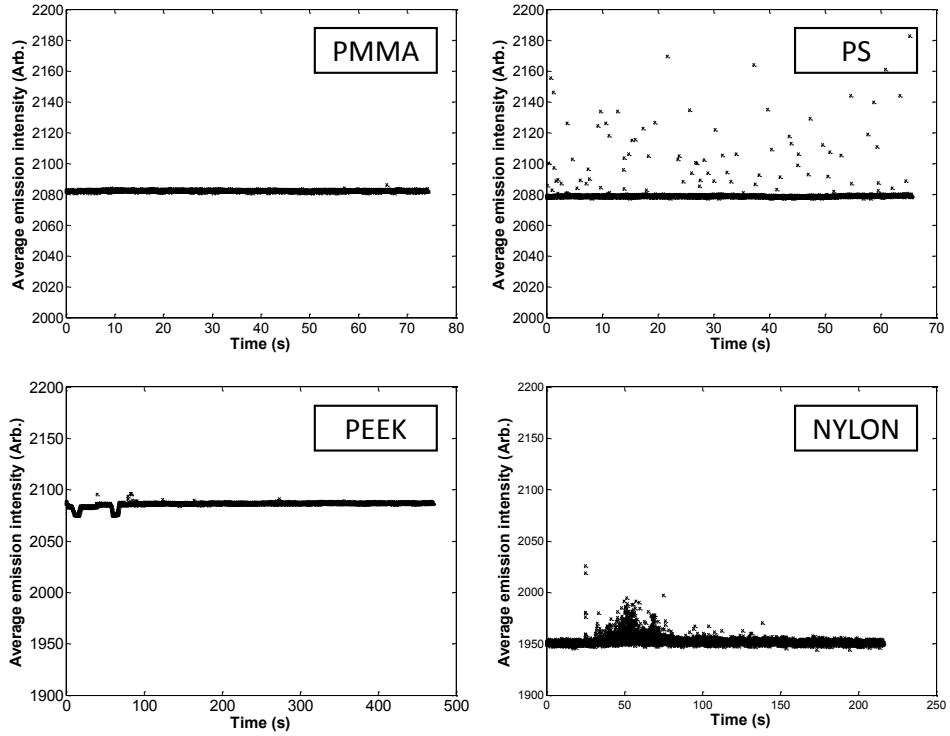

Figure C.1: No/Low emission-variation in average photon emission intensity with time for PMMA/ Al_2O_3, PS/Al_2O_3, PEEK/Al_2O_3 and NYLON/Al_2O_3 contacts, loaded with 1 N and sliding at a speed of 2.8 m/s.

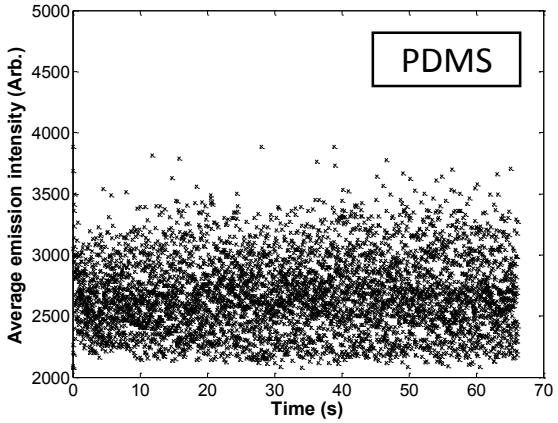

Figure C.2: Constant emission - variation in average photon emission intensity with time for PDMS/Al_2O_3 contact, loaded with 1 N and sliding at a speed of 2.8 m/s.

Figure C.3 shows an initial peaking then drop to low emission as observed for PVDF/ Al_2O_3 and HDPE/ Al_2O_3 contacts, loaded with 1 N and sliding at a speed of 2.8 m/s. Figure C.4 shows an initial peak followed by continued a steady emission observed in case of for Oil filled Nylon/ Al_2O_3 contact, loaded with 1 N and sliding at a speed of 2.8 m/s.

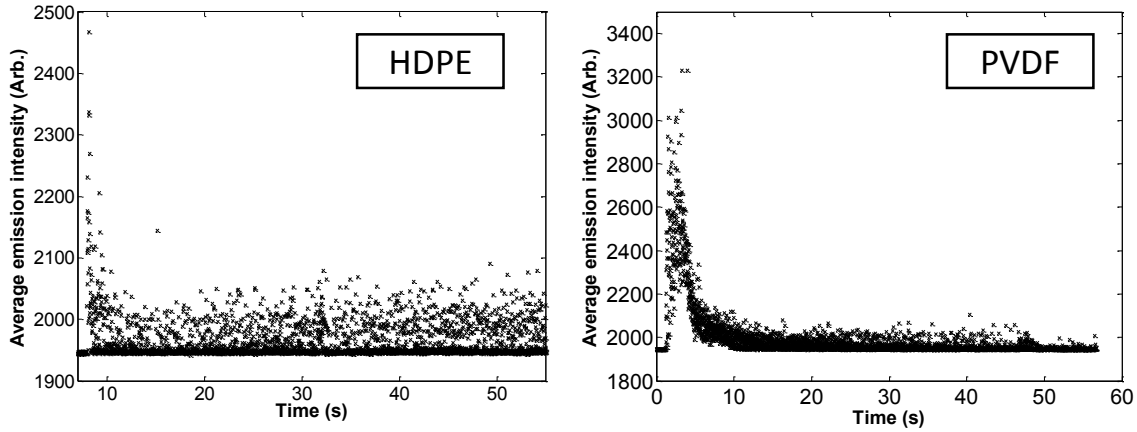

Figure C.3: Initial peak then drop to low emission – variation in average photon emission intensity with time for PVDF/ Al_2O_3 and HDPE/ Al_2O_3 contact, loaded with 1 N and sliding at a speed of 2.8 m/s.

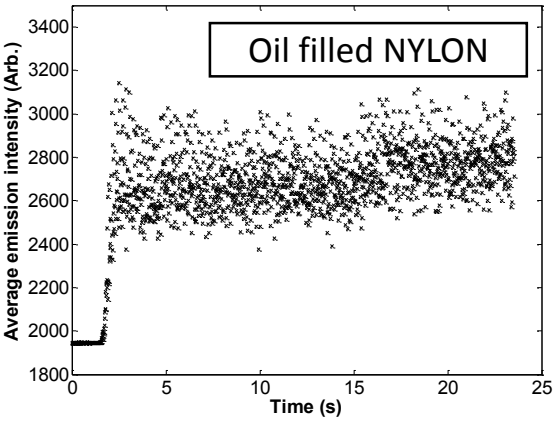

Figure C.4: Initial peak then continue a steady emission – variation in average photon emission intensity with time for Oil filled Nylon/ Al_2O_3 contact, loaded with 1 N and sliding at a speed of 2.8 m/s.

Figure C.5 shows gradually increasing overall intensity in a cyclic manner observed in case of polyvinylchloride PVC/ Al_2O_3 contact. A gradually increasing emission trend is exhibited by polycarbonate (PC), copolymer of polypropylene (PP(C)) and homopolymer of polypropylene (PP(H)). The variation in average photon emission intensity with time for PP(C)/ Al_2O_3, PP(H)/Al_2O_3, and PC/Al_2O_3 contacts is shown in Figure C.6.

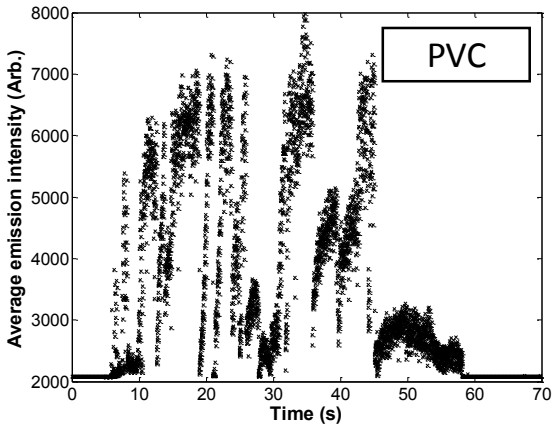

Figure C.5: Gradually increasing overall intensity in a cyclic fluctuation – variation in average photon emission intensity with time for PVC/ Al_2O_3 contact, loaded with 1 N and sliding at a speed of 2.8 m/s.

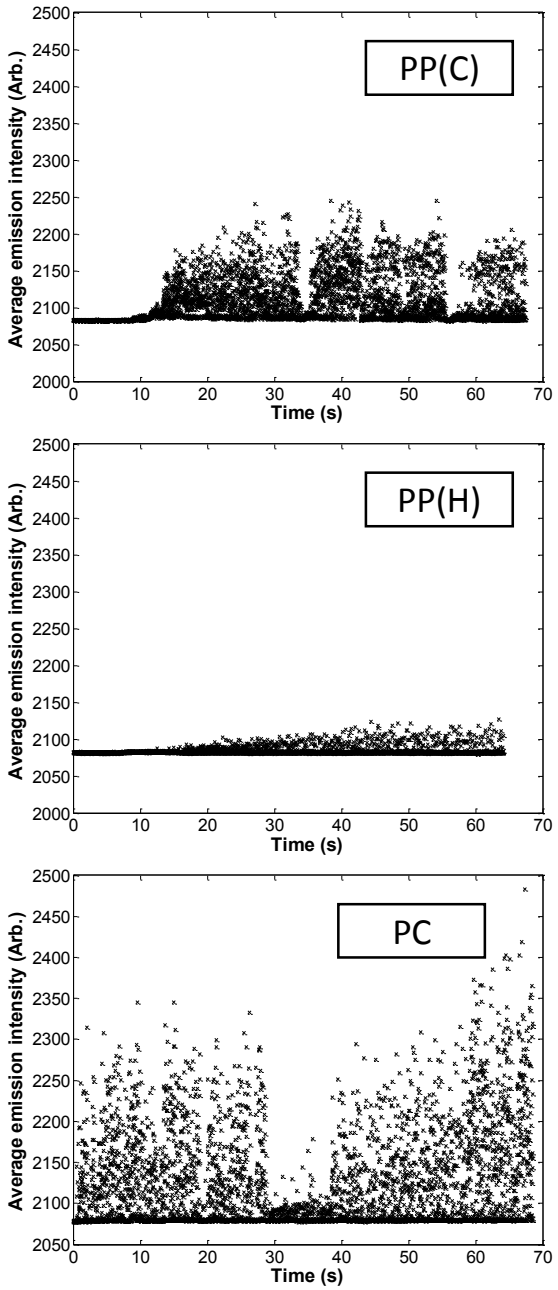

Figure C.6: Gradually increasing emission–variation in average photon emission intensity with time for PP(C)/ Al_2O_3, PP(H)/Al_2O_3, and PC/Al_2O_3 contacts, loaded with 1 N and sliding at a speed of 2.8 m/s.

Appendix D Submerged tests

Appendix D shows the various submerged tests conducted utilizing the dye fluorescence technique for UHMWPE-sapphire contact and PTFE-Sapphire contacts which were not shown in section 6.2 for brevity. This study only highlights the dye-debris interaction but further in-depth studies are needed to understand the exact mechanism.

The observations were made with a UHMWPE-Sapphire contact were similar to PTFE/Sapphire contact presented in **Section 6.2 of Chapter 6**. In Figure D.1, (a), (b) and (c) shows the images of a UHMWPE-Sapphire contact when submerged in deionized water while (c), (d) and (f) show the images of a UHMWPE-Sapphire contact when submerged in dye mixed deionized water. Images (a) and (d) are white light images of the contact. Images (b) and (e) are fluorescent images before sliding while Images (c) and (f) are the fluorescent images after sliding. There is very little change in the contact before sliding and after sliding. This is because UHMWPE is a wear resistant material and therefore the contact area does not increase significantly as compared to PTFE. Consequently, the apparent interaction of the dye with the rubbed polymer is also diminished. The black dots in image (f), accumulated around the edge of the contact suggests some level of agglomeration and/or quenching of florescence at these locations. It should note that images (b) and (c) are of low light intensity. They are made brighter by auto adjustment function of the ImageJ image processing software. The presence of dye, makes the image brighter because of the dye's fluorescence activity. This is also seen in PTFE-sapphire contact shown in **Figure 6.7**:PTFE –Sapphire contact– submerged during sliding in water (no dye) – in situ fluorescence images (a) white light image (b) fluorescence microscope image before test (c) fluorescence microscope image after test [excited by 450-490 and observed in wavelength in range of 500-550 nm].PTFE –Sapphire contact– submerged during sliding in 1mM CF in water (a) white light image (b) in-situ fluorescence image before test (c) in-situ fluorescence image after test. in **Chapter 6**.

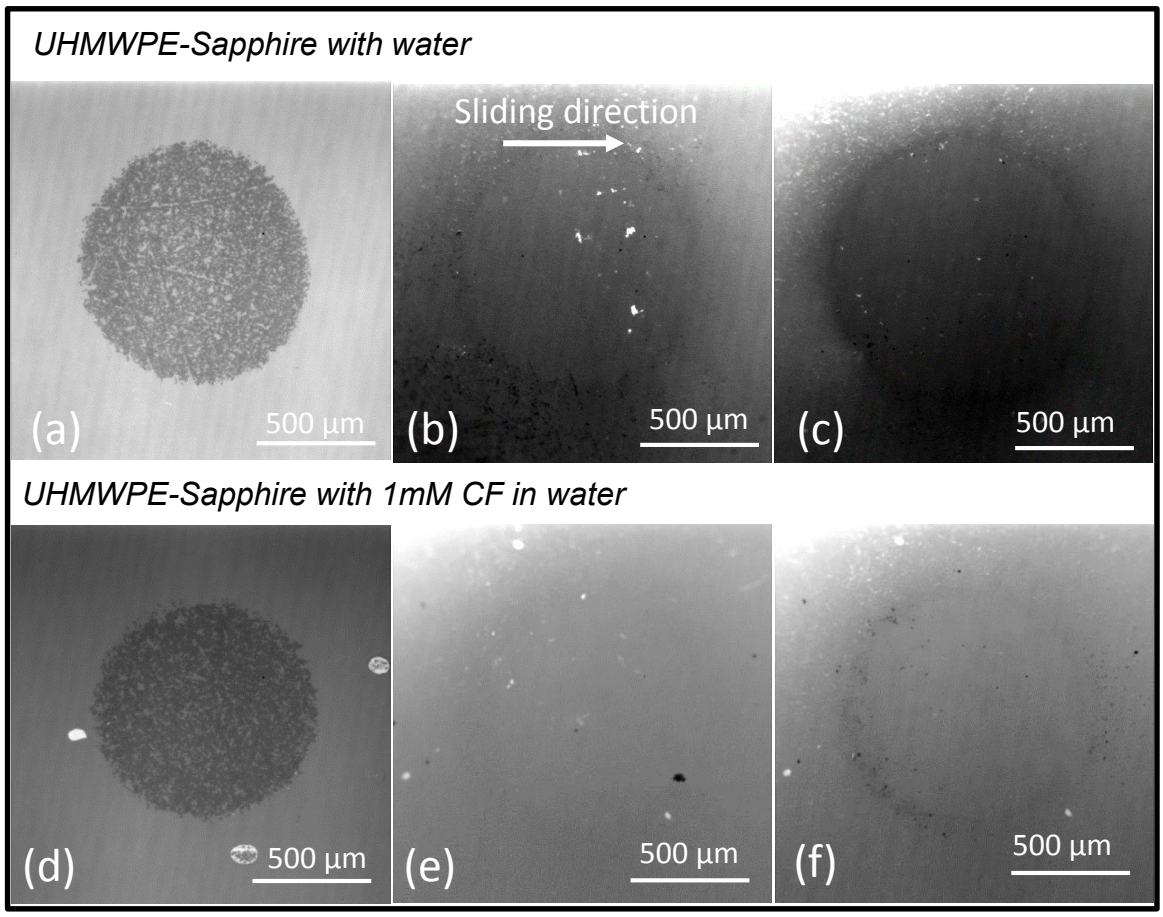

Figure D.1: UHMWPE – Sapphire contact submerged during sliding. (a),(b), and (c) are in deionized water; (d),(e), and (f) are in 1mM CF dye mixed water (a) and (d) are white light image; (b) and (e) are in-situ fluorescence image before test; (c) and (f) are in-situ fluorescence image after test.

Figure D.2 shows an ex-situ optical microscope image of the rubbed UHMWPE ball surface. There is no apparent change in the contact surface in comparison to PTFE-Sapphire contact. The agglomerated dye can be noticed along the edges of the contact although the hemispherical shape of the ball makes it impossible to focus on each point to the same degree.

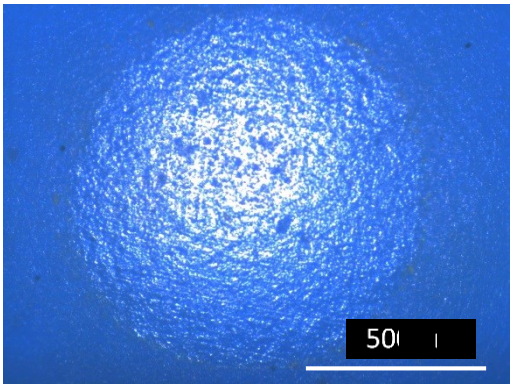

Figure D.2: Contact area of the UHMWPE ball visualized under optical microscope after sliding tests.

Next, in the liquid submerged series of tests, the contact was submerged in oil or dye mixed oil and sliding tests were conducted. CF was mixed with group II base oil to obtain a concentration of 1 mM. **Figure D.3** shows images of a PTFE-Sapphire contact while **Figure D.4** shows images of a UHMWPE-Sapphire contact in oil submerged conditions. Images (a), (b) and (c) show the contact submerged in oil only while images (d), (e), and (f) show the contact submerged in 1mM CF dye mixed with oil. Images (a) and (d) are white light image of the contact, (b) and (e) are in-situ fluorescence image before test, (c) and (f) are in-situ fluorescence image after test. On comparing **Figure D.3** (b) and (c), it is evident that rubbing in presence of an oil generates fluorescent strands of PTFE debris which are mostly accumulated at the contact inlet. The bright spots dispersed in the contact, as seen in **Figure D.3** (c) and (f) could be due to dye-debris interaction.

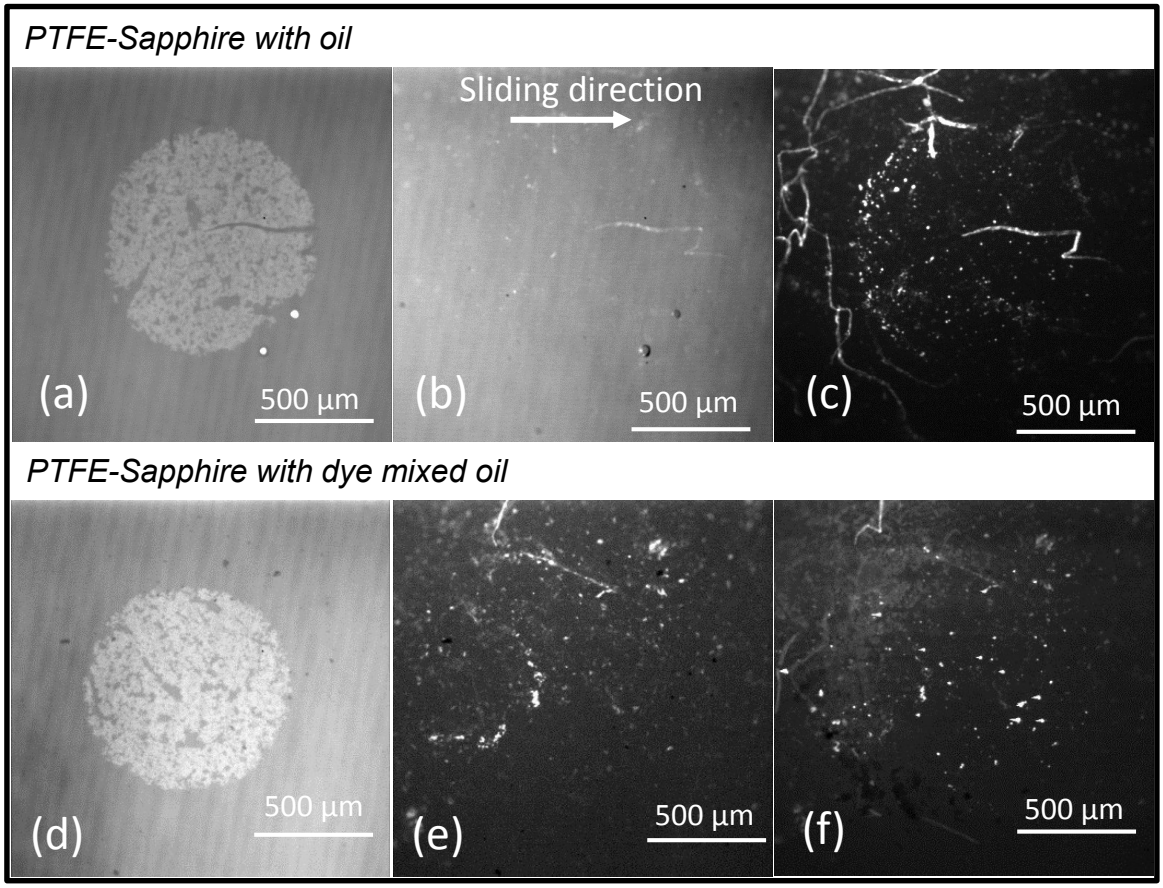

Figure D.3: PTFE –Sapphire contact submerged during sliding. (a),(b), and (c) are in oil; (d),(e), and (f) are in 1mM CF dye mixed with oil (a) and (d) are white light image; (b) and (e) are in-situ fluorescence image before test; (c) and (f) are in-situ fluorescence image after test.

Images (a) and (b) in **Figure D.4** are similar to images (a) and (b) in **Figure D.3** which shows PTFE- Sapphire oil submerged contact but fluorescent images (c), (e) and (f) in both figures are very different, particularly, image (c) in **Figure D.4**. It does not show distribution of any

bright spots in the contact. Some agglomerated dye is already present in the dye mixed oil which appear as black spots in images (e) and (f) in both **Figure D.3** and **Figure D.4**. Fluorescent images (c) and (f) show that UHWPE debris accumulates at the front of the contact after sliding stops. In the presence of dye mixed oil, black debris or dye-debris aggregate is also observed at front of the contact. The proportion of these black agglomerates increases as sliding continues. Moreover, the accumulated debris appear brighter in image (f) than image (c) which contains only oil. This is a clear evidence of dye interaction with charged polymer debris. Additionally, in case of UHMWPE-sapphire contact, there is very few brightly dispersed spots inside the contact which is in contrast with the PTFE-sapphire contact. This suggests that the bright spots seen in images (b), (c), (e) and (f) in **Figure D.3** are indeed PTFE debris interaction with the CF dye. As mentioned earlier, the black regions or spots could be a result of dye agglomeration during sliding or/and due to quenching of fluorescence at those locations due to interaction with charged polymer debris during sliding.

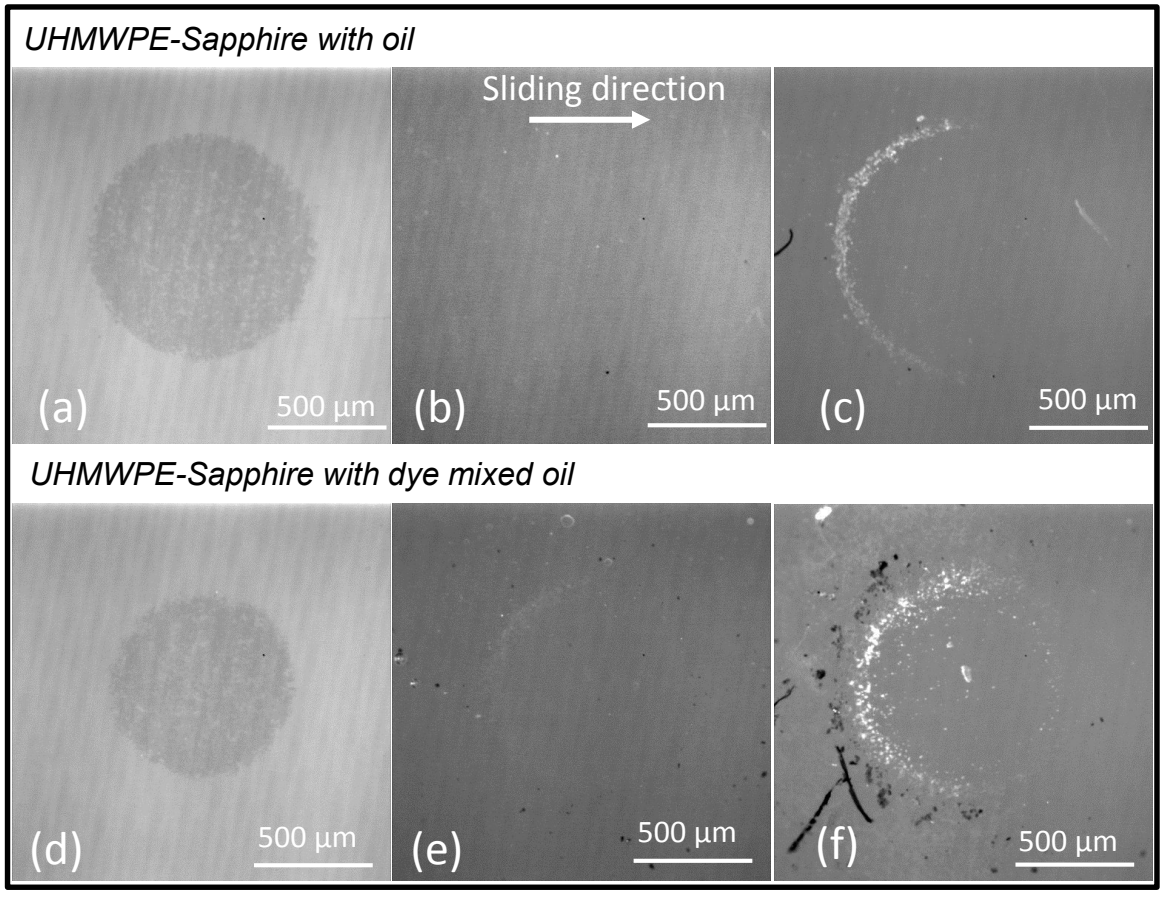

Figure D.4: UHMWPE –Sapphire contact submerged during sliding. (a),(b), and (c) are in oil; (d),(e), and (f) are in 1mM CF dye mixed with oil (a) and (d) are white light image; (b) and (e) are in-situ fluorescence image before test; (c) and (f) are in-situ fluorescence image after test.

Figure D.5 shows ex-situ optical images of (a) PTFE ball and (b) UHMWPE ball submerged in dye mixed oil during sliding. It provides evidence of two kind of dye-debris interaction. The PTFE debris interacts with the dye mixed oil in the same manner as with dye mixed water. This further confirms the charged entity interaction where the positive dye ion is attracted to negatively charged debris. On the contrary, UHMWPE shows a different kind of interaction with the dye mixed water as compared to dye mixed oil. In case of water submerged UHMWPE-sapphire contact, debris generation is low hence no major change in fluorescent image is observed after sliding. While in the case of oil submerged UHMWPE-sapphire contact, the debris is seen to accumulate at the entry, some of which is fluorescent while some are not. These black regions could be attributed to dye-debris interaction leading to quenching of the fluorescence or agglomeration.

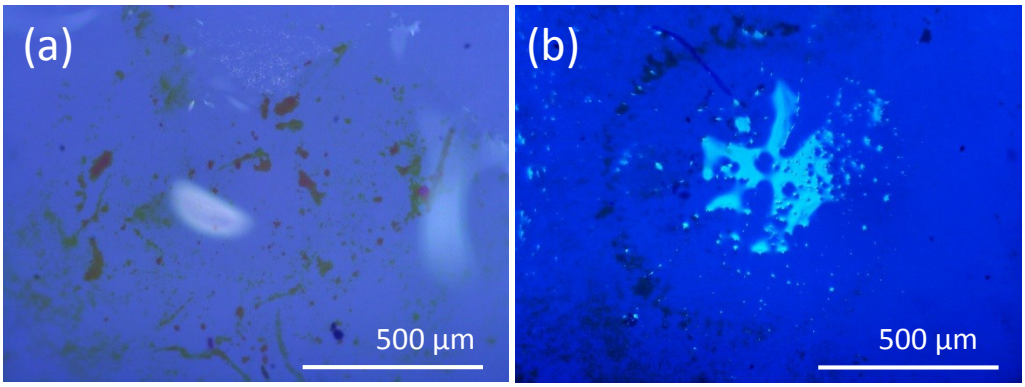

Figure D.5: Ex situ optical images (a) PTFE ball (b) UHMWPE ball – submerged during sliding in dye mixed oil.

It was shown in **Chapter 5** that debris has a net charge in either polarity and therefore there is a strong possibility that, depending upon the interaction with the triboemission, (electrons and ions) some dye molecules (fluorophore) will cease to fluoresce. This may be the reason for the differences in fluorescent images (f and c) in water submerged PTFE-sapphire contact and oil PTFE-sapphire submerged contact in Figure D.3. To further confirm if the dye interaction was specific to the selected CF dye, another dye, neutral red was used that was mixed with deionized water to obtain a concentration of 1mM. A similar dye interaction was observed at and around the contact as shown in **Figure D.6**. It is evident that the dye precipitates out of the solution and adsorbs at the contact inlet.

Additional rubbing tests in dye submerged conditions were carried on a high frequency reciprocating rig (HFRR) and UV-VIS absorption spectroscopy was done on the dye mixed liquid before and after the test. There was a substantial decrease in absorption intensity of dye

mixed liquid collected after the in-situ rubbing (**See Appendix E**). The intensity is directly proportional to concentration according to Beer Lambert Law. Thus, it was concluded that the decrease in concentration was due to dye aggregates deposited at the contact. This kind of aggregations arise from a competition between cohesive forces and flow rupture at the contact. The size of the aggregates is related to concentration and shear rates.

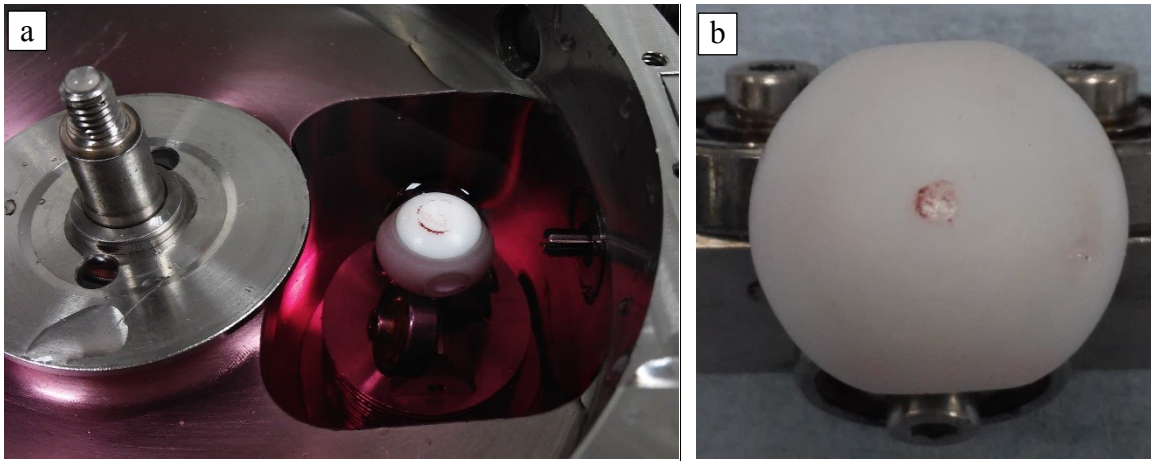

Figure D.6: (a) After test images of the contact area of PTFE ball after being slid against a transparent sapphire disc submerged in 1mM neutral red mixed deionized water. (b) After test images of the contact area of PTFE ball after drying from another test.

Appendix E UV-VIS absorption spectra

In Appendix E, UV-VIS absorption spectra of 0.05 mM neutral red dye in de-ionized water (referred here on as solution) under various conditions such as (i) fresh solution, (ii) after immersion of unrubbed sample for 30 minutes, (iii) after immersion of rubbed sample for 30 minutes, (iv) after extraction of the solution which submerged a unrubbed tribo-pair kept in stationary position in the high frequency reciprocating rig (HFRR) for 30 minutes (v) after extraction of the solution which submerged the tribo-pair in reciprocating action in the HFRR for 30 minutes are shown in Figure E.1 and Figure E.2 . The two sets of tribopair used were UHMWPE/Al_2O_3 and PTFE/Al_2O_3 contacts. There appears to be some peak shift as well attenuation of absorption spectra in all repeats test carried. Rubbing decreases the absorbance at the first peak at 450 nm while increased on the second peak at 535 nm. Since, these studies were carried in neutral pH both NR and NRH^+ forms coexist in the solution. Thus at neutral pH the absorption spectrum of neutral red shows both the absorption peaks due to neutral (NR) and protonated (NRH^+) forms of the dye at 450 and 535 nm respectively. The decrease in the absorbance at 450 nm and slight increase in absorbance at 532 nm after rubbing are due to enhanced protonation of NR to form NRH^+. This protonation is promoted by shearing of polymeric chains. But any conclusive inference could not be derived because of change of concentration of the solution under various conditions mentioned above, the uncertainty regarding change in pH level after rubbing, as well as the effect of charged surfaces on neutral red absorption spectra. Similar decrease in absorbance peaks of carboxyfluorescein dye was also observed. Figure E.3 shows absorption as well aggregation of neutral red dye onto the wear track of the polymer disc when rubbing is carried while submerged in the solvent.

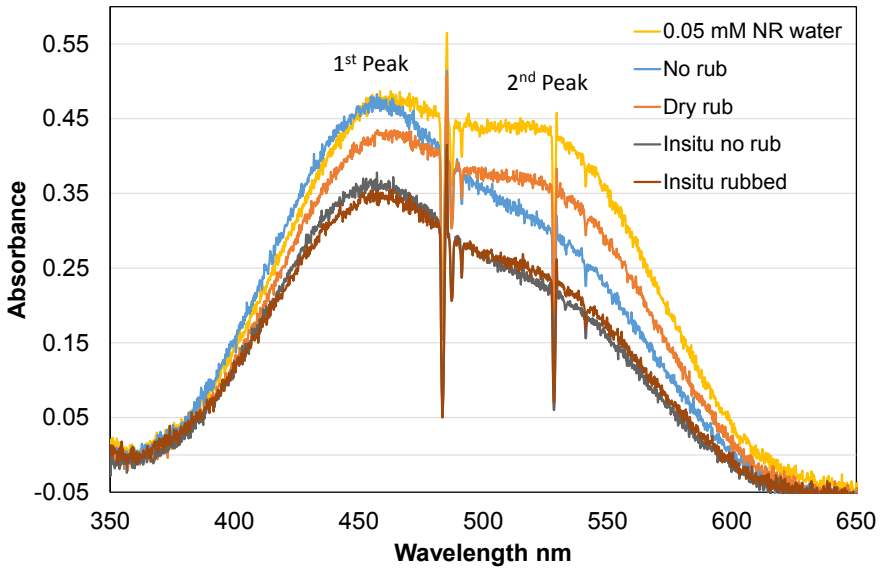

Figure E.1: Absorption spectra of 0.05 mM neutral red dye in water under various conditions in UHMWPE/Al_2O_3 contact.

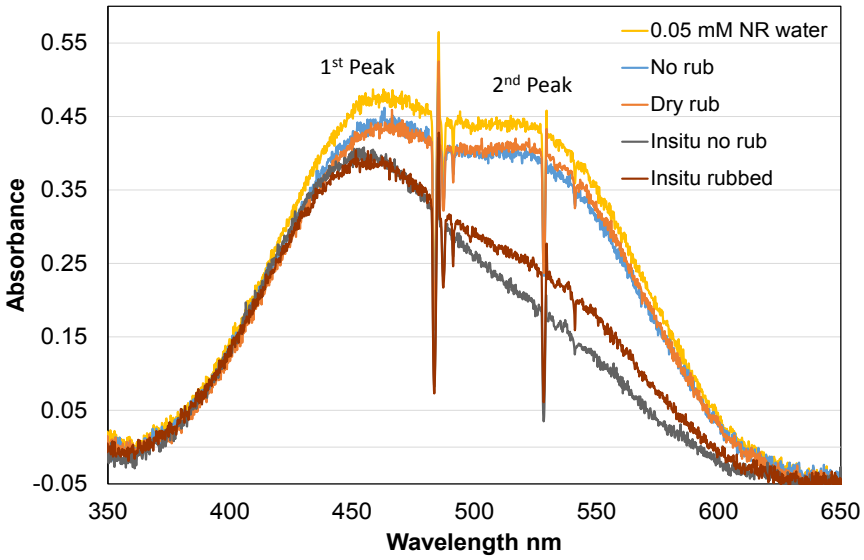

Figure E.2: Absorption spectra of 0.05 mM neutral red dye in water under various conditions in PTFE/Al_2O_3 contact.

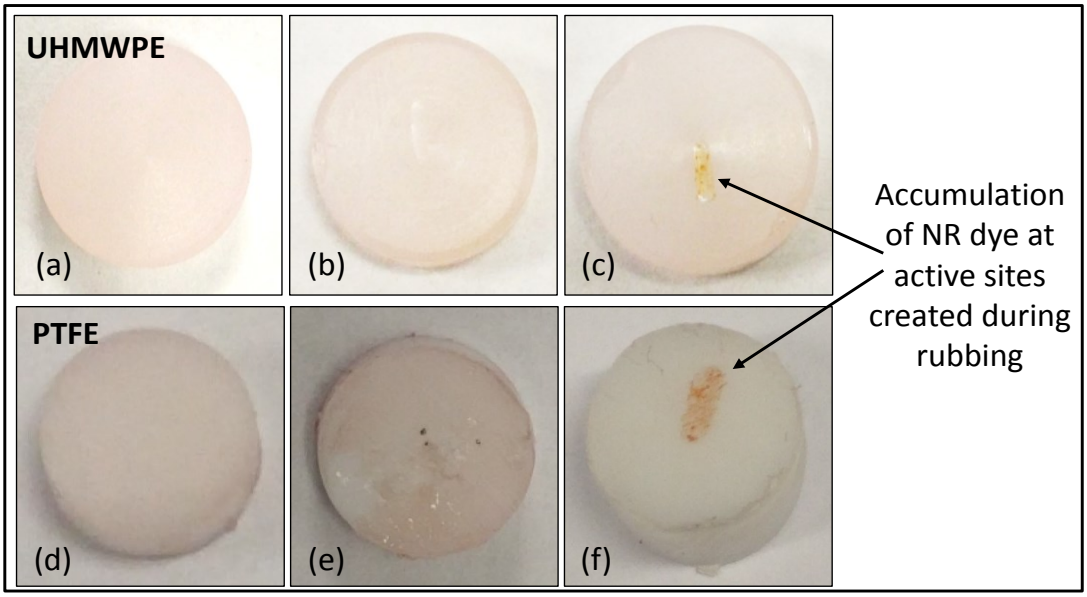

Figure E.3: Images (a)-(c) show UHMWPE disc (10 mm diameter) while images (d)-(f) show PTFE disc after rubbed with a Al_2O_3 hemisphere in a high frequency reciprocating rig (HFRR). Sample in image (a) and (d) are unrubbed fresh samples; samples in images (b) and (e) are rubbed dry then immersed in NR dye; samples in images (c) and (f) are rubbed while immersed in 0.05 mM neutral red dye in water.

Appendix F List of Publications

The following is the list of conference and journal publications, where parts of this work were presented.

1. **Puhan, Debashis** and Tom Reddyhoff, *Triboplasma from Polymer Contacts* 21st International Conference on Wear of Materials, Hilton Long Beach, California, USA, 26-30 March 2017.

2. **Puhan, Debashis** and Tom Reddyhoff, *Transient characteristics of triboplasma generation*, Proceedings of the 43rd Leeds-Lyon Symposium on Tribology, Leeds, United Kingdom, 6-9 September 2016

3. **Puhan, Debashis** and Tom Reddyhoff, *Triboplasma generation at polymer contacts*, Proceedings of the 42th Leeds-Lyon Symposium on Tribology, Lyon, France 7-9 September 2015.

4. **Puhan, Debashis** and Tom Reddyhoff, *An Experimental Study into the Effects of Triboemission,* International Tribology Conference, Tokyo 2015, Tokyo University of Science, Tokyo, Japan, 16-20 September 2015.

5. Reddyhoff, Tom and **Debashis Puhan**, *Transient Triboplasma Measurements*, International Tribology Conference, Tokyo 2015, Tokyo University of Science, Tokyo, Japan, 16-20 September 2015.